



# Reynolds Number Effects in Wall-Bounded Turbulent Flows

P. R. Bandyopadhyay  
Weapons Technology and Undersea Systems Department

M. Gad-el-Hak  
University of Notre Dame



**UNCLASSIFIED**  
NAVAL UNDERSEA WARFARE CENTER  
DIVISION NEWPORT  
NEWPORT, RHODE ISLAND 02841-1708  
RETURN TO: TECHNICAL LIBRARY

**Naval Undersea Warfare Center Division  
Newport, Rhode Island**

## **PREFACE**

This work was funded under IR/IED Project No. A10301, "Microfabrication," principal investigator P. R. Bandyopadhyay (Code 8233). Publication of this report was supported by the Director for Science and Technology (Code 10).

The technical reviewer for this report was J. S. Uhlman (Code 8233).

The second author of this report, M. Gad-el-Hak, was an ONR Distinguished Faculty Fellow who worked at NUWC Division Newport during the summer of 1993; his permanent address is Department of Aerospace and Mechanical Engineering, University of Notre Dame, Notre Dame, IN 46556.

Professor Gad-el-Hak wishes to acknowledge the financial support of the Office of Naval Research.

**Reviewed and Approved: 18 March 1994**



**F. L. White**  
**Head, Weapons Technology and**  
**Undersea Systems Department**

# REPORT DOCUMENTATION PAGE

Form Approved  
OMB No. 0704-0188

Public reporting for this collection of information is estimated to average 1 hour per response, including the time for reviewing instructions, searching existing data sources, gathering and maintaining the data needed, and completing and reviewing the collection of information. Send comments regarding this burden estimate or any other aspect of this collection of information, including suggestions for reducing this burden, to Washington Headquarters Services, Directorate for Information Operations and Reports, 1215 Jefferson Davis Highway, Suite 1204, Arlington, VA 22202-4302, and to the Office of Management and Budget, Paperwork Reduction Project (0704-0188), Washington, DC 20503.

1. AGENCY USE ONLY (Leave blank)		2. REPORT DATE 18 March 1994		3. REPORT TYPE AND DATES COVERED Final	
4. TITLE AND SUBTITLE  Reynolds Number Effects in Wall-Bounded Turbulent Flows				5. FUNDING NUMBERS	
6. AUTHOR(S)  P. R. Bandyopadhyay M. Gad-el-Hak					
7. PERFORMING ORGANIZATION NAME(S) AND ADDRESS(ES)  Naval Undersea Warfare Center Division Newport, Rhode Island 02841-1708				8. PERFORMING ORGANIZATION REPORT NUMBER  TR 10,296	
9. SPONSORING/MONITORING AGENCY NAME(S) AND ADDRESS(ES)				10. SPONSORING/MONITORING AGENCY REPORT NUMBER	
11. SUPPLEMENTARY NOTES					
12a. DISTRIBUTION/AVAILABILITY STATEMENT  Approved for public release; distribution is unlimited.				12b. DISTRIBUTION CODE	
13. ABSTRACT (Maximum 200 words)  This report reviews the state-of-the-art of Reynolds number effects in wall-bounded shear-flow turbulence, with particular emphasis on the canonical zero-pressure-gradient boundary layer and two-dimensional channel flow problems. The Reynolds numbers encountered in many practical situations are typically orders of magnitude higher than those studied computationally or even experimentally. High Reynolds number research facilities are expensive to build and operate, and the few existing ones are heavily scheduled with mostly developmental work. For wind tunnels, additional complications due to compressibility effects are introduced at high speeds. Full computational simulation of high Reynolds number flows is beyond the reach of current capabilities. Understanding of turbulence and the use of modeling will continue to play vital roles in the computation of high Reynolds number practical flows using the Reynolds-averaged Navier-Stokes equations. Because the existing knowledge base, accumulated mostly through physical as well as numerical experiments, is skewed toward the low Reynolds numbers, the key question in such high Reynolds number modeling in addition to devising novel flow control strategies is: What are the Reynolds number effects on the mean and statistical turbulence quantities and on the organized motions? The coherent structures in low Reynolds number wall-bounded flows have been reviewed several times since the 1960s. However, the Reynolds number effects on the higher order statistical turbulence quantities and on the coherent structures have not been reviewed thus far, and there are some unresolved aspects of the effects on even the mean flow at very high Reynolds numbers. Furthermore, a considerable volume of experimental and full-simulation data has been accumulated since 1962. This report aims at further assimilation of those data, pointing to obvious gaps in the present state of knowledge and highlighting the misunderstood and the ill-understood aspects of Reynolds number effects.					
14. SUBJECT TERMS Reynolds Number Effects  Wall-Bounded Turbulent Flows  Mean Flow Turbulence  Coherent Structures				15. NUMBER OF PAGES 152	
				16. PRICE CODE	
17. SECURITY CLASSIFICATION OF REPORT Unclassified	18. SECURITY CLASSIFICATION OF THIS PAGE Unclassified	19. SECURITY CLASSIFICATION OF ABSTRACT Unclassified		20. LIMITATION OF ABSTRACT  SAR	

0262

NAVAL UNDERSEA WARFARE CENTER DIVISION  
NEWPORT, RI

Change to Technical Report


To all holders of NUWC-NPT TR 10,296  
dated 18 March 1994:

1. Subject TR, recently distributed, is being changed to correct an error in figure 3.
2. Please make the following pen-and-ink changes to the subcaptions of figure 3 on page 4:

(a)  $Re_\theta = 2060$ ;  $\delta^* = 887$ ;  $\delta = 13.1$  cm  
(Kline et al., 1967)

(b)  $Re_\theta = 38,000$ ;  $\delta^* = 17,350$ ;  $\delta = 12.8$  cm  
(Tu and Willmarth, 1966)

25 April 1994

  
\_\_\_\_\_  
F. L. White  
Head, Weapons Technology and  
Undersea Systems Department

# TABLE OF CONTENTS

Section	Page
LIST OF ILLUSTRATIONS .....	ii
LIST OF TABLES .....	v
LIST OF SYMBOLS .....	vi
1 INTRODUCTION .....	1
1.1 Field Versus Laboratory Flows.....	1
1.2 Reynolds Number .....	1
1.3 Outline of Present Review .....	5
2 CONTEMPORARY RELEVANCE .....	7
2.1 Primary Issues .....	7
2.2 Turbulence Modeling .....	8
2.3 Flow Control and Post-Transition Memory.....	9
3 FLOW REGIMES .....	11
3.1 Viscous Region .....	12
3.2 Constant Reynolds Stress Region .....	13
3.3 Outer Layer.....	15
4 COMPARISON TO OTHER SHEAR FLOWS.....	17
5 MEAN FLOW .....	23
5.1 Streamwise Velocity.....	23
5.2 Von Kármán Constant .....	26
5.3 Illusory Asymptotic State .....	27
5.4 Is Self-Preservation Ever Achieved? .....	32
5.5 Alternatives to Logarithmic Profile .....	33
6 HIGHER ORDER STATISTICS .....	35
6.1 RMS Velocity Fluctuations.....	35
6.2 Reynolds Stress .....	47
6.2.1 Reynolds Number Effects .....	47
6.2.2 Peak Location .....	51
6.2.3 Asymptotic Theory.....	55
6.3 Spectra.....	56
6.4 Skewness and Flatness Factors .....	62
6.5 Wall-Pressure Fluctuations .....	68

## TABLE OF CONTENTS (Cont'd)

Section	Page
7 COHERENT STRUCTURES .....	71
7.1 Overview .....	71
7.2 Open Issues.....	76
7.2.1 Origin of Different Structures .....	76
7.2.2 Inner/Outer Interaction and Regeneration Mechanisms .....	77
7.3 Reynolds Number Effects .....	81
7.3.1 Bursting Period .....	82
7.3.2 High Reynolds Number .....	84
7.3.3 Small Structures in Outer Layer.....	88
7.3.4 Inner Structures.....	93
8 FLOW CONTROL.....	95
8.1 Introductory Remarks .....	95
8.2 Riblets.....	96
8.3 Recovery Response .....	97
8.3.1 Disturbances in Outer Layer .....	98
8.3.2 Disturbances Close to Wall.....	101
8.4 Control of High Reynolds Number Flows .....	102
9 NUMERICAL SIMULATIONS.....	103
9.1 General Remarks.....	103
9.2 Direct Numerical Simulations .....	106
10 NON-CANONICAL BOUNDARY LAYERS .....	109
11 CONCLUSIONS .....	113
12 BIBLIOGRAPHY .....	117

## LIST OF ILLUSTRATIONS

Figure	Page
1 Energy Spectra at Low and High Reynolds Numbers .....	3
2 Qualitative Effect of Reynolds Number on Features Composing Outer Region of a Turbulent Boundary Layer .....	4
3 Mean Velocity Profiles at Low and High Reynolds Numbers .....	4

## LIST OF ILLUSTRATIONS (Cont'd)

Figure	Page
4	Distribution of Viscous and Turbulence Shear Stresses in Wall-Bounded Flows..... 11
5	Normalized Turbulence Kinetic Energy Production Rate as Function of Normal Distance From Wall ..... 16
6	Turbulence Energy Balance in Typical Plane Wake..... 19
7	Mean Streamwise Velocity and Mean Spanwise Vorticity Distributions in Different Shear Flows ..... 20
8	Comparison of Mean Velocity Profiles With Logarithmic Law at Low Reynolds Numbers..... 24
9	Non-Dimensional Mean Velocity Profiles at High Reynolds Numbers..... 24
10	Mean Velocity Profiles Non-Dimensionalized on Inner Variables..... 25
11	Reproduction of Coles' Strength of Wake Component in Equilibrium Turbulent Boundary Layers at Low Reynolds Numbers ..... 28
12	Reproduction of Coles' Strength of Wake Component at Large Reynolds Numbers ..... 29
13	Strength of Wake Component vs Reynolds Number on Semi-Log Plot (Subsonic Data of Smith and Walker (1959) at Four Different Downstream Stations) (Mabey, 1979) ..... 30
14	Strength of Wake Component vs Reynolds Number on Semi-Log Plot (Supersonic Data of Mabey et.al., (1976) at Six Different Mach Numbers) (Mabey, 1979) ..... 31
15	Low Reynolds Number Effects on Clauser's Shape Parameter..... 31
16	Variation of Distribution of Turbulence Intensity in Wall Variables With Reynolds Number ..... 36
17	Distribution of Turbulence Intensity in Wall Variables at Four Different Downstream Locations ..... 37
18	Normal Profiles of RMS Streamwise Velocity, RMS Normal Velocity, and Reynolds Stress..... 39
19	Peak Value of $u$ Turbulence Intensity in Turbulent Boundary Layers ..... 40
20	Streamwise Turbulence Intensity Profiles Non-Dimensionalized With Respect to Inner Variables..... 41
21	Normal Turbulence Intensity Profiles Non-Dimensionalized With Respect to Inner Variables..... 42
22	Profiles of Turbulence Intensity in Streamwise Direction (Open Points) and Direction Normal to Wall (Solid Points), Non-Dimensionalized on Local Mean Velocity..... 43
23	Profiles of Turbulence Intensity in Streamwise Direction (Open Points) and Direction Normal to Wall (Solid Points), Non-Dimensionalized on Inner Variables..... 44
24	Profiles of Turbulence Intensity in Streamwise Direction and Direction Normal to Wall, Non-Dimensionalized on Inner Variables..... 45
25	Peak Value of $u$ Turbulence Intensity in Two-Dimensional Channel Flows..... 46
26	Streamwise Turbulence Intensity Profiles Non-Dimensionalized With Respect to Inner Variables..... 47

## LIST OF ILLUSTRATIONS (Cont'd)

Figure	Page
27 Reynolds Stress Profiles in Wall Units vs Distance From Wall Normalized With Channel Half-Width (Compiled by Wei and Willmarth, 1989) .....	48
28 Reynolds Stress Profiles in Wall Units vs Distance From Wall Normalized With Channel Half-Width (Channel-Flow Data of Wei and Willmarth, 1989).....	50
29 Reynolds Stress Profiles Non-Dimensionalized on Inner Variables (Channel-Flow Data of Wei and Wilmarth, 1989).....	50
30 Reynolds Stress Profiles Non-Dimensionalized on Inner Variables (Channel-Flow Data of Harder and Tiederman, 1991) .....	52
31 Turbulence Kinetic Energy Production Profiles.....	52
32 Location of Peak Reynolds Stress as Function of Reynolds Number .....	53
33 Power Spectra of Streamwise Velocity Fluctuations at $y^+ = 15$ .....	57
34 Power Spectra of Normal Velocity Fluctuations at $y^+ = 15$ .....	58
35 Power Spectra of Reynolds Stress Fluctuations at $y^+ = 15$ .....	58
36 Power Spectra of Streamwise Velocity Fluctuations at $y^+ = 125$ .....	60
37 Power Spectra of Normal Velocity Fluctuations at $y^+ = 125$ .....	60
38 Power Spectra of Reynolds Stress Fluctuations at $y^+ = 125$ .....	61
39 Normalized Power Spectra of Streamwise Velocity Fluctuations .....	61
40 Profiles of Skewness Factor of Streamwise Velocity Fluctuations at Four Reynolds Numbers.....	63
41 Skewness of Velocity Derivative $du/dt$ in Inner Region of Pipe Flow .....	65
42 Distribution of Skewness Factor of Velocity Fluctuations Normal to Wall .....	65
43 Distribution of Skewness Factor of Velocity Fluctuations Normal to Wall (Near-Wall Region Results From Four Different Facilities).....	67
44 Profiles of Flatness Factor of Streamwise Velocity Fluctuations at Four Reynolds Numbers.....	67
45 Side View of Low Reynolds Number Turbulent Boundary Layer; $Re_\theta = 725$ .....	73
46 Top View of Low Reynolds Number Turbulent Boundary Layer; $Re_\theta = 742$ .....	73
47 Top View of Low Reynolds Number Turbulent Boundary Layer; $Re_\theta = 725$ .....	74
48 Sketch of Large Eddy Structures as Collection of Smaller-Scale Hairpin Vortices.....	78
49 Hairpin Structures in Smoke-Filled Turbulent Boundary Layer at Three Reynolds Numbers .....	80
50 Mean Bursting Frequency vs Reynolds Number .....	83
51 Comparison of Shear Correlation Coefficient in High and Low Reynolds Number Boundary Layers .....	85

## LIST OF ILLUSTRATIONS (Cont'd)

Figure	Page
52	Comparison of Intermittency Factor in High and Low Reynolds Number Boundary Layers.....86
53	Two-Dimensional Spectra $\mathcal{P}(k_z^+, \omega^+)$ for $Re_a = 10,000$ ; $y^+ = 1.56$ .....87
54	Two-Dimensional Spectra $\mathcal{P}(k_z^+, \omega^+)$ for $Re_a = 100,000$ ; $y^+ = 13.9$ .....87
55	Reynolds Number Dependence of Ratio of Outer to Inner Scale .....89
56	Reynolds Number Variation of Maximum Mixing Length, Typical Eddy, and Taylor's Micro-Scale Lengths .....90
57	Smoke-Filled Turbulent Boundary Layer Illuminated Using Laser Sheet Inclined Upstream at $45^\circ$ to Flow Direction.....92
58	Reynolds Number Effects on Viscous Drag Reduction Due to OLD for $2500 \leq Re_\theta \leq 18,000$ .....99
59	Large Area Drag Balance Measurements Showing Reynolds Number Effects on Viscous Drag Reduction Due to Outer Layer Devices for $1300 \leq Re_\theta \leq 3600$ .....100
60	Approach to Equilibrium After Tripping Device at Moderately High Reynolds Numbers.....101
61	Ranges of Momentum Thickness Reynolds Number for Different Facilities and Field Conditions.....103
62	Vortical Structures in Simulated Turbulent Boundary Layers.....107
63	Reynolds Number Dependence of Fractional Increase in Skin Friction Caused by Freestream Turbulence.....111

## LIST OF TABLES

Tables	Page
1	Wall-Pressure Fluctuation Statistics.....69

## LIST OF SYMBOLS

$a$	Pipe radius or channel half-width
$c_x$	Longitudinal phase velocity
$C_f$	Local skin-friction coefficient $= \tau_w / \left( \frac{1}{2} \rho U^2 \right)$
$C_{f_0}$	Skin-friction value for negligible freestream turbulence
$C_x, C_y, C_z$	Typical eddy lengths along $x$ , $y$ , and $z$
$d$	Vortex diameter
$D_{KE}$	Dissipation of turbulence kinetic energy
$DR$	Drag reduction with respect to reference (unaltered) case
$E$	Energy
$f$	Bursting frequency, Hz
$f_s$	Freestream turbulence parameter $= \left\{ [u' / U_o] / [(L_o / \delta) + 2] \right\}$
$f\beta$	Freestream turbulence parameter modified by a damping factor $= f_s B^n$
$F_u$	Flatness factor (or kurtosis) of streamwise velocity fluctuations $= (\overline{u^4}) / (u_{rms}^4)$
$F_v$	Flatness factor of normal velocity fluctuations
$G$	Clauser's velocity-profile shape parameter $= \int_0^\delta \left( \frac{U_o - U}{U_r} \right)^2 dy / \int_0^\delta \left( \frac{U_o - U}{U_r} \right) dy$
$h$	Riblet height
$H$	Shape factor $= \delta^* / \theta$
$k$	Wavenumber
$k_z$	Spanwise wavenumber

$\ell$	Mixing length or hot-wire length
$L$	Size of largest eddies in the flow
$L_o$	Longitudinal dissipation length-scale in the freestream
$M_\infty$	Freestream mach number
$P_w$	Fluctuating wall pressure
$P_{K.E.}$	Production of turbulence kinetic energy
$\mathcal{P}$	Two-dimensional spectrum = $\mathcal{P}(k_z^+, \omega^+)$
$q^2$	Twice the turbulence kinetic energy
$R_{uv}$	Shear correlation coefficient = $-\overline{uv} / (u_{rms} v_{rms})$
$Re_a$	Channel or pipe Reynolds number based on centerline velocity and channel half-width or radius
$Re_c$	Critical value of $Re$ above which the turbulence structure changes
$Re_L$	Reynolds number based on plate length and freestream velocity
$Re_t$	Turbulence Reynolds number = $uT/\nu$
$Re_x$	Surface-length Reynolds number = $U_\infty x / \nu$
$Re_\theta$	Momentum-thickness Reynolds number = $U_\infty \theta / \nu$
$Re^*$	Ratio of outer-length scale ( $\delta^+$ or $a^+$ to inner-length scale ( $\nu / U_\tau$ ) ( $\delta^*$ or $a^*$ is also used to notate same quantity)
$Re_\Gamma$	Vortex Reynolds number $\Gamma / \nu$
$s$	Spanwise spacing of V-groove riblets
$S_u$	Skewness factor of streamwise velocity fluctuations = $(\overline{u^3}) / (u_{rms})^3$
$S_v$	Skewness factor of normal velocity fluctuations
$S_{(du/dt)}$	Skewness factor of velocity derivative with respect to time
$t$	Time

$T$	Bursting period
$T_u$	Freestream turbulence intensity = $u_{rms} / U_\infty$
$u, v, w$	Components of velocity fluctuations along $x, y$ , and $z$ , respectively
$u'$	Root-mean-square value of the streamwise velocity fluctuations
$-\overline{uv}$	Time-mean (kinematic) Reynolds shear stress
$U$	Mean velocity within the boundary layer in the $x$ -direction
$U_\ell$	Centerline velocity in pipe or channel
$U_\tau$	Local friction velocity = $(\tau_w / \rho)^{1/2}$
$U_o$	Velocity at edge of shear layer
$U_\infty$	Freestream velocity in boundary layer
$Wy/\delta$	Universal wake function
$x, y, z$	Longitudinal, surface normal, or spanwise coordinates, respectively
$y_p$	Location of peak Reynolds stress
$\beta$	Damping factor = $\left[1 + 3e^{-(Re_\theta/425)}\right] \left[1 + 3e^{-(Re_\theta/425)}\right]$
$\gamma$	Intermittency factor
$\gamma(x)$	Circulation per unit length of a vortex sheet
$\Gamma$	Total circulation in a vortex tube
$\delta$	Boundary-layer thickness
$\delta^*$	Displacement thickness
$\Delta U^+$	Strength of the wake component in wall units
$\Delta C_f$	Change in skin friction due to freestream turbulence
$\theta$	Momentum thickness
$\eta$	Appropriately normalized transverse distance in a wake flow

$\kappa$	Von Kármán's constant
$\lambda_x, \lambda_y, \lambda_z$	Taylor's micro-scales or wavelengths along $x, y$ , or $z, x, y$ , or $z$ , respectively
$\mu$	Coefficient of dynamic viscosity
$\nu$	Kinematic viscosity $\mu / \rho$
$\rho$	Density
$\tau_w$	Wall-shear stress = $\mu(\partial U / \partial y)_w$
$\Phi$	Power spectrum of turbulent velocity or Reynolds stress fluctuations
$\omega$	Radian frequency = $2\pi f$
$\omega_x, \omega_y, \omega_z$	Components of vorticity fluctuations along $x, y$ , and $z$
$\Omega_x, \Omega_y, \Omega_z$	Mean vorticity components along $x, y$ , and $z$

### Subscripts:

max	Maximum value
ref	Reference (unaltered) case
RMS	Root-mean-square
w	Variable computed at wall
$\tau$	Value based on the shear stress at the wall
$\infty$	Freestream condition

### Superscripts:

+	Non-dimensionalized with wall-layer scales, viz., $U_\tau$ for velocity, $\nu / U_\tau$ for length, and $\nu / U_\tau^2$ for time
'	Root-mean-square (RMS) value

# REYNOLDS NUMBER EFFECTS IN WALL-BOUNDED TURBULENT FLOWS

## 1. INTRODUCTION

### 1.1 FIELD VERSUS LABORATORY FLOWS

To overstate the technological importance of the turbulent wall-bounded flow would be done so with great difficulty. A vast amount of energy is spent in overcoming the turbulence skin-friction drag in pipelines and on air, water, and land vehicles. For blunt bodies, e.g., trucks and trains, the pressure drag resulting from boundary-layer separation can be several orders of magnitude higher than the skin friction, wasting even more energy. Heat transfer and mixing processes crucially depend on the turbulent transport for their efficient attainment. The Reynolds numbers encountered in many practical situations are typically orders of magnitude higher than those studied computationally or even experimentally. Yet, our knowledge of high Reynolds number flows is very limited and a complete understanding is yet to emerge. The existing knowledge base, accumulated mostly through physical as well as numerical experiments, is clearly skewed toward low Reynolds numbers. For many practical applications, the key question is then what are the Reynolds number effects on the mean and statistical turbulence quantities and on the organized motions of turbulence? One always hopes that the flow characteristics become invariant at sufficiently high Reynolds number. That merely shifts the question to what is high enough?

Consider the simplest possible turbulent wall-bounded flow, that over a smooth flat-plate at zero incidence to a uniform, incompressible flow or its close cousin the two-dimensional channel flow. Leaving aside for a moment the fact that such idealized flow does not exist in practice, where three-dimensional, roughness, pressure-gradient, curvature, wall compliance, heat transfer, compressibility, stratification, and other effects might be present individually or collectively, the canonical problem itself is not well understood. Most disturbing from a practical point of view are the unknown effects of Reynolds number on the mean flow, the higher-order statistical quantities, and the flow structure. The primary objective of this report is to review the state-of-the-art of Reynolds number effects in wall-bounded shear-flow turbulence, with particular emphasis on the canonical boundary layer and channel-flow problems.

### 1.2 REYNOLDS NUMBER

Reynolds-number effects are intimately related to the concept of dynamic similarity. In a given flow geometry, if  $L$  and  $U$  are the length and velocity scales, respectively, the non-dimensional equation of motion for an effectively incompressible fluid is given by

$$\frac{\partial \mathbf{u}}{\partial t} + (\mathbf{u} \cdot \nabla) \mathbf{u} = -\nabla \mathcal{P} + \frac{1}{Re} \nabla^2 \mathbf{u}, \quad (1)$$

where  $Re = UL/\nu$ ,  $P$  is pressure and  $\nu$  is kinematic viscosity. This seemingly superficial non-dimensionalization reveals two important properties. The first is the concept of dynamic similarity. No matter how  $L$ ,  $U$ , and  $\nu$  are varied, as long as  $Re$  is the same in two geometrically similar flows, they have the same solution. Small-scale model testing of large-scale real-life flows is based on this property. Secondly, for a given geometry and boundary condition, the effect of changing  $L$ ,  $U$ , or  $\nu$ , or any combination of them, can be described uniquely by the change of  $Re$  alone. Although, the importance of  $Re$  was recognized earlier by Stokes, it has come to be termed Reynolds number in recognition of Osborne Reynolds' telling demonstration of its effect on the onset of turbulence (Reynolds, 1883; 1895). Even today, the laminar-to-turbulence transition is one of the most dramatic Reynolds-number effects and its rational computation continues to be a research challenge.

Equation (1) shows that  $Re$  represents the relative importance of viscous and inviscid forces. Because three forces, viz., inertia, pressure, and viscous, are in equilibrium, the balance can be described by the ratio of any two. It is customary to characterize the flow by the ratio of inertia to viscous forces.

In this report, only turbulent flows are considered because they are widely prevalent. The understanding of the effects of Reynolds number relies on our understanding of viscous forces. For a wall-bounded flow, this is true no matter how high the Reynolds number is. Experience shows that there is no practical Reynolds number where the no-slip boundary condition, which owes its origin to viscous effects, switches off. Because the net viscous force on an element of incompressible fluid is determined by the local gradients of vorticity, the understanding of the vorticity distribution is the key to determining Reynolds number effects. Vorticity can be produced only at a solid boundary and cannot be created or destroyed in the interior of a homogeneous fluid under normal conditions.

The qualitative effects of Reynolds number on the scales of turbulence are demonstrated in the two velocity-fluctuations spectra depicted in figure 1. The large scale is only weakly dependent on Reynolds number (Townsend, 1976). However, as Reynolds number increases, the small scales become physically smaller (larger wavenumbers), and the diversity of intermediate scales between the large and small increases.

In terms of organized motions in a turbulent boundary layer, the effect of Reynolds number on the omnipresent elongated vortex loops (horseshoes) is as sketched in figure 2, from Head and Bandyopadhyay (1981). With increasing Reynolds number, the aspect ratio of the constituent hairpin vortices increases while the vortices become skinnier. The related result, viz., the relative shrinking of the inner layer where viscous effects are stronger is shown in the mean-velocity profiles depicted in figure 3. Significantly, the two flows have approximately the same boundary layer thickness (13 cm). While the inner layer occupies most of the boundary layer for the low Reynolds number flow, it shrinks to a very small proportion at high Reynolds number.

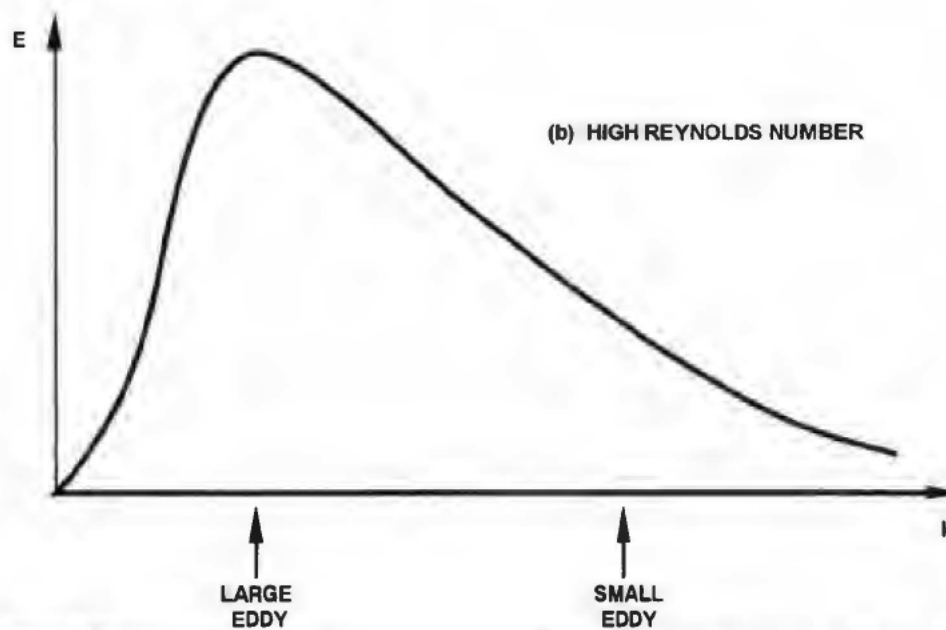
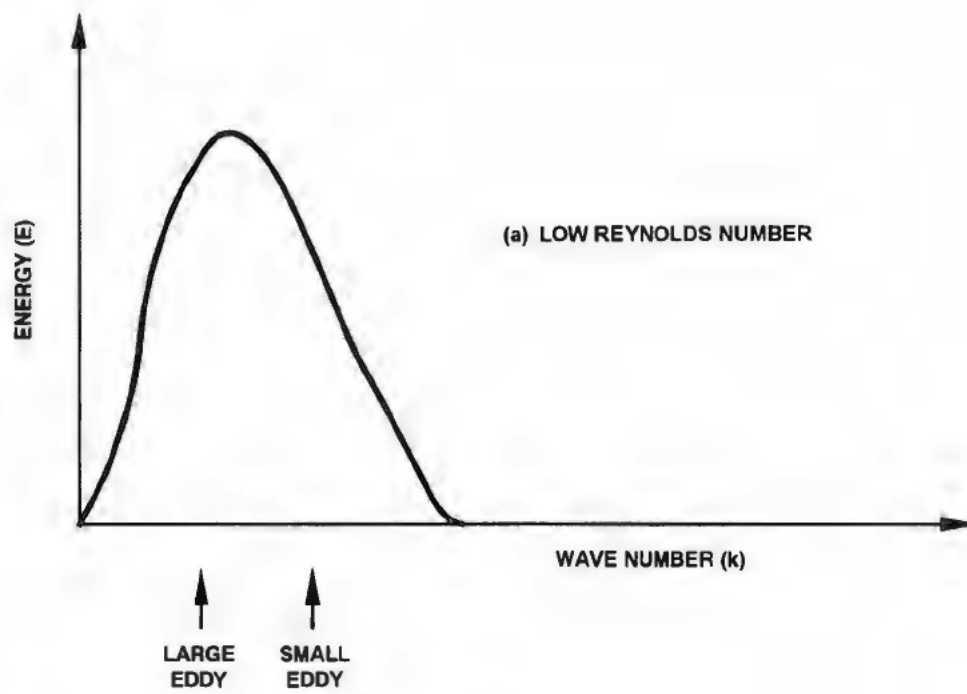


*Figure 1. Energy Spectra at Low and High Reynolds Numbers*

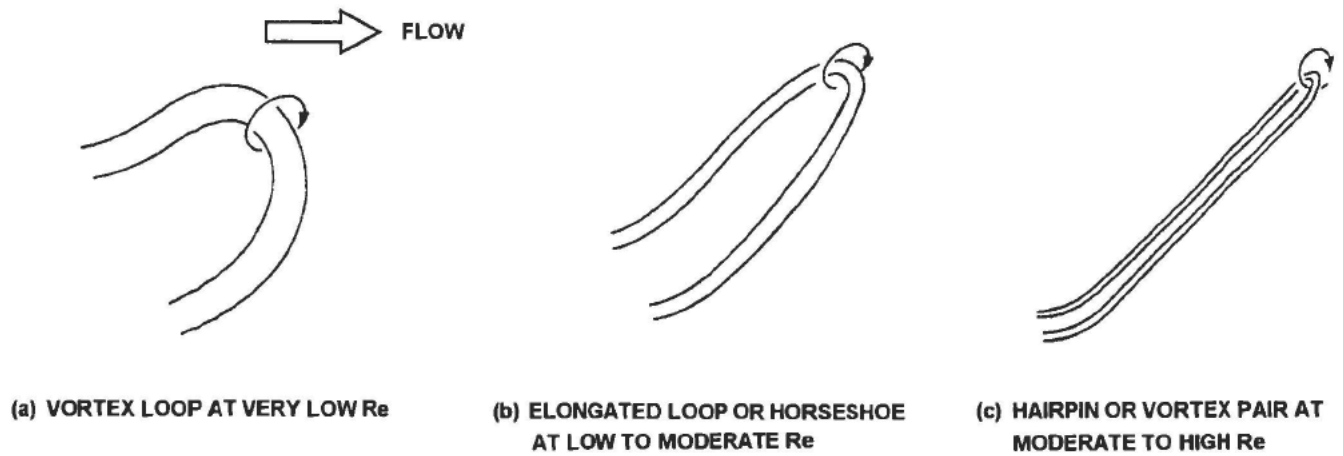


**Figure 2. Qualitative Effect of Reynolds Number on Features Composing Outer Region of a Turbulent Boundary Layer (Head and Bandyopadhyay, 1981)**

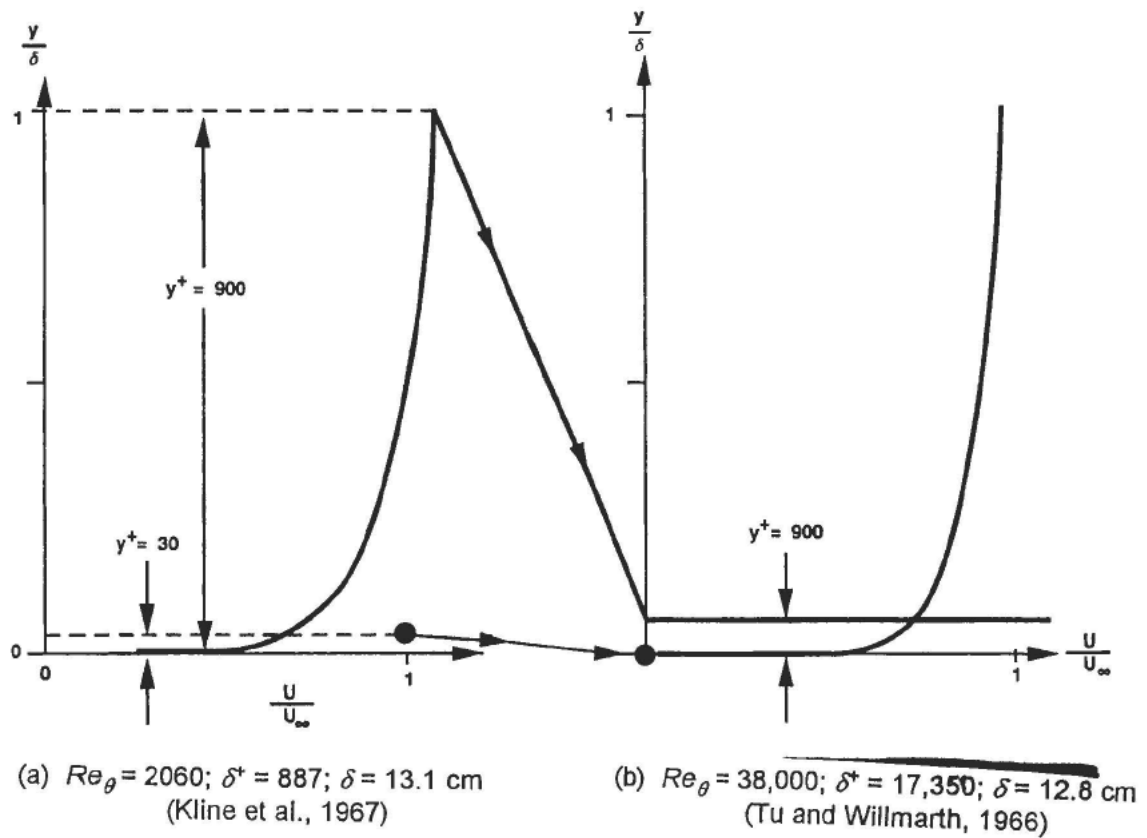


**Figure 3. Mean Velocity Profiles at Low and High Reynolds Numbers**

### 1.3 OUTLINE OF PRESENT REVIEW

In this report, the effects of Reynolds number on the mean flow, coherent structures and statistics of turbulent boundary layers and channel flows are reviewed. Published data are re-examined in light of the following questions:

1. Does the boundary-layer turbulence structure change after the well-known Reynolds number limit, viz., when  $Re_\theta > 6 \times 10^3$ ?
2. Is it possible to disturb a high Reynolds number, flat-plate turbulent boundary layer near the wall such that the recovery length is  $O(100\delta)$ ?
3. How close is the numerically simulated low-Reynolds number, flat-plate turbulence structure to that observed experimentally? The turbulence structure appears to change continuously with Reynolds number virtually throughout the boundary layer and sometimes in unexpected manners at high Reynolds numbers (Bandyopadhyay, 1991).

It is relevant to acknowledge two recent doctoral theses by Kailasnath (1993) and Smith (1994), which came to our attention after the bulk of this report was written. Both dissertations address somewhat similar questions to those raised herein. Kailasnath (1993) amplifies on the notion of scale similarity using a statistical approach for obtaining valuable information on the structure of the instantaneous momentum flux within laboratory as well as atmospheric turbulent boundary layers. Smith (1994) emphasizes Reynolds number effects on the structural aspects of boundary layers.

This report is organized into 11 sections. Following the present introductory remarks, the contemporary relevance of the general topic of Reynolds number effects and of the specific problems of flow control and post-transition memory is given in section 2. The different regions of the boundary layer are reviewed in the following section. Section 4 highlights the qualitative differences between wall-bounded layers and free-shear flows. Reynolds number effects on the mean flow and on higher-order statistics are given in sections 5 and 6, respectively. Outer and inner coherent structures and their interactions are recalled in section 7. Brief remarks are made on flow control, numerical simulations, and non-canonical boundary layers in the following three sections; concluding remarks are given in section 11.

## 2. CONTEMPORARY RELEVANCE

### 2.1 PRIMARY ISSUES

Most studies on the structure of flat-plate turbulent boundary layers are being carried out at rather low Reynolds numbers. The few existing high Reynolds number wind or water tunnels are expensive to build and operate and are heavily scheduled with mostly developmental work. Full computational simulation of high Reynolds number turbulent flows is beyond the reach of current computers. Because many practical flows have very high Reynolds numbers, the question is how relevant are the low Reynolds number studies to practical situations? For this reason alone, the issue of Reynolds number effects is important.

Because the Reynolds number scaling laws are usually given by the wall-layer, outer-layer, or any mixed-layer length, time, and velocity scales that govern the variation of a mean or turbulence quantity with Reynolds number, the Reynolds number effects will be examined in terms of the applicability of these scaling laws.

The subject is too broad and here it is discussed chiefly in light of four questions. One of the earliest studies of the Reynolds number effect in turbulent boundary layers was due to Coles (1962). When measurements of mean-velocity profiles were expressed in inner-layer form based on directly measured local friction values, a logarithmic region was found to exist even at an  $Re_\theta$  of  $50 \times 10^3$ , where  $Re_\theta$  is the Reynolds number based on momentum thickness and freestream velocity. The wall-layer variables appear to describe the mean flow in the inner layer universally in flat plates, pipes, and channels at all Reynolds numbers (see section 5.5).

In a boundary layer, the behavior of the outer layer, when expressed in terms of wall-layer variables by the strength of the wake component  $\Delta U^+$ , which is the maximum deviation of the mean-velocity profile from the log law, appeared to reach an asymptotic value for  $Re_\theta > 6 \times 10^3$ . Above this limit, the inner- and outer-layer mean flows are expected to reach an asymptotic state, which the turbulence quantities are also hypothesized to follow. This is, however, not the case because the wake component starts decreasing, albeit slowly, at about  $Re_\theta > 15 \times 10^3$ . This decrease raises the question, does the mean flow ever achieve true self-preservation?

The situation is murkier for higher-order statistics. Measurements in pipes (Morrison et al., 1971), channels (Wei and Willmarth, 1989), and boundary layers (Andreopoulos et al., 1984; Erm et al., 1985) are beginning to show that turbulence quantities do not scale with wall-layer variables even in the inner layer. Therefore, the question arises: Can the mean-flow scales be applied to turbulence?

Furthermore, the outer-layer-device drag reduction experiments of Anders (1990a) show that above this Reynolds number limit, the maximum skin-friction reduction and the recovery length (the latter with some exception) do not remain constant but reduce with increasing Reynolds number. The loss of performance at higher Reynolds numbers is puzzling and Anders attributed it

to a significant change in the turbulence structure. In this background, the question "Does the turbulence structure change when  $Re_\theta > 6 \times 10^3$ ?" is discussed.

Consider another puzzling high Reynolds number behavior. In the 1950s, Clauser had experimentally shown that in a turbulent boundary layer at a given Reynolds number, disturbances survive much longer in the outer layer ( $y/\delta > 0.2$ ) than in the inner layer. This was demonstrated by placing a circular rod in the outer and inner layers of a fully developed wall layer. Incidentally, some consider Clauser's demonstration as the predecessor of the modern-day drag reduction experiments employing modifications to the outer layer (Bushnell and Hefner, 1990). Note that Clauser (1956) compared the response of the inner and outer layers at a low Reynolds number and did not consider any Reynolds number effect. In viscous drag reduction techniques where a device drag penalty is involved, as with the use of an outer layer device, a recovery length of  $O(100\delta)$  is desirable to achieve a net gain. To date, with outer-layer devices, such recovery lengths have been achieved only at low Reynolds numbers as mentioned earlier. One normally expects the recovery length to be far less if the disturbances are applied near the wall, and the length to reduce even more as  $Re_\theta$  is increased. However, published data are re-examined here, which shows that, in fact, at higher Reynolds numbers, an opposite trend sometimes takes place. This unexpected result indicates a serious difficulty in the extrapolation of low Reynolds number results. The third question is concerned with this aspect of the Reynolds number effect.

Spalart (1986) has numerically simulated a smooth flat-plate turbulent boundary layer at  $Re_\theta = 300, 670$ , and  $1410$ . Robinson et al. (1989) have analyzed the database at  $Re_\theta = 670$  and identified the organized structures. In the last part of the paper, the numerically obtained low Reynolds number structures are compared with experimental observations.

## 2.2 TURBULENCE MODELING

Full computational simulation of high Reynolds number turbulent flows is beyond the reach of current capabilities. Understanding of turbulence and modeling will continue to play vital roles in the computation of high Reynolds number practical flows using the Reynolds-averaged Navier-Stokes equations. The mean-flow review by Coles (1962) has had a great impact on turbulence modeling. However, that article did not cover any turbulence quantities. Additionally, as will be discussed in section 5, the effects of Reynolds number on even the mean flow quantities at truly high Reynolds numbers (momentum thickness-based Reynolds number  $Re_\theta \geq 1.5 \times 10^4$ ) are still, unfortunately, not understood and are even misunderstood and erroneously simplified.

After the work of Coles, interest in organized motion or the so-called coherent structures, had increased. The coherent structures of turbulent boundary layers, particularly for low  $Re$  flows, have been reviewed several times (Willmarth, 1975a; 1975b; Willmarth and Bogar, 1977; Blackwelder, 1978; Cantwell, 1981; Hussain, 1983; Fiedler, 1986; Robinson, 1991). In these reviews, the kinematic features of coherent structures are discussed, but the Reynolds number dependence is largely not covered. Furthermore, although these developments have greatly improved our understanding of the turbulence production mechanism, their impact on turbulence modeling and flow control have been minimal. The structural modeling works of Perry and

Chong (1982), Nagano and Tagawa (1990), and Bandyopadhyay and Balasubramanian (1993, 1994) are exceptions and hold some promise.

The direct numerical simulation (DNS) of turbulent boundary layers have so far been carried out up to an  $Re_\theta$  of 1410 (Spalart, 1986). Because the computational resource required varies approximately as the cube of the Reynolds number, it would not be possible to simulate very high Reynolds number turbulent shear flows any time soon (Karniadakis and Orszag, 1993). This has created a resurgence of interest in turbulence modeling particularly for high Reynolds number wall-bounded flows. Thus, there is a need to review the state-of-the-art of Reynolds number effects on the mean flow, turbulence statistics, and coherent structures so that the flow physics input to any new turbulence model or flow control device is up-to-date. To be useful to modeling or to flow management, seven requirements of this report can be specified:

1. Evaluate state-of-the-art aspects of the mean flow at truly high Reynolds numbers left open by Coles (1962).
2. Examine experimental and numerical simulation data to determine the Reynolds number effects on conventional statistical turbulence quantities, particularly those that appear in the various forms of the Reynolds-averaged Navier-Stokes equations.
3. Determine if the scaling laws of the mean flow apply to the higher-order turbulence statistics as commonly assumed.
4. Investigate the issues of post-transition memory and probe resolution of existing turbulence measurements, including such statistical quantities as root-mean-square (RMS) and spectrum.
5. Establish state-of-the-art Reynolds number effects on the coherent structures or organized motions, while keeping an eye on the need of structural modeling.
6. Attempt to bridge the gap between the coherent structure flow physics and Reynolds-averaged quantities and thereby make the former useful to a practicing engineer.
7. Finally, it is more useful to review the mean flow, the turbulence quantities, and the organized motions in a unified manner than to treat them separately. The advantage is that it will then be possible to examine if the mean-flow scaling laws can indeed be extrapolated to turbulence.

## **2.3 FLOW CONTROL AND POST-TRANSITION MEMORY**

Apart from that in turbulence modeling, the knowledge of the Reynolds number effects is useful to flow control because experimental investigations at low Reynolds numbers, i.e., lower speeds and smaller length scales, are less expensive. Most flow-control devices are, therefore, developed and tested at rather low speeds. Extrapolation to field conditions is not always straightforward though, and it often comes to grief. The relevance of Reynolds number

effects to flow control is particularly telling in case of full numerical simulation because it is currently limited to Reynolds numbers that are not that far from transitional values.

One objective of this review article is to highlight the misunderstood and ill-understood aspects of the Reynolds number effects. This should help guide flow-control, turbulence modeling research, and data gathering for code validation in the right direction. Two examples would serve to make the point.

1. In viscous drag-reduction techniques where a device drag penalty is involved, as with outer layer devices (OLD), a recovery length  $\sim 100\delta$  is desirable to achieve a net gain. As indicated in section 2.1, this does happen at low  $Re_\theta (< 6 \times 10^3)$  (Anders, 1990a). However, when Anders examined his outer layer devices at higher Reynolds numbers, to his surprise, the drag reduction performance was reduced and the device was no longer a viable candidate for viscous drag reduction. For both low  $Re_\theta (< 6 \times 10^3)$  and high  $Re_\theta (> 6 \times 10^3)$ , the effectiveness of OLD diminishes with the increase of Reynolds number (Bandyopadhyay, 1986a; Anders, 1990a).

2. The continued drop in the drag reduction comes as a surprise because the mean flow analysis of Coles (1962) indicates an asymptotic state of the outer layer to have been reached above  $Re_\theta > 6 \times 10^3$ . Anders attributed the irreproducibility of the low Reynolds number behavior at higher values to a significant change in the turbulence structure at higher  $Re_\theta$ . As discussed by Head and Bandyopadhyay (1981), a continuous change in the ratio of the outer to the inner layer,  $U_\tau \delta / \nu$ , is observed even beyond  $Re_\theta = 6 \times 10^3$ . This change also suggests that  $U_\tau \delta / \nu$  may be more important to turbulence production than the wake component  $\Delta U^+$ .

The above example shows that the 1962 review work of Coles is not always providing sufficient guidance on the Reynolds number effects to the research application engineer. The reason seems to be that our knowledge of the Reynolds number effects on the mean flow is not enough for many applications (and modeling), and that there is also a need to know the *Reynolds number effects on the turbulence*. Considerable amounts of statistical mean and turbulent flow data have come out of the experimental and numerical simulations since 1962, and it would be useful to review the state-of-the-art.

That, being armed with the knowledge of Reynolds number effects on the mean turbulent flow alone does not allow one to address all practical problems, can be demonstrated in the following post-transition unexpected result. Klebanoff and Diehl (1952) have made measurements on artificially-thickened boundary layers at zero pressure gradients. The first 60 cm of their splitter plate was covered with No. 16 floor sanding paper. The measurements were carried out over a length of 3.2 m at free-stream velocities of 11, 17, and 33 m/s, giving three ranges of Reynolds numbers the maximum  $Re_\theta$  being  $1.49 \times 10^4$ . The value of  $Re_\theta$  at the end of the sand roughness (at  $x = 60$  cm) was  $2.64 \times 10^3$ ,  $4.05 \times 10^3$ , and  $7.99 \times 10^3$  at the three respective speeds. One normally expects the recovery response of the turbulent boundary layer from the same wall disturbances to be the shortest (in  $x$ ) at the highest Reynolds number. However, in contrary, Klebanoff and Diehl's measurements showed that the return to the "equilibrium" state is slowed down as the reference Reynolds number is increased and not decreased. This raises the question, are the near-wall transition-trip disturbances surviving even

beyond an  $x / \delta$  of 100 at such high Reynolds numbers as  $1.5 \times 10^4$ ? This question is clearly important to model testing and code validation data, where roughness is used to trip and thicken the boundary layer to simulate high Reynolds numbers or flight conditions. Thus, there is also a need to review available experimental data containing the Reynolds number dependence of the distance up to which transition memory survives.

### 3. FLOW REGIMES

An inspection of the distribution of viscous and turbulence shear stresses in a typical wall-bounded flow demonstrates the presence of three distinct regions. Figure 4, adapted by Sreenivasan (1989) from the smooth pipe-flow data of Nikuradse (1932) and Laufer (1954), shows such distribution in wall units (friction velocity,  $U_\tau = (\tau_w / \rho)^{1/2}$ , used as velocity scale, and the ratio of the kinematic viscosity to friction velocity used as length scale).

Pipe- (or channel-) flow data are preferable to flat-plate boundary layer experiments because the Reynolds stress, a rather difficult quantity to measure accurately, can be computed exactly for fully developed channel flows from the relatively simple measurements of mean velocity profile and pressure gradient (section 6.2). The semi-log plot in figure 4 enhances the importance of the thin near-wall region relative to the rest of the shear layer.

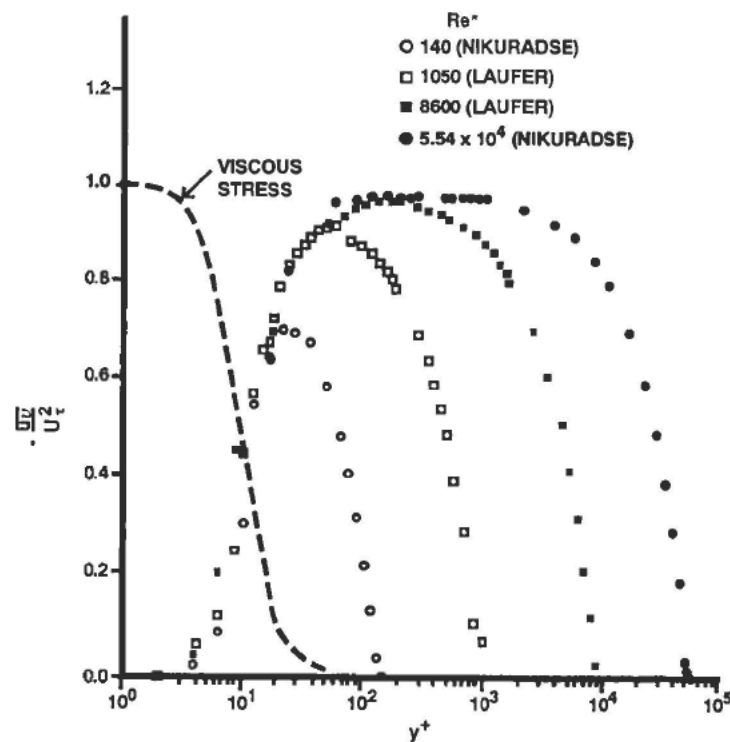


*Figure 4. Distribution of Viscous and Turbulence Shear Stresses in Wall-Bounded Flows (Sreenivasan, 1989)*

The broken line in the figure is the time-averaged viscous stress distribution computed by differentiating the mean-velocity profile. Note that this laminar flow concept of shear may not be relevant to the time-dependent turbulent flow because turbulence models based on the mean velocity gradients have not been widely successful (e.g., Bradshaw et al., 1967). Nevertheless, it is clear from the figure that the mean viscous stress,  $\mu(\partial U / \partial y)$ , is important only near the wall. This wall layer is followed by a region of approximately constant Reynolds stress. Finally, an outer layer (called core region in internal flows) is characterized by a diminishing turbulence shear stress, reaching zero at the centerline of the pipe. Unlike the second and third regimes, the extent of the first region does not depend on Reynolds number. Both the viscous region and the constant Reynolds stress region are similar in all wall-bounded flows. In contrast, the outer layer is different in internal flows and boundary layers. Profiles of the mean velocity and other turbulence statistics can be constructed from scaling considerations of the three distinct regimes, as will be seen in the following three subsections.

Note that the Reynolds number used as a parameter in figure 4 is defined as  $Re^* = U_\tau a / \nu$ ; that is the channel half-width (or boundary-layer thickness) expressed in wall units  $a^+$  (or  $\delta^+$ ). Although numerically  $Re^*$  and  $\delta^+$  are the same, their difference in significance and usage should be clarified. The variable  $\delta^+$  denotes the ratio of the outer- to the inner-layer thickness and represents the degree of shrinking of the latter with respect to the former, which changes little with Reynolds number (see figure 3). It emphasizes the disparity of the two scales and the diversity of the intermediate and interacting scales at higher Reynolds numbers. As will be seen in section 7,  $\delta^+$  indicates the reduction of the hairpin vortex diameter and the increase in its aspect ratio as the Reynolds number increases (Head and Bandyopadhyay, 1981). The value of  $\delta^+$  in a typical laboratory experiment is  $O(1000)$ , while it approaches 100,000 in the boundary layer developing over the space shuttle (Bandyopadhyay, 1990). This variable is pertinent to the understanding of the mechanism of drag reduction by outer layer devices (Anders, 1990b). On the other hand,  $Re^*$  is a Reynolds number, also called a stability parameter by Black (1968). In Black's work and later in Sreenivasan's (1988),  $Re^*$  indicates a Reynolds number associated with the quasi-periodic instability and breakup process that is hypothesized to be responsible for the regeneration of turbulence in a wall-bounded flow (sections 4 and 7). Note that, for a smooth wall,  $Re^*$  increases monotonically with  $Re_\theta$  and never reaches an asymptote.

### 3.1 VISCOUS REGION

Viscosity appears to be important only up to  $y^+ = 30$ . The viscous region can be subdivided into two subregions: the viscous sublayer and the buffer layer. Very close to the wall,  $0 \leq y^+ \leq 5$ , the turbulence shear stress is nearly zero, which implies that the only relevant quantities are the kinematic viscosity  $\nu$  and friction velocity  $U_\tau$ .<sup>†</sup> In this viscous sublayer, several turbulence statistics can be asymptotically estimated from considerations of the no-slip condition and

---

<sup>†</sup> For *hydraulically rough* walls, i.e., where the average roughness height is greater than the viscous sublayer thickness, the relevant scaling parameters are the characteristic roughness height and friction velocity.

continuity and dynamical equations. Following Monin and Yaglom (1971) and using experimental data, Sreenivasan (1989) gives the following Taylor's series expressions in wall units for the mean streamwise velocity, the RMS of the three fluctuating velocity components, and the Reynolds stress, respectively:

$$U^+ = y^+ - 1 \times 10^{-4} y^{+4} + 1.6 \times 10^{-6} y^{+5} + \dots, \quad (2)$$

$$u'^+ = 0.3 y^+ + c_1 y^{+2} + \dots, \quad (3)$$

$$v'^+ = 0.008 y^{+2} + c_2 y^{+3} + \dots, \quad (4)$$

$$w'^+ = 0.07 y^+ + c_3 y^{+2} + \dots, \quad (5)$$

$$-\overline{uv}^+ = 4 \times 10^{-4} y^{+3} - 8 \times 10^{-6} y^{+4} + \dots \quad (6)$$

For  $y^+ < 5$ , the leading term of each of the above expansions suffices. With three terms, equation (2) for the mean velocity is valid up to  $y^+ = 20$ . Note that the *constants* in the above equations are not necessarily universal. As will be discussed in section 6, clearly discernible Reynolds number effects will be demonstrated for all higher-order statistical quantities, even in the near-wall region.

The buffer layer is where both the viscous stress and the turbulence shear stress are important and where the peak production and dissipation of turbulence kinetic energy occur (at about  $y^+ = 12$ , seemingly independent of the global Reynolds number). Here, the characteristic local Reynolds number of  $yU_\tau / \nu = 30$  is exceedingly low and turbulence cannot be maintained unless buffeted constantly by strong disturbances, presumably from the outer layer. This region merges with the constant Reynolds stress layer.

### 3.2 CONSTANT REYNOLDS STRESS REGION

In a pipe flow, this region, loosely interpreted to include all points within the -3 dB points of the peak Reynolds stress, extends from  $y^+ = 30$  to  $y/a = 0.2$ , where  $a$  is the pipe radius. Here, the distance from the wall  $y$  is much larger than the viscous length scale  $\nu/U_\tau$  but much smaller than the pipe radius (or the boundary layer thickness  $\delta$  for an external flow). Note that the upper extent of this region is a constant fraction of the boundary layer thickness but varies with Reynolds number when expressed in wall units.

In this region, viscous stresses are negligible and the momentum flux is accomplished almost entirely by turbulence. The only relevant length scale is  $y$  itself, and the square root of the nearly constant Reynolds stress  $(-\overline{uv}_{max})^{1/2}$  is the appropriate velocity scale. Therefore, the mean

velocity gradient can be expressed as:

$$\partial U / \partial y = \left( -\overline{uv}_{max} \right)^{1/2} / y. \quad (7)$$

The well-known logarithmic velocity profile follows directly from integrating equation (7) and using the velocity at the edge of the viscous sublayer as a boundary condition:

$$U^+ = (1/\kappa) \ln(y^+) + B, \quad (8)$$

where  $\kappa$  is the von Kármán constant. Both  $\kappa$  and B are presumably universal constants and are determined empirically for flat-plate boundary layers to be approximately 0.41 and 5.0, respectively. Slightly different values are used for the two constants in the case of pipe or channel flows, in which case, equation (8) holds almost up to the centerline of the channel. As the Reynolds number increases, the extent of the logarithmic region (in wall units) increases and the maximum Reynolds stress approaches the value of the viscous stress at the wall ( $-\overline{uv}_{max} / U_\tau^2 \rightarrow 1$ ).

Several other methods can be used to derive the logarithmic velocity profile. A mixing length, based on momentum transport, that simply varies linearly with distance from the wall,  $\ell = \kappa y$ , again yields equation (8). Millikan's (1939) asymptotic analysis recovers the log relation by assuming the existence of a region of overlap where both the inner and outer laws are simultaneously valid (see also the rarely cited albeit relevant article by Izakson, 1937). All models invariably rely on the presence of the constant-stress layer experimentally observed at high Reynolds number. Despite the copious evidence for the existence of a logarithmic region in the mean-velocity profile, the whole log-law scenario has been periodically questioned (see, for example, Barenblatt, 1979; 1993; Malkus, 1979; Long and Chen, 1981; George et al., 1992; Barenblatt and Prostokishin, 1993). (Further explanation can be found in section 5.1.)

The arguments used by Millikan (1939) to derive the logarithmic relation for the boundary layer are analogous to those employed to establish the universal equilibrium theory of turbulence, called the theory of local similarity by its originator Kolmogorov (1941a; 1941b; 1941c; 1962). For the boundary layer, an *inertial sublayer* exists at sufficiently large Reynolds numbers and the overall flow dynamics is independent of viscosity, which merely provides a momentum sink of prescribed strength at the wall. Similarly, an *inertial subrange* exists in the turbulence energy spectrum when the Reynolds number is large enough. There, the wavenumber is larger than that for the large eddies but smaller than the dissipative wavenumbers. The viscosity again provides the dissipative sink for kinetic energy at the small-scale end of the turbulence spectrum. The spectral shape in the inertial subrange is completely determined by the energy flux across the wavenumber domain.

Similar scaling arguments to those leading to equations (7) and (8) can be used in the constant-turbulent stress region to show that<sup>†</sup>

$$u' / U_\tau = \text{constant} = 2.0, \quad (9)$$

$$v' / U_\tau = \text{constant} = 1.0, \quad (10)$$

$$w' / U_\tau = \text{constant} = 1.4, \quad (11)$$

$$P_{k.E.} = D_{k.E.} = U_\tau^3 / \kappa y, \quad (12)$$

where  $P_{k.E.}$  and  $D_{k.E.}$  are the production and dissipation of turbulence kinetic energy, respectively. Additionally, a portion of the power spectrum for each of the three velocity components exhibits a -1 power law in this same region governed by a constant turbulence shear stress transmitted across its different fluid layers.

The total stress is approximately constant throughout the viscous layer and the constant Reynolds stress region. This is the so-called inner layer (see figure 5) and for a smooth wall the mean velocity profile given by the unique similarity law of the wall, first formulated by Prandtl (1925):

$$U^+ = f(y^+), \quad (13)$$

where  $f$  is a universal function presumably independent of Reynolds number and streamwise location. The inner law is the same for both internal and external flows.

### 3.3 OUTER LAYER

Beyond the constant-stress region, an outer layer is characterized by a diminishing turbulence shear stress. Note that some researchers include the constant Reynolds stress region as part of the outer region. This is perhaps an accurate inclusion because the part of the boundary layer where the logarithmic law is valid is, strictly speaking, the region of overlap between the inner and outer layers (see figure 5).

In internal flows, intermittency of turbulence and interaction with potential freestream are absent. There is, however, an interaction of turbulence from the opposite wall in case of a two-dimensional channel and this is even more complex in case of a circular pipe. Furthermore, fully-developed conditions for pipes and channels are defined as that all time-averaged flow quantities (except static pressure) are independent of  $x$ . Therefore, the core region of a pipe or channel flow differs from the outer layer of a growing boundary layer.

---

<sup>†</sup> The value of the constants in equations (9) through (12) are determined empirically from mostly low Reynolds number experiments. Section 6 will reveal that these constants depend in fact on the Reynolds number.

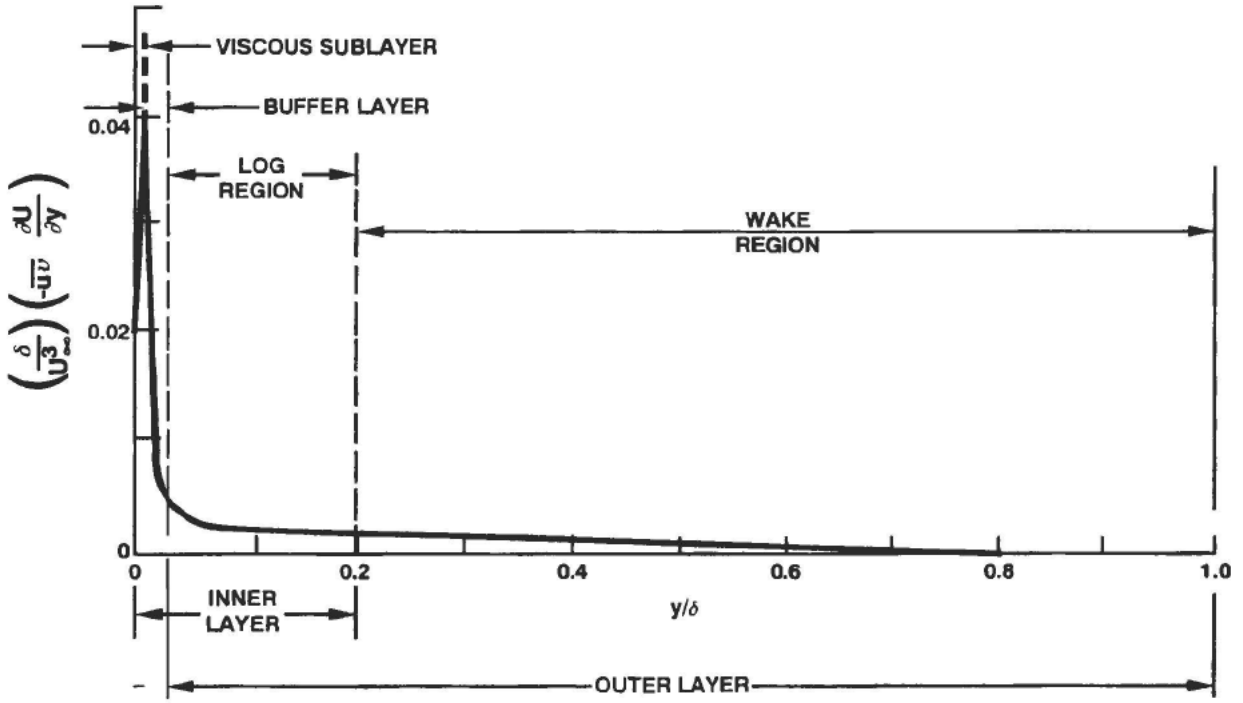


**Figure 5. Normalized Turbulence Kinetic Energy Production Rate as Function of Normal Distance From Wall (Data for Typical Laboratory Flat-Plate Boundary Layer) (Kline et al., 1967)**

The appropriate length scale in the core region is the pipe radius  $a$  (or the boundary-layer thickness  $\delta$  for an external flow). The mean-velocity profile is characterized by the velocity defect  $(U_o - U)$ , where  $U_o$  is the velocity at the edge of the shear layer (centerline velocity  $U_c$  for a pipe flow or freestream velocity  $U_\infty$  for a boundary layer). The velocity-defect (or, more appropriately, momentum-defect) law, formulated by von Kármán (1930), is given by a second universal function:

$$(U_o - U) / U_\tau = g(y / \delta). \quad (14)$$

This equation is valid even in the logarithmic region and is well confirmed experimentally.

For a turbulent boundary layer, Coles (1956) combined the defect law and the inner law to give the following empirical velocity profile valid throughout the entire wall-bounded shear layer:

$$U^+ = f(y^+) + (\Pi/\kappa)W(y/\delta), \quad (15)$$

where  $\kappa$  is the von Kármán constant and  $\Pi$  is a profile parameter that depends strongly on  $Re$  for small Reynolds numbers. Coles' idea is that a typical boundary layer flow can be viewed as a wake-like structure, which is constrained by a wall. Intermittency and entrainment give rise to the wake-like behavior of the outer part of the flow, which is sensitive to pressure gradient and freestream turbulence. The wall constraint is closely related to the magnitude of the surface shear stress, and is sensitive to the wall roughness and other surface conditions.

For equilibrium flows, the profile parameter  $\Pi$  is independent of streamwise location (Clauser, 1954). The universal wake function  $W(y/\delta)$  is the same for all two-dimensional boundary-layer flows. Its form is similar to that describing a wake flow or, more precisely, the mean-velocity profile at a point of separation or reattachment. For example, the wake function can be adequately represented by

$$W\left(\frac{y}{\delta}\right) = 2 \sin^2\left[\frac{\pi}{2} \frac{y}{\delta}\right]. \quad (16)$$

At the same Reynolds number, deviation of the actual mean-velocity distribution from the logarithmic profile in the core region of a pipe or channel flow is smaller than that in the outer region of a boundary layer. In fact, as mentioned in section 3.2, the logarithmic velocity profile, equation (8) with slightly modified constants  $\kappa$  and  $B$ , holds approximately up to the centerline of the pipe.

#### 4. COMPARISON TO OTHER SHEAR FLOWS

Before proceeding to investigate the specific effects of Reynolds number on the mean and turbulence quantities of wall-bounded flows, it is instructive to give a coarse comparison between such flows on the one hand and free-shear flows on the other. As it will be illustrated, the presence of the wall is of paramount importance to the issue at hand. No matter how large the Reynolds number is, viscosity must be important in a progressively shrinking region close to the wall and *Reynolds number dependence persists indefinitely*.

Wakes, jets, and mixing layers are profoundly different from channel and pipe flows and boundary layers. The absence of the wall in free-shear flows implies that at sufficiently high Reynolds numbers, the flow is nearly inviscid and, by implication, Reynolds number-independent. For wall-bounded flows, on the other hand, there is always a small, progressively shrinking region near the surface where viscosity must be important, no matter how large the Reynolds number is.

In boundary layers and channel flows, the overall behavior and gross structure of turbulence is always affected by viscosity near the wall, while the direct effect of viscosity gradually diminishes away from the surface. This implies that the velocity and length scales must be different near the wall and away from it. The disparity of scales for wall-bounded flows increases with Reynolds number and true self-preservation may never be achieved, unless the inner and outer scales are forced to be proportional at all Reynolds numbers. This latter scenario can be realized, for example, in the very special case of flow between two planes converging at a prescribed angle.

In wall-bounded flows, very large levels of turbulent fluctuations are maintained close to the wall despite the strong viscous as well as turbulent diffusion. As indicated in figure 5, at a typical laboratory Reynolds number of  $Re_\theta =$  on the order of  $10^3$  ( $O(10^3)$ ) more than about one-third of the total turbulence kinetic energy production (and dissipation) occurs in the 2 percent of the boundary-layer thickness adjacent to the wall. The fraction of this thickness decreases as the Reynolds number increases (figure 3). The near-wall region is directly affected by viscosity<sup>†</sup> and its importance to the maintenance of turbulence is clearly disproportional to its minute size.

The thinness of the viscous sublayer presents a great challenge to both physical and numerical experiments. Because this region is closest to the wall and is where drag acts, it is extremely important at all Reynolds numbers. Yet in contemporary direct numerical simulations, the viscous sublayer of 5 wall units is resolved only up to 1.4 wall units. In measurements, probe resolutions are even worse; other than in low-Reynolds number or oil-channel experiments, a probe length of  $\ell^+ < 7$  is indeed rare (Bandyopadhyay, 1991).

In free-shear layers, energy production peaks near the inflection points of the mean-velocity profile. Both production and dissipation are spread over the entire flow width as shown in figure 6 depicting the turbulence energy balance for a typical two-dimensional wake. Above a reasonably modest Reynolds number,  $O(10^3)$ , all turbulence quantities become invariant to additional changes in Reynolds number.

Despite these differences between boundary layers and free-shear flows, there are also some similarities. The outer region of a boundary layer is characterized by an intermittent rotational/irrotational flow, much the same as that observed in all free-shear flows. Moreover, the outer flow is more or less inviscid at sufficiently high Reynolds numbers, again being similar to jets, wakes, and mixing layers. The interaction between the outer, or *wake*, region of a turbulent boundary layer and the potential flow in the freestream is also similar to that in wakes and other free-shear flows. The above are observational similarities and differences between the wall-bounded turbulent flows and the free-shear layers. In the following, they are compared based on dynamic issues like the applicability of an inflectional inviscid breakdown mechanism, and it is shown that the subject is still wide open.

---

<sup>†</sup> Through action of viscous stresses for a smooth wall, or through the action of pressure drag resulting from the separated flow around discrete elements of sufficient size for rough walls.

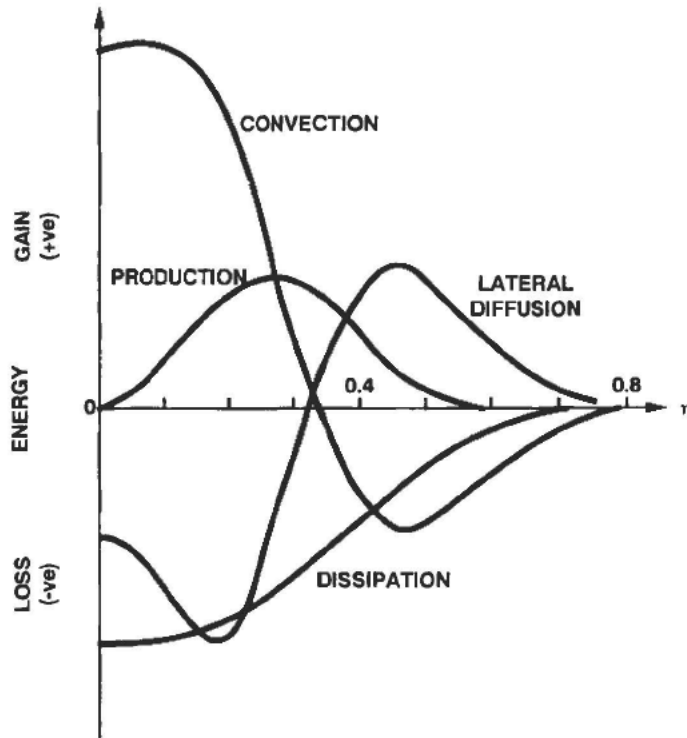


**Figure 6. Turbulence Energy Balance in Typical Plane Wake  
(Townsend, 1976)**

Inviscid stability theory has been successfully used to predict the observed coherent structures in turbulent free-shear flows, but it is not clear that similar arguments can be made when a wall is present. In other words, it is not obvious that the same inviscid, mean-flow breakdown mechanism responsible for generating the large eddies in, say, a mixing layer is operable in the case of a boundary layer. Consider the mean streamwise velocity and mean spanwise vorticity distributions sketched in figure 7, from Roshko (1992), for four different shear flows. A two-dimensional mixing layer is modeled as a single vortex sheet placed at the location of peak vorticity (at the point of inflection of the mean-velocity profile). The local circulation per unit length of the vortex sheet,  $\gamma(x)$ , is equal to the integral of the mean spanwise vorticity  $\Omega_z$  across the shear layer.

This vortex sheet is inviscidly unstable to two-dimensional perturbations and the resulting Kelvin-Helmholtz instability eventually evolves into the omnipresent two-dimensional vortices, observed even in high Reynolds number mixing layers; the resulting vortex blobs correspond to the saturation state of this instability. As indicated in the figure, circulation in the blobs is conserved,  $\Gamma = \gamma(x)\Delta x$ . Secondary instabilities of the roll-up structures result in smaller longitudinal vortices and other three-dimensional, hairpin-like eddies.

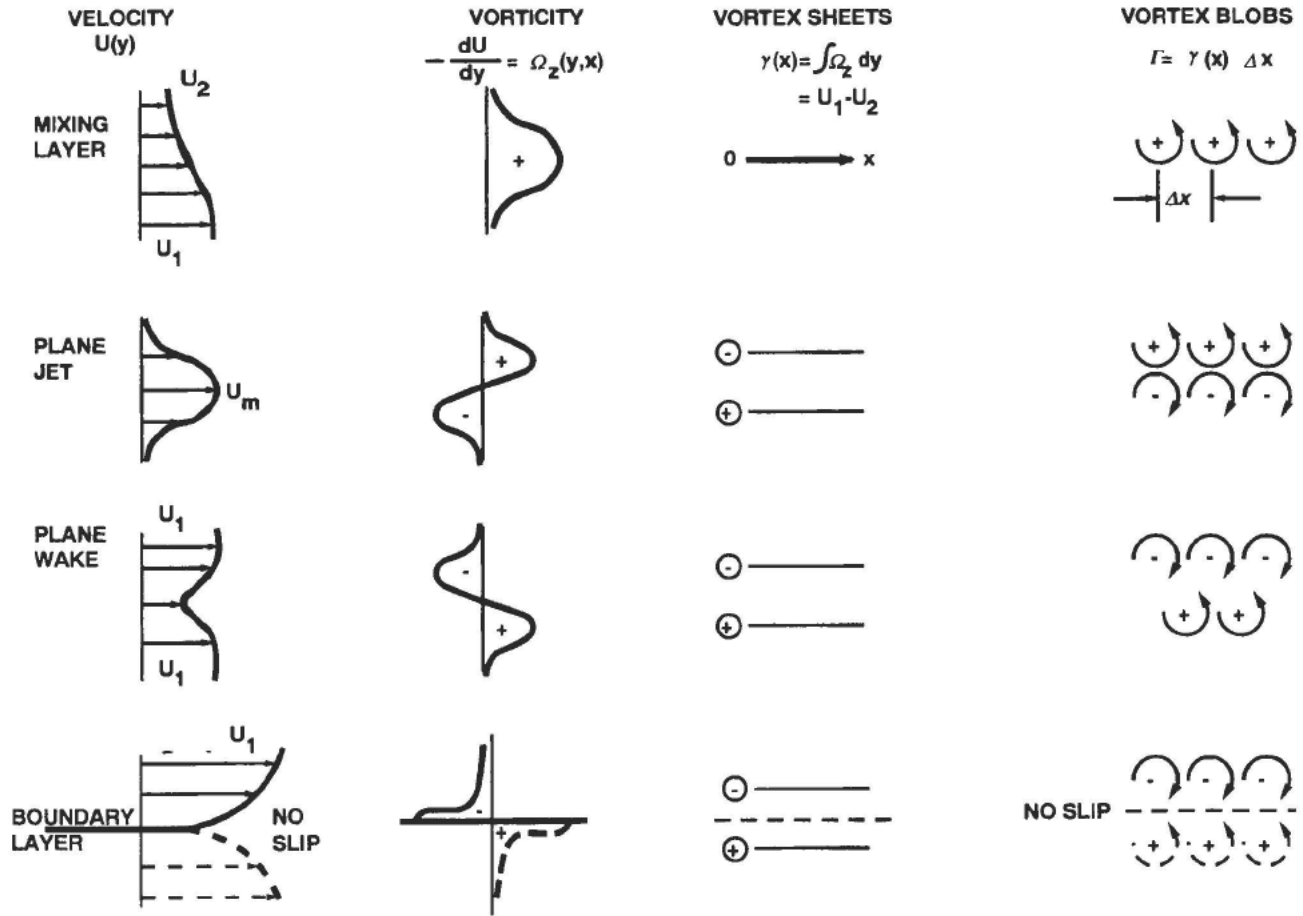


**Figure 7. Mean Streamwise Velocity and Mean Spanwise Vorticity Distributions in Different Shear Flows (Roshko, 1992)**

Similar reasoning lead to the in-phase counter-rotating vortices for plane jets and the staggered Kármán vortex street for two-dimensional wakes. As depicted in figure 7, both jets and wakes can be modeled as two vortex sheets with opposite signs of vorticity. Again, each sheet is located at the location of spanwise vorticity extrema, and total circulation is conserved.

For a turbulent wall-bounded flow, however, it is not obvious that the observed large-eddy structures (section 7) can be derived using similar inviscid arguments. If the boundary layer is modeled by a vortex sheet in which the entire mean flow vorticity has been concentrated, the presence of the wall imposes a boundary condition that necessitates the use of an image vortex sheet of opposite sign of vorticity. Such considerations led Sreenivasan (1988) to propose that the large eddies are the result of an instability of a *caricature* of the real boundary layer. Two- and three-dimensional instabilities, both inviscid and viscous, of this caricature flow lead to a plausible explanation for many observed features including the double-roller structures, hairpin eddies, and low speed streaks (see section 7 of this report).

It turns out that a somewhat similar argument was advanced two decades earlier by Black (1968). He treats the mean-flow breakdown as an intermittent, three-dimensional, inviscid process, where a mechanism analogous to the starting vortex of an impulsively started airfoil is in play. He thereby successfully predicts the formation of an array of hairpin vortices caused by a passing instability wave (Head and Bandyopadhyay, 1978). Note that while Theodorsen (1955) predicted the formation of hairpin vortices, the aspect of an array of them is absent in his work. In Black's work,  $U_\tau \delta / \nu$  appears as an important stability parameter. Mention should also be made of the waveguide theory developed by Landahl (1967; 1972; 1977; 1980; and 1990) to explain the cause and effect relationships for the variety of coherent structures observed in turbulent boundary layers.

In Sreenivasan's model, a *fat* vortex sheet and its image are located on either side of the wall at a distance corresponding to the position of the peak Reynolds stress. Because of the absence of inflection points in the interior of the canonical turbulent flow, Sreenivasan (1988) chose the alternative location of peak  $-\overline{uv}$  based on experience with transitional boundary layers.<sup>†</sup> From all available boundary layers as well as channel-flow data, this location appears to scale with the geometric mean of the inner and outer scales. Sreenivasan (1988) termed that position the *critical layer*,<sup>‡</sup> although any evidence for the existence of such a two-dimensional layer, where small perturbations are presumed to grow rapidly, is lacking. Using linear stability theory, Sreenivasan successfully showed that the primary instability of the vortex sheet and its image yields two-dimensional roll-up structures, which in turn excite low speed streaks and bursting. Subsequent instability of the roll-up structures leads to hairpin eddies and double-roller structures. One problem with this picture is that, unlike the case of free-shear flows, the predicted two-dimensional structures have never been observed in an actual turbulent wall-bounded flow. Sreenivasan (1988) allows that his simplistic model is unfinished and has a number of weaknesses but offers it as a target for useful criticism.

The arguments above indicate that the existence of an inviscid breakdown mechanism responsible for the self-sustenance of the turbulence has not been firmly established. In other words, it is not clear that the observed coherent structures in a boundary layer or channel flow are the result of an instability of the mean flow or its caricature. Until this issue is resolved, progress in the understanding of wall-bounded flows will remain lagging behind that of free-shear flows. Despite the importance of this dynamical issue, research on the organized nature of turbulent boundary layers has remained confined to the kinematics, and high-payoff turbulence control strategies are yet to be developed.

---

<sup>†</sup> Note that in the past, both Clauser (1956) and Corrsin (1957) have also attempted to treat the turbulent regenerative process as primarily similar to the breakdown mechanism of a critical laminar layer.

<sup>‡</sup> In a transitional wall-bounded flow, the location of peak Reynolds stress coincides with the critical-layer position. Because this position shows similar trends with Reynolds number to that in a turbulent flow (see the lowermost two data points in figure 32b), Sreenivasan (1988) chose to place his proposed vortex sheet at this location.

## 5. MEAN FLOW

Before investigating the issue of Reynolds number effects on coherent structures, available data for the mean velocity and higher-order statistics of wall-bounded flows are reviewed in the present and following sections. Section 5 focuses on the Reynolds number effects on the mean streamwise velocity, and section 6 discusses these effects on RMS velocity fluctuations, Reynolds stress, spectra, skewness and flatness factors, and RMS and spectrum of wall-pressure fluctuations.

### 5.1 STREAMWISE VELOCITY

The mean flow velocity in the streamwise direction is a relatively easy quantity to measure and almost every paper on wall-bounded flows has such measurements (see, for example, Laufer, 1951; Comte-Bellot, 1965; Eckelmann, 1974; Purtell et al., 1981; Andreopoulos et al., 1984; and Wei and Willmarth, 1989). Requirements for probe resolution are modest and, except very near the wall, most published data are reliable to better than 1 percent. This is obviously not the case for measurements of higher-order statistics, and this point will be revisited in the following section.

For a turbulent wall-bounded flow, the region directly affected by viscosity, the viscous sublayer plus the buffer layer, occupies progressively smaller proportion of the boundary-layer thickness as the Reynolds number increases (see figure 3). The rest of the flow is more or less independent of viscosity. It is not surprising, therefore, that the Reynolds number has a considerable effect on the velocity profile. As  $Re_\theta$  increases, the mean-velocity profile becomes fuller and the shape factor  $H$  decreases accordingly. For example, at  $Re_\theta = 2000$ ,  $H = 1.41$ , and at  $Re_\theta = 10,000$ ,  $H = 1.33$ . The effect is even more pronounced at Reynolds numbers lower than 2000. In a laminar flat-plate flow, in contrast, viscosity is important across the entire layer and the shape factor is independent of Reynolds number.

Available data indicate that the wall-layer variables universally describe the streamwise mean velocity in the inner layer of smooth flat plates, pipes, and channels at all Reynolds numbers. Figures 8 through 10 illustrate this for boundary layers and channel flows for a wide range of Reynolds numbers. The low Reynolds number boundary layer data of Purtell et al. (1981) in figure 8 indicate the presence of a logarithmic region for  $Re_\theta$  as low as 500. This is rather surprising considering that at this Reynolds number a constant-stress region is virtually non-existent and the maximum Reynolds stress is substantially less than  $U_\tau^2$ . However, in deriving the log law, equation (8), the presumably constant-velocity scale has a weak, square-root dependence on the Reynolds stress. The extent of the log region, expressed in wall units, increases with Reynolds number but is a constant fraction of the boundary layer thickness.

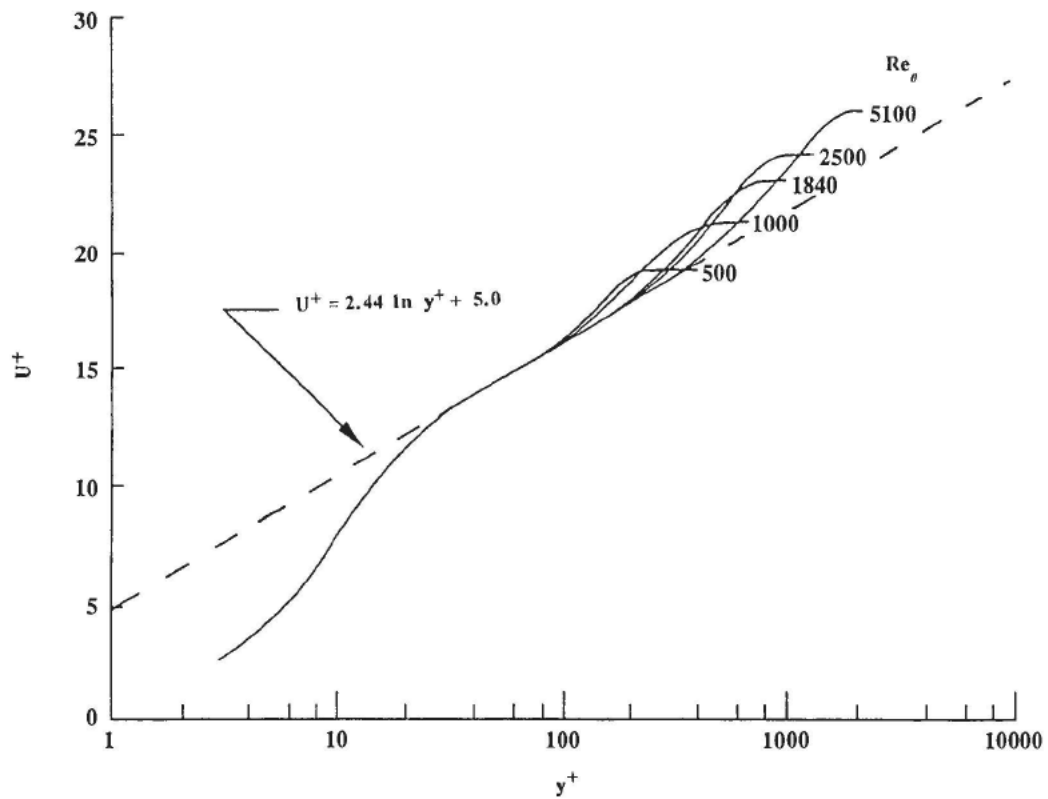


**Figure 8. Comparison of Mean Velocity Profiles With Logarithmic Law at Low Reynolds Numbers (Boundary Layer Data From Purtell et al., 1981)**

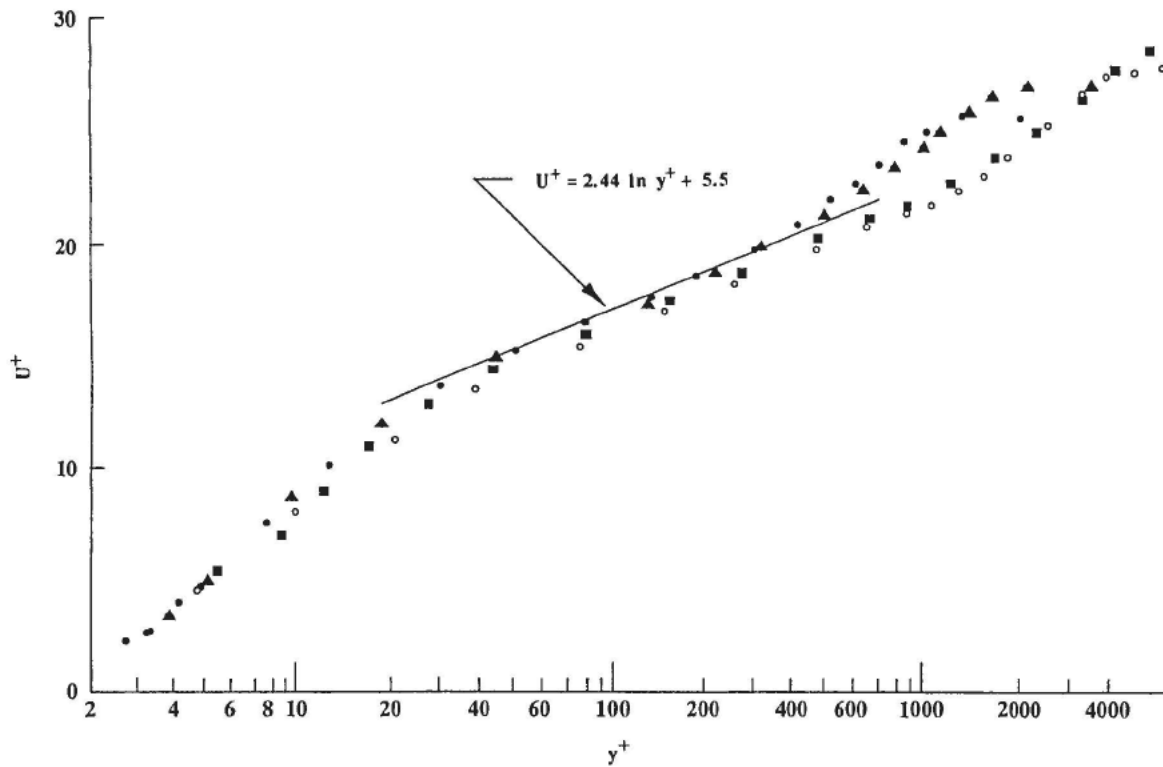


**Figure 9. Non-Dimensional Mean Velocity Profiles at High Reynolds Numbers (Boundary Layer Data From Andreopoulos et al., 1984)**

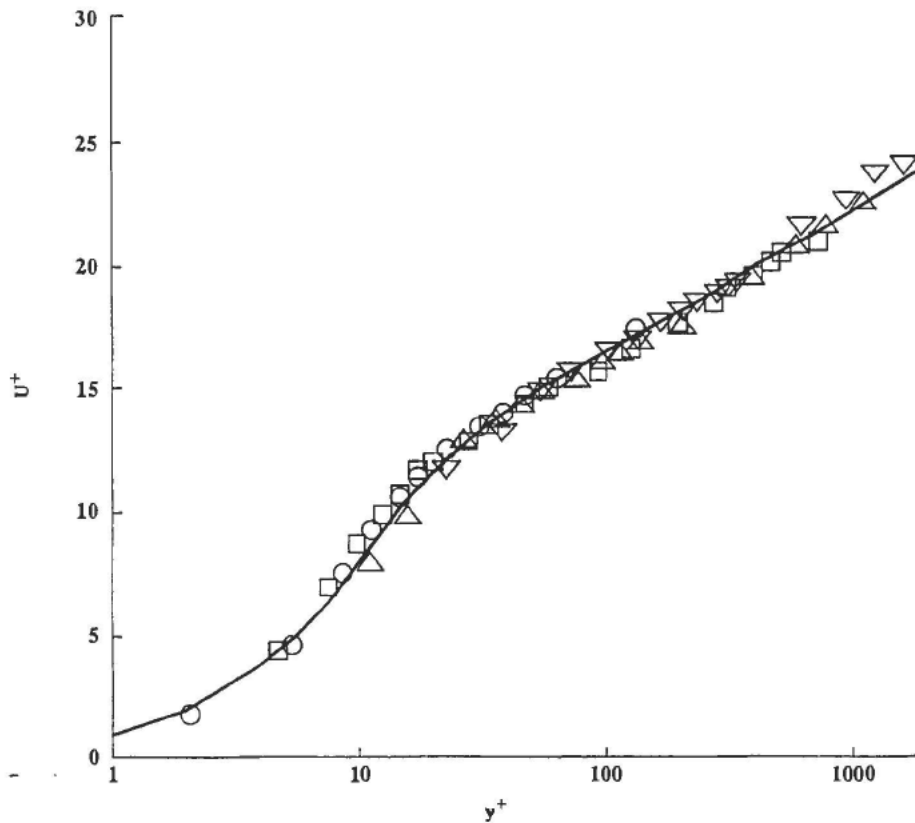


**Figure 10. Mean Velocity Profiles Non-Dimensionalized on Inner Variables  
(Channel-Flow Data From Wei and Willmarth, 1989)**

The single straight line in figure 8 does not support Simpson's (1970; 1976) claim that the law-of-the-wall, especially  $\kappa$ , varies with Reynolds number, nor the assertion by Landweber (1953), Preston (1958), and Granville (1977) that the logarithmic region disappears altogether at low Reynolds numbers. An important question is: What is the minimum  $Re_\theta$  at which a log region is first established? Coles (1962) analysis of wake component indicates that it is zero at  $Re_\theta \leq 600$ . The data of Bandyopadhyay and Ahmed (1993) indicate that Clauser's outer-layer shape parameter  $G$  reaches zero at  $Re_\theta = 425$ . These can be regarded as two indications of a minimum value, supporting the experimental findings of Purtell et al. (1981) depicted in figure 8.

At low Reynolds numbers, the large scales of the turbulent fluctuations dominate its dynamics. The logarithmic region appears to be an inherent characteristic of the turbulent boundary layer and to be associated with the large eddies. Because of the persistence of the log region to Reynolds numbers just above transition, Purtell et al. (1981) suggest that the large-scale structures in the turbulent boundary layer are related to, if not simply comprises, the hairpin eddies produced during the final stages of laminar-to-turbulence transition.

Andreopoulos et al. (1984) provide mean-flow data for higher Reynolds number boundary layers. Figure 9 depicts their normalized data for the four Reynolds numbers  $Re_\theta = 3624, 5535, 12,436, \text{ and } 15,406$ . All three flow regimes described in section 3 are apparent in the different mean-velocity profiles. Again, inner scaling collapses the data in the inner layer (viscous plus logarithmic regions) onto a single curve.

Similar results are observed in the channel-flow data of Wei and Willmarth (1989) depicted in figure 10. Here the Reynolds number is based on the centerline velocity and the channel half-width and ranges from  $Re_a = 2970$  to  $Re_a = 39,582$ . As expected, the wake component in the mean-velocity profiles of the channel flow is much weaker than that in the boundary layer data.

## 5.2 VON KÁRMÁN CONSTANT

As discussed in section 5.1, Purtell et al.'s (1981) measurements in low-Reynolds number boundary layers confirm that the law of the wall does not vary with Reynolds number, thus implying a truly constant value of the von Kármán's constant. This result refutes an earlier claim by Simpson (1970) that  $\kappa$  varies with Reynolds number. Additionally, as illustrated below, a rather simple kinematic argument can be invoked to support the universality of  $\kappa$  (Bandyopadhyay, 1991).

Based on two-point velocity-correlation measurements, Townsend (1976) proposes the double-cone wall grazing eddy as the prototypal coherent structure in the near-wall region. This vortex, which satisfies the wall constraint, is the attached analog to his double-roller eddy of free-shear flows. The coherent structure is in contact with the wall over its whole length, and vortex stretching is ignored. Its diameter must then be  $d = 2y$ , where  $y$  is the location of the vortex center.

Of relevance here is Robinson's (1990) observation that the near-wall streamwise vortices frequently detected in low-Reynolds number direct numerical simulations have mean diameters that vary with distance from the wall according to the linear relation:

$$d^+ = \kappa y^+, \quad (17)$$

where  $d$  is the mean vortex diameter and  $\kappa$  is the von Kármán constant. Now, the simple-momentum-transport model used in section 3.2 to derive the log law assumes a local mixing length that varies according to

$$\ell = \kappa y. \quad (18)$$

This means that in the constant-Reynolds stress region,

$$d^+ = \ell^+ = \kappa y^+. \quad (19)$$

Notice that  $\ell$  reaches its maximum value at the end of the constant-stress region, i.e., at  $(y/\delta) = 0.2$ , such that

$$(\ell/\delta)_{\max} = \kappa(y/\delta)_{\text{top of log region}} = 0.082. \quad (20)$$

Thereafter,  $\ell$  is a constant throughout the rest of the boundary layer. Although  $(\ell/\delta)_{\max}$  is independent of the Reynolds number, it is clear that  $\ell_{\max}^+$  is not a constant. In fact,  $\ell_{\max}^+$  is a strong function of the Reynolds number for  $\delta^+ < 10^3$  (Bushnell et al., 1975).

If the near-wall region within which  $\ell_{\max}$  is first reached is simply modeled to comprise Townsend's double-cone eddies, it is then encouraging that the von Kármán constant of 0.41 is within the value of the constant of proportionality for the upper limit of the vortex size, viz., 2. The kinematic behavior supports the contention that  $\kappa$  is independent of Reynolds number and type of flow (pipe, channel, or boundary layer).

### 5.3 ILLUSORY ASYMPTOTIC STATE

While inner scaling collapses wall-layer mean-flow data onto a single curve regardless of the Reynolds number, the situation is not that simple in the outer layer. As discussed in section 3, Coles (1956) proposed to represent the entire mean-velocity profile in any two-dimensional turbulent boundary layer by a linear superposition of two universal functions, the law of the wall and the law of the wake. In fact, Coles suggested a simple extension of his empirical law to represent even yawed and three-dimensional flows. Recall equation (15):

$$U^+ = f(y^+) + (\Pi/\kappa)W(y/\delta).$$

The first term on the right-hand side is valid for any smooth wall-bounded flow, and available evidence indicates that the function  $f$  is independent of Reynolds number, pressure gradient, and freestream turbulence. This term supposedly represents all mixing processes in the wall layer governed primarily by viscosity. The wall constraint is felt mainly in the viscous sublayer, the buffer layer, and the logarithmic portion of the velocity profile. For rough walls, particularly when the roughness is sufficiently pronounced, the viscous length scale is simply replaced by the characteristic roughness height. For both smooth and rough walls, the appropriate velocity scale is derived from the magnitude of the surface shear stress.

The second term, representing turbulent mixing processes dominated by inertia, is the product of the universal wake function  $W(y/\delta)$  and the ratio of the profile parameter  $\Pi$  to the von Kármán constant  $\kappa$ . The parameter  $\Pi$  depends on the pressure gradient, the freestream turbulence, and whether the flow is internal or external, but is not directly affected by wall conditions such as roughness, etc. For a flat-plate boundary layer, the profile parameter increases with Reynolds number but presumably asymptotes to a constant value at high enough  $Re$ . This is illustrated in figure 11, from Coles (1962), depicting the change of the maximum deviation of the mean velocity from the logarithmic law,  $\Delta U^+$ , with Reynolds number. Here, the maximum deviation, or the strength of the wake component, is expressed in wall units and the Reynolds

number is based on freestream velocity and momentum thickness. The maximum Reynolds number shown is 15,000. Because the maximum deviation occurs close to the edge of the boundary layer and since  $W(y/\delta)$  has been normalized such that  $W(1) = 2$ , the strength of the wake component is approximately related to the profile parameter by

$$\Delta U^+ = 2\pi/\kappa. \quad (21)$$

It is clear that the strength of the wake depends upon the somewhat arbitrary way in which the logarithmic portion of the velocity profile is fitted, i.e., on the particular values of  $\kappa$  and  $B$  chosen.

Figure 11 shows the strength of the wake component reaches a constant value for  $Re_\theta \geq 6000$ . Coles (1962) termed the flow at this high Reynolds number "equilibrium," which led to the wide-spread perception that the flow becomes independent of Reynolds number beyond this value. Unfortunately, when the plot in figure 11 is extended to larger values of Reynolds numbers, it becomes clear that the presumed asymptotic state is merely an illusion. As shown in figure 12,  $\Delta U^+$  starts decreasing again at about  $Re_\theta > 15,000$ , although very slowly compared with the rise rate for  $Re_\theta < 6000$ . After excluding all data containing certain anomalies, Coles (1962) was puzzled by the persistent change in behavior and the variation between data sets for  $Re_\theta > 15,000$ . The drop cannot be explained from experimental uncertainties such as those caused by probe calibration problems, improper tripping devices, three-dimensional effects, high levels of freestream turbulence and pressure-gradient effects, and Coles left the issue open

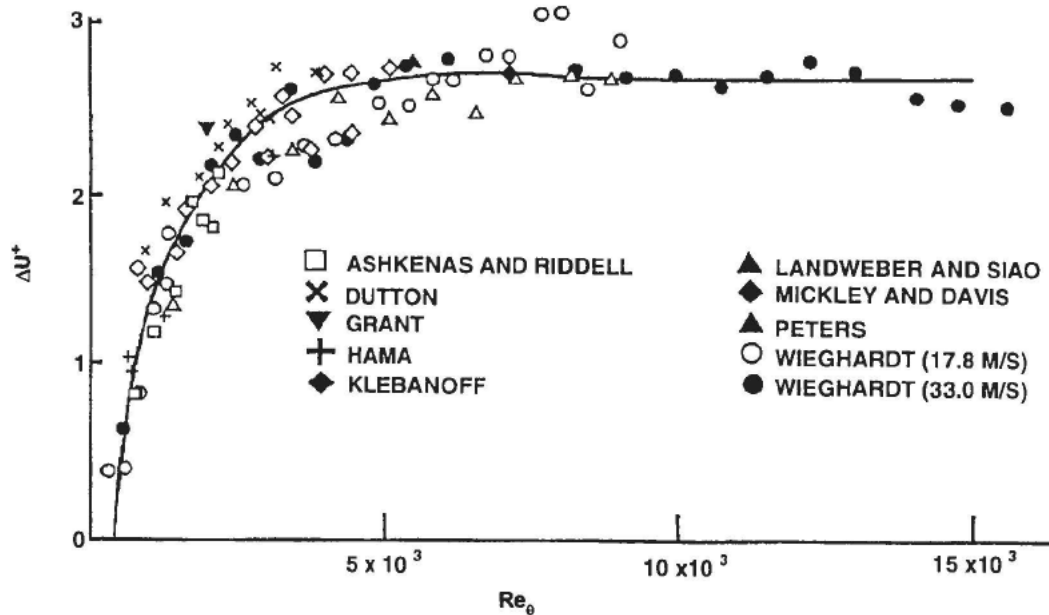


**Figure 11. Reproduction of Coles' (1962) Strength of Wake Component in Equilibrium Turbulent Boundary Layers at Low Reynolds Numbers**

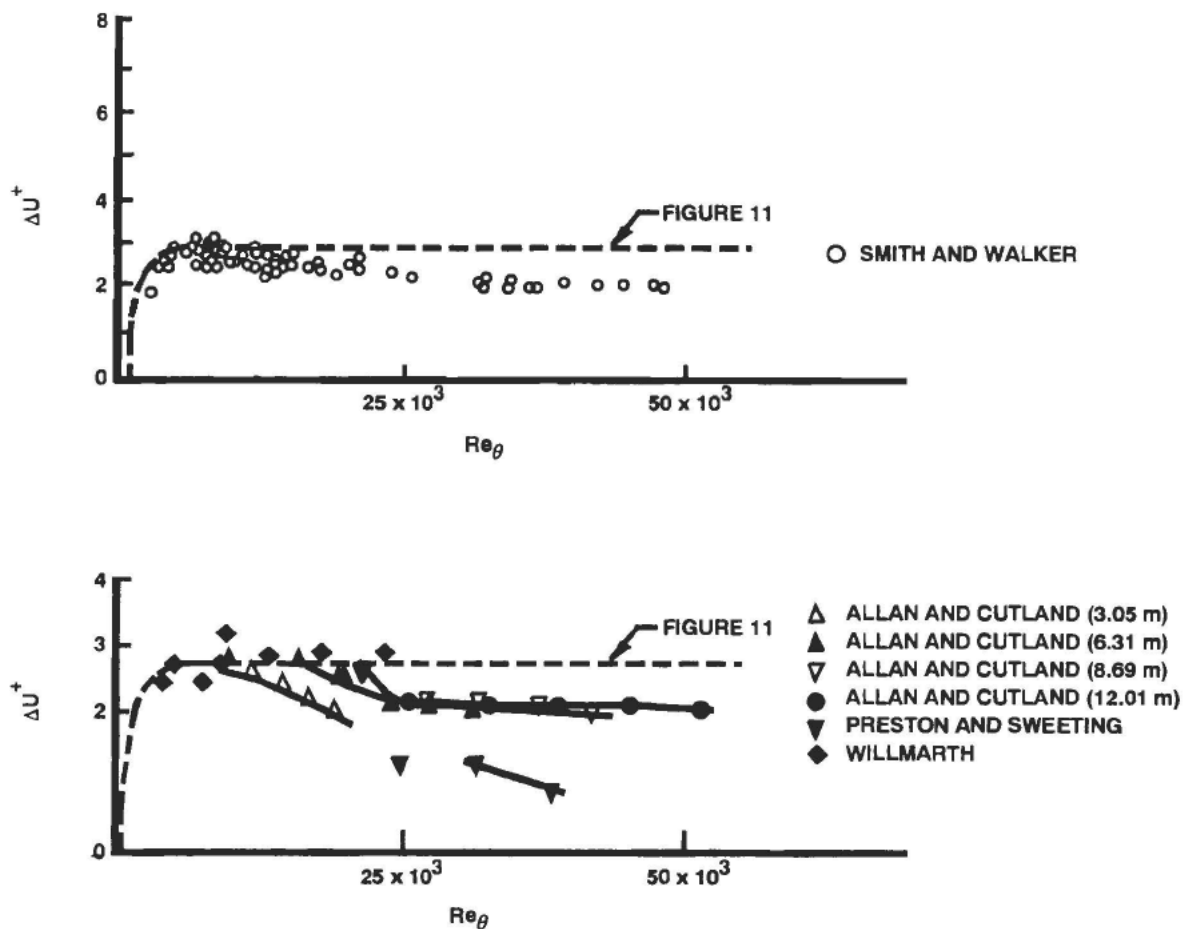


**Figure 12. Reproduction of Coles' (1962) Strength of Wake Component at Large Reynolds Numbers**

The rapid rise and the subsequent gradual fall of  $\Delta U^+$  with  $Re_\theta$  appear to be genuine and have been confirmed in several other experiments as summarized by Mabey (1979). The maximum  $\Delta U^+$ , reached at about  $Re_\theta = 6000$ , is 2.7 for subsonic flows (Smith and Walker, 1959) but is higher by 30 percent or more for supersonic flows (Lee et al., 1962; Hopkins et al., 1972; Mabey et al., 1976).

Smith and Walker's (1959) subsonic data, shown previously in the top part of figure 12, are replotted on a semi-log scale in figure 13 for four different measuring stations. The forward station,  $x = 400$  mm, shows a different trend as compared with the three downstream locations. Using the two curves fitted to the data in figure 13, Mabey (1979) analyzed the effects of the variation of the wake component with Reynolds number on skin-friction and total drag predictions. These are important parameters when extrapolating model tests to actual vehicle configurations. The curve marked  $W_1 = 1.8$  corresponds to a constant wake component of 1.8 above  $Re_\theta = 5600$  but falls to zero at  $Re_\theta = 600$ . The second curve marked  $W_1 = 2.8$  peaks at  $Re_\theta = 5600$ , but drops at higher and lower Reynolds numbers. Particularly at low  $Re_\theta$ , the skin friction computed from the first curve fits the law-of-the-wall estimates, while predictions based on the second curve fit the directly measured drag better.

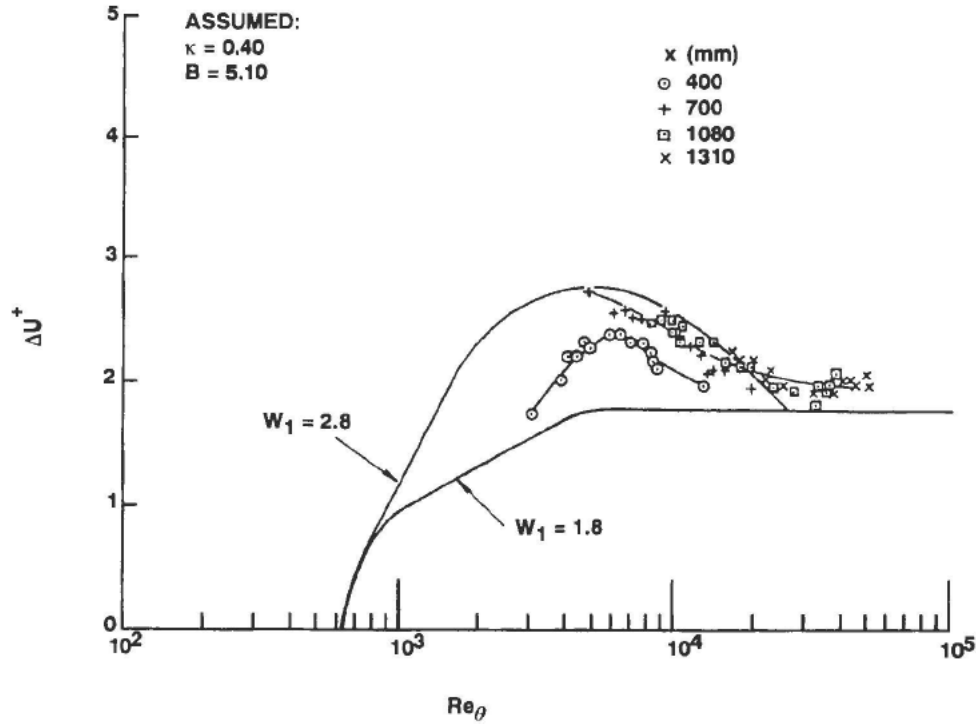


**Figure 13. Strength of Wake Component vs Reynolds Number on Semi-Log Plot (Subsonic Data of Smith and Walker (1959) at Four Downstream Stations) (Mabey, 1979)**

The supersonic data of Mabey et al. (1976) are depicted in figure 14, where there seems to be no significant variation with Mach number. Despite artificial tripping, the boundary layer was laminar or transitional for  $Re_\theta < 600$ , and no wake component can be extracted from the velocity profiles. As in the subsonic case, Mabey (1979) used the two fitted curves in figure 14 to analyze the effects of the variation of the wake component with Reynolds number on skin friction.

The Reynolds number effect on the mean flow can also be verified independently from Clauser's shape parameter:

$$G = \int_0^\delta \left( \frac{U_o - U}{U_r} \right)^2 dy / \int_0^\delta \left( \frac{U_o - U}{U_r} \right) dy, \quad (22)$$

where  $U(y)$  is the velocity profile and  $U_o$  is the velocity at the edge of the boundary layer,  $y = \delta$ . Bandyopadhyay (1992) compiled the findings of several recent experiments to show the variation of  $G$  with  $Re_\theta$ . The results are shown in figure 15, and include the high-aspect ratio<sup>†</sup> data of Anders (1989). The trend parallels that of  $\Delta U^+$ . The value of  $G$  first rises rapidly with  $Re_\theta$  and then drops gradually. Figure 15 also corrects the loose notion found in the literature that  $G$  varies between 6.5 and 7.5.

<sup>†</sup> Ratio of tunnel span to  $\delta$ .

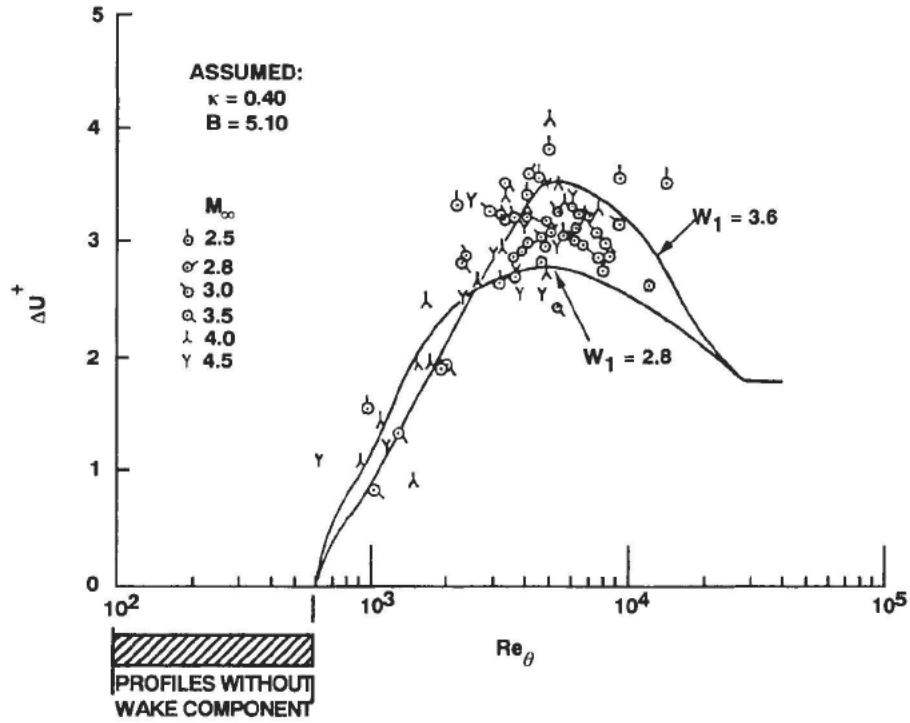


Figure 14. Strength of Wake Component vs Reynolds Number on Semi-Log Plot (Supersonic Data of Mabey et al. (1976) at Six Different Mach Numbers) (Mabey, 1979)

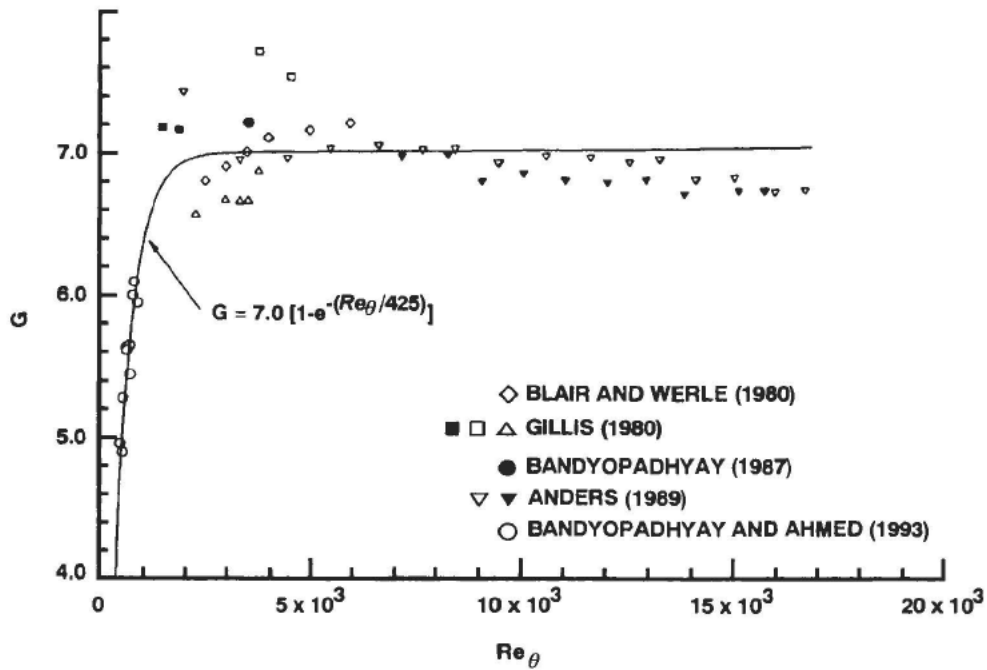


Figure 15. Low Reynolds Number Effects on Clauser's Shape Parameter (Bandyopadhyay, 1992)

## 5.4 IS SELF-PRESERVATION EVER ACHIEVED?

At approximately  $Re_\theta > 15 \times 10^3$ , the gradual departure of  $\Delta U^+$  from the apparent low  $Re_\theta$  asymptote suggests that some new effects are gradually appearing in the turbulence production process. A new, lower asymptote appears to have been reached when  $Re_\theta = 50,000$ , but the boundary layer might also continue to change indefinitely as the inner and outer scales are forever departing. The paucity of high Reynolds number reliable data makes it difficult to make a definitive conclusion.

Without definitive experiments at even higher Reynolds numbers, one can never be sure of the universality of the defect law. Very few existing facilities can deliver the required ultra-high Reynolds number flows, while maintaining relatively low Mach numbers (in the so-called low speed, high Reynolds number tunnels) to avoid the added complication of compressibility effects. The largest available water tunnels and towing tanks can deliver a momentum thickness Reynolds number of approximately  $3 \times 10^4$  and  $9 \times 10^4$ , respectively. Cryogenic tunnels, for example the National Transonic Facility at NASA Langley, typically use nitrogen and run as high as  $Re_\theta = 6 \times 10^4$ , but their Mach numbers are near one and are rather expensive, as well as heavily scheduled (Bushnell and Greene, 1991). Tunnels using liquid helium I are an attractive, low-cost alternative to the much larger nitrogen tunnels (Donnelly, 1991). Helium facilities can match the Reynolds numbers of the transonic wind tunnels but with essentially zero Mach number and much smaller sizes (e.g., 1 cm x 1 cm test section). Instrumenting the smaller facilities with high-resolution velocity or pressure probes is at present problematic, although the rapidly developing microfabrication technology has the potential for producing inexpensive megahertz frequency and micron-size sensors (see, for example, Löfdahl et al., 1989; 1991; 1992).

A commonly accessible large-scale, high Reynolds number facility is the atmospheric boundary layer. The flow is virtually incompressible and the momentum thickness Reynolds number in the atmosphere can be as much as four orders of magnitude higher than that in typical laboratory experiments. Unfortunately, such a natural laboratory has several faults. Firstly, the “wall” in this case is almost always rough and direct comparison with the canonical boundary layer is difficult. Secondly, the atmospheric experiments are not well controlled, the flow conditions are neither precisely repeatable nor documentable to the needed detail (see however the recent thesis by Kailasnath, 1993, who was able to carry out useful comparison between low Reynolds number laboratory data and high Reynolds number atmospheric data).

The so-called *super-pipe* facility is currently being constructed at Princeton University (A. J. Smits, private communications). The pipe has a diameter of 12.7 cm and a length-to-diameter ratio of 200. When completed, this high-pressure-air (200 atm.) pipe flow will provide a very high Reynolds number of up to  $Re_\theta = 2.3 \times 10^7$  at a reasonably large scale and low Mach number, and hopefully will help in answering some of the questions raised in the present review.

For the present at least, it is simply not known if the mean flow in a wall-bounded flow ever achieves true self-preservation. As will be shown in the following section, the situation is less clear for higher-order statistics.

## 5.5 ALTERNATIVES TO LOGARITHMIC PROFILE

Despite copious evidence for the existence of the log law, the whole scenario leading to it has been questioned (see references cited in section 3.2). From a purely practical point of view, a portion of the streamwise mean velocity profile could equally well fit either a logarithmic relation or a power law. If the mean velocity profile for a pipe flow (or boundary layer) is to be fitted with a power law of the form

$$\frac{U}{U_a} = c \left( \frac{y}{a} \right)^{\frac{1}{n}}, \quad (23)$$

the value of the exponent ( $1/n$ ) will decrease as the velocity profile becomes fuller. In other words,  $n$  increases as  $H$  decreases and  $Re$  increases. For example, the smooth pipe-flow data of Nikuradse (1932) indicate that  $n$  changes from 6 to 10 as the Reynolds number varies in the range of  $Re_a = 2.53 \times 10^3 - 1.85 \times 10^6$  (Schlichting, 1979).

Sreenivasan (1989) argues that although the power law used by engineers to describe the mean velocity profile has been discredited by scientists since Millikan (1939) derived the logarithmic law from asymptotic arguments, the basis for the power law is *a priori* as sound as that for the log law, particularly at low Reynolds numbers (see also Barenblatt, 1979, 1993; Barenblatt and Prostokishin, 1993). The behavior of the exponent ( $1/n$ ) as  $Re_a \rightarrow \infty$  is of particular interest. If it tends to zero, the log law is recovered. If, on the other hand, the limiting value of the exponent is a non-zero constant, the log law does not strictly hold. This implies that an inertial sublayer is lacking and, therefore, that viscous effects persist even at infinitely large Reynolds number. Such a scenario is consistent with the suggestion by Long and Chen (1981) that the inner flow is the outcome of an interplay between wall effects and outer effects; it is strange that the matched layer between one characterized by inertia and another characterized by viscosity depends only on inertia. Long and Chen suggest that a "mesolayer" intrudes between the inner and outer regions preventing the overlap assumed in the derivation of the classical logarithmic velocity profile. Unfortunately, experimental or numerical mean velocity data can not be used to explore this important issue since the difference between a logarithmic relation and a power law with a large but finite  $n$  is imperceptible (see Kailasnath, 1993, for a comprehensive review of available data).

George et al. (1992, 1993, 1994) provide the most serious challenge to the validity of the log law for external wall-bounded flows. The assertion that boundary layer data taken at different Reynolds numbers collapse in the log region only if the shear stress is calculated from a method (i.e., the Clauser's method) that forces it to by assuming such a layer exists. Such superficial collapse compromises the collapse in the viscous sublayer where no adjustable constants or Reynolds number dependence should exist. As an alternative, George et al. (1992) used measured shear stress to normalize the data of Purtell et al. (1981) and showed that the profiles collapse very close to the wall but not in the log region where clearly discernible Reynolds number dependence is depicted. To remedy the situation, George et al., propose matching a new velocity defect law with explicit Reynolds number dependence and the traditional law of the wall. The

result in the matched region is a power law velocity profile of the form

$$\frac{U}{U_\infty} = C_o \left( \frac{y}{\delta} \right)^n + B_o, \quad (24)$$

$$\frac{U}{U_\tau} = C_i \left( \frac{U_\tau y}{\nu} \right)^n + B_i, \quad (25)$$

where coefficients  $B_i$ ,  $B_o$ ,  $C_i$ ,  $C_o$ , and the exponent  $n$  are Reynolds number dependent, but all are asymptotically constant. The corresponding friction coefficient is then expressed as the Reynolds number to the power  $-2n/(1 + n)$ .

George et al. (1994) assert that their approach removes many of the unsatisfying features of the classical Millikan's (1939) theory. Furthermore, it is argued that a clear distinction should be made between internal and external wall-bounded flows. For fully developed pipe and channel flows, the streamwise homogeneity ensures that the pressure gradient and wall shear stress are not independent, thus  $U_\tau$  is the correct scaling velocity for the problem. This results in a log law although the flow has no constant stress layer. The growing, inhomogeneous boundary layer, in contrast, is governed by a power law even though it does, at least for zero pressure gradient and high  $Re$ , have a constant stress layer. The matched region of a boundary layer retains a dependence on streamwise distance, and hence, never becomes Reynolds-number independent.

George and Castillo (1993) have recently extended the new scaling law described above for the flat-plate flow to boundary layers with pressure gradient. Inclusion of roughness or compressibility effects could proceed along similar attempts made in the past for the classical theory (Hama, 1954; Coles, 1962).

The fresh look at the turbulent boundary layer by George and his colleagues is intriguing and deserves further scrutiny. Independent confirmation of their claims is needed, and carefully controlled boundary layer experiments over a wide range of Reynolds numbers would be most useful. If validated, their new theory indicates that boundary layer is governed by a different scaling law than commonly believed. Explicit, albeit weak, Reynolds number dependence is shown for the mean velocity profile all the way down to the edge of the viscous sublayer. The matched region retains a dependence on streamwise distance, consequently, Reynolds number effects will always persist for all turbulence quantities.

The difference in the inner layer between flat-plate boundary layers and pipe flows, as proposed by George, has a serious implication on the principle and use of Preston tube, which is widely used for the measurement of local mean skin friction. Because Preston tubes rely on the universality of the inner layer, the validity of the calibration of Preston tubes in a pipe flow to smooth flat-plate boundary layers is questionable. Direct measurement of the wall-shear stress, clearly, should be preferred over indirect methods like Preston tubes.

## 6. HIGHER ORDER STATISTICS

Compared with the mean flow, higher order statistical quantities are more difficult to measure, and the issue of Reynolds number effects is cloudy. For quantities such as RMS, Reynolds stress, skewness, and spectrum, the issues of spatial as well as temporal probe resolutions, three-dimensional effects, and boundary-layer tripping devices become much more critical. In contrast to mean flow, reliable data for higher order statistics are scarce.

A measurement probe essentially integrates the signal over its active sensing area or volume. This means that velocity or pressure fluctuations having scales smaller than the sensor size are attenuated by the averaging process, and the resulting RMS of the fluctuations, for example, is smaller than it actually is. Several studies have shown the importance of probe size in the detection of small-scale structures in the near-wall region (for example, Willmarth and Bogar, 1977; Schewe, 1983; Johansson and Alfredsson, 1983; Blackwelder and Haritonidis, 1983; Luchik and Tiederman, 1986; Karlsson and Johansson, 1986; Ligrani and Bradshaw, 1987; Wei and Willmarth, 1989; and Löfdahl et al., 1992). As a rule of thumb, probe length much larger than the viscous sublayer thickness is not acceptable for accurately measuring turbulence levels and spectra anywhere across the boundary layer, and even smaller sensing elements are required to resolve dynamical events within the sublayer itself.

The issue of sufficient probe resolution is particularly acute when studying Reynolds number effects. A probe that has high fidelity at low  $Re$  might give erroneous results when the Reynolds number is increased and the scales to be resolved become smaller relative to the probe size. The probe resolution should be expressed in wall units, and as mentioned above  $\ell^+$  should not be much larger than 5, where  $\ell$  is the probe length.

The classic idea of inner scaling is that any turbulence quantity measured at different Reynolds numbers and in different facilities will collapse, at least in the inner layer, to a single universal profile when non-dimensionalized using inner-layer variables. In contrast to mean-velocity profiles, higher order statistics do not, in general, scale with wall-layer variables even deep inside the inner layer. In the following five subsections, there is a review of Reynolds number effects on the RMS values of the velocity fluctuations, Reynolds stress, spectra, skewness and flatness factors, and RMS and spectrum of the wall-pressure fluctuations.

### 6.1 RMS VELOCITY FLUCTUATIONS

The intensity of turbulent fluctuations is defined by its RMS value. The streamwise velocity fluctuations are more readily measured using, for example, a single hot-wire probe or a two-beam laser Doppler velocimeter. Measuring the other two velocity components, in contrast, requires two hot wires either in an X-array or a V-array or four intersecting laser beams. Especially very close to the wall, few reliable measurements of the normal velocity components are reported in the literature, and even fewer are available for the spanwise component. A notable exception is the oil-channel data reported by Kreplin and Eckelman (1979), who measured all three velocity components inside the viscous sublayer. Here, boundary layer data for both low and high Reynolds numbers are presented followed by channel and pipe-flow data.

Figure 16 shows the variation of the normal distribution of turbulence intensity in wall variables with Reynolds number. Measurements of the streamwise velocity component were conducted by Purtell et al. (1981) in a low Reynolds number, flat-plate boundary layer. Four Reynolds numbers based on momentum thickness are presented in the figure, ranging from  $Re_\theta = 465$  to 5100. It is clear that Reynolds number effects penetrate into the boundary layer much deeper in terms of the turbulence intensity than it does for the mean velocity. Approximate similarity in wall units is maintained only out to  $y^+ \approx 15$ , compared with mean velocity, which is similar throughout the entire inner layer. Close inspection of the figure reveals that even in the viscous region itself, some weak dependence on Reynolds number is observed in the RMS value of the streamwise velocity fluctuations, as seen at the lowest Reynolds number of  $Re_\theta = 465$ . Purtell et al., attributed the systematic decrease in  $u'$  across most of the boundary layer to the suppression of all but the largest turbulence eddies as the Reynolds number is reduced.

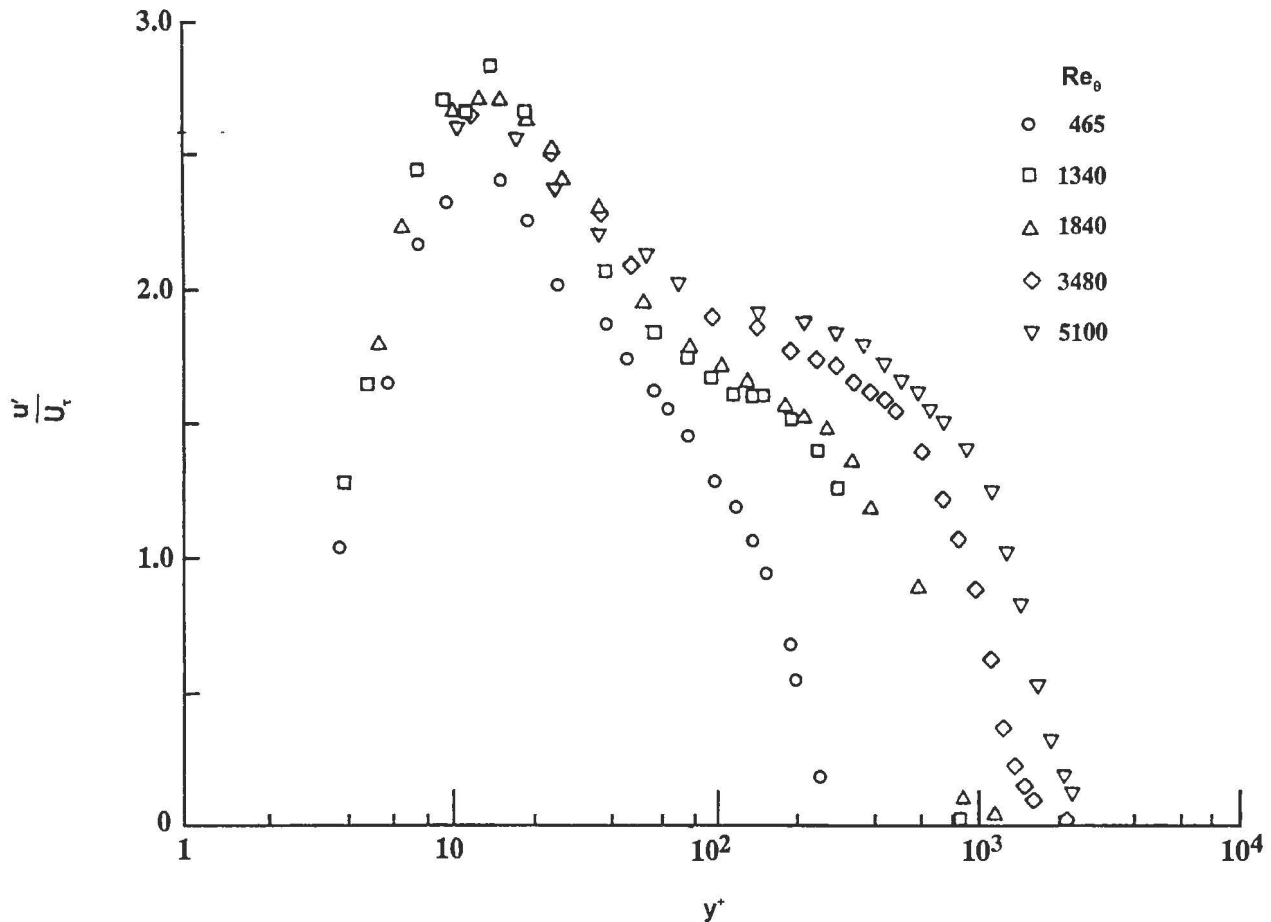


**Figure 16. Variation of Distribution of Turbulence Intensity in Wall Variables With Reynolds Number  
(Boundary Layer Data From Purtell et al., 1981)**

Reynolds number can of course be changed either by varying the freestream velocity at a fixed streamwise location or by holding the tunnel speed constant and conducting the measurements at increasing downstream locations. To check the state of development of the flow, Purtell et al. (1981) measured, for a fixed freestream velocity, the mean velocity profiles at four downstream distances from the tripping device. At the station closest to the distributed roughness, they report under development in the outer region of the mean flow, but an undistorted logarithmic region that produces friction velocity values in agreement with directly measured  $U_\tau$  values computed from near-wall measurements of  $\partial U / \partial y$ . The same trends were observed at higher Reynolds numbers by Klebanoff and Diehl (1951).

When normalized with the freestream velocity,  $u'$  also shows distortion in the outer region for measurements not sufficiently far downstream of the tripping device. However, as shown in figure 17, the RMS data plotted in inner variables at a freestream velocity of 2.3 m/s and four downstream stations  $x = 91, 122, 152$ , and  $183$  cm, exhibit such a strong Reynolds number dependence in the outer layer that the distortion mentioned above is obscured. Close inspection of figure 17 shows a small but systematic Reynolds number effect even below  $y^+ = 10$ . Barring the first measurement station ( $x = 91$  cm), which is non-typical due to its close proximity to the tripping device, at a given  $y^+$ ,  $u'_{rms}$  increases with  $x$ , i.e., with  $Re_\theta$ .

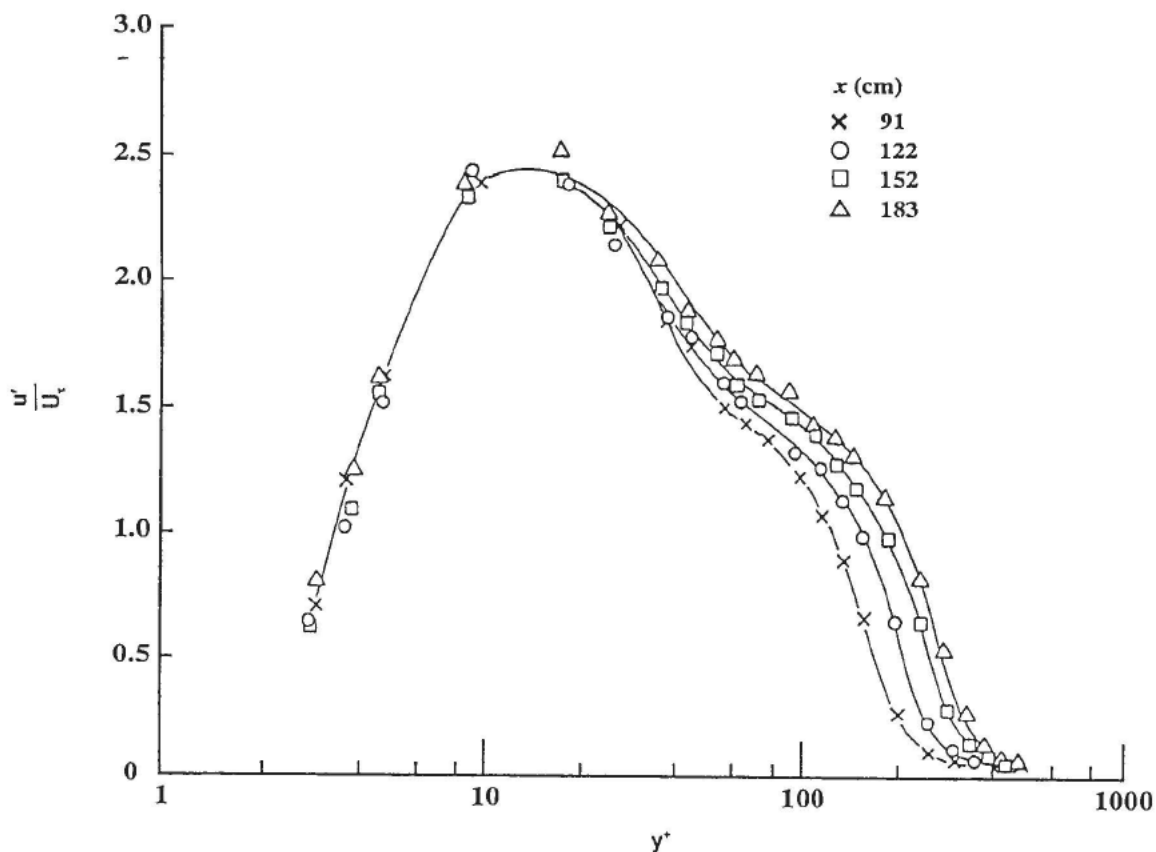


**Figure 17. Distribution of Turbulence Intensity in Wall Variables at Four Different Downstream Locations (Flat-Plate Boundary Layer at  $U_\infty = 2.3$  m / s (Purtell et al., 1981))**

One might argue that the strong Reynolds number effects shown above will eventually subside at sufficiently high Reynolds number. This is not the case, at least up to  $Re_\theta$  of 15,406, as shown in the flat-plate data (figure 18a) of Andreopoulos et al. (1984). The RMS values of the longitudinal velocity fluctuations show strong Reynolds number dependence all the way to the edge of the viscous sublayer. In the buffer layer,  $u'/U_\tau$  decreases as the Reynolds number increases from 3624 to 12,436, thereafter reaching what seems to be a constant value. An opposite trend, that continues for all four Reynolds numbers, is observed in the logarithmic and wake regions. Andreopoulos et al. (1984) indicated that the behavior of their  $u'$  data in the buffer region is in general agreement with the channel-flow results of Laufer (1950), Comte-Bellot (1965), and Zaric (1972).

Andreopoulos et al. (1984) were able to measure the normal velocity component only at the lowest Reynolds number,  $Re_\theta = 3620$ , as shown in figure 18b. The weak second peak in  $v'/U_\tau$  appearing at  $y^+ = 4$  seems to be unique to this particular experiment, but the authors do not comment on this. Reliable  $v'$  measurements could not be obtained by Andreopoulos et al., for higher Reynolds numbers due to limitations of the applicable velocity range of their triple-wire sensor.

The effect of Reynolds number on the inner-layer turbulence in boundary layers is summarized in figure 19; the plot, from four different experiments and a single direct numerical simulation, demonstrates the effect of outer-layer scales on inner-layer turbulence. The peak value of  $u$  turbulence intensity, which occurs at  $12 \leq y^+ \leq 15$ , is plotted normalized by wall variables versus the logarithm of  $Re_\theta$ . In Ueda and Hinze's (1975) experiment, the freestream turbulence  $T_u$  is 0.03 percent, hot wire,  $\ell^+$  is between 2.4 and 6.7, and the measurements have been carried out at 3.4 m downstream of a trip wire. In Erm et al.'s (1985) experiment,  $\ell^+ < 5$  and the measurements have been carried out 0.18 to 1.94 m downstream of stimulator pins. Two sets of Purtell et al.'s (1981) experiments are included where No. 4 floor sanding paper has been used to trip the boundary layer,  $T_u = 0.05$  percent and  $0.8 \leq \ell^+ \leq 3$ . The  $Re_\theta = 465$  data point is from a station 1.07 m downstream of a 15-cm long fetch of sandpaper. The higher  $Re_\theta$  data points are from runs where the sand roughness extended over 61 cm and the measurements were carried out 2.69 m downstream. Note the higher value of the maximum turbulence intensity at the lowest  $Re_\theta$  of the second data set. In the Andreopoulos et al. (1984) experiment,  $1.7 \leq \ell^+ \leq 6.4$ , and the measurements were carried out 3-4 m downstream of a 1 cm-long sandpaper trip (grit height  $\approx 1$  mm).

In figure 19,  $T_u$  or  $\ell^+$  does not explain the variation between the different facilities. Despite the scatter in the different data sets, the general trend is for increasing values of the normalized peak value of  $u_{RMS}$  with Reynolds number, at least initially. The paucity of data at  $Re_\theta > 6000$  precludes making any definitive statement regarding the asymptotic behavior of  $u_{RMS}^+$ . Because  $Re_\theta$  represents outer-layer scales, the figure shows that the outer layer affects the inner-layer  $u$  turbulence. The outer-layer effect seems to be facility dependent even at  $Re_\theta \sim 5 \times 10^3$  and 3.4 m from the trip. The stronger trip effects on turbulence at the higher Reynolds number is

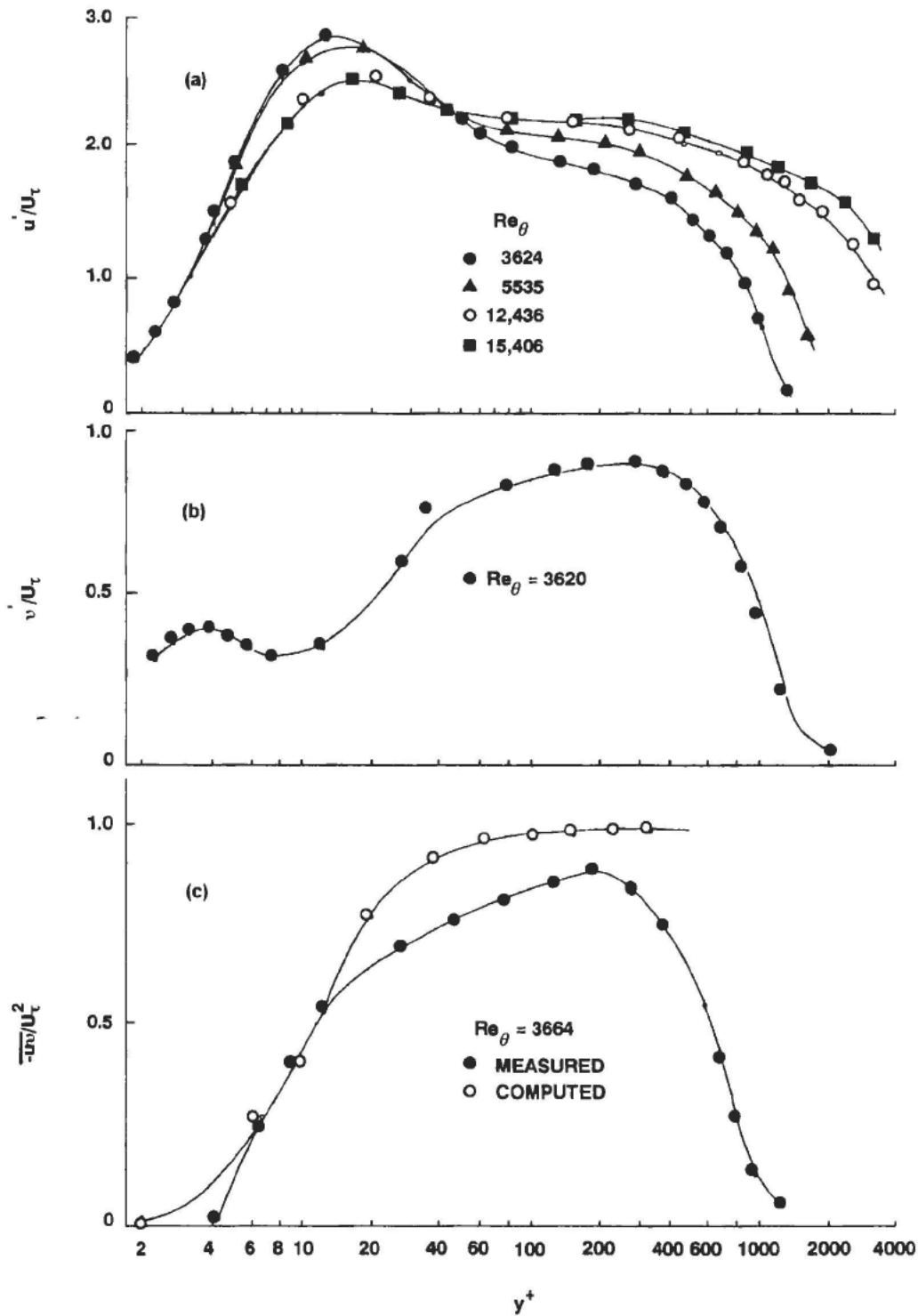


**Figure 18. Normal Profiles of RMS Streamwise Velocity, RMS Normal Velocity, and Reynolds Stress: (a) Root-Mean-Square Values of Longitudinal Velocity Fluctuations at Four Different Reynolds Numbers; (b) Root-Mean-Square Values of Normal Velocity Fluctuations at  $Re_\theta = 3620$ ; (c) Measured and Computed Reynolds Stress Distributions at  $Re_\theta = 3664$  (Andreopoulos et al., 1984)**

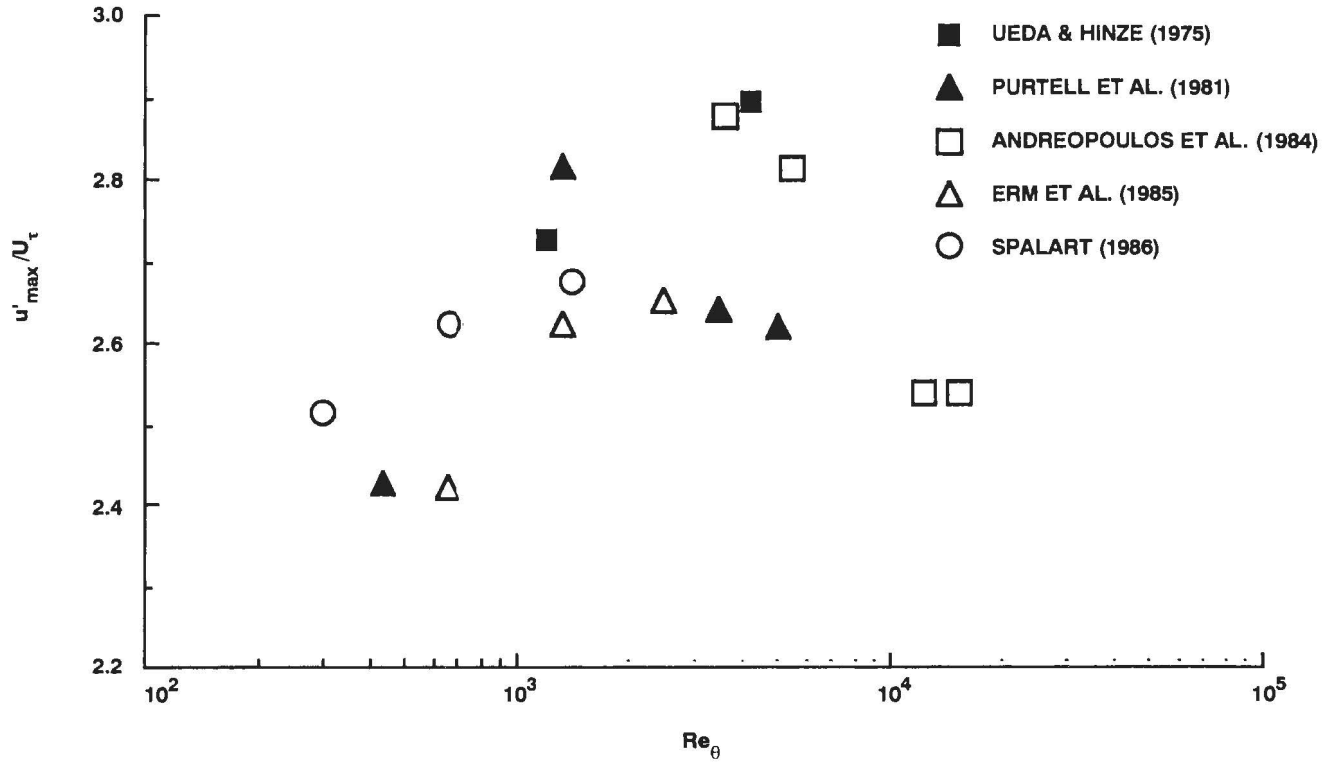


**Figure 19. Peak Value of  $u$  Turbulence Intensity in Turbulent Boundary Layers (Bandyopadhyay, 1991)**

surprising although, as will be shown in section 8.3.2, the mean flow also exhibits a similar behavior.

In figure 19, in three experiments, the maximum value of  $u_{rms} / U_\tau$  first increases rapidly (above 2.8) with Reynolds number before dropping slowly. This behavior is similar to the high Reynolds number mean flow behavior downstream of a trip. The reason for this is not understood; but it is known for the effect of freestream turbulence, length scales  $O(\delta)$  introduced into the outer layer by the trips could be involved. In that case, it is interesting that certain transition devices could affect the turbulence in a boundary layer at high Reynolds numbers even beyond  $85\delta$ . Three data points from the direct numerical simulation of Spalart (1986) are included in the figure and they indicate similar trends to those of the low Reynolds number experiments.

Relatively more data are available for two-dimensional channel flows. Figure 20 depicts Reynolds number effects on the normal profiles of the streamwise turbulence intensity in four different channel flows. Laufer's (1951) experiments were conducted at three Reynolds numbers, based on channel half-width and centerline velocity, of  $Re_a = 12,300$ ;  $30,800$ ; and  $61,600$ . Comte-Bellot (1965) covered the higher range of  $Re_a = 57,000$  and  $230,000$ . Kreplin and Eckelmann's (1979) experiments were conducted at  $Re_a = 3850$ . Johansson and Alfredsson (1982) provided data for  $Re_a = 6900$ ;  $17,300$ ; and  $24,450$ .

Probe resolution problems appear to exist in both Laufer's and Comte-Bellot's high Reynolds number data. In the former experiment, the hot-wire length increased from 3 wall units at the lowest Reynolds number investigated to 13 wall units at the highest Reynolds number, a fourfold loss in spatial resolution. Laufer (1951) observed (erroneously) a corresponding decrease in the peak value of  $u' / U_\tau$  with increasing Reynolds number. Comte-Bellot's (1965) probe length increased from 13-36 viscous lengths as  $Re_\tau$  increased from 57,000 to 230,000. Correspondingly, she also observed (erroneously) a decrease in the peak value of the non-dimensional streamwise turbulence intensity from 2.85 to 2.5. High-quality turbulence data obtained using sufficiently small probes and facilities void of significant trip-memory effects are clearly lacking. In any case, the data in figure 20 indicate that the turbulence intensity profiles do not collapse even deep into the inner layer.

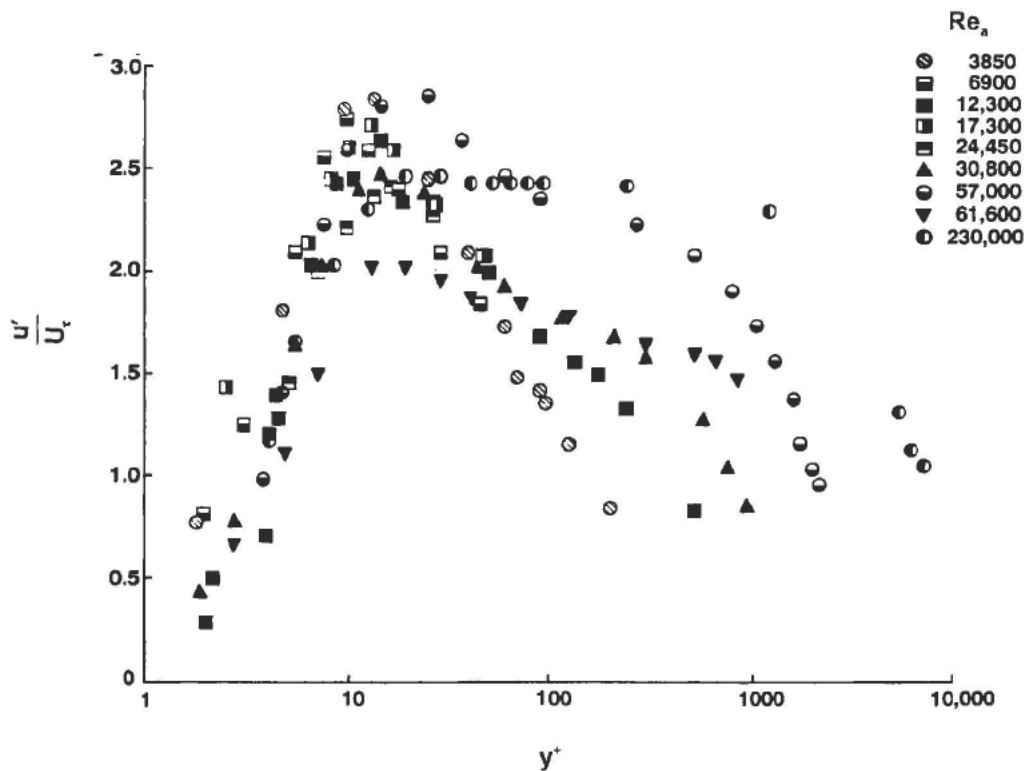


**Figure 20. Streamwise Turbulence Intensity Profiles Non-Dimensionalized With Respect to Inner Variables (Compiled by Wei and Willmarth, 1989)**

Similar trends are observed in the RMS values of the velocity fluctuations normal to the wall. Figure 21 depicts the  $v'$  profiles taken from four different facilities. Laufer's (1951) experiments were conducted at  $Re_a = 12,300$ ; 30,800; and 61,600. Comte-Bellot (1965) covered the higher values of  $Re_a = 57,000$  and 230,000. Eckelmann (1974) provided data for  $Re_a = 2800$  and 4100. Alfredsson and Johansson's (1984) experiments were conducted at  $Re_a = 7500$ . The peak  $v'$  is lower than that for the streamwise fluctuations and occurs further away from the wall. Validity of inner scaling deep into the viscous region cannot be ascertained from this figure because of the scarcity of data for  $y^+ < 30$ .

Due to the poor quality of most of the data in figures 20 and 21, Wei and Willmarth (1989) systematically investigated the Reynolds number effects using a unique high resolution, two-component laser-Doppler anemometer (LDA). To reduce the amount of ambient light in the vicinity of the measuring volume and thus to improve the signal-to-noise ratio of the LDA system, four laser beams were entered and exited into the test section via two narrow slits located at the two side walls of a two-dimensional water channel. Both slots were covered with an extremely thin (17 microns) window of heat shrinking Mylar film, which virtually eliminated optical refraction by the window. The laser beams intersected at a single point away from the wall, and the effective probe length ranged from 0.66 to 6.43 wall units as the Reynolds number was varied in the range of  $Re_a = 3000$  to 40,000. Beam refraction in the path between the laser source and the measuring station was minimized using a specially designed optical head.

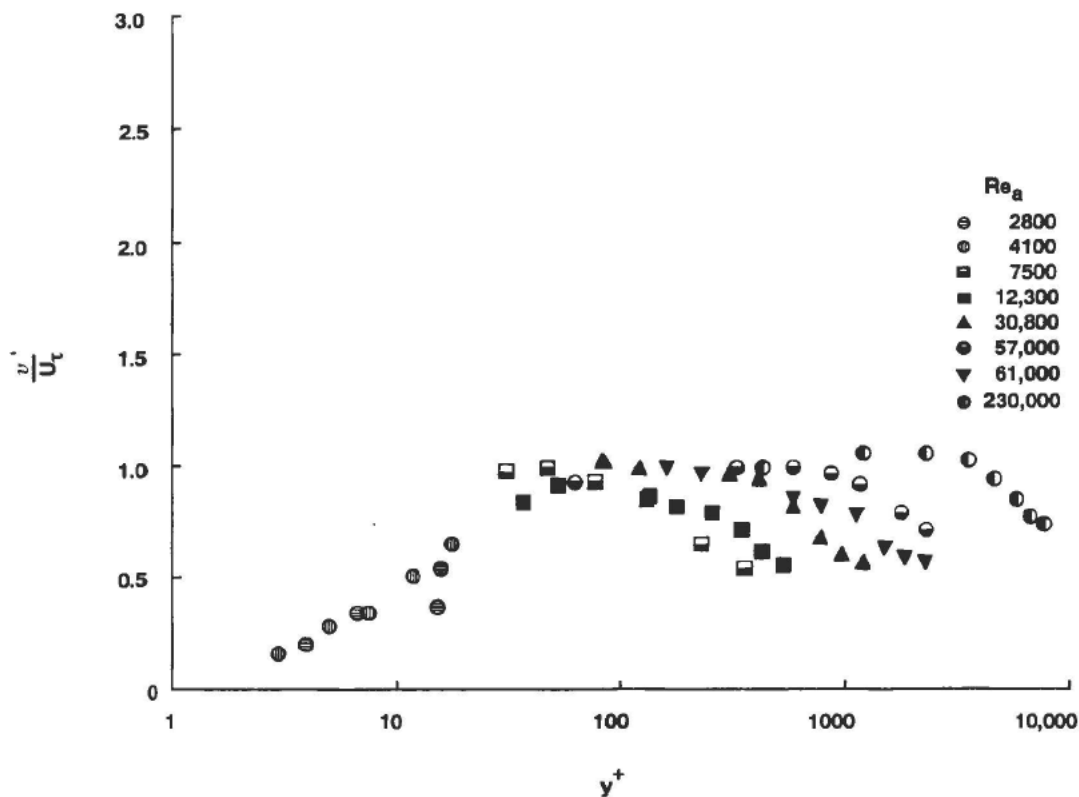


**Figure 21. Normal Turbulence Intensity Profiles Non-Dimensionalized With Respect to Inner Variables (Compiled by Wei and Willmarth, 1989)**

The combination of high spatial resolution and high data rates enabled Wei and Willmarth (1989) to reconstruct accurate time-dependent velocity traces. Their results for the streamwise and normal turbulence intensities are presented in figures 22 and 23. In the former figure,  $u'$  and  $v'$  are non-dimensionalized with the local mean velocity  $U$ , while  $U_\tau$  is used as a velocity scale in figure 23. In figure 22, the intensity of turbulent fluctuations is described relative to the square root of the mean kinetic energy per unit mass at a given distance from the wall. The apparent increase in  $v'/U$  as the surface of the channel is approached violates the continuity equation and is probably caused by reduced measurement resolution very close to the wall.

The inner variable plot in figure 23 allows some instructive comparison with other data in the literature (figures 20 and 21). Wei and Willmarth (1989) ascribe the slight disagreement between the different data sets to a decreased spatial resolution of the hot wires used by Laufer (1951), Comte-Bellot (1965), and Johansson and Alfredsson (1982) at high Reynolds numbers. But, even in the newer data set, the fluctuating turbulence quantities do not scale with wall variables even at as close as 10 viscous lengths from the wall. In fact, inner scaling does not seem to apply to  $v'$  across the entire portion of the viscous region where measurements are available.

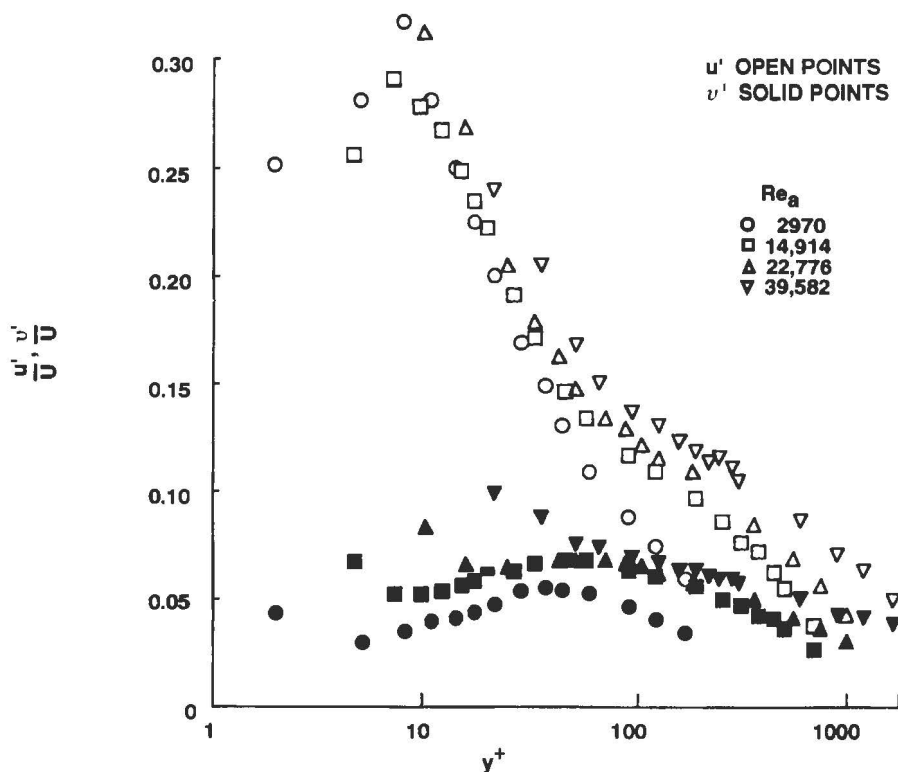


**Figure 22. Profiles of Turbulence Intensity in Streamwise Direction (Open Points) and Direction Normal to Wall (Solid Points), Non-Dimensionalized on Local Mean Velocity (Channel-Flow Data of Wei and Willmarth, 1989)**

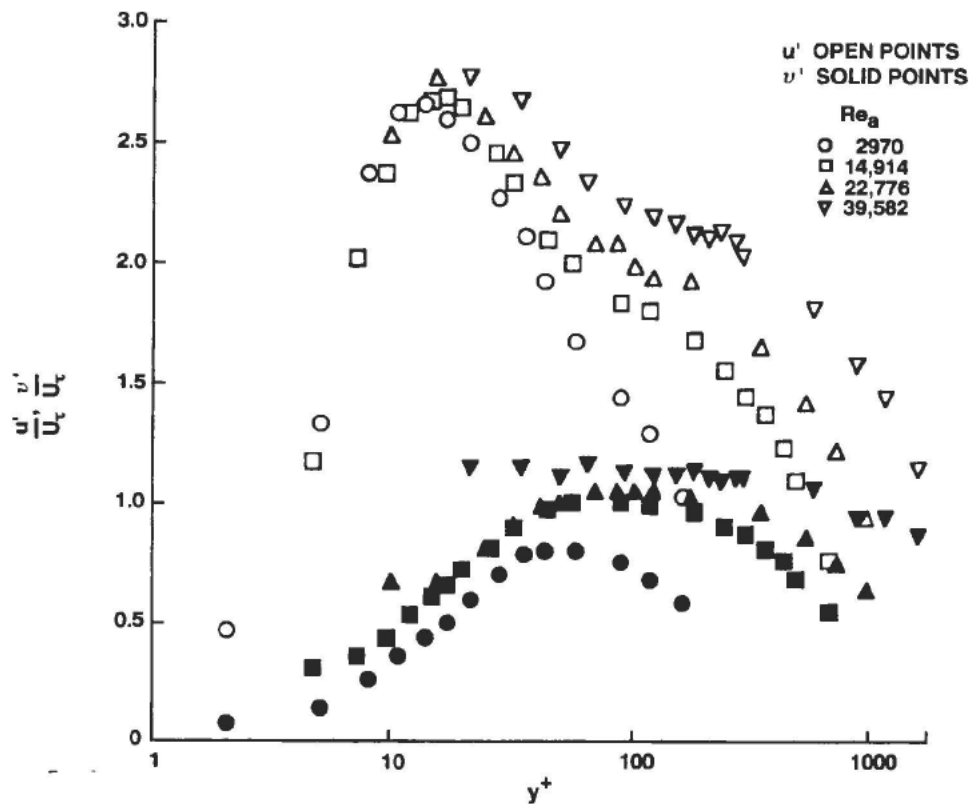


**Figure 23. Profiles of Turbulence Intensity in Streamwise Direction (Open Points) and Direction Normal to Wall (Solid Points), Non-Dimensionalized on Inner Variables (Channel-Flow Data of Wei and Willmarth, 1989)**

More recently, Harder and Tiederman (1991) have studied the behavior of the RMS of the fluctuating streamwise and normal velocities as a function of distance from the wall of a two-dimensional water channel. Their results are depicted in figure 24 for  $Re_a = 9019$ ; 12,663; 19,013; and 21,650. In here,  $u'_{rms}$  peaks at 2.76 for a  $y^+ \approx 15$ , while  $v'_{rms}$  peaks at a  $y^+ \approx 75$  with a value of 1.12. The data are generally 7 percent lower than those of Walker and Tiederman's (1990) experiments indicated by the solid lines in figure 24, but 7 percent higher than the experimental values obtained by Hussain and Reynolds (1975) or the numerical simulation results of Kim et al. (1987).

Harder and Tiederman (1991) assert that, in disagreement with Wei and Willmarth (1989), inner scaling does correlate the data for all Reynolds numbers in the wall region ( $y^+ < 50$ ). However, in the present authors opinion, the range of Reynolds numbers investigated by Harder and Tiederman (1990) is too narrow to make such a claim. The dependence on Reynolds number in the inner region is a rather weak one, and a substantial change in  $Re_a$  is needed to ensure a measurable effect. Typically, the turbulence intensity changes by only a few percentage points when the Reynolds number changes by 100 percent. The ratio of the largest to smallest  $Re_a$  in Wei and Willmarth's study is about 13, while it is only 2.4 in Harder and Tiederman's.

Additional support for Wei and Willmarth's (1989) basic conclusion that turbulence quantities in the near-wall region do not scale on wall variables comes from the boundary layer experiments of Purtell et al. (1981) and Andreopoulos et al. (1984), referenced earlier in this section, as well as from the physical and numerical channel-flow experiments conducted by Antonia et al. (1992) and the flat-plate experiments of Murlis et al. (1982), Wark and Nagib (1991), and Naguib and Wark (1992). It is, of course, conceivable that wall-layer scaling might apply over the entire inner layer provided that the Reynolds number is high enough, but at the moment at least such ultra-high Reynolds number experiments cannot be conducted with sufficient probe resolution.

The effect of Reynolds number on the inner-layer turbulence in channel flows is summarized in figure 25, compiled by Bandyopadhyay (1991). The peak value of  $u$  turbulence intensity, which occurs at  $12 \leq y^+ \leq 15$ , is plotted normalized by wall variables. The data in the figure are compiled from the experiments conducted by Laufer (1951), Grass (1971), Eckelman (1974), Johansson and Alfredsson (1982), and Wei and Willmarth (1989) in five different facilities. For all the data points shown in figure 25, probe resolution is better than 7 wall units. The data follow the general trends reported by Wei and Willmarth (1989), and the solid line in the figure is a least-square fit to all the points. The peak value in channel flows seems to be increasing monotonically with Reynolds number, at least up to  $Re_a = 23,000$ . Confidence in the data in this figure is, in general, higher than that for the boundary layer results summarized in figure 19. There, post-transition memory effects may have played a role, that remains ill understood, in the observed trends.

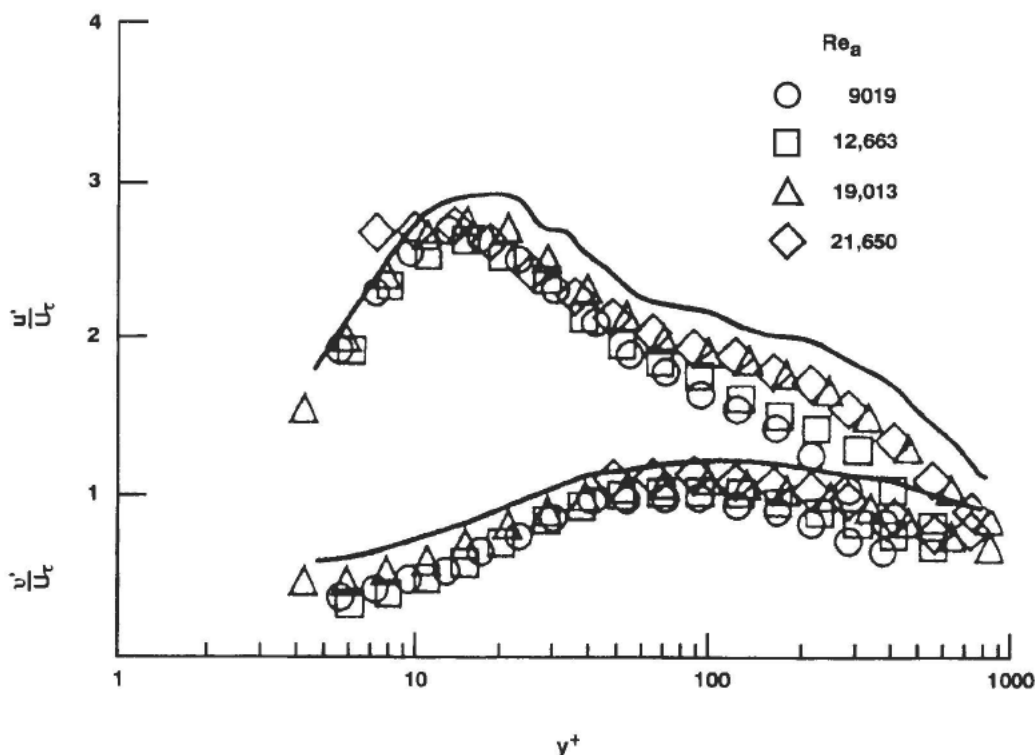


**Figure 24. Profiles of Turbulence Intensity in Streamwise Direction and Direction Normal to Wall, Non-Dimensionalized on Inner Variables (Channel-flow data of Harder and Tiederman, 1991. Solid lines are best fit to Walker and Tiederman's 1990 data.)**

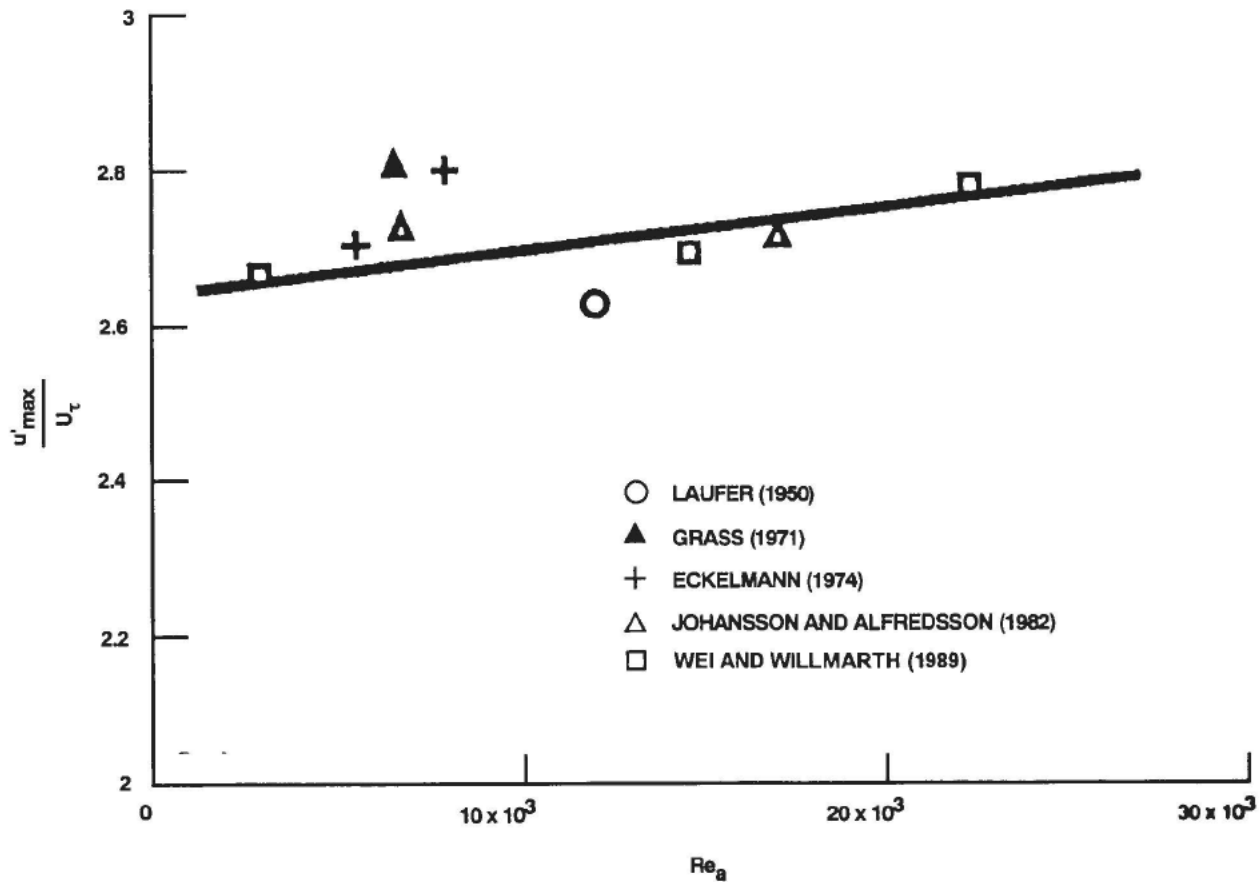


**Figure 25. Peak Value of  $u$  Turbulence Intensity in Two-Dimensional Channel Flows (Bandyopadhyay, 1991)**

Perry and Abell (1975) provide pipe-flow data for the Reynolds number range of  $Re_a = 40,000$ -130,000. An example of their data is shown in figure 26. The streamwise turbulence intensity in wall units is plotted versus  $y^+$  for four different Reynolds numbers. As a consequence of the existence of a constant-stress regime, a distinct region of constant turbulence level appears for each of the four Reynolds numbers investigated (section 3.2 and equation (9)). Although scaling with inner variables appears to collapse the pipe-flow data in the inner region, contrary to the boundary-layer and channel-flow data discussed earlier, it should be noted that the data in figure 26 have been obtained with a hot wire whose length has ranged from 35 to 100 wall units as the Reynolds number changed in the indicated range. According to the criterion that have been established earlier in this report, Perry and Abell's probe resolution is insufficient to prove or refute the existence of similarity with inner variables.

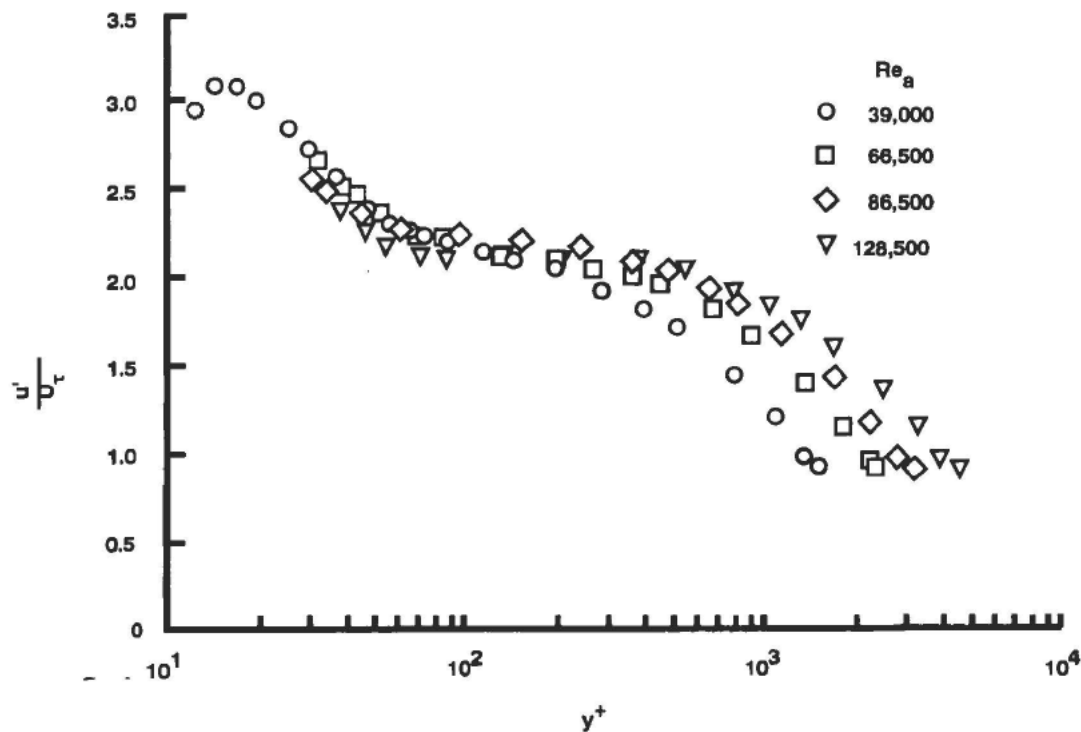


**Figure 26. Streamwise Turbulence Intensity Profiles Non-Dimensionalized With Respect to Inner Variables**  
*(High Reynolds Number Pipe-Flow Experiments of Perry and Abel, 1975)*

## 6.2 REYNOLDS STRESS

### 6.2.1 Reynolds Number Effects

Turbulence shear stress, or Reynolds stress  $-\rho \overline{uv}$ , is the most important dynamical quantity affecting the mean motion. The major portion of the momentum transported in a two-dimensional turbulent wall-bounded flow is accomplished by  $-\overline{uv}$ . Therefore, modeling the behavior of Reynolds stress is one of the primary objectives of various prediction schemes. Simultaneous measurements of the streamwise and normal velocity fluctuations are required to compute the Reynolds stress at any particular point in the flow field. Provided this is done with high fidelity in the low to moderate Reynolds number laboratory experiments, extrapolation to the higher Reynolds number field conditions is only possible if Reynolds number effects are well understood. A review of those effects in boundary layers, channels, and pipes are found in this subsection.

In boundary layers, the normalized cross correlation  $-\overline{uv}$  was plotted in figure 18c, for a single Reynolds number of  $Re_\theta = 3664$ . Again, Andreopoulos et al. (1984) were unable to measure the Reynolds stress reliably at higher Reynolds numbers due to limitations of the applicable velocity range of their triple-wire probe. The directly measured turbulence shear stress is on the average 10 percent smaller than theoretical distribution deduced from the momentum balance and mean-flow data shown by the open symbols in figure 18c.

More data are available for two-dimensional channel flows. The (kinematic) Reynolds stress normalized with the friction velocity is plotted versus the distance normal to the wall normalized with the channel half-width in figures 27 and 28. In both figures, the data points are directly computed by averaging the product of the measured  $u$  and  $v$  velocity fluctuations, and the solid line represents the theoretical total shear stress profile. In figure 27, data from four different experiments are presented; the solid line represents total shear stress profile. Eckelmann (1974), using an oil channel, covered the low Reynolds numbers of 2800 and 4100. Alfredsson and Johansson (1984) conducted their experiment at  $Re_a = 7500$ , while Kastrinakis and Eckelmann (1983) conducted theirs at  $Re_a = 12,600$ . Comte-Bellot (1965) covered the higher range of Reynolds number of 57,000 and 230,000.

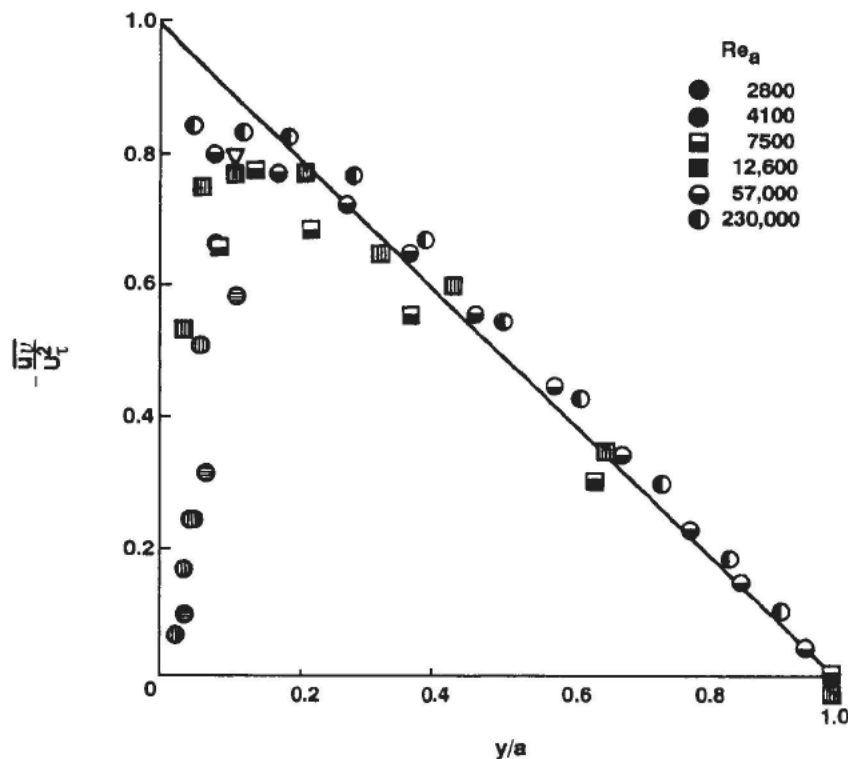


**Figure 27. Reynolds Stress Profiles in Wall Units vs Distance From Wall Normalized With Channel Half-Width (Compiled by Wei and Willmarth, 1989)**

The data of Wei and Willmarth (1989) covered the Reynolds number range (four different Reynolds numbers) of 2970 to 39,582, and are reproduced in the linear plot shown in figure 28. Their high-resolution LDA allows measurements very close to the wall where the Reynolds stress is decreasing. The maxima of the non-dimensional turbulence shear stress profiles increase in magnitude and are closer to the wall as the Reynolds number increases.

The same data above are plotted versus  $y^+$  in figure 29. Here, the semi-log plot allows closer inspection of the near-wall region, and Reynolds number effects are demonstrated more clearly. The maximum value of the normalized turbulence shear stress is not the same for each profile, indicating the lack of inner scaling in the Reynolds number range investigated. When expressed in wall units, the location of peak Reynolds stress moves away from the wall as the Reynolds number increases.

One advantage of investigating fully developed pipe or channel flows is the ability to compare measurements with the computed Reynolds stress using the mean-velocity profile and pressure gradient, two quantities that are easier to measure. This has the advantage of being able to check the accuracy of the directly measured Reynolds stress, especially near the wall where probe resolution problems are particularly acute. In a fully-developed channel or pipe flow, the average normal and spanwise velocities vanish, there are no mean longitudinal velocity or Reynolds stress variations in the streamwise and spanwise directions, and the pressure gradient is a constant. The longitudinal momentum equation could then be integrated to give an exact relation between the Reynolds stress and mean-velocity distribution:

$$-\overline{uv} = -\nu (dU / dy) + U_\tau^2 (1 - y / a), \quad (26)$$

where  $U(y)$  is the streamwise mean-velocity distribution and  $a$  is the channel half-width or pipe radius. The friction velocity, or the slope of the velocity profile at the wall, is related to the constant pressure gradient through

$$U_\tau^2 = \nu (dU / dy)_w = -(a / \rho)(dP / dx), \quad (27)$$

where  $P$  is the static pressure and  $\rho$  and  $\nu$  are the fluid density and kinematic viscosity, respectively. In wall units, the momentum balance equation (24) reads

$$-\overline{uv}^+ = -(dU^+ / dy^+) + (1 - y^+ / a^+). \quad (28)$$

Wei and Willmarth (1989) used equation (26) to compute the Reynolds stress profiles shown by the solid lines in figure 29. Again, the non-dimensional profiles at different Reynolds numbers do not collapse in the outer and logarithmic regions and even well into the viscous region. Except very close to the wall, the agreement between the directly measured Reynolds stress and that computed from the measured mean velocity and pressure gradient is very good and attests to the accuracy of the instantaneous velocity traces reconstructed, filtered, and smoothed from the Doppler burst detector and processor signals. Wei and Willmarth speculate that the divergence

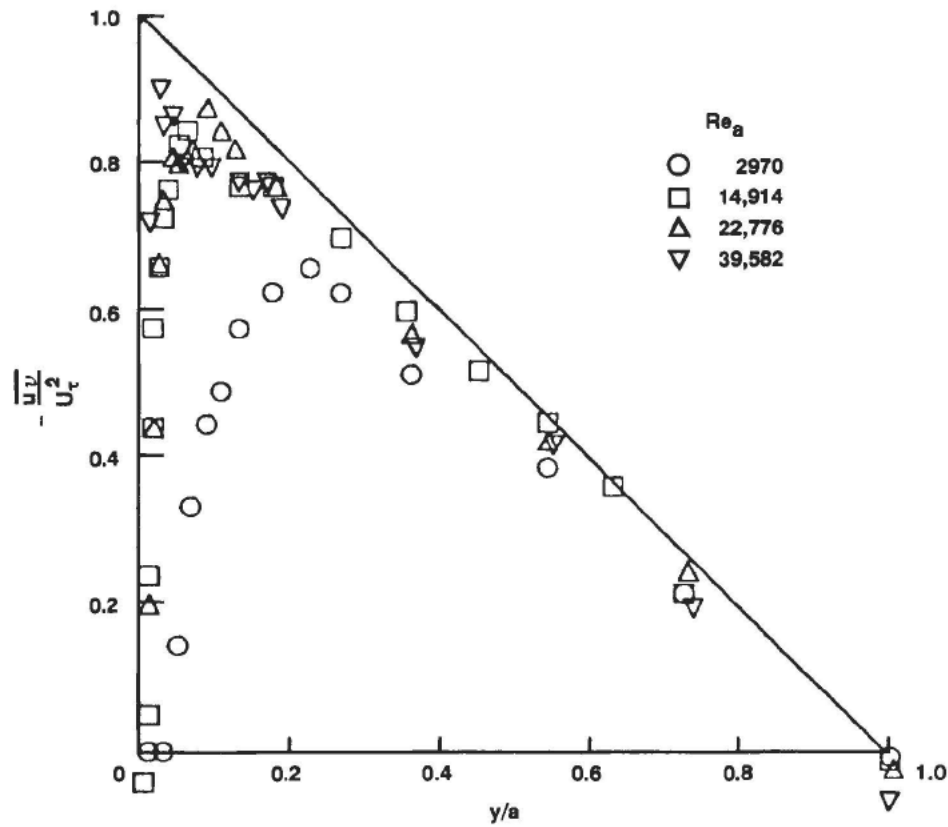


**Figure 28. Reynolds Stress Profiles in Wall Units vs Distance From Wall Normalized With Channel Half-Width (Channel-Flow Data of Wei and Wilmarth, 1989)**

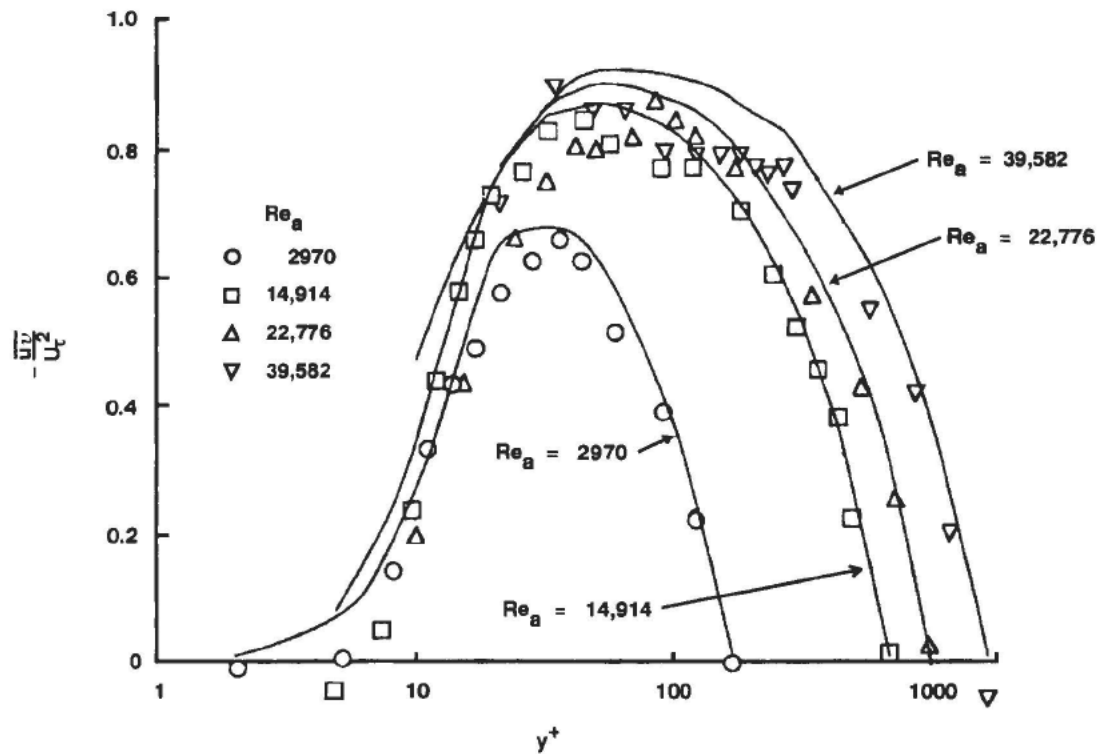


**Figure 29. Reynolds Stress Profiles Non-Dimensionalized on Inner Variables (Channel-Flow Data of Wei and Willmarth, 1989)**

between the directly measured and computed Reynolds stresses is due to insufficient spatial and temporal resolution in the direct LDA measurement very close to the wall.

The Reynolds stress profiles measured in a water channel by Harder and Tiederman (1991) are reproduced, non-dimensionalized with inner variables, in figure 30. The range of Reynolds numbers investigated,  $Re_a = 9019$  to  $21,650$ , is narrower than that studied by Wei and Willmarth (1989). Not surprisingly, then, Harder and Tiederman assert that, for  $y^+ < 50$ , inner scaling correlates their data for all four Reynolds numbers.

Wei and Willmarth (1989) also computed the turbulence kinetic energy production using both the directly measured Reynolds stress and the momentum balance equation. The profiles for four different Reynolds numbers are shown non-dimensionalized with inner variables in figure 31. Excepting very close to the wall, the two methods of computing  $-\overline{uv} (dU/dy)$  agree within 10 percent. Neither method leads to a profile collapse even in the viscous region. The maximum value of kinetic energy production obtained from the momentum balance (indicated by the solid lines) increases with Reynolds number. The data point nearest to the wall measured at  $Re_a = 22,776$  appears to be in error. Interestingly, while the position of peak Reynolds stress, expressed in wall units, moves away from the wall as the Reynolds number increases (figure 29), the peak turbulence production seems to be fixed at  $y^+ \approx 12 - 15$ . This point will be discussed later in this section and once more in section 7.

The measurements of mean velocity and pressure drop in the smooth-pipe-flow experiments of Nikuradse (1932) and Laufer (1954) were used to compute the Reynolds stress profiles shown previously in figure 4. The Reynolds number in that figure,  $Re^* = U_\tau a / \nu$ , is the ratio of the pipe radius to the viscous length scale and varies over the wide range of  $140$ - $55,400$ . A constant-turbulent-shear-stress region is clear at the highest Reynolds number. As in the channel flows, the peak value of normalized Reynolds stress increases and its location, relative to the viscous length scale, moves away from the wall as the Reynolds number increases.

### 6.2.2 Peak Location

Sreenivasan (1989) analyzed several different wall-bounded flow experiments. The distance from the wall, expressed in inner variables, where the streamwise turbulence intensity peaks appears to be independent of Reynolds number (figure 16 of his paper). In contrast, the location of the largest normal fluctuations occur is a strong function of Reynolds number (figure 17 of his paper):

$$[y^+]_{v'_{max}} = [Re^*]^{0.75}, \quad (29)$$

where  $Re^*$  is the pipe radius or boundary layer thickness in wall units. Available data on the spanwise intensity are scarce and no conclusion can be reached on the scaling of its peak position. For the total turbulence kinetic energy, however, the position of its peak does scale on wall variables, much the same as  $u'$ . This is because the near-wall value of the total fluctuation energy is essentially overwhelmed by the streamwise component.

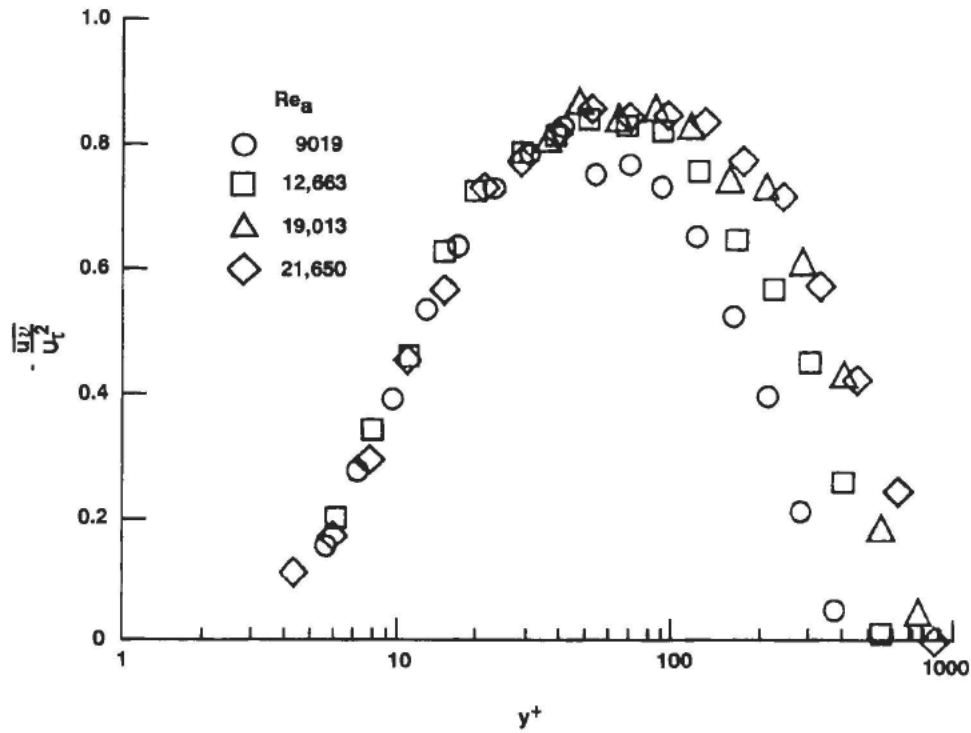


**Figure 30.** *Reynolds Stress Profiles Non-Dimensionalized on Inner Variables (Channel-Flow Data of Harder and Tiederman, 1991)*

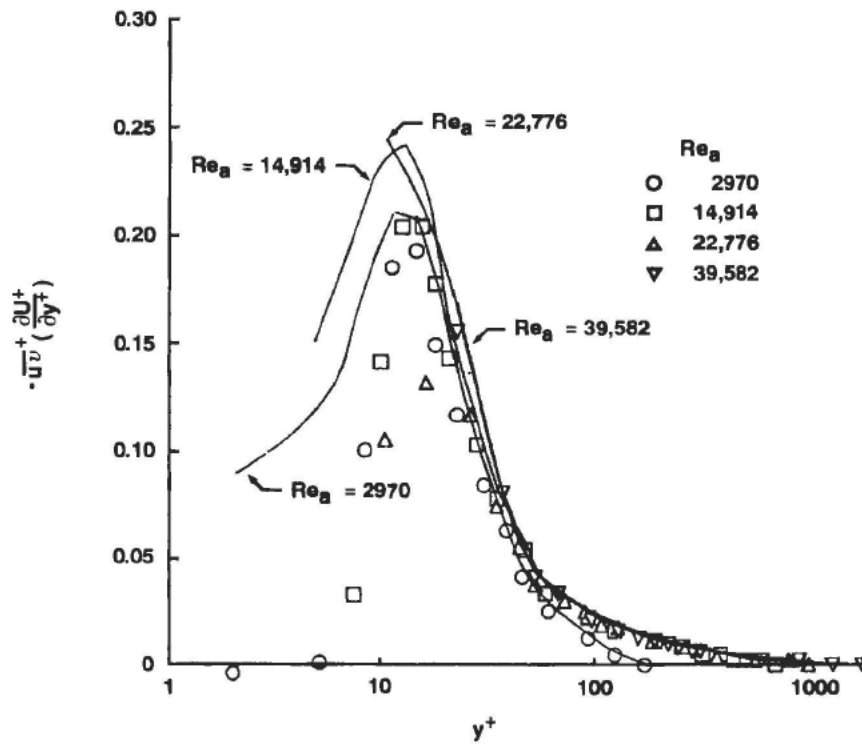


**Figure 31.** *Turbulence Kinetic Energy Production Profiles (Channel-Flow Data of Wei and Willmarth, 1989)*

Similar to the normal fluctuations, the peak Reynolds stress occurs at increasingly higher values of  $y^+$  as the Reynolds number increases as shown in figures 32a and 32b, compiled from directly measured and computed turbulence shear stress data, respectively. The lowermost two data points in figure 32b correspond to the location of the peak Reynolds stress, or the critical layer position, in typical transitional boundary layer and channel flows.

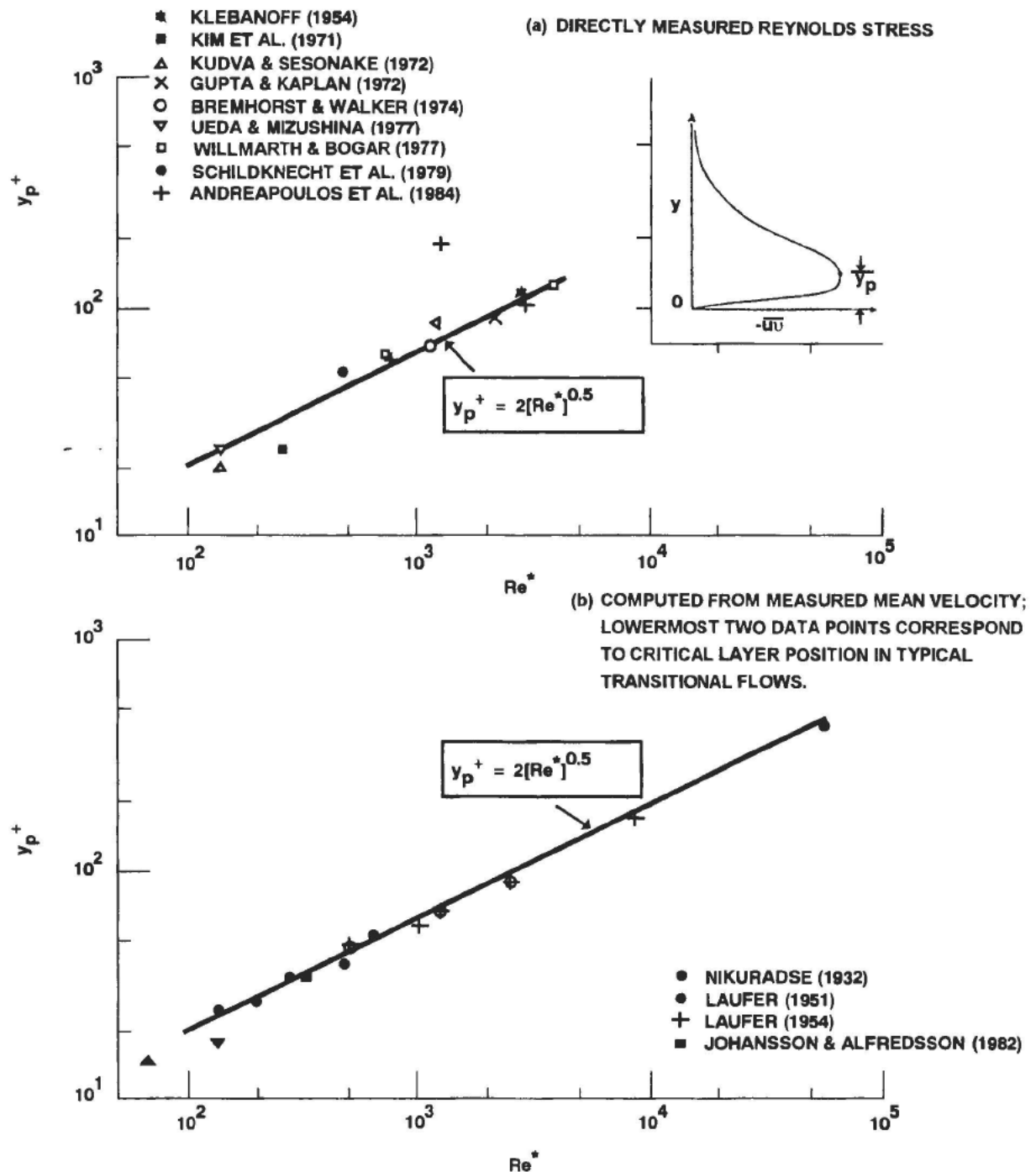


Figure 32. Location of Peak Reynolds Stress as Function of Reynolds Number  
(Data Compiled by Sreenivasan, 1988)

A least-squares fit (solid lines) of all the data points in both figures leads to the same equation:

$$[y_p^+] = 2[Re^*]^{0.5}, \quad (30)$$

where  $y_p$  is the location of peak Reynolds stress. Note that although probe resolution has a significant effect on the magnitude of turbulence intensity, Reynolds stress, or other higher-order statistics, a relatively long probe should have less effect on the accuracy of determining the peak location of these quantities. Therefore, it is not surprising that Sreenivasan (1989) could use a variety of data sources, including some with insufficient probe resolution, to arrive at the correlations in equations (29) and (30).

Equation (30) indicates that the location of the peak turbulence stress scales on the geometric mean of the inner and outer scales. Recall that, because this is the position in Sreenivasan's (1988) model discussed in section 4, where all the mean vorticity of a turbulent boundary layer has been assumed to be concentrated into a single sheet, the correlation in equation (30) gives some credence to his hypothesis.

Note that if a velocity profile is assumed for the case of fully developed channel flow, exact expressions for the location of the peak Reynolds stress and turbulence kinetic energy production could be derived from equation 26. For example, if the logarithmic mean velocity profile,<sup>†</sup> equation (8) is used, the peak Reynolds stress occurs at  $y_p^+ = 1.56 Re^{*0.5}$ , while the peak production occurs at a fixed  $y^+$ .

At high Reynolds numbers, the peak Reynolds stress occurs substantially outside the viscous region. Note however that, due to the shrinking of the inner layer as the Reynolds number increases, this peak location moves closer to the wall as a fraction of the boundary layer thickness. Interestingly, while the most significant Reynolds stress-producing activity does not occur at a universal value of  $y^+$ , the production of turbulence kinetic energy,  $-\overline{uv}(dU/dy)$ , does always peak at  $y^+ \approx 15$ . This implies that, at high Reynolds numbers where the two positions dispart, the scales producing the Reynolds stress are quite different from those responsible for the turbulence kinetic energy production. This observation led Townsend (1961) to hypothesize the existence of an *active motion* and an *inactive motion* within the inner layer. The former is due to the vorticity field of the inner-layer proper and is responsible for Reynolds stress production. The statistical properties of the active motion are presumably universal functions of the distance from the wall. The inactive, larger-scale motion is partly caused by the irrotational field sloshing associated with the pressure fluctuations in the outer layer and partly by the large-scale vorticity field of the outer-layer turbulence, which the inner layer sees as an unsteady external stream (see also the substantive measurements of Bradshaw, 1967). The inactive motion does not scale with inner variables, and is characterized by intense velocity fluctuations. The effect of increasing the Reynolds number can then be thought of as the increasing significance of the inactive motion.

---

<sup>†</sup> Not an accurate assumption for  $y^+ < 30$ .

The primary conclusion of this subsection is that Reynolds number does have an effect on the turbulence shear stress even in the inner layer. Inner scaling fails to collapse the Reynolds stress profiles. The peak value of  $-\overline{uv}$  increases with Reynolds number and its position moves outward when expressed in wall units.

### 6.2.3 Asymptotic Theory

The results depicted in sections 6.1, 6.2.1, and 6.2.2 indicate that inner scaling fails to collapse the profiles for the Reynolds stress and for the RMS values of the velocity fluctuations. Considerable Reynolds number effects are exhibited even for  $y^+$  values less than 100. Panton (1990a) points out that a turbulent wall-bounded flow is fundamentally a two-layer structure, which is a classical single perturbation situation. At finite Reynolds numbers, neither the inner layer representation nor the outer layer representation is a uniformly valid approximation to the true answer in the matching region. As  $Re^*$  varies, the overlap layer changes in size and the proportions of inner and outer effects are altered.

A uniformly valid answer for the present singular perturbation problem could be obtained by forming an additive composite expansion from the inner and outer expansions. Matching essentially replaces the two lost boundary conditions at  $y = 0$  and  $y = \infty$ , and the additive composite expansion is simply the sum of the inner and outer ones minus the common part (e.g., Van Dyke, 1974). Systematic changes with Reynolds numbers that are considered anomalies when turbulence quantities are expressed as inner expansions could then be considered as proper first-order trends that are expected when viewed in the proper light. Such treatments were demonstrated for the mean flow (Panton, 1990b), for the RMS turbulence fluctuations (Panton, 1991) and for the Reynolds stress (Panton, 1990a). RMS values of the velocity fluctuations or Reynolds stress expressed as additive composite expansions are equivalent in accuracy to the mean velocity expressed as the law of the wall plus the law of the wake.

For the mean flow, Panton (1990a) suggests the use of an inner velocity scale that is different from the friction velocity (see equation (7) in this report), the two being equal only in the limit of infinite Reynolds number. Within the framework of an asymptotic theory (Yajnik, 1970; Afzal, 1976; Afzal and Bush, 1985), the lowest-order equation for the mean flow shows weak Reynolds number dependence while that for the Reynolds stress indicates a much stronger effect. According to Panton (1990a), the logarithmic nature of the inner, outer, and composite expansions for the mean flow dictates minimal Reynolds number effects. On the other hand, the Reynolds stress behaves algebraically and the inner/outer effects are mixed in different proportions and occur at different locations, resulting in strong Reynolds number dependency even in the first-order theory. Moreover, the additive composite expansion for the Reynolds stress does not evince a constant-stress region; only the inner expansion does so.

### 6.3 SPECTRA

It is often useful to analyze the kinetic energy of the turbulent fluctuations according to its distribution over the various frequencies occurring in these fluctuations. The energy (or power) density spectrum of the fluctuating velocity components or Reynolds stress is computed from the respective instantaneous, digitized signals, and can yield information regarding structural evolution as the Reynolds number changes. Consider the channel-flow data of Wei and Willmarth (1989) taken at  $y^+ = 15$  at three different Reynolds numbers:  $Re_a = 2970$ ; 14,914; and 22,776. The power spectra of the streamwise velocity fluctuations non-dimensionalized with inner variables are plotted versus the angular frequency in wall units on a semi-log scale in figure 33a and on a log-log scale in figure 33b. The normalization employed in these figures is that used by Perry and Abell (1975) and is such that the area under each curve is the mean-square of the velocity fluctuations in wall units. Essentially

$$\Phi^+(\omega^+) = \omega^+ \Phi(\omega) / \nu, \quad (31)$$

$$\omega^+ = \omega \nu / U \tau^2, \quad (32)$$

where  $\Phi(\omega)$  is the power spectral density of the velocity (or Reynolds stress) fluctuations,  $\omega$  is the radian frequency, and  $\omega^+$  is the frequency scaled with inner variables.

Although there is appreciable scatter at lower frequencies (in the semi-log plot),<sup>†</sup> the  $u$  power spectra in figure 33 suggest that the energy-containing eddies scale on inner variables in the vicinity of the kinetic energy production peak,  $y^+ = 15$ . However, at high frequencies, the spectra begin to diverge from inner-layer scaling and greater energy is available with increasing Reynolds number (see the log-log plot in figure 33b, which emphasizes the low-energy portion of the spectrum). This is consistent with the appearance of smaller eddies and increased vortex stretching at higher Reynolds numbers (discussed in section 7). Notice that the increase in the streamwise turbulence kinetic energy with Reynolds number is very slight, consistent with the near collapse of  $u'$  data for  $y^+ \leq 15$  (figure 23).

Normalized plots similar to figure 33a but for the near-wall normal velocity fluctuations and Reynolds stress are given in figures 34 and 35, respectively. Neither set of plots scale on inner variables over a large portion of the energy-containing frequency range. This is consistent with Wei and Willmarth's (1989) assertion that neither the  $v'$  profiles nor the  $-\overline{uv}$  profiles scale on inner variables even very close to the wall (figures 23 and 29 in this report).

---

<sup>†</sup> As will be shown in figures 34 and 35, there is even more scatter in the  $v$ - and  $uv$ -spectra when similarly plotted on semi-log plots.

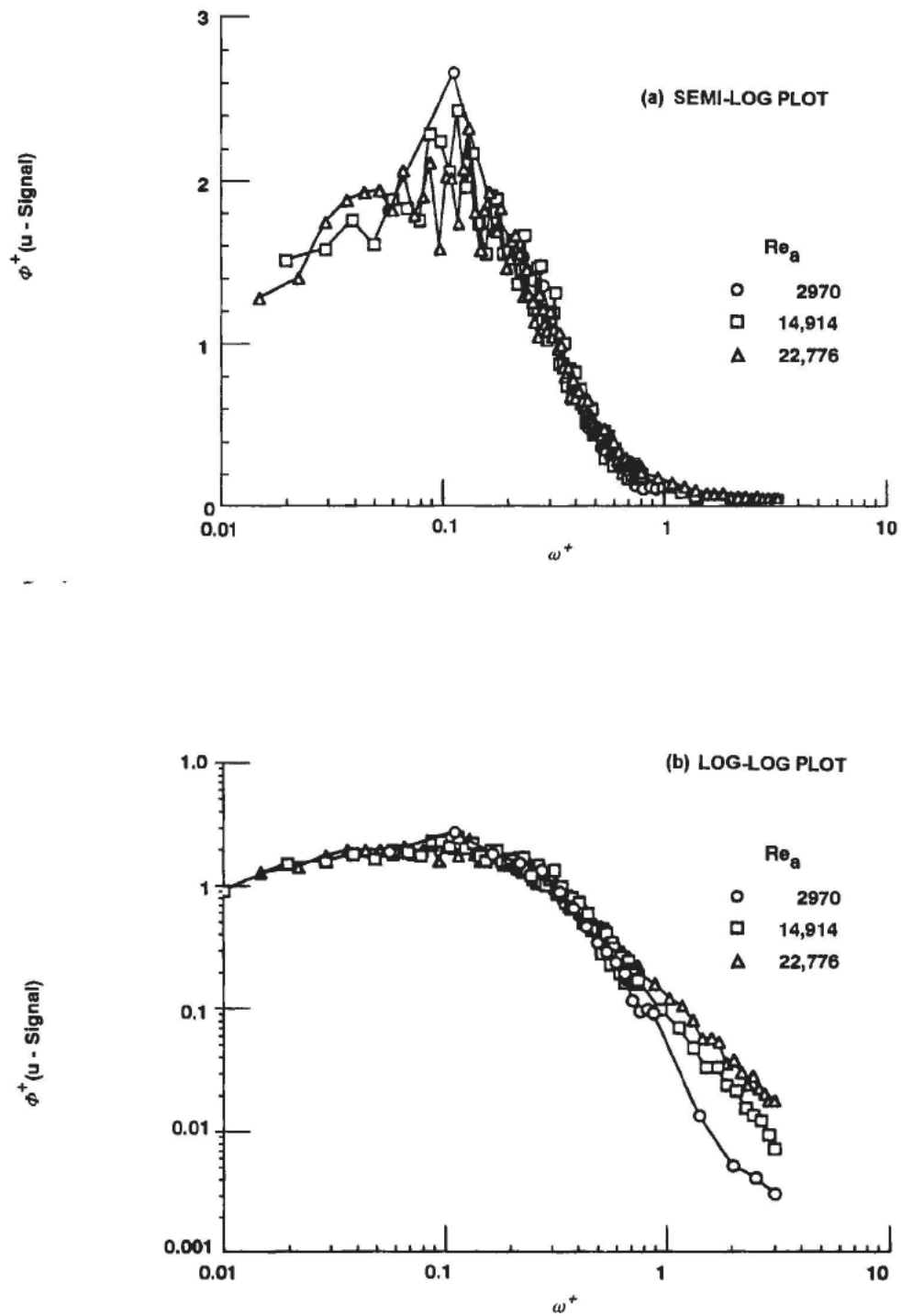


**Figure 33. Power Spectra of Streamwise Velocity Fluctuations at  $y^+ = 15$  (Wei and Willmarth, 1989)**

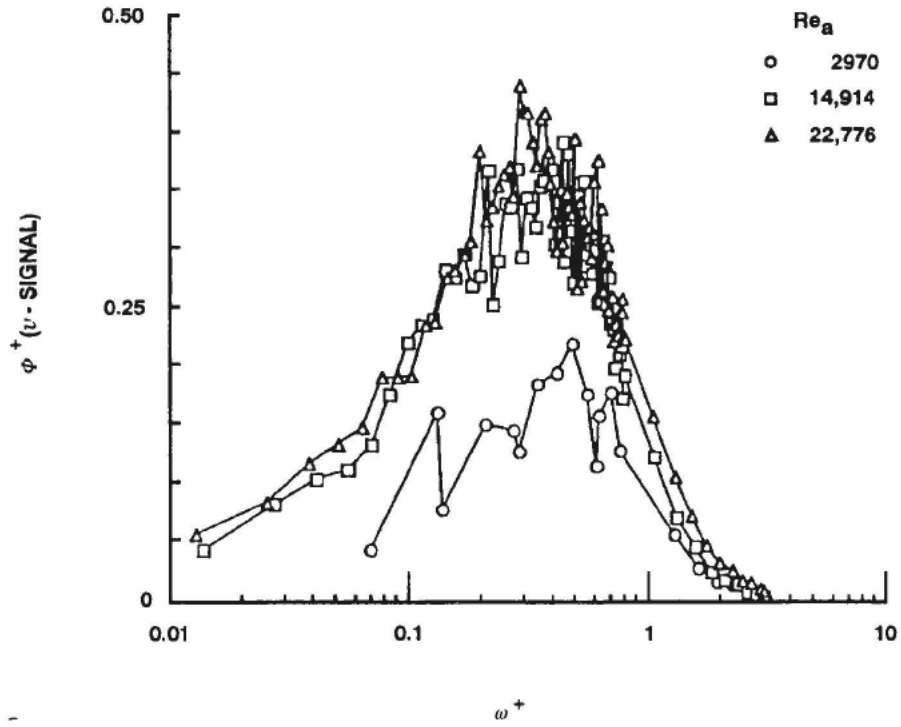


**Figure 34. Power Spectra of Normal Velocity Fluctuations at  $y^+ = 15$**   
(Channel-Flow Data From Wei and Willmarth, 1989)

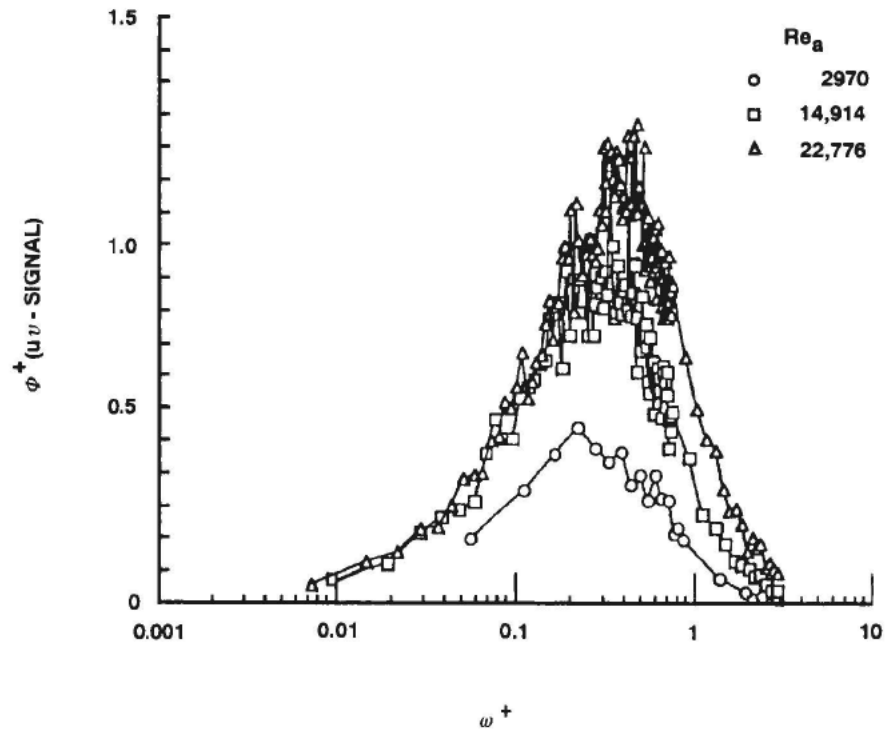


**Figure 35. Power Spectra of Reynolds Stress Fluctuations at  $y^+ = 15$**   
(Channel-Flow Data From Wei and Willmarth, 1989)

The power spectra of the streamwise velocity, normal velocity, and Reynolds stress in the same channel flow as above, but near the edge of the inner layer,  $y^+ = 125$ , are shown in figures 36, 37, and 38, respectively. Again, the area under each spectrum represents the mean square of the corresponding velocity or Reynolds stress fluctuations normalized with inner variables. Reynolds number effects on the high frequency portion of the spectrum appear to be less pronounced at this distance farther away from the wall as compared with the spectra in the near-wall region depicted in figures 33-35. Because the mean-velocity gradient decreases with increasing distance from the wall; Wei and Willmarth (1989) attribute the weaker Reynolds number-dependence to a diminished stretching of vorticity farther away from the wall. On the other hand, in the low-frequency portion of the spectra, Reynolds number effects are stronger. The lack of scaling with inner variables at  $y^+ = 125$  is consistent with the measurements of Bradshaw (1967) and is due to the large-scale inactive motion.

The power spectra of the streamwise velocity fluctuations in the high Reynolds number pipe-flow experiment of Perry and Abell (1975) are shown in figure 39. In this normalized log-log plot,  $\Phi(ky)/U\tau^2$  is plotted versus  $ky$ , where  $k$  is the wavenumber. The data points represent several Reynolds numbers in the range of  $Re_a = 40,000$ -130,000, and several distances from the wall in the range of  $y^+ = 150$ -444. These distances correspond to the region of overlap where  $y$  is much larger than the viscous length scale but much smaller than the outer scale (see section 3.2). In this constant-Reynolds stress regime, the spectrum does not change with wall distance. The straight line in the log-log plot has the slope of -1, predicted for the equilibrium range of the spectrum using scaling arguments (see Sreenivasan, 1989). The large-scale fluctuations outside this equilibrium range constitute the so-called inactive motion mentioned earlier. At the other end of the scale, the smaller eddies (high wavenumbers) either obey the usual -5/3 Kolmogorov law provided the Reynolds number is high enough to create an inertial subrange, or simply be dominated by viscosity at low Reynolds numbers.

In summary, only the  $u$  turbulence spectra scale with inner variables very close to the wall ( $y^+ \leq 15$ ), while those for  $v$  and  $uv$  do not. In the constant stress layer and over a wide range of Reynolds numbers, the spectrum of the longitudinal velocity fluctuations has a -1 slope in the equilibrium range of eddies.

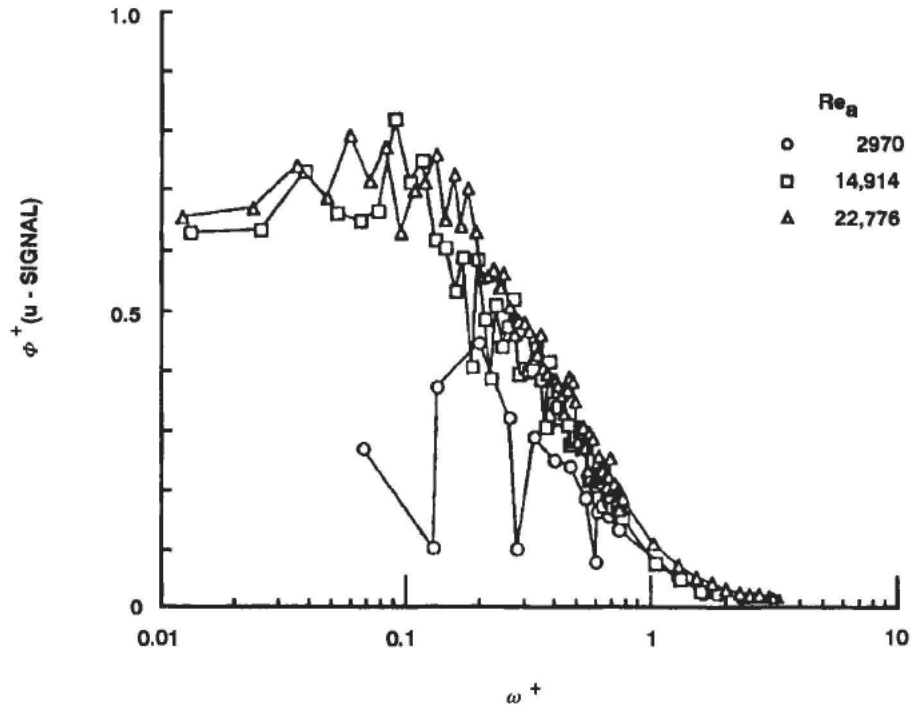


**Figure 36. Power Spectra of Streamwise Velocity Fluctuations at  $y^+ = 125$  (Channel-Flow Data From Wei and Willmarth, 1989)**

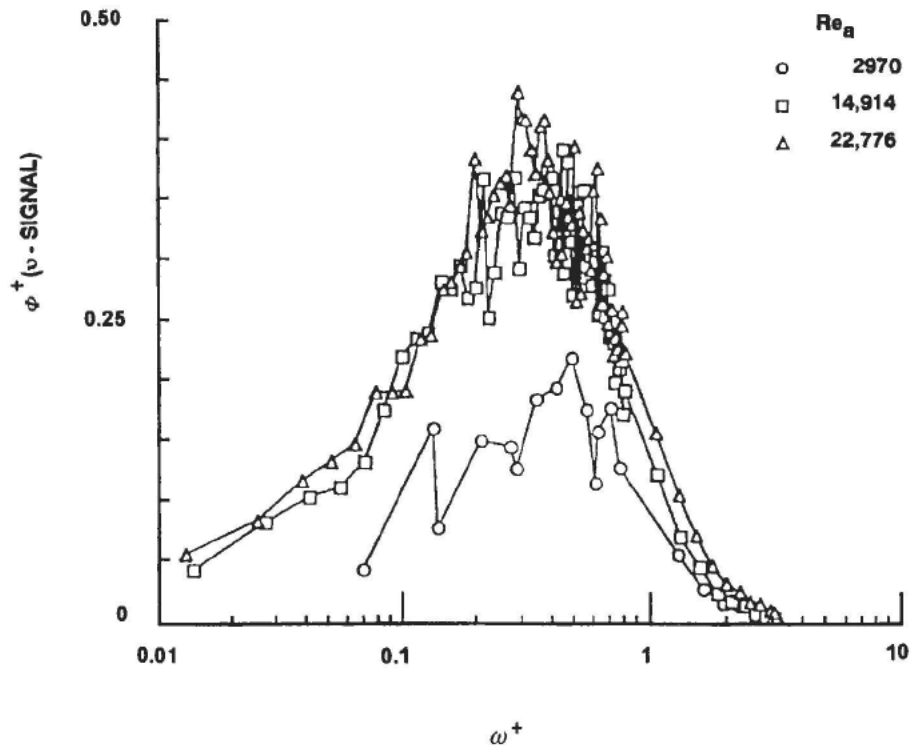


**Figure 37. Power Spectra of Normal Velocity Fluctuations at  $y^+ = 125$  (Channel-Flow Data From Wei and Willmarth, 1989)**

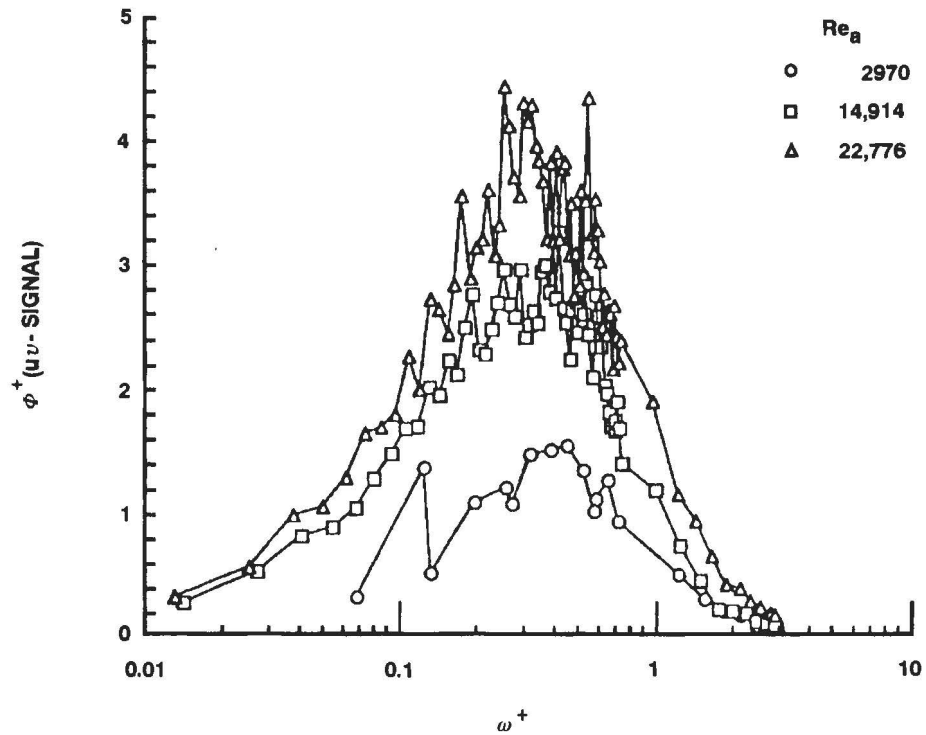


**Figure 38. Power Spectra of Reynolds Stress Fluctuations at  $y^+ = 125$  (Channel-Flow Data From Wei and Willmarth, 1989)**

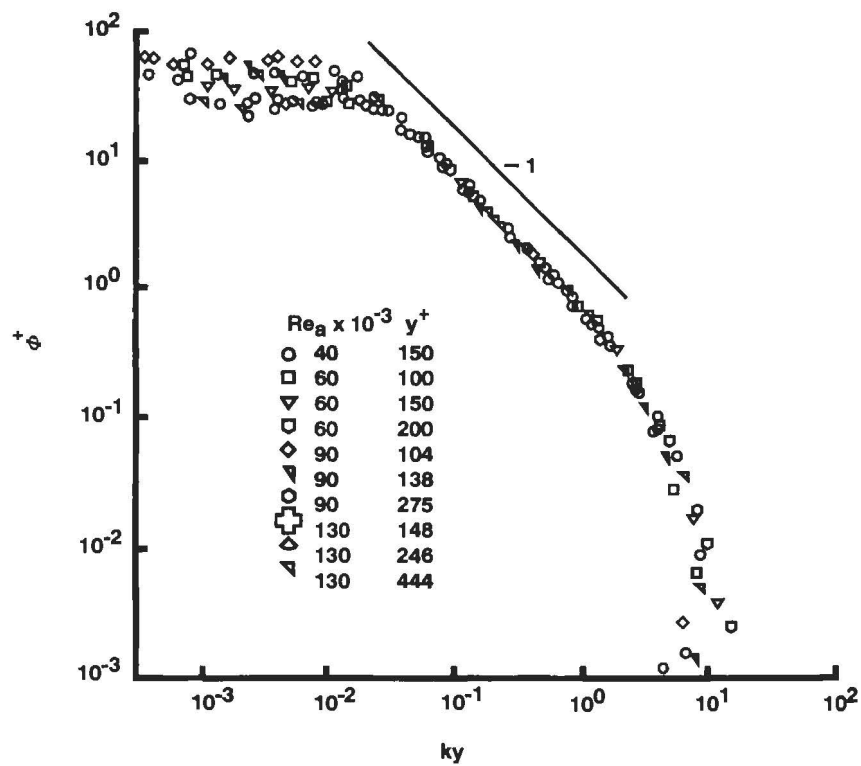


**Figure 39. Normalized Power Spectra of Streamwise Velocity Fluctuations (Pipe-Flow Data From Perry and Abell, 1975)**

## 6.4 SKEWNESS AND FLATNESS FACTORS

The third and fourth moments of a random signal give useful statistical information regarding the temporal distribution of its fluctuations around an average value. When non-dimensionalized using the RMS value of the fluctuations, these become the skewness and flatness factors, respectively. For example, for the streamwise velocity fluctuations the skewness and flatness factors are defined as follows:

$$S_u = (\overline{u^3}) / (u_{rms})^3, \quad (33)$$

$$F_u = (\overline{u^4}) / (u_{rms})^4. \quad (34)$$

Similar expressions can be written for the skewness and flatness factors for the other two velocity components, the Reynolds stress, the velocity derivative with respect to time, etc.

For a Gaussian signal, the probability distribution is symmetric around the mean value and those factors are, respectively,  $S = 0$  and  $F = 3$ . A non-zero skewness factor indicates the degree of temporal skewness of the random fluctuations, e.g., acceleration versus deceleration or sweep versus ejection. Flatness factor larger than 3 is associated with a signal that is rapidly changing with time, as for example, that produced by intermittent turbulent events.

Unlike the second and higher even moments, the third and all higher odd-number moments retain the sign information and thus contain valuable statistical information related to the coherent structures. The skewness of a turbulence quantity can be thought of as representing the flux of a stress that is directly attributable to coherent structures. For example,  $\overline{u^3}$  is the streamwise flux of the streamwise turbulence kinetic energy  $\overline{u^2}$ ,  $-\overline{u^2v}$  is the streamwise flux of the Reynolds stress  $\overline{uv}$ ,  $-\overline{uv^2}$  is the normal flux of  $\overline{uv}$ , etc.

A combination of positive  $\overline{u^3}$  and negative  $\overline{v^3}$  is associated with sweep events, while a combination of negative  $\overline{u^3}$  and positive  $\overline{v^3}$  is attributable to ejection events (see section 7). Similarly,  $-\overline{u^2v}$  and  $-\overline{uv^2}$  denote streamwise flux and outward transport of shear stress, respectively. Note that, via triple moments, structural information can be extracted without ambiguity, that is, without the recourse of any subjective threshold setting as in the so-called VITA and VISA -- variable interval time- or space-averaging techniques (Blackwelder and Kaplan, 1976), respectively. The flatness factor, on the other hand, is always positive. Near the rotational/irrotational interface of a turbulent boundary layer and in the near-wall region where intermittent bursting events take place, the normalized fourth moment attains large values.

Profiles of the skewness factor of the streamwise velocity fluctuations in the boundary-layer flow of Andreopoulos et al. (1984) are plotted in figure 40 for four Reynolds numbers in the range of  $Re_\theta = 3624$ -15,406. High positive values of  $S_u$  are observed in the viscous sublayer,

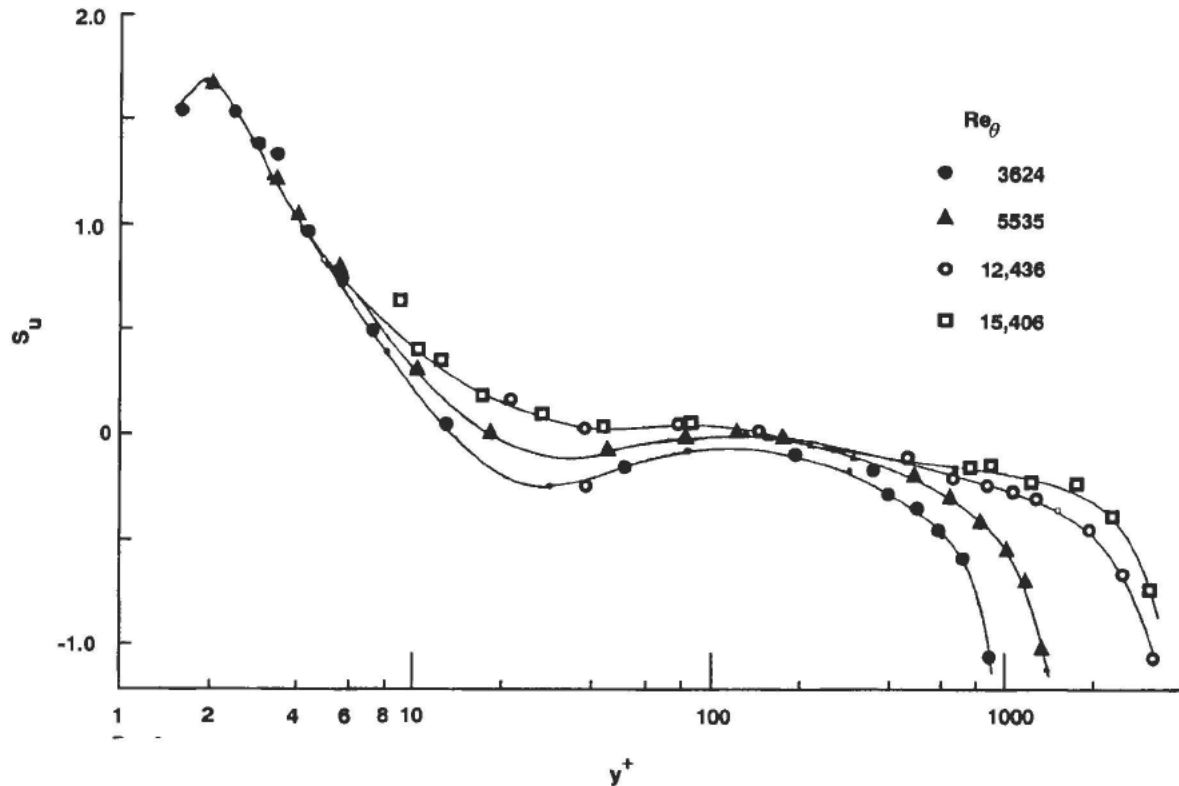


**Figure 40. Profiles of Skewness Factor of Streamwise Velocity Fluctuations at Four Reynolds Numbers (From Andreopoulos et al., 1984)**

indicating the skewed nature of the acceleration-dominated velocity fluctuations there. As a result of the arrival of high-speed fluid from regions away from the wall (sweep events), large positive values of  $u$  occur more frequently than large negative values in the near-wall region. In the log region, the skewness factor is only slightly different from that for a Gaussian probability density distribution. Farther away from the wall, the skewness is negative consistent with the arrival of low-speed fluid from the wall region (deceleration-dominated ejection events). Reynolds number effects are stronger in the wake region of the flow where the skewness is negative, although some effects penetrate all the way to the edge of the viscous sublayer. Figure 40 indicates the strong Reynolds number effects on streamwise flux of the longitudinal turbulence kinetic energy due to both sweep and ejection events.

Kline (1967) has proposed that the near-wall value of  $S_u$  is related to the width of the low-speed streaks (section 7.1). In low Reynolds number flows, the most probable location of the breakup stage of the bursting process is at  $y^+ = 15$ . According to the data in figure 40, the value of  $S_u$  changes sign at that  $y^+$  at  $Re_\theta = 3624$ , but at the higher Reynolds number of  $Re_\theta = 15.4 \times 10^3$ , the skewness does not change sign until  $y^+ \approx 200$ .

Smits et al. (1989) have compared the skewness factor  $S_u$  for subsonic low-Reynolds number ( $M_\infty = 0.1$ ;  $Re_\theta = 5 \times 10^3$ ) and supersonic high-Reynolds number ( $M_\infty = 2.9$ ;  $Re_\theta = 80 \times 10^3$ ) turbulent boundary layers. Because the effect of Mach number appears to be weak and can be taken into account by considering the local fluid properties, the comparison primarily shows the effect of  $Re_\theta$ . It is interesting that in Smits et al.'s experiments,  $S_u$  changes sign at  $y/\delta = 0.17$  for  $Re_\theta = 5 \times 10^3$ , but at  $y/\delta = 0.68$  for  $Re_\theta = 80 \times 10^3$ . Thus, the point of crossover from the sweep- to ejection-dominated motions moves outward as  $Re_\theta$  increases and shows no sign of reaching an asymptote. Admittedly, the available data are scarce, but it is clear that Reynolds number effects on third- and higher-order moments are stronger than those on the first- and second-order moments.

In isotropic turbulence, the skewness of the velocity derivative  $du/dx$  signifies the inertial transfer of energy across the wavenumber domain and is proportional to the production of mean-square vorticity by vortex stretching. For the anisotropic wall-bounded flow, Sreenivasan (1989) argues that such interpretations may hold at least qualitatively. Figure 41 depicts  $S_{(du/dt)}$  for the pipe-flow data of Elena and Dumas (1978). In a high-shear flow, time derivative is very roughly related to space derivative through the Taylor's frozen-flow hypothesis. The skewness profile in figure 41 is typical and peaks at roughly  $S_{(du/dt)} = 1$  around  $y^+ = 12$ , indicating strong nonlinear effects, or vortex stretching, in the same region where production of turbulence kinetic energy also reaches a maximum. The value of  $S_{(du/dt)}$  drops to 0.4 in the outer layer and toward zero at the wall. Similar trends are observed in channel flows (Comte-Bellot, 1963) and other boundary layers (Ueda and Hinze, 1975).

For the reasons indicated in section 6.1, Andreopoulos et al. (1984) measured the normal velocity fluctuations only at the single low Reynolds number of  $Re_\theta = 3624$ . Their results for the skewness factor of the surface-normal fluctuations are depicted in figure 42. Unlike the skewness of the streamwise velocity fluctuations, the value of  $S_v$  is negative near the wall and positive in the outer-flow region, signaling the more frequent occurrence of negative and positive normal velocity fluctuations in the inner and outer layer, respectively. The skewness is again near zero in the overlap region.

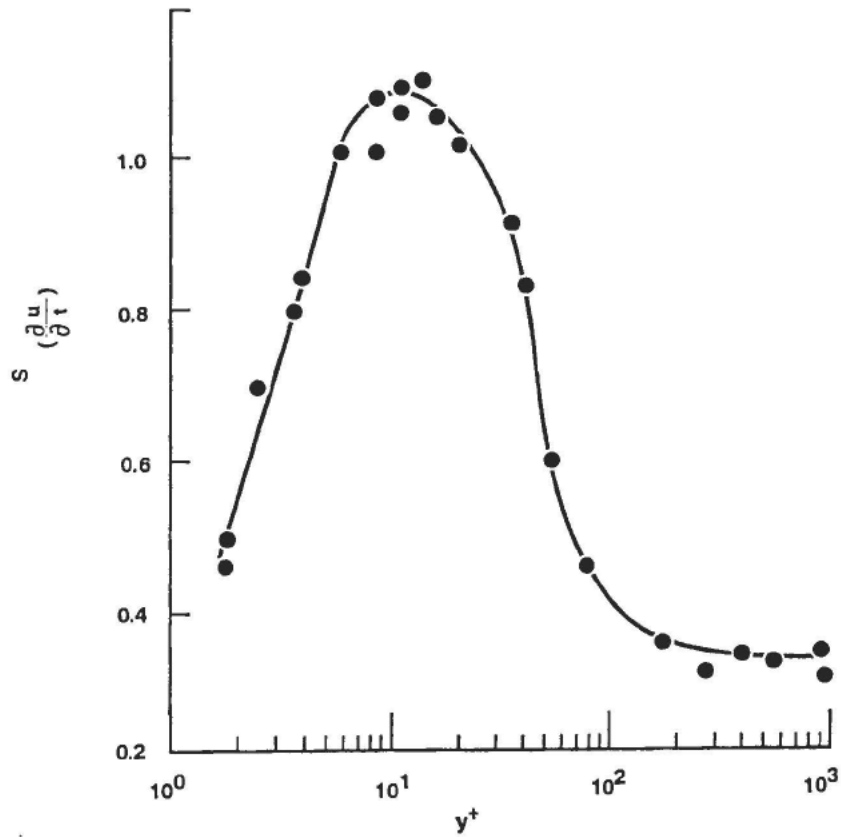


**Figure 41. Skewness of Velocity Derivative  $du/dt$  in Inner Region of Pipe Flow (Andreopoulos et al., 1984)**

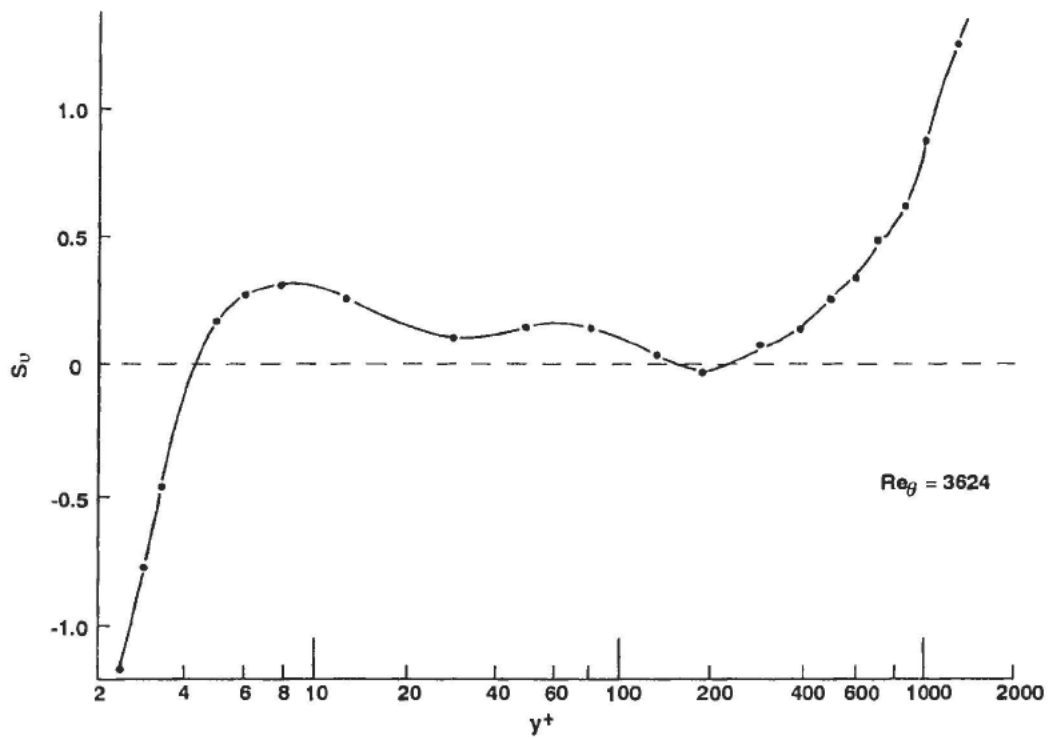


**Figure 42. Distribution of Skewness Factor of Velocity Fluctuations Normal to Wall (Andreopoulos et al., 1984)**

Andreopoulos et al.'s (1984) data follows the general trends of those measured by Gupta and Kaplan (1972) but differ somewhat from the data of Kreplin and Eckelmann (1979) and more strongly from those due to Kutateladze and Khabakhpasheva (1978). The disagreements are particularly noticeable in the near-wall region, which is not surprising considering the spatial and temporal probe-resolution difficulties associated with the measurement of higher-order moments. The near-wall distribution of the skewness of the normal velocity fluctuations is compared for the four different experiments in figure 43. Note that a linear scale is used for the abscissa in this figure. Except for the data of Kutateladze and Khabakhpasheva (1978),  $S_u$  is positive only for  $y^+ > 5$  and negative only for  $y^+ < 5$ . It is intriguing that as the wall is approached, the increased viscous effects and wall constrain are incapable of damping the wall-ward component of the velocity fluctuations.

Profiles of the flatness factor of the streamwise velocity fluctuations in the boundary layer flow of Andreopoulos et al. (1984) are plotted in figure 44 for four different Reynolds numbers in the range of  $Re_\theta = 3624 - 15,406$ . The kurtosis has high values near the wall and in the outer layer, indicating that the turbulence is highly intermittent in both places. In the overlap region,  $F_u$  is nearly 3, and Reynolds number effects are weak. But Reynolds number effects penetrate all the way to the edge of the viscous sublayer, being particularly noticeable in the buffer layer, and are much stronger in the outer layer, much the same as the corresponding effects on the skewness factor  $S_u$  depicted in figure 40.

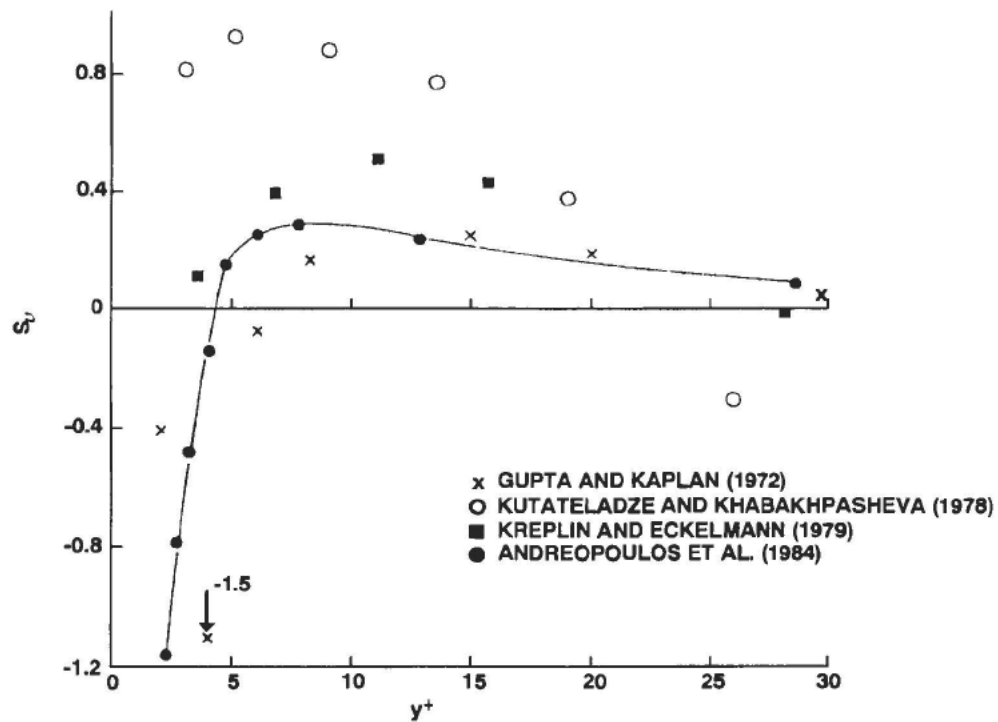


**Figure 43.** Distribution of Skewness Factor of Velocity Fluctuations Normal to Wall  
(Adapted by Andreopoulos et al., 1984)

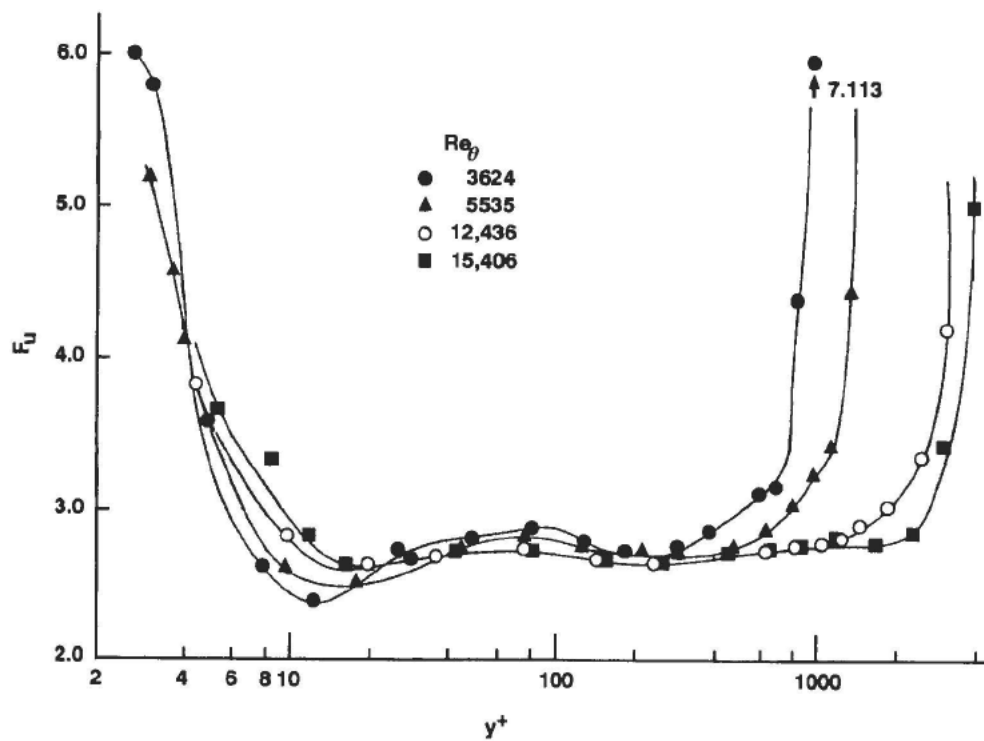


**Figure 44.** Profiles of Flatness Factor of Streamwise Velocity Fluctuations at Four Reynolds Numbers (Andreopoulos et al., 1984)

## 6.5 WALL-PRESSURE FLUCTUATIONS

Important physics of the turbulent wall-bounded flow can be learned from the measurements of the instantaneous static pressure. Pressure fluctuations are often proposed as an important mechanism by which the outer region of a boundary layer could influence and even initiate dynamically significant events in the wall region. Additionally, pressure fluctuations in a boundary layer induce structural vibrations on the wall and are believed to be responsible for radiated noise. Solving practical engineering problems that deal with reducing this flow-induced noise, for example to improve the performance of sonar domes on submarines or to suppress unpleasant noise in the interior of commercial aircraft, requires documenting the important statistics of the random pressure field, such as RMS, spectrum, and cross correlation.

The local static pressure fluctuations across a shear flow cannot yet be measured; the only location where it can be measured is at the wall. This is often advantageous because information on convective structures within the boundary layer can be obtained nonintrusively by using wall-pressure sensors. The subject of wall-pressure measurements has been reviewed by Willmarth (1975b). Johansson et al. (1987) and Farabee and Casarella (1991) describe the current status. The latter authors show that the applicable scaling laws change with the frequency range of the spectrum. As anticipated earlier by Panton and Lineberger (1974), the friction velocity and boundary layer thickness are the appropriate scales at low wave numbers. At high wave numbers, the friction velocity and viscous length scale seem to collapse the data (Robert 1993; Panton and Robert 1993, 1994).

Reliable laboratory measurements of pressure fluctuations are particularly difficult because extraneous freestream turbulence and acoustic noise are unavoidably sensed by the wall-mounted microphones. To partially alleviate this problem, Panton et al. (1980) conducted pressure measurements on the fuselage of a sail plane. Contributions from potential motion outside the boundary layer were measured and show a slight Reynolds number dependence.

Currently, the state-of-the-art of probe resolution is a much more serious problem for wall pressure than it is in velocity-based variables. For example, pressure sensors as large as 450 wall units have been used in the past. Schewe (1983) used one of the smallest probes, having an effective diameter of  $19\nu/U_\tau$ . More recently, Lauchle and Daniels (1987) used sensors with diameters in the range of 0.7-1.5 wall units. However, the glycerin pipe-flow facility they used was acoustically noisy, and elaborate noise-removal techniques were used to process the pressure-fluctuations data. The wall-pressure spectra measured by Lauchle and Daniels in the range of Reynolds numbers of  $Re_a = 7000$ -16,500 are consistent with the flow physics: higher Reynolds number flow supports smaller scales and, hence, higher frequency pressure fluctuations. When non-dimensionalized with wall variables, however, the spectra, in that range of Reynolds numbers, seem to collapse.

Keith et al. (1992) assert that attenuations resulting from inadequate spatial resolution of a sensor are of primary concern. Variations among different data sets are reduced at higher frequencies when resolution effects are accounted for. Keith et al., clearly show the Reynolds number effects in the scaling of the low-frequency portion of wall-pressure spectra; while at low  $Re_\theta (< 4.5 \times 10^3)$  a mixed scaling applies, but outer scaling holds better at higher  $Re_\theta (> 4.5 \times 10^3)$ .

In their work, the outer scaling of the low-frequency end of the spectrum is related to the mixed scaling by the factor  $(U_\tau / U_\infty)^4$ , which decreases as  $Re_\theta$  increases. This observed change in the scaling laws with Reynolds number is intriguing. Inner scaling seems to be effective, on the other hand, at the high frequency portion of the spectra over the entire range of Reynolds numbers where reliable data are available.

Note that even a weak Reynolds number dependence in a wavenumber space will be accentuated in frequency space. The reason being that a large eddy moving at a high speed would produce the same frequency as a small eddy moving at a low speed. For this reason, Panton (1989) developed his inner/outer layer theory in wavenumber-phase velocity space and a reasonable agreement with experimental data was obtained (Panton and Roberts, 1994).

Table 1, adapted from Bandyopadhyay and Balasubramanian (1993, 1994), is a summary of RMS wall pressure normalized with the square of the friction velocity from measurements and simulations. Both the physical and numerical experiments indicate a slight increase with Reynolds number, a result that is also theoretically anticipated (Bradshaw, 1967). In the structural model of Bandyopadhyay and Balasubramanian, higher Reynolds number effects in  $p'_w$  are better simulated by higher vortex Reynolds number sweep motions.

**Table 1. Wall-Pressure Fluctuation Statistics**

Measurements					
$p'_w / U_\tau^2$	2.3-2.6			3.38 (Average)	
$Re_\theta$	up to $4 \times 10^4$			$Re_x \approx 10^8$ ; $M \leq 0.6$	
	Laboratory Measurements (Willmarth, 1975b)			Flight: Boeing 737 Forward (Bhatt, 1971)	
Flat Plate and Channel Simulations					
$p'_w / U_\tau^2$	2.3-2.4	2.8	1.9	2.7	1.4
$Re_\theta$	353-505	576	300	1410	$Re_D = 1.38 \times 10^4$
	LES (Tsai & Leslie, 1990)		DNS (Spalart, 1988)		DNS (Kim et al., 1987)
Structural Model (Bandyopadhyay and Balasubramanian, 1993, 1994)					
$p'_w / U_\tau^2$	1.28	1.26	3.59	2.32	
$Re_\Gamma$	200	100	200	100	
Vortex Model	Ejection	Ejection	Sweep	Sweep	

## 7. COHERENT STRUCTURES

The classical view that turbulence is essentially a stochastic phenomenon having a randomly fluctuating velocity field superimposed on a well-defined mean has been changed in the last few decades by the realization that the transport properties of all turbulent shear flows are dominated by quasi-periodic, large-scale vortex motions (Laufer, 1975; Townsend, 1976; Cantwell, 1981). Despite the extensive research work in this area, no generally accepted definition of what is meant by coherent motion has emerged. In physics, coherence stands for well-defined phase relationship. For the present purpose, the rather restrictive definition given by Hussain (1986) is adopted: *a coherent structure is a connected turbulent fluid mass with instantaneously phase-correlated vorticity over its spatial extent*. In other words, underlying the random, three-dimensional vorticity that characterizes turbulence, a component of large-scale vorticity exists that is instantaneously coherent over the spatial extent of an organized structure. The apparent randomness of the flow field is, for the most part, due to the random size and strength of the different type of organized structures that field comprises.

In a wall-bounded flow, a multiplicity of coherent structures has been identified mostly through flow visualization experiments, although some important early discoveries have been made using correlation measurements (e.g., Townsend, 1961 and 1970; Bakewell and Lumley, 1967). Although the literature on this topic is vast, no research community-wide consensus has been reached particularly on the issues of the origin of and interaction between the different structures, regeneration mechanisms, and Reynolds number effects. Following are somewhat biased remarks addressing those issues. At times, diverse viewpoints will be presented but for the most part particular scenarios, which in the present authors' opinion are most likely to be true, will be emphasized. The interested reader is referred to the large number of review articles available (e.g., Kovasznay, 1970; Laufer, 1975; Willmarth, 1975a, 1975b; Saffman, 1978; Cantwell, 1981; Fiedler, 1986, 1988; Blackwelder, 1988; Robinson, 1991). The last reference, in particular, summarizes many of the different, sometimes contradictory, conceptual models offered thus far by different research groups. Those models are aimed ultimately at explaining how the turbulence maintains itself and range from the speculative to the rigorous, but none, unfortunately, are self-contained and complete. Furthermore, they dwell largely on the kinematics of organized motion and are weak on the dynamics of the turbulence regeneration process.

### 7.1 OVERVIEW

With few exceptions, most of the available structural information on wall-bounded flows come from many but rather low Reynolds number experiments and a handful of, again, low Reynolds number numerical simulations. Organized structures appear to be similar in all wall-bounded flows only in the inner layer. The outer region of a boundary layer is, by necessity, different from the core region of a pipe or channel flow. Before getting to the issue of Reynolds number effects, an overall view, whose source of information is predominately low Reynolds number experiments, is first presented. As will become clear throughout the discussion following

the present subsection, the picture that emerges at high Reynolds numbers is quite different, and structural information gleaned from low Reynolds number physical and numerical experiments may not be very relevant to high Reynolds number flows.

In (low Reynolds number) external flows, the turbulence production process is dominated by three kinds of quasi-periodic eddies: the large outer structures, the intermediate Falco-Newman eddies, and the near-wall eddies. Examples of these coherent structures visualized in rather low Reynolds number boundary layers are depicted in figures 45-47. Laser sheet illumination is used in all three photographs. Large eddies forming on a flat plate towed in a water channel are seen in the side view in figure 45. The flow is from left to right. The artificially tripped boundary layer has a Reynolds number at the observation station of  $Re_\theta = 725$ , and is marked with fluorescein dye. The smoke-filled boundary layer shown in top view in figure 46 depicts the characteristic pockets believed to be induced by the motion of Falco-Newman eddies over the wall. In here, the experiments are conducted in a wind tunnel at a momentum thickness Reynolds number of  $Re_\theta = 742$ , and the boundary layer is again artificially tripped. Finally, the top view in figure 47 depicts the low speed streaks in the near-wall region of the same turbulent boundary layer previously shown in side view in figure 45. Flow direction is again from left to right.

The large, three-dimensional bulges (figure 45) scale with the boundary layer thickness  $\delta$  and extend across the entire layer (Kovaszny et al., 1970; Blackwelder and Kovaszny, 1972). These eddies control the dynamics of the boundary layer in the outer region, such as entrainment, turbulence production, etc. They appear randomly (quasi-periodically) in space and time, and seem to be, at least for moderate Reynolds numbers, the residue of the transitional Emmons spots (Zilberman et al., 1977; Gad-el-Hak et al., 1981). Note, however, that at higher Reynolds numbers ( $Re_\theta \approx 17,000$ ) the very existence of the large eddy as an isolated coherent structure has been questioned by Head and Bandyopadhyay (1981), and this point will be discussed in section 7.2.2.

The Falco-Newman eddies<sup>†</sup> are also highly coherent and three-dimensional. Falco (1974, 1977) named them typical eddies because they appear in wakes, jets, Emmons spots, grid-generated turbulence, and boundary layers in zero, favorable and adverse pressure gradients. They have an intermediate scale of about 100 wall units. The Falco-Newman eddies appear to be an important link between the large structures and the near-wall events. In the plan view shown in figure 46, smoke fills the near-wall region of a boundary layer and the roughly circular regions devoid of marked fluid are called pockets.<sup>‡</sup> Falco (1980) asserts that these pockets are the *footprints* of some outer structures that induce fluid toward the wall. Robinson et al. (1989) analyzed the database generated from the direct numerical simulations of Spalart (1988). They concur that the pockets are the signature of local wall-ward motions, evidenced by spanwise divergence of streamlines, above regions of high wall pressure. Low pressure regions, on the other hand, occur along lines of converging streamlines associated with outward motion.

---

<sup>†</sup> Discovered at about the same time by Newman (1974).

<sup>‡</sup> These undulations are very similar to the so-called folds observed by Perry et al. (1981) in turbulent spots.

FLOW  
→ →



*Figure 45. Side View of Low Reynolds Number Turbulent Boundary Layer;  $Re_\theta = 725$   
(Gad-el-Hak et al., 1984)*

FLOW  
→ →



*Figure 46. Top View of Low Reynolds Number Turbulent Boundary Layer;  $Re_\theta = 742$   
(Falco, 1980)*

FLOW  
→ →



*Figure 47. Top View of Low Reynolds Number Turbulent Boundary Layer;  $Re_\theta = 725$  (Gad-el-Hak et al., 1984)*

The third kind of eddies exists in the wall region ( $0 \leq y^+ \leq 100$ ) where the Reynolds stress is produced in an intermittent fashion. Half of the total production of turbulence kinetic energy  $-\overline{uv}(dU/dy)$  takes place near the wall in the first 5 percent of the boundary layer at typical laboratory Reynolds numbers (smaller fraction at higher Reynolds numbers), and the dominant sequence of intense organized motions there are collectively termed the bursting phenomenon. This dynamically significant process, identified during the 1960s by researchers at Stanford University (Kline and Runstadler, 1959; Runstadler et al., 1963; Kline et al., 1967; Kim et al., 1971; Offen and Kline, 1974; 1975), was reviewed by Willmarth (1975a) and Blackwelder (1978), and most recently by Robinson (1991).

Qualitatively, the process, according to at least one school of thought, begins with elongated, counter-rotating, streamwise vortices having diameters of approximately  $40\nu/U_\tau$ . This estimate for the diameter of the vortex is obtained from the conditionally averaged spanwise velocity profiles reported by Blackwelder and Eckelmann (1979). There is a distinction, however, between vorticity distribution and a vortex (Saffman and Baker, 1979; Robinson et al., 1989;

Robinson, 1991), and the visualization results of Smith and Schwartz (1983) may indicate a much smaller diameter. In any case, the counter-rotating vortices exist in a strong shear and induce low- and high-speed regions between them. The vortices and the accompanying eddy structures occur randomly in space and time. However, their appearance is sufficiently regular that an average spanwise wavelength of approximately  $80-100 \nu/U_\tau$  has been identified by Kline et al. (1967) and others.

It may be instructive at this point to emphasize that the distribution of streak spacing is very broad. The standard of deviation is 30-40 percent of the more commonly quoted mean spacing between low-speed streaks of 100 wall units. Both the mean and standard deviation are roughly independent of Reynolds number in the rather limited range of reported measurements ( $Re_\theta = 300-6500$ , see Smith and Metzler, 1983; Kim et al., 1987). Butler and Farrell (1993) have shown that the mean streak spacing of  $100 \nu/U_\tau$  is consistent with the notion that this is an optimal configuration for extracting "the most energy over an appropriate eddy turnover time." In their work, the streak spacing remains 100 wall units at Reynolds numbers, based on friction velocity and channel half-width, of  $a^+ = 180-360$  that is a factor of 2.

Kim et al. (1971) observed that the low-speed regions (figure 47) grow downstream, lift up, and develop inflectional  $U(y)$  profiles. At approximately the same time, the interface between the low- and high-speed fluid begins to oscillate, apparently signaling the onset of a secondary instability. The low-speed region lifts up away from the wall as the oscillation amplitude increases, and then the flow rapidly breaks up into a disorganized motion. The streak oscillations commence at  $y^+ \approx 10$ , and the abrupt breakup takes place in the buffer layer, although the ejected fluid reaches all the way to the logarithmic region. Because the breakup process occurs on a very short time scale, Kline et al. (1967) called it a *burst*. Virtually all of the net production of turbulence kinetic energy in the near-wall region occurs during these bursts.

Corino and Brodkey (1969) showed that the low-speed regions are quite narrow, i.e.,  $20\nu/U_\tau$ , and may also have significant shear in the spanwise direction. They also indicated that the ejection phase of the bursting process is followed by a large-scale motion of upstream fluid that emanates from the outer region and cleanses (sweeps) the wall region of the previously ejected fluid. The sweep phase is, of course, required by the continuity equation and appears to scale with the outer-flow variables. The sweep event seems to stabilize the bursting site, in effect, preparing it for a new cycle.

Considerably more has been learned about the bursting process during the last decade. For example, Falco (1980, 1983) has shown that when a typical eddy, which may be formed in part by ejected wall-layer fluid, moves over the wall it induces a high  $uv$  sweep (positive  $u$  and negative  $v$ ). The wall region is continuously bombarded by pockets of high-speed fluid originating in the logarithmic and possibly the outer layers of the flow. These pockets appear to scale, at least in the limited Reynolds number range where they have been observed,  $Re_\theta = O(1000)$ , with wall variables and tend to promote or enhance the inflectional velocity profiles by increasing the instantaneous shear leading to a more rapidly growing instability. The relation between the pockets and the sweep events is not clear, but it seems that the former molds the highly irregular interface between the latter and the wall-region fluid.

Other significant experiments were conducted by Tiederman and his students (Donohue et al., 1972; Reischman and Tiederman, 1975; Oldaker and Tiederman, 1977; Tiederman et al., 1985) and Smith and his colleagues (Smith and Metzler, 1982, 1983; Smith and Schwartz, 1983). The first group conducted extensive studies of the near-wall region, particularly the viscous sublayer, of channels with Newtonian as well as drag-reducing non-Newtonian fluids. Smith's group, using a unique, two-camera, high-speed video system, was the first to indicate a symbiotic relationship between the occurrence of low-speed streaks and the formation of vortex loops in the near-wall region.

## 7.2 OPEN ISSUES

There are at least four unresolved issues regarding coherent structures in wall-bounded flows; not all are necessarily independent. How does a particular structure originate? How do different structures (especially the ones having disparate scales) interact? How does the turbulence continue to regenerate itself? Does the Reynolds number affect the different structures in any profound way? The primary difficulty in trying to answer any of those queries stems from the existence of two scales in the flow that become rather disparate at large Reynolds numbers (figure 1). The closely related issues of origin, inner/outer interaction and regeneration will be addressed in the following two subsections. Reynolds number effects on the coherent structures are reserved for the four subsections in section 7.3.

### 7.2.1 Origin of Different Structures

Faced with the myriad of coherent structures existing in the boundary layer, a legitimate question is where do they all come from and which one is dynamically significant? Sreenivasan (1988) offers a glimpse of the difficulties associated with trying to answer this question. The structural description of a turbulent boundary layer may not be that complicated, however, and some of the observed structures may simply be a manifestation of the different aspects of a more basic coherent structure. For example, some researchers argue that the observed near-wall streamwise vortices and large eddies are, respectively, the legs and heads of the omnipresent hairpin vortices (Head and Bandyopadhyay, 1981). Nevertheless, that still leaves us with a minimum number of *building blocks* that must be dealt with.

If the large eddies are assumed to be dynamically significant, then how are they recreated? It is easy to argue that the conventional laminar-to-turbulence transition cannot be responsible, because the same large eddies appear even in heavily tripped boundary layers where the usual transition routes are by-passed. Wall events cannot be responsible for creating large eddies because of their extremely small relative scale at high Reynolds number. Furthermore, no hierarchical amalgamation of scales has been observed to justify such proposition.

If, alternatively, wall events are assumed to dominate, then where do the streamwise vortices or the low-speed streaks come from and what mechanism sustains the bursting cycle? Mechanisms that assume local instability cannot be valid at large Reynolds numbers where the wall layer is, for example, 0.1 percent of the boundary layer thickness,<sup>†</sup> and it is difficult to conceive that 99.9 percent of the boundary layer has no active role in the generation and maintenance of turbulence. On the other hand, assuming the bursting events are triggered by the large eddies, brings us back to the original question: Where do the latter come from?

The above difficulties explain the lack of a self-consistent model of the turbulent boundary layer, despite the enormous effort expended to establish one. None of the existing models is complete in the sense that *none* accounts for each aspect of the flow in relation to every other aspect. Developing a complete, self-consistent model is more than an academic exercise; for a proper conceptual model of the flow gives researchers the necessary tools to compute high Reynolds number practical flows using the Reynolds-averaged Navier-Stokes equations, to devise novel flow control strategies, and to extend known laboratory-scale control devices to field conditions.

### 7.2.2 Inner/Outer Interaction and Regeneration Mechanisms

There is no doubt that significant interactions between the inner and outer layers take place. On energy grounds alone, it is known that in the outer layer the dissipation is larger than the turbulence kinetic energy production (Townsend, 1976). Therefore, it is necessary for energy to be transported from the inner layer to the outer layer simply to sustain the latter. How that is accomplished and whether coherent structures are the only vehicle to transport energy is not clear, but two distinct schools of thought have emerged. In the first, the large-scale structures dominate and provide the strong buffeting necessary to maintain the low Reynolds number turbulence in the viscous region ( $Re \leq 30$ ). In the second view, rare, intense wall events are assigned the active role and, through outward turbulent diffusion, provide the necessary energy supply to maintain the outer region. As mentioned in the previous subsection, both views have some loose ends.

Based on a large number of space-time two-point correlation measurements of  $u$  and  $v$ , Kovasznay et al. (1970) suggested that the outer region of a turbulent boundary layer is dominated by large eddies. The interface between the turbulent flow and the irrotational fluid outside the boundary layer is highly corrugated with a RMS slope in the ( $x$ - $y$ ) plane of roughly 0.5. The three-dimensional bulges are elongated in the streamwise direction with an aspect ratio of approximately 2:1 and have a characteristic dimension of between  $0.5\delta$  and  $\delta$  in the wall normal direction. They appear quasi-periodically and are roughly similar to each other. Kovasznay et al., allowed that the large eddies are passive in the sense that the wall events and not these eddies are responsible for producing the Reynolds stress. Kovasznay (1970) advanced the hypothesis that wall bursting starts a chain reaction of some sort at all intermediate scales

---

<sup>†</sup> This is the near-wall region of thickness  $y = 30\nu/U_\tau$  as a percentage of the boundary layer thickness when the Reynolds number is  $Re_\theta \approx 100,000$ .

culminating into a sequence of amalgamations, which eventually leads to the large structures. As mentioned earlier, such hierarchical amalgamation of scales has not been directly observed in the laboratory.

Head and Bandyopadhyay (1981), on the other hand, suggested that the very existence of the large eddies at high Reynolds numbers is in doubt. Their combined flow visualization/hot-wire probe experiments are unique in that an unusually large range of Reynolds numbers was investigated,  $Re_\theta = 500-17,500$ , allowing them to clarify unambiguously Reynolds number effects on the structure of the boundary layer. Head and Bandyopadhyay maintained that a large structure seen in typical flow visualization experiments is nothing but the slow overturning of a random collection of smaller-scale hairpin vortices, just a few or even a single isolated vortex loop at low Reynolds numbers (for example,  $Re_\theta < 1000$ ) but a large number of them at high Reynolds numbers (for example,  $Re_\theta > 5000$ ). This is sketched for typical low and high Reynolds number boundary layers in figures 48a and 48b, respectively. A brisker rate of rotation of the isolated (fat) vortex loop is observed at the lowest Reynolds number, consistent with prior observations of large eddies in low-speed experiments. The hairpins are inclined at around  $45^\circ$  to the plane of the flow over a major part of the layer thickness. In Head and Bandyopadhyay's (1981) view, the entire turbulent boundary layer consists very largely of vortex loops that become increasingly elongated as the Reynolds number increases (see figure 2). The so-called large eddies, on the other hand, do not appear to exhibit any particular coherent motion beyond a relatively slow overturning or toppling due to shear.

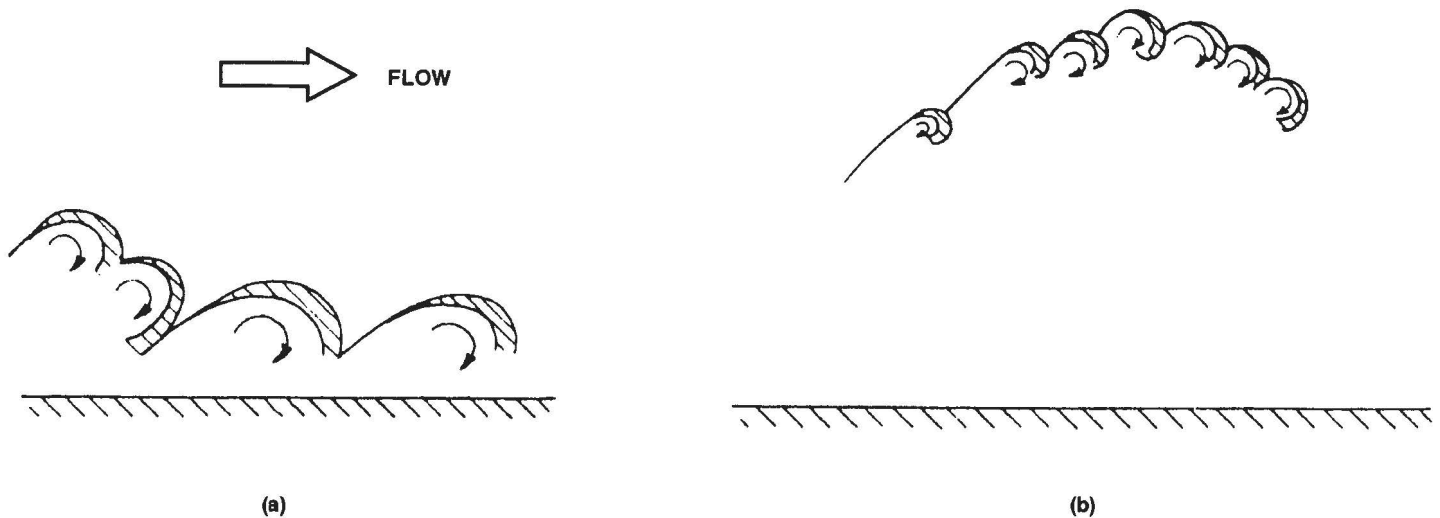


**Figure 48. Sketch of Large Eddy Structures as Collection of Smaller-Scale Hairpin Vortices: (a) Typical Low Reynolds Number Boundary Layer; (b) Typical High Reynolds Number Boundary Layer (Head and Bandyopadhyay, 1981)**

Corroborative evidence for the hairpin angle of inclination of  $45^\circ$  comes from the simultaneous, multiple-point hot-wire measurements of Alving et al. (1990) in both a canonical turbulent boundary layer and a boundary layer recovering from the effects of strong convex curvature. Their cross-correlation results are consistent with the observation of large-scale structures spanning the entire shear layer and inclined at angles in the range of  $35^\circ$ - $45^\circ$  near the outer edge of the boundary layer, but at continuously decreasing angles as the wall is approached.

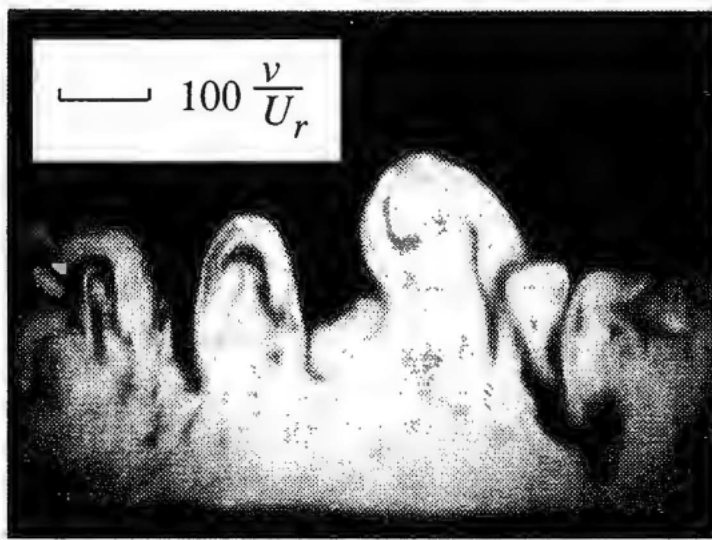
The sketch in figure 48b for a typical large eddy at high Reynolds number is consistent with the statistical findings of Brown and Thomas (1977), who have shown by using conditional averaging techniques that a typical large structure in a turbulent boundary layer has an upstream rotational/irrotational interface inclined at  $18^\circ$  to the flow direction. Head and Bandyopadhyay (1981) have observed such individual structures only at higher  $Re_\theta$  ( $> 5000$ ). It is possible to arrive precisely at this slope by modeling the large structure to be composed of hairpin vortices formed at regular intervals (Bandyopadhyay, 1980). Such large structures comprising many hairpin vortices have not been observed in the low Reynolds number DNS simulations.

Samples of Head and Bandyopadhyay's (1981) visualization experiments at three Reynolds numbers are depicted in figure 49. A laser light sheet illuminates a section of the smoke-filled boundary layer making  $45^\circ$  with the downstream plane. The vortex loops seen in this figure at  $Re_\theta = 600$ , 1700, and 9400 correspond roughly to the vortex loop, horseshoe vortex, and hairpin vortex sketched previously in figure 2 of this report. The increased elongation of the vortex loops as the Reynolds number increases over one order of magnitude is evident in the three photographs depicted in figure 49.

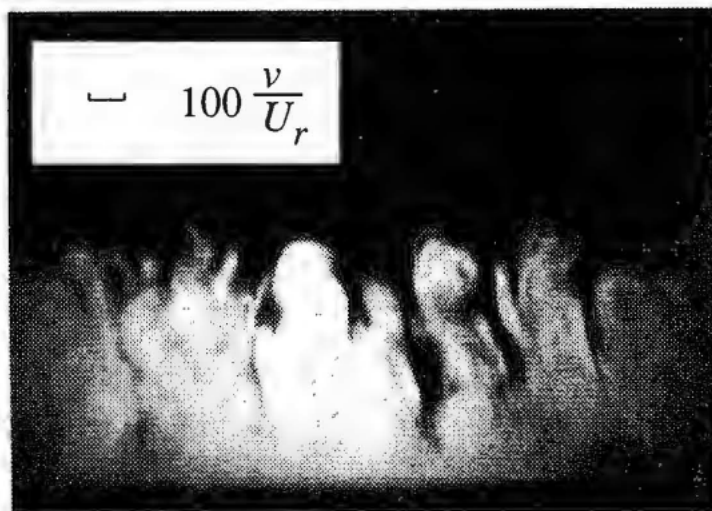
Robinson (1991) summarizes many of the conceptual models advanced by different researchers to explain how a wall-bounded turbulent flow maintains itself. Among those reviewed are the models advocated by Willmarth and Tu (1967); Black (1968); Offen and Kline (1975); Hinze (1975); Praturi and Brodkey (1978); Thomas and Bull (1983); Acarlar and Smith (1987a, 1987b); and Robinson (1990). Some of those conceptual models emphasize a particular aspect of the flow dynamics, for example the bursting cycle, while others are more ambitious and attempt to include both the inner and outer structures and their interaction.

Robinson (1991) also lists significant contributions that use structural information to predict statistical quantities or invoke a simplified form of the governing equations to model the dynamics of the near-wall turbulence-production process. Among the predictive models discussed are those by Landahl (1967, 1980, 1990); Townsend (1976); Perry and Chong (1982); Perry et al. (1986, 1989); Walker and Herzog (1988); Aubry et al. (1988); Hanratty (1989); and Berkooz et al. (1991).

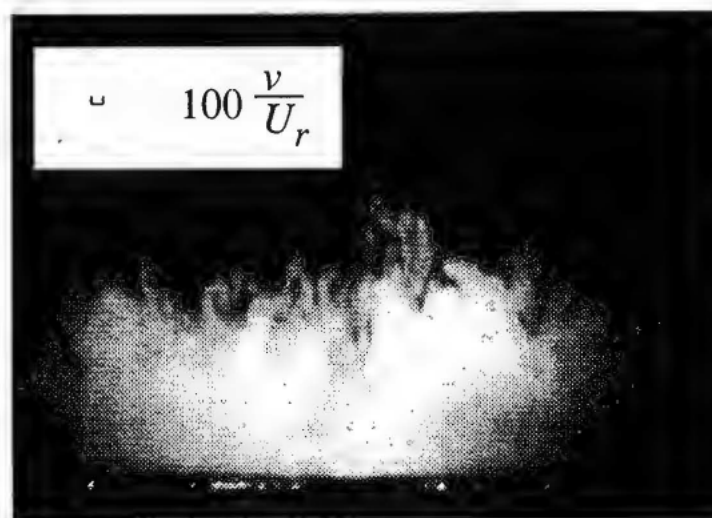
Other, potentially useful, predictive models not discussed by Robinson (1991) include those based on stability considerations (Malkus, 1956; 1979), based on the turbulence energy equation (Bradshaw et al., 1967), based on the  $u$   $v$  velocity quadrant statistical description of the organized motions (Nagano and Tagawa, 1990), and based on a single hairpin-like vortex in a unit domain of turbulence production (Bandyopadhyay and Balasubramanian, 1993, 1994). These models account explicitly for Reynolds number effects and may, therefore, be useful for practical Reynolds numbers.



$Re_\theta = 600$



$Re_\theta = 1700$



$Re_\theta = 9400$

*Figure 49. Hairpin Structures in Smoke-Filled Turbulent Boundary Layer at Three Reynolds Numbers (Head and Bandyopadhyay, 1981)*

Inevitably, in almost all the conceptual models, the omnipresent hairpin vortex (or horseshoe at low  $Re$ ) plays a key role. Such a vortex has been proposed earlier by Theodorsen (1952) on intuitive grounds as the primary structure responsible for turbulence production and dissipation in the boundary layer. His tornado-like vortices form astride near-wall, low-speed regions of fluid and grow outward with their heads inclined at  $45^\circ$  to the flow direction.

Black (1966, 1968) conducted a more rigorous analytical work to show the fundamental role of hairpin vortices in the dynamics of wall-bounded flows. His basic premise is that the primary role of the random turbulent motion is not to transfer mean momentum directly but rather to excite strong, three-dimensional instability of the sublayer, which is a powerhouse of vorticity. In Black's model, trains of discrete horseshoes are generated by repetitive, localized nonlinear instabilities within the viscous sublayer. The vortical structures are shed and outwardly migrate from the near-wall region in a characteristic, quasi-frozen spatial array. The horseshoes inviscidly induce an outflow of low-speed fluid from within the vortex loops, creating motions that would be seen by a stationary probe as sharp, intermittent spikes of Reynolds stress. Because of the continuous creation of new vortex loops that replace older elements, the lifetime of the vortical array is much longer than that for its individual members. According to Black (1968), such organized structures are responsible for the efficient mass and momentum transfer within a turbulent boundary layer.

Sreenivasan (1987) offers a similar model to that of Black (1968). The essential structures of the boundary layer, including the hairpin vortices, result from the instability of a caricature flow in which all the mean flow vorticity has been concentrated in a single fat sheet. Sreenivasan's conclusions were briefly discussed in section 4 of this report.

As a parting remark in this subsection, it may be instructive to recall that hairpin vortices play an important role also in the laminar-to-turbulence transition of boundary layer flows. Essentially, these hairpins are the result of the nonlinear tertiary instability of the three-dimensional peak/valley pattern, which itself is the secondary instability of the primary Tollmien-Schlichting waves (Klebanoff et al., 1962).

### 7.3 REYNOLDS NUMBER EFFECTS

The last question to be discussed in this section relates to Reynolds number effects on the coherent structures in wall-bounded flows. There are several facets to this issue and the present section is divided into four subsections. To be addressed are proper scaling for the period between bursts, possibility of profound structural changes after the well known Reynolds number mean flow limit of  $Re_\theta = 6000$ , small-structures existing in the outer layer, and Reynolds number effects on inner structures.

### 7.3.1 Bursting Period

Because of threshold setting and probe resolution, problems, bursting frequency and its scaling have become the source of continuing controversy. Cantwell (1981), based on a review of available literature, has concluded that this frequency scales on outer variables, thus establishing a strong link between the inner and outer regions of a wall-bounded flow. On the other hand, Blackwelder and Haritonidis (1983) have shown that frequent occurrence of these events scales with the viscous parameters consistent with the usual boundary layer scaling arguments. Their results, depicted in figure 50, were obtained with a hot-wire probe whose length varied in the range of  $\ell^+ = 4.5 - 20^\dagger$  as the Reynolds number increased in the range of  $Re_\theta = 1000 - 10,000$ . In figure 50a, outer variables are used to normalize the bursting frequency (or its inverse, the period between bursts). The non-dimensional frequency increases with Reynolds number, thus clearly indicating that outer scaling is not applicable. On the other hand, the same data plotted in figure 50b using the viscous time scale to normalize the frequency indicate the validity of inner scaling.<sup>‡</sup> Thus, the properly non-dimensionalized bursting period is independent of the Reynolds number, in agreement with the observations of Kline et al. (1967), Corino and Brodkey (1969), Donohue et al. (1972), Achia and Thompson (1977), and Blackwelder and Eckelmann (1978). Blackwelder and Haritonidis (1983) have suggested that past erroneous results are caused by insufficient spatial resolution of the sensors used to detect the bursts.

Based on measurements in the atmospheric boundary layer where the Reynolds number is several orders of magnitude higher than in typical laboratory experiments, Narasimha and Kailas (1986, 1987, 1990) still maintain that bursting events scale on outer variables. To do otherwise, the insufficient time resolution of the atmospheric data would simply not have allowed the detection of any dynamically significant events. Narasimha and Kailas cite other laboratory experiments to support their position (e.g., Rao et al., 1977; Ueda and Hinze, 1975; Willmarth, 1975a; Shah and Antonia, 1989; Rajagopalan and Antonia, 1984).

Adding to the present confusion, Bandyopadhyay (1982) has shown that the bursting period is not a universal function and both inner and outer variables are involved in its scaling with  $Re_\theta$ . He reviewed existing data and concluded that a universal value of the bursting frequency scaled with either inner or outer variables in various boundary layers ranging from relaminarized to separated does not exist. Because a turbulent boundary layer is characterized by three integral variables,  $C_f$ ,  $H$ , and  $Re_\theta$ , verification of universality with  $Re_\theta$  alone is clearly inadequate, and the apparent confusion stems in part from the lack of experiments over a sufficiently wide range of shape factors  $H$ . Johansson and Alfredsson (1982) have also suggested that the bursting period scale with intermediate scaling proportional to the geometric mean of the inner and outer scales.

---

<sup>†</sup> The upper end of this range may not provide sufficient probe resolution according to the criterion established earlier in this report.

<sup>‡</sup> Three additional data points (inverted triangles) from an untripped boundary layer are also shown in figure 50b.

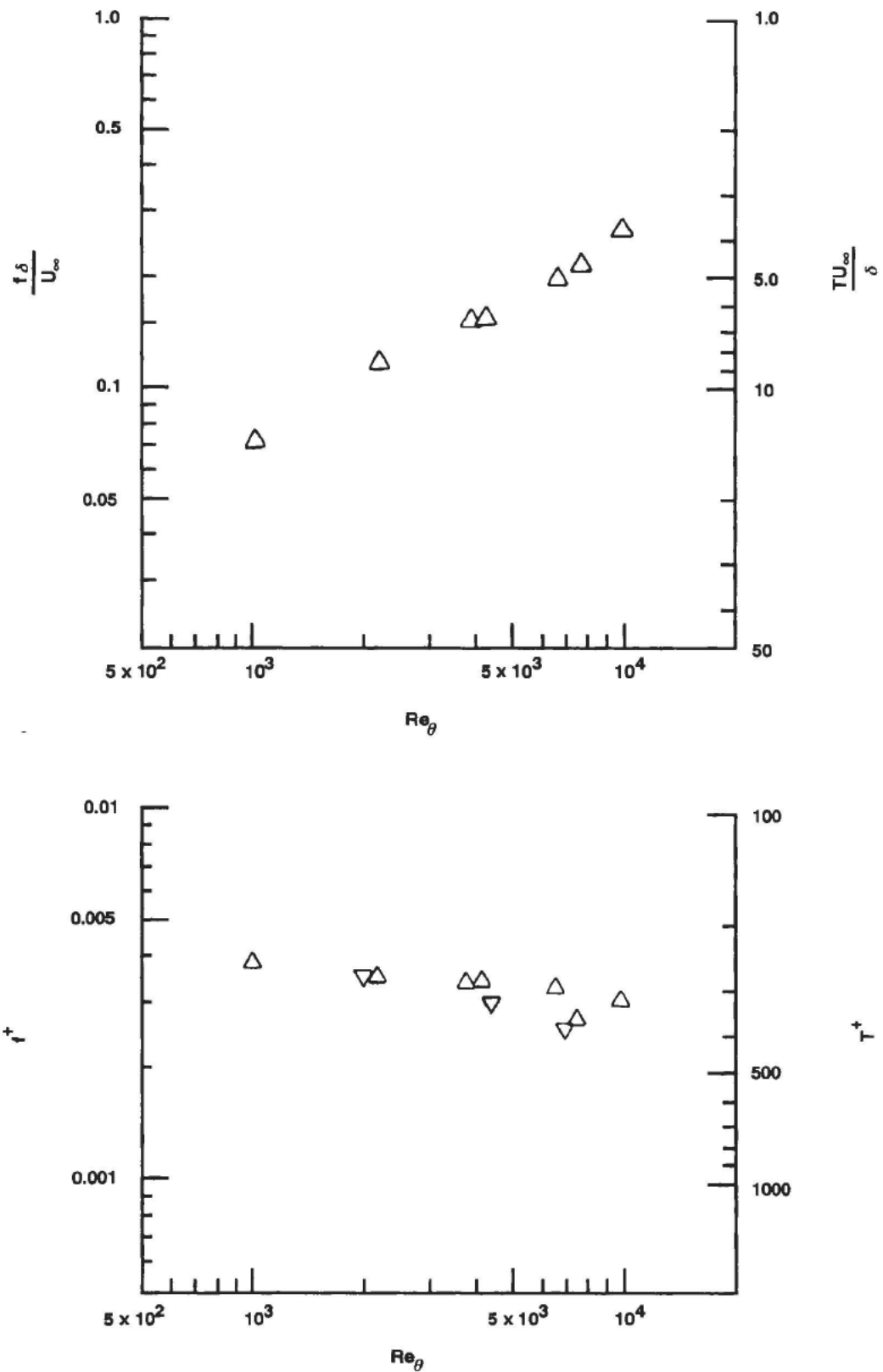


**Figure 50. Mean Bursting Frequency vs Reynolds Number:**  
**(a) Outer-Flow Variables Scaling; (b) Inner-Flow Variables Scaling**  
*(The inverted triangles represent three additional data points from an untripped boundary layer.)*  
*(Blackwelder and Haritonidis, 1983)*

The arguments by both Blackwelder and Haritonidis (1983) and Narasimha and Kailas (1987) are compelling, and the issue of scaling of the bursting events must, for the moment at least, stay open. The laboratory experiments of the former group are well controlled, but the range of Reynolds numbers and range of shape factors investigated are not large enough. The latter group experiments are conducted with sufficient probe resolution, but the atmosphere can neither be controlled nor fully documented. Moreover, the effects of roughness on the scaling is simply not known. Controlled high Reynolds number experiments using smooth walls and probes with sufficient resolution should settle the question.

### 7.3.2 *High Reynolds Number*

Does the boundary layer structure change when  $Re_\theta > 6 \times 10^3$ ? The Reynolds number variations of  $\Delta U^+$  due to Coles (1962) were reproduced in this report in figures 11 and 12 up to  $Re_\theta$  values of  $15 \times 10^3$  and  $50 \times 10^3$ , respectively. Figure 11 does suggest that an asymptotic state is reached approximately when  $Re_\theta > 6 \times 10^3$ . But, the higher Reynolds number data in figure 12 show that beyond that limit  $\Delta U^+$  drops, although very slowly compared with the rise rate for  $Re_\theta > 6 \times 10^3$ . The gradual departure of  $\Delta U^+$  from the apparent low  $Re_\theta$  asymptote suggests that some new effects are appearing in the turbulence production process at approximately  $Re_\theta (6 \text{ to } 15) \times 10^3$ . Experiments conducted in several different facilities are briefly described below and show that profound changes in the coherent structures of different wall-bounded flows may indeed take place at very high Reynolds numbers.

Relevant to the issue of structural changes when  $Re_\theta > 6 \times 10^3$  is the recent assertion by Kailasnath (1993) that the skin friction, the pressure fluctuations, and the mean-velocity profiles all show a distinct change of behavior at about the same Reynolds number. For example, a power-law fit to existing skin-friction data for both boundary layers and pipe flows<sup>†</sup> indicates a break point at  $Re_\theta \approx 5000$ , that separates two ranges of Reynolds numbers. This and other evidence promoted Kailasnath (1993) to propose a transitional behavior for wall-bounded flows from a low to a high Reynolds number regime and to suggest further that the turbulence regeneration mechanism is different in the two regimes.

The results of Head and Bandyopadhyay (1981) discussed earlier indicate that the hairpin structures exhibit strong dependence on Reynolds number for  $Re_\theta < 7000$ , and hence the hairpins are atypical. At higher Reynolds numbers, on the other hand, the hairpin vortex is found unambiguously. In Head and Bandyopadhyay's view, Falco-Newman's (1977) typical eddies are merely the longitudinal cross-sections of the tips of the hairpins. Perry and Chong (1982) and Perry et al. (1986) concur with this view. Their model of the turbulent boundary layer emphasizes a hierarchy of hairpin eddies as the essential structure of the outer region. In wavenumber space, the analogous idea of a hierarchy of interacting scales and energy transfer from large eddies to

---

<sup>†</sup> The pipe Reynolds number based on its radius and the centerline velocity could be related to an equivalent Reynolds number based on the momentum thickness.

smaller ones is, of course, not new and has been proposed as early as 1922 by Richardson<sup>†</sup> and formalized by Kolmogorov (1941a).

Turbulent boundary layers ranging from relaminarized to separated cover the entire range of possible shape factor  $H$ . The statistical properties of the turbulent/irrotational fluid interface as well as the bursting period in such diverse layers can be described by  $H$  (Fiedler and Head, 1966; Bandyopadhyay, 1982). As can be expected, the location of the maximum deviation of the mean velocity from the logarithmic law also correlates with the mean location of the intermittent layer. Changes in the properties of the intermittent layer can take place when  $H$  drops below 1.3, that is, approximately when  $Re_\theta > 10 \times 10^3$ . This is supported by the flow visualization results of Head and Bandyopadhyay (1981) at  $Re_\theta = 17.5 \times 10^3$ , which shows that the outer part of the boundary layer is noticeably sparser; fewer of the hairpin vortices reach  $\delta$  although more of them are produced per unit (dimensional) wall area. Figure 51, which shows the variations of the shear correlation coefficient across a subsonic and supersonic boundary layer, seems also to echo that, as the Reynolds number is drastically increased,  $u$  and  $v$  fluctuations are not as well correlated in the outer layer. Note that the trends in this figure are primarily due to changing the Reynolds number; the effect of varying the Mach number has already been accounted for by considering local fluid properties.

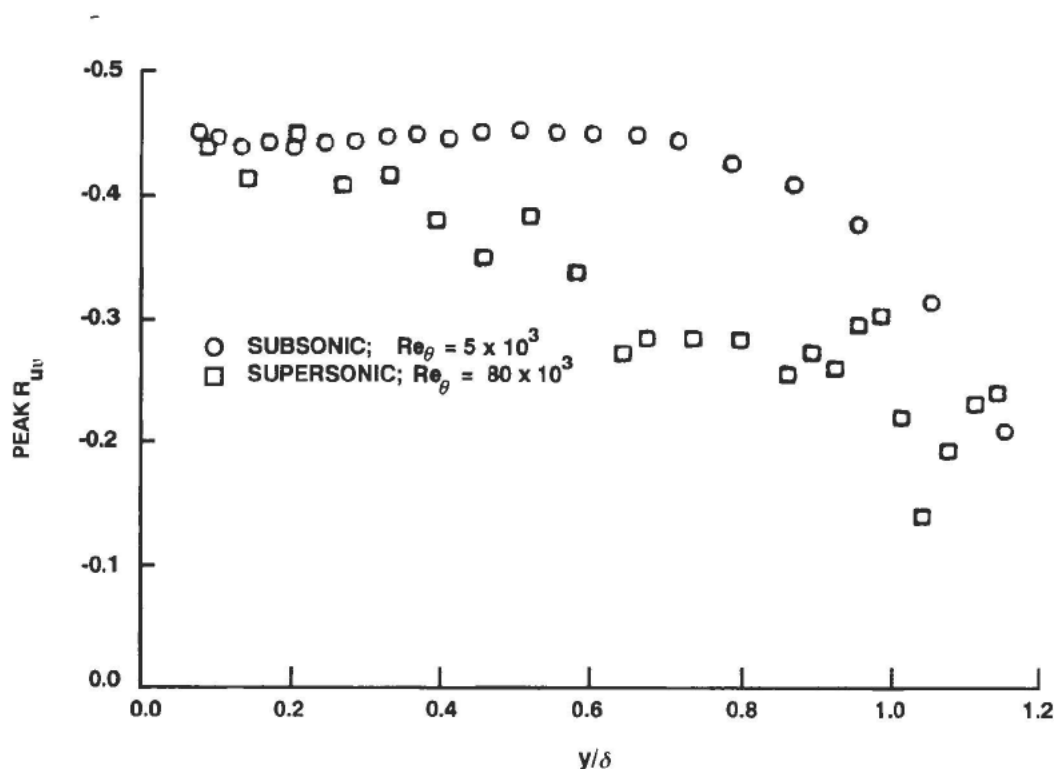


**Figure 51. Comparison of Shear Correlation Coefficient in High and Low Reynolds Number Boundary Layers (Smits, 1990)**

<sup>†</sup> Richardson's (1922) poetic description of turbulent clouds reads: Big whorls have little whorls that feed on their velocity, and little whorls have lesser whorls and so on to viscosity.

In high-speed, high Reynolds number turbulent boundary layers, the mean location of the intermittent layer and its standard deviation change significantly according to the results of Owen et al. (1975) at  $M_\infty = 7.0$  and  $Re_\theta = 85 \times 10^3$ . This is shown in figure 52, where the supersonic data are compared with the low-Reynolds number and low Mach number results of Klebanoff (1954). The intermittency profile for the supersonic boundary layer is clearly fuller. Furthermore, at these high Reynolds numbers, *the boundary layer structures do not exhibit much overturning motion that is typical of lower Reynolds numbers*. In the statistical measurements of conventional boundary layer properties at high Reynolds numbers these changes may not always seem dramatic, but their critical importance might lie in the efficiency of flow control devices similar to outer-layer devices for drag reduction (section 8.3.1).

Morrison et al. (1971) compared the sublayer spectra,  $P(k_z^+, \omega^+)$ , at low and high Reynolds number pipe flows. Their results are depicted in figures 53 and 54.<sup>†</sup> Over a sufficiently wide range of Reynolds numbers, the shape of the two-dimensional spectra expressed in wall-layer variables is not universal. This result contradicts the earlier low Reynolds number, one- and two-dimensional spectral observations made by Bakewell and Lumley (1967) and Morrison (1969). As the Reynolds number is increased from  $Re_\theta = 10,000$ -100,000, more energy appears in the low frequency, low wavenumber region. The additional energy results from disturbances that convect at twice the characteristic velocity of the sublayer of  $8U_\tau$ . The high Reynolds numbers appear to have the effect of randomizing the phase velocity, whereby the disturbances are no longer phase-correlated in the sublayer. This additional evidence also suggests much change in the turbulence production mechanism at very high Reynolds numbers. In fact, Morrison et al. (1971) have strongly suggested that the low speed streaks are unique to low Reynolds number wall-bounded flows. Streaks would no longer appear at very high Reynolds numbers, where a phase-correlated, wave-like turbulence may not exist within the viscous sublayer.

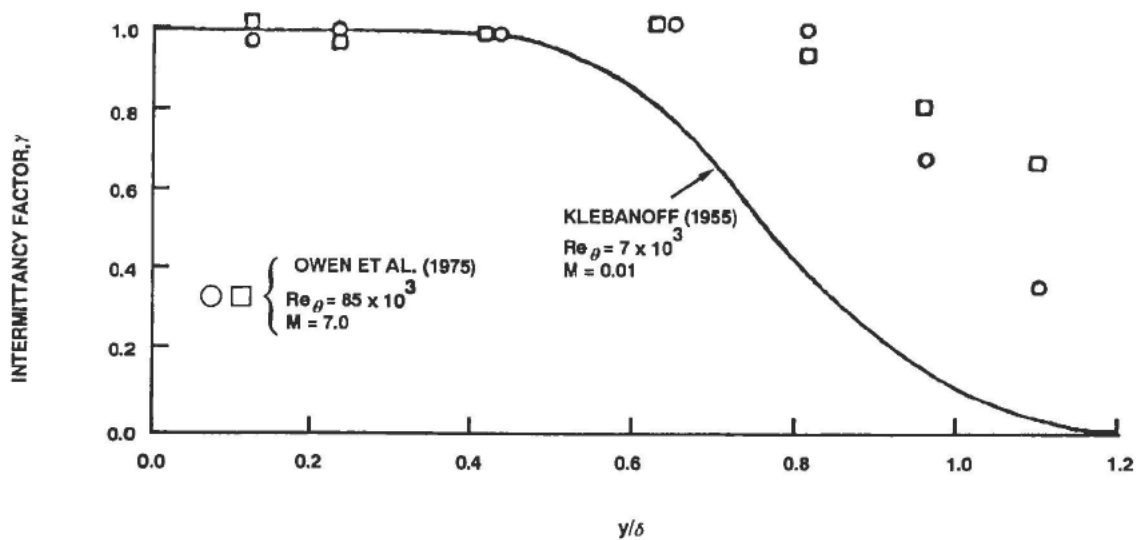


**Figure 52. Comparison of Intermittency Factor in High and Low Reynolds Number Boundary Layers (Smits, 1990)**

<sup>†</sup> Although the spectra in figure 54 were measured outside the viscous sublayer (at  $y^+ = 13.9$ ), Morrison et al. (1971) argue that the energy distribution at the sublayer edge is not substantially different from the distribution within the viscous sublayer.

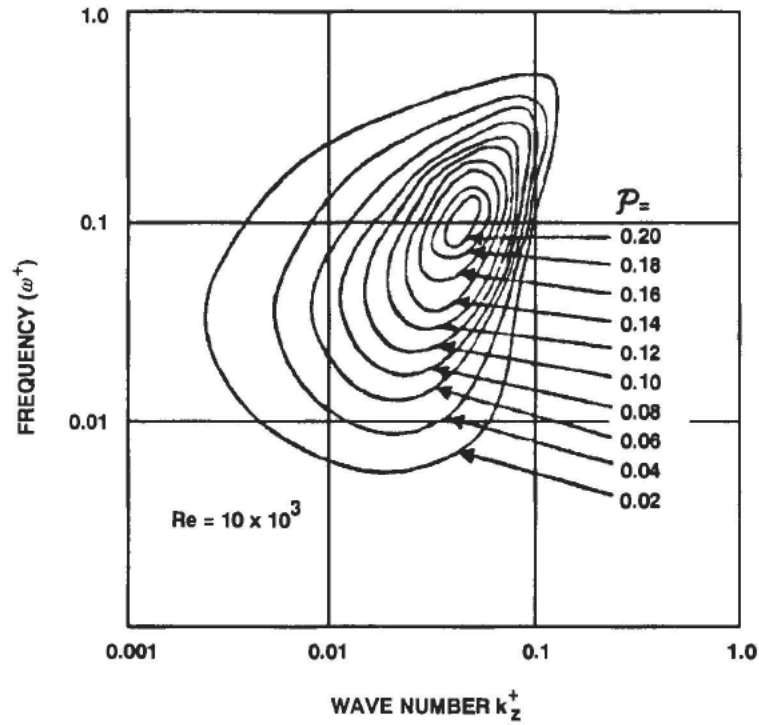


Figure 53. Two-Dimensional Spectra  $P(k_z^+, \omega^+)$  for  $Re_a = 10,000$ ;  $y^+ = 1.56$  (Morrison et al., 1971)

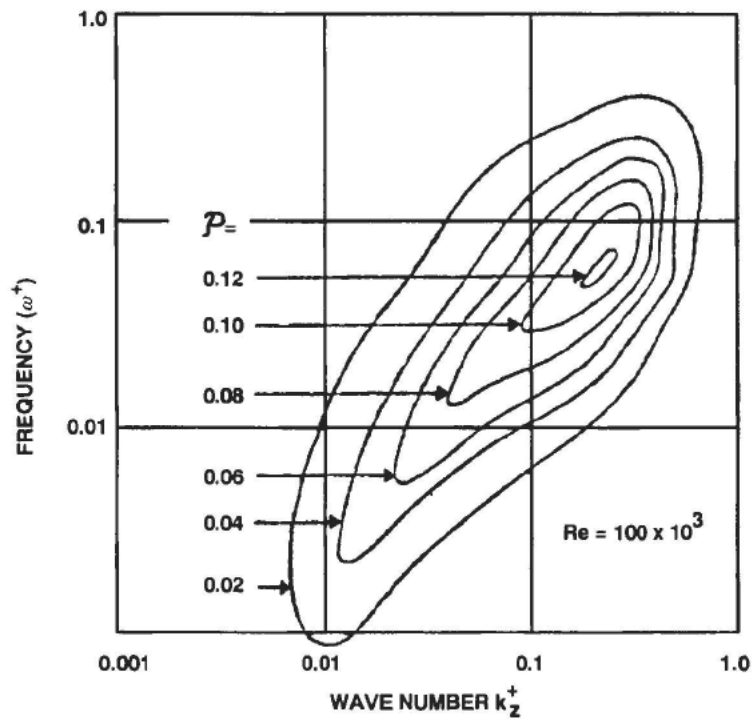


Figure 54. Two-Dimensional Spectra  $P(k_z^+, \omega^+)$  for  $Re_a = 100,000$ ;  $y^+ = 13.9$  (Morrison et al., 1971)

Using a rake of X-wires and conditional averaging techniques, Antonia et al. (1990) have examined the effects of Reynolds number on the topology of the large structures in the range  $1360 \leq Re_\theta \leq 9630$ . The instantaneous longitudinal sectional streamlines in a moving frame of reference contain many rotational structures  $O(\delta/2)$  at the lowest Reynolds number. Very significant  $Re_\theta$  effects can be observed in the instantaneous frames (see figure 5 that appears in Antonia et al., 1990). As  $Re_\theta$  is gradually increased to 9630, the large rotational structures become much smaller and no longer dominate the outer layer. When the large structures are selectively sampled and averaged, their foci are found to be more circular at lower Reynolds numbers. As  $Re_\theta$  is increased from 1360 to 9630, the location of the foci moves closer to the wall from  $0.83\delta$  to  $0.78\delta$ , which is consistent with the effect of Reynolds number on the mean location of the intermittent layer for similar values of the shape factor  $H$  (Fiedler and Head, 1966).

### 7.3.3 Small Structures in Outer Layer

In this subsection, an alliance is developed relating the ratio of outer to inner scales to Reynolds number changes. Reynolds number effects on small structures existing in the outer layer are then discussed. Finally, brief remarks are made on vortex-vortex interaction in the outer region.

The boundary-layer thickness in wall units  $\delta^+$  is related to the Reynolds number  $Re_\theta$  via the skin-friction coefficient and the ratio of boundary layer thickness to momentum thickness:

$$\delta^+ = \frac{\delta U_\tau}{\nu} = \frac{U_\tau}{U_\infty} \frac{\delta}{\theta} Re_\theta, \quad (35)$$

$$\delta^+ = \left( \frac{C_f}{2} \right)^{1/2} \frac{\delta}{\theta} Re_\theta. \quad (36)$$

For a smooth flat plate, an approximate empirical relation can be obtained by using the modified pipe resistance formula viz.,  $c_f = 0.0296(Re_x)^{-1/5}$  and the 1/7th-power-law velocity profile. The ratio of the outer scale to inner scale is thus given by

$$\delta^+ = 1.168(Re_\theta)^{0.875}. \quad (37)$$

Figure 55, taken from Bandyopadhyay (1991), shows that equation (35) describes the data over the entire Reynolds number range where measurements are available. The straight line is computed from modified pipe resistance formula and power-law mean-velocity profile.

---

† The notation  $Re^*$  is also used as discussed in section 3.

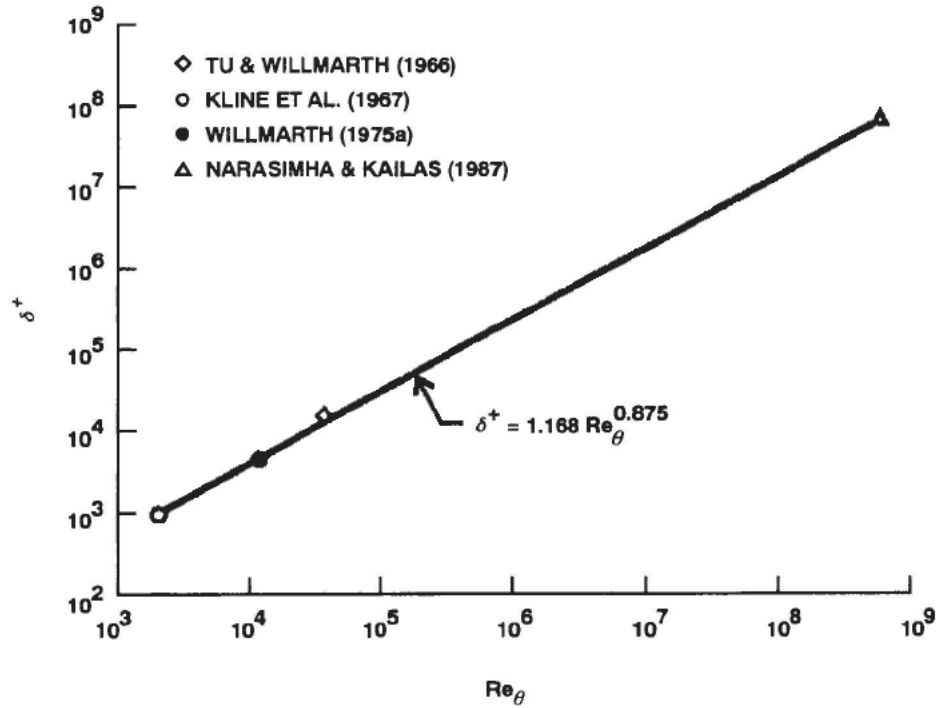


**Figure 55. Reynolds Number Dependence of Ratio of Outer to Inner Scale (Data Compiled by Bandyopadhyay (1991) From Different Experiments)**

Falco (1977) used simultaneous hot-wire anemometry and flow visualization to measure the characteristic dimensions of the typical eddy in the outer region of a boundary layer ( $C_x$  and  $C_y$ ; see insert in figure 56). His conclusion is that while large eddies appear to be Reynolds number independent, the typical eddies do depend on the Reynolds number.

Figure 56, taken from Bandyopadhyay (1991), shows a compilation of data from widely different physical as well as numerical experiments. The emphasis is on Reynolds number effects on organized small scales in the outer layer. Equation (37) is used to rescale Bushnell et al.'s (1975) compilation of the variation of the maximum mixing length ( $\ell$ ) with Reynolds number, shown by the shaded area in figure 56. The streamwise and normal characteristic dimensions of the typical eddy  $C_x$  and  $C_y$  are obtained from Falco's (1977) experiments referenced above. These data are represented, respectively, by the broken and solid lines in figure 56. Data for the Taylor's streamwise and normal micro-scales,  $\lambda_x$  and  $\lambda_y$ , are compiled by Falco (1974) and are indicated here by the slanted dashes. Finally, the range of variation of the diameter  $d$  of the characteristic hairpin near the edge of the boundary layer is computed from Spalart's direct numerical simulations by Robinson (1990). This is indicated in figure 56 at a single Reynolds number by the open circle and the *error bar*. The large variability of the vortex diameter in the simulations is intriguing.

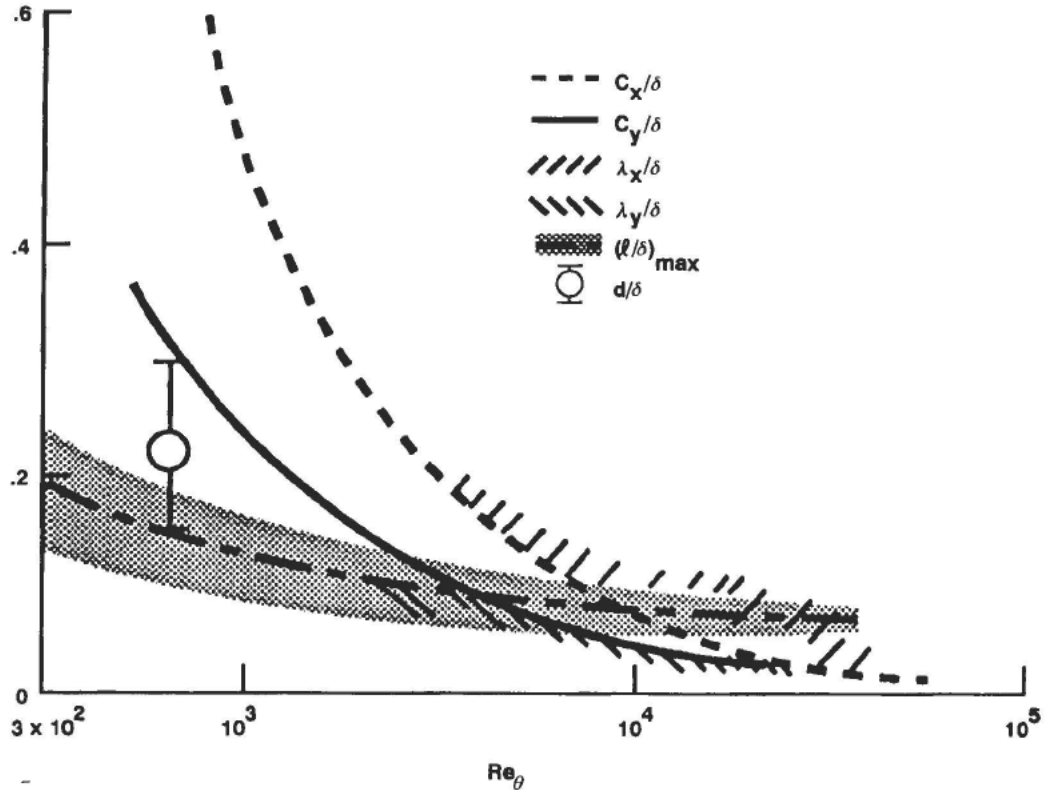


**Figure 56. Reynolds Number Variation of Maximum Mixing Length, Typical Eddy, and Taylor's Micro-Scale Lengths (Data Compiled by Bandyopadhyay, 1991)**

All scales are normalized with the appropriate boundary layer thickness,  $\delta$ . At  $Re_\theta > 10 \times 10^4$ , the characteristic size of all the organized small structures appears to asymptote to the value of the maximum mixing length:

$$\lambda_x / \delta \approx \lambda_y / \delta \approx C_x / \delta \approx C_y / \delta \approx (\ell / \delta)_{\max}. \quad (38)$$

In the same range of Reynolds numbers, the above scales are probably also equal to  $\lambda_z / \delta$  and  $C_z / \delta$ . This does not necessarily imply an approach to isotropy, but rather that  $x$ - $y$  and  $x$ - $z$  sections of the same hairpin vortex are being observed.

Smits et al. (1989) and Smits (1990) have compared a supersonic ( $Re_\theta = 80 \times 10^3$ ) and a subsonic ( $Re_\theta = 5 \times 10^3$ ) turbulent boundary layer, which primarily reflects the effect of  $Re_\theta$  and not  $M_\infty$ . In the high-Reynolds number flow, for  $y / \delta > 0.25$ , the peak value of the shear correlation coefficient  $R_{uv}$  is lower than the corresponding value in the low Reynolds number flow, e.g., by 40 percent at  $y / \delta = 0.65$  (see figure 51). Comparison of the probability density function shows that for  $y / \delta > 0.25$ , the vertical component of the Reynolds-stress-contributing motion is weaker in the high  $Re_\theta$  case.

If the Reynolds stress-production module is qualitatively unchanged, the drop in the coefficient  $R_{uv}$ , referred henceforth to the peak value, represents a disproportionate increase in the denominator. A large drop in the value of  $R_{uv}$  could happen if the turbulence becomes partially stochastic, whereby  $u$  and  $v$  are decorrelated while the kinetic energy production continues to contribute to the RMS values of  $u$  and  $v$ . But since such a situation will come largely due to high-frequency components that do not have much energy, the decreased  $R_{uv}$  must come from an increased contribution from the large scales that are energetic but are unable to produce turbulence. The growth, at higher Reynolds numbers, of an approximately flow-aligned, large-scale swirling motion in the cross-stream plane in the outer part of the boundary layer satisfies this requirement. Long-time two-dimensionality requires that swirls of both signs be produced. The development of the swirl suggests an increase in the  $v$  and  $w$  turbulence. Because the outer layer  $u$  turbulence intensity in supersonic boundary layers still scales with  $y/\delta$  exactly as at low  $Re_\theta$  (Smits 1990), the lower  $R_{uv}$  is attributable to increased  $v$  turbulence only. Accordingly, in the cross-stream plane, the  $v$  and  $w$  motions must be correlated over distances  $O(\delta)$  at high Reynolds numbers. With increasing Reynolds numbers, the vortex-vortex interactions in intra- and inter-hairpin vortices could lead to the formation of such new scales described as double helix and tornadoes, respectively, in Bandyopadhyay (1989).

The sequence of photographs in figure 57 shows that double-helix spiraling of a hairpin vortex in a turbulent boundary layer can indeed take place. The smoke-filled flow is illuminated with a sheet of laser inclined upstream at  $45^\circ$  to the flow direction, and the Reynolds number is approximately  $Re_\theta = 600$ . At this low Reynolds number, a typical vortex loop has a relatively low aspect ratio and vortex stretching is not pronounced. Nevertheless, the photographs in figure 57 adequately illustrate the phenomenon. Increased vortex stretching and vortex-vortex interaction could cause a hairpin vortex to first spiral around itself into a double helix and then onto further spiraling between neighboring double helices. The process contributes to crinkling and increase in surface area of the vorticity layer. The hierarchies of spiraling leading to many miniature tornadoes continues as long as they contribute to enstrophy amplification. These special behaviors become more pronounced as the Reynolds number is increased. As the double helix crosses the static light plane, the cross-section moves wall-ward and the direction of the inner-induced flow rotates. In this example, the maximum vortex diameter happens to be the same as the maximum mixing length and it decreases in size both as  $y \rightarrow 0$  and  $y \rightarrow \delta$ .

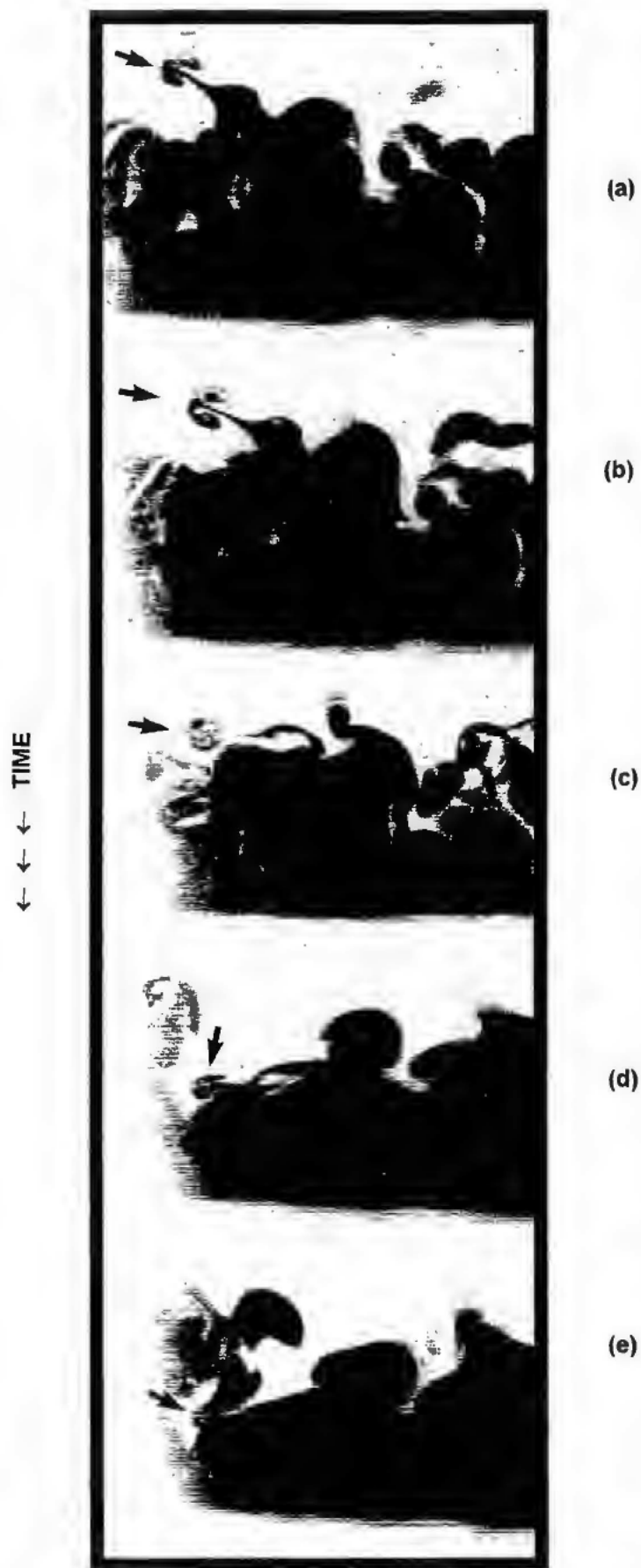


**Figure 57. Smoke-Filled Turbulent Boundary Layer Illuminated Using Laser Sheet Inclined Upstream at  $45^\circ$  to Flow Direction (Bandyopadhyay, 1989)**

### 7.3.4 Inner Structures

In this subsection, Reynolds number effects on the inner structures are discussed. It will be argued that vortex stretching is enhanced at higher Reynolds numbers, and that the low speed streaks, commonly observed in low Reynolds number experiments, may become less important at higher speeds.

Wei and Willmarth (1989) have argued that in turbulent channel-flow literature where an inner-layer scaling has been claimed to hold, errors have crept into measurements that are ascribable to large invasive probes, and that sometimes small but systematic variations with Reynolds number have been overlooked because such a scaling was assumed *a priori*. Their measurements, described previously in section 6 of this report, show that  $u_{rms}/U_\tau$  turbulence intensity scales on inner variables only up to  $y^+ \approx 10$ , which is well inside the inner region. The  $v_{rms}/U_\tau$  turbulence intensity and the Reynolds shear stress  $-\overline{uv}/U_\tau^2$  distributions do not scale on inner variables anywhere in the channel. Interestingly, the maximum normalized Reynolds stress and normal turbulence intensity increase with Reynolds number. This increase has been attributed to the enhancement of the vortex-stretching mechanism in the inner region with increasing Reynolds number.

Because the Reynolds number  $Re_a$  or  $Re_\theta$  is a dimensionless grouping of outer variables, failure of the turbulence quantities in the inner region to scale only on inner variables is an indication that the dynamics of the inner region structure are affected by outer as well as inner variables. Wei and Willmarth argue that these Reynolds number dependencies are caused by *changes in the coherent structure of the turbulence close to the wall*, and that the turbulent flow structure at high Reynolds number near solid boundaries, i.e., the hairpin vortex structure and interactions, will differ significantly from lower-Reynolds number inner structures.

Morrison et al. (1971) have studied the organized motion in the sublayer region of a pipe flow. As discussed in section 7.3.2, they have measured the two-point frequency-wavenumber spectra of the longitudinal velocity fluctuations at  $10.6 \times 10^3 \leq Re_a \leq 96.5 \times 10^3$ . An appeal of these data lies in its long-time averaged statistical nature and the absence of any troublesome, subjective threshold setting as used in VITA or VISA techniques. For  $Re_a < 30 \times 10^3$ , the streamwise phase velocity  $c_x^+$  in the sublayer is independent of wavenumber and remains a constant throughout the sublayer. Because this constant velocity coordinates the phase of the periodic motions at different wall-normal locations, Morrison et al., concluded that the sublayer turbulence is wave-like and, in fact, at low Reynolds numbers, it is likely that the sublayer consists of relatively periodic waves.

The critical-layer height is estimated to be  $9\nu/U_\tau$  because at that location, the average fluid velocity equals  $c_x^+ = 8$ . At  $Re_a < Re_c = 30 \times 10^3$ , the characteristic spanwise wavelength  $\lambda_z^+$  of 135 agrees with Kline et al.'s (1967) streak-spacing estimate of 130. However, for  $Re_a > Re_c$ , the frequency-wavenumber spectra for the laterally spaced points lose their universal shape, and the relative amount of low frequency, low wavenumber ( $k_z^+$ ) energy increases with Reynolds numbers

(see figures 53 and 54). This additional energy, which becomes significant at higher Reynolds numbers, results from disturbances that convect at velocities much greater (the average being  $16 U_\tau$ ) than the characteristic sublayer velocity of  $8 U_\tau$ . This led Morrison et al. (1971) to conclude that at higher Reynolds numbers, the character of the sublayer will be substantially altered, with an increasing amount of low frequency, low wavenumber energy being introduced. The disturbances responsible for this additional energy have propagation velocities much larger than that which characterizes the sublayer at low Reynolds numbers. The “streaky” structure, which has been assumed to be characteristic of the sublayer, will become less important as Reynolds number is increased, and it is probable that the streaks may not be apparent at sufficiently large values.

By trial and error, Walsh (1990) has optimized the dimensions of drag reducing V-groove riblets ( $h^+ = s^+ = 12$ , where  $h$  and  $s$  are the riblet height and spanwise spacing, respectively) at low Reynolds numbers ( $Re_\theta < 6 \times 10^3$ ). The value of  $s^+$  does not scale with the spanwise mean-streak-spacing  $\lambda_z^+ (\approx 100)$ . The findings of Walsh et al. (1989) and Walsh (1990) that the riblet performance does not change at transonic speeds and high Reynolds numbers ( $M_\infty = 0.7; 20 \times 10^3 \leq Re_\theta \leq 50 \times 10^3$ ) do not, therefore, invalidate the conclusion of Morrison et al. (1971) that the low-speed streaks will gradually become unimportant at high Reynolds numbers.

Grass (1971) investigated the nature of inner/outer interaction in smooth as well as rough wall-bounded flows. He maintains that the essential features of this interaction do not change despite the presence of three-dimensional roughness elements that protrude as much as 80 wall units into the inner layer, well outside the viscous region. Because low-speed streaks are not observed on walls with three-dimensional roughness, Grass' results minimize the importance of the streaks in the maintenance of turbulence.

A related issue is the importance of the intense, but rare, bursting events at high Reynolds numbers. Kailasnath (1993) used a statistical approach to obtain useful information on the structure of the instantaneous momentum flux, thus sidestepping analysis conditioned on specific episodes and focused instead on the contribution to the momentum flux associated with various magnitudes of velocity fluctuations. Kailasnath's non-episodic approach reveals that the contribution to the flux is dominated by medium amplitude velocity fluctuations in the range of  $\pm 1.5u'$ , which are not rare events. This implies a diminishing importance of the rare, intense events taking place in a progressively shrinking near-wall region as the Reynolds number increases.

## 8. FLOW CONTROL

### 8.1 INTRODUCTORY REMARKS

The ability to actively or passively manipulate a flow field to affect a desired change is of immense technological importance. The term boundary layer control includes any mechanism or process through which the boundary layer of a fluid flow is made to behave differently than it normally would were the flow developing naturally along a smooth flat surface. The topic has been reviewed by, among others, Bushnell (1983), Bandyopadhyay (1986b), Wilkinson et al. (1988), Bushnell and McGinley (1989), Gad-el-Hak (1989, 1990, 1993), Bushnell and Hefner (1990), Fiedler and Fernholz (1990), and Gad-el-Hak and Bushnell (1991). A boundary layer could be manipulated to achieve transition delay, separation postponement, lift enhancement, drag reduction, turbulence augmentation, or noise suppression. These objectives are not necessarily mutually exclusive. For example, by maintaining as much of a boundary layer in the laminar state as possible, the skin-friction drag and the flow-generated noise are reduced. However, a turbulent boundary layer is, in general, more resistant to separation than a laminar one. By preventing separation, lift is enhanced and the form drag is reduced. An ideal method of control that is simple, inexpensive to build and operate, and does not have any trade-off does not exist, and the skilled engineer has to make continuous compromises to achieve a particular goal.

Of all the various types of shear flow control now extant, control of flow separation is probably the oldest and economically most important. The tremendous increases in the capability of computational fluid dynamics (CFD), which have occurred as a direct result of increases in computer storage capacity and speed, are transforming flow separation control from an empirical art to a predictive science. Control techniques such as mitigation of imposed pressure gradients, blowing, and suction are all readily parameterized via viscous CFD. Current inaccuracies in turbulence modeling can severely degrade CFD predictions once separation has occurred; however, the essence of flow separation control is the calculation of attached flows, estimation of separation location (and indeed whether or not separation will occur), and tasks that CFD can in fact perform reasonably well within the uncertainties of the transition location estimation.

Techniques to reduce the pressure drag are more well established than turbulent skin-friction reduction techniques. Streamlining and other methods to postpone separation can eliminate most of the pressure drag. The wave and induced drag contributions to the pressure drag can also be reduced by geometric design.

The skin friction constitutes about 50 percent, 90 percent, and 100 percent of the total drag on commercial aircraft, underwater vehicles, and pipelines, respectively. Most of the current research effort concerns reduction of skin-friction drag for turbulent boundary layers. For that purpose, three flow regimes are identified. First, for  $Re_x < 10^6$ , the flow is laminar, and skin friction may be lowered by reducing the near-wall momentum. Adverse pressure gradient, blowing, and surface heating/cooling could lower the skin friction but increase the risk of transition and separation. Secondly, for  $10^6 < Re_x < 4 \times 10^7$ , active and passive methods to delay transition could be used, thus avoiding the much higher turbulent flow drag. Thirdly, at the Reynolds number encountered after the first few meters of a fuselage or a submarine, methods to

reduce the large skin friction associated with turbulent flows are sought. These methods are classified in the following categories: reduction of near-wall momentum; introduction of foreign substance; geometrical modification; relaminarization; and synergism.

The second category above leads to the most impressive results. Introduction of small concentration of polymers, surfactants, particles, or fibers into a turbulent boundary layer leads to a reduction in the skin-friction coefficient of as much as 80 percent. Recently introduced techniques often fall under the third category above and seem to offer more modest net drag reduction. These methods are, however, still in the research stage and include riblets ( $\approx 8$  percent), large eddy breakup devices (or outer-layer devices, OLD) ( $\approx 20$  percent), and convex surfaces ( $\approx 20$  percent).

The knowledge of the Reynolds number effects is useful to flow control because experimental investigations at low Reynolds numbers, i.e., lower speeds and smaller length scales, are less expensive. Most flow control devices are, therefore, developed and tested at rather low Reynolds numbers, for example,  $Re_\theta = 1000$ . Extrapolation to field conditions is not always straightforward though, and it often comes to grief. While the riblets results seem to extrapolate favorably to field conditions, the verdict on OLD is disappointing. These points will be discussed in sections 8.2 and 8.3.

## 8.2 RIBLETS

Properly optimized, longitudinally grooved surfaces, called riblets, could lead to a modest skin-friction drag reduction in the range of 5-10 percent in turbulent boundary layers. The subject dates back to the mid-1960s but has attracted much attention during the 1970s and 1980s. Walsh (1990) provides a recent up-to-date review. The exact mechanism through which riblets achieve net drag reduction despite the substantial increase in wetted surface area is still controversial. For the present purpose, however, the issue of Reynolds number effects on riblets performance is more pertinent. Flight tests and transonic tunnel experiments all indicate that the inner variables are the proper scaling for the dimensions of the riblets, as discussed in section 7.3.4.

Choi's (1989) spectrum measurements show that the energy of skin-friction fluctuations in the riblet groove drops by a decade compared with that of the smooth surface over more than a decade of the flow frequency range. Typically, over time expressed in wall units of  $t^+ = 170$ , the skin friction in the groove can remain below average and at a quiescent state as if the fluid in the groove is partially relaminarized. The dye flow visualization of Gallagher and Thomas (1984) also shows that the tracer remained quiescent and viscous pool-like between the ribs and leaves the groove only when a burst passes overhead. Like Gallagher and Thomas, Narasimha and Liepmann (1988) have also suggested that the riblets create pools of slow viscous flow in the valleys, and thereby modify the interaction of the wall flow with the outer flow. Black (1968) has analytically described the dynamics of the mean-velocity profile of a canonical turbulent boundary layer in terms of a periodic competition between the wall and outer layers, whereby the thickness of the sublayer changes with phase. The maximum thickness of the sublayer that the outer layer will allow can be obtained from the extrapolation of the log law to the sublayer profile.

Consider the equality

$$U^+ = y^+ = 2.41 \ln(y^+) + 5.4. \quad (39)$$

This is given by  $y^+ = 11$ , which is nearly the same as the optimized riblet height.

Once it is accepted that the riblet performance is unrelated to streaks, it comes as no surprise that sand-grain roughness also has a drag-reducing behavior exactly like riblets. Tani (1987, 1988) has reanalyzed Nikuradse's (1933) experimental data on sand-grain roughness and has shown that its performance also changes from drag reducing to drag increasing with increasing  $h^+$ , where  $h$  is the characteristic roughness height. The skin friction remains lower than that of the smooth wall for  $h^+ < 6$ . Compared with the optimized riblets, the drag reduction is lower in magnitude but is still of the same order. Tani has also suggested that the mechanism of drag reduction is likely to originate in the nearly quiescent regions of the flow between the interstices of the roughness elements, as observable deep within riblets.

Grass (1971) has shown in a channel flow that the intrush and outrush phases of the production cycle are also present when the wall has a three-dimensional roughness. Note, however, that walls with three-dimensional roughness elements do not have smooth, wave-like, low-speed streaks, and although the outer-layer structure is similar to that in a smooth wall, the near-wall stress-flux has a different behavior (Bandyopadhyay and Watson, 1988).

### 8.3 RECOVERY RESPONSE

There are at least two modes of interaction between the inner and outer regions of a boundary layer. In the first, the outer structures obtain at least part of their energy by convection and turbulent transport from the inner region of the upstream part of the boundary layer. This view is supported by the near-constancy of the ratio between turbulence stress and twice the turbulence kinetic energy,  $-\overline{uv} / \overline{q^2}$ , across a major portion of the boundary layer. This is true even in the wake region, i.e.,  $y / \delta \geq 0.2$ , where both the Reynolds stress and the RMS velocity fluctuations are rapidly decreasing. According to Townsend (1976), the turbulent fluid in that region has been sheared sufficiently long to attain its equilibrium structure. The second mode of inner/outer interaction involves the pressure effects of the inactive motion. Compared with the convective mode, the pressure mode is much less extended in the streamwise direction. In other words, the first mode points toward long memory while the second is associated with short memory. This may be relevant to the performance of different control devices as discussed in the following two subsections.

### 8.3.1 Disturbances in Outer Layer

The long memory associated with the outer structure dependence on upstream conditions contrasts the short memory of the inner region. This was demonstrated by Clauser (1956) who has shown that in a turbulent boundary layer at a given Reynolds number, disturbances survive much longer in the outer layer ( $y/\delta > 0.2$ ) than in the inner layer. He demonstrated this by placing a circular rod in the outer and inner regions of a fully-developed wall layer. For the rod placed at  $y/\delta = 0.16$ , the decay of the maximum deviation of the distorted mean-velocity profile from the equilibrium value was reduced to one-half of its initial value at a downstream distance of  $2\delta$ . In contrast, the outer-layer rod at  $y/\delta = 0.6$  caused a distortion in the velocity profile that lasted four times longer,  $8\delta$ , and that did not completely disappear even at  $16\delta$  downstream of the rod (see figure 13 of Clauser's article).

In viscous drag reduction techniques where a device drag penalty is involved, as with OLDs, a recovery length  $\approx 100\delta$  is desirable to achieve a net gain. To date, such recovery lengths have been achieved only at low Reynolds numbers,  $Re_\theta < 6 \times 10^3$  (Anders, 1990a). However, when Anders examined his outer-layer devices at higher Reynolds numbers, to his surprise, the drag reduction performance was reduced and the device was no longer a viable candidate for viscous drag reduction. Anders' measurements in the range of Reynolds numbers of  $2500 \leq Re_\theta \leq 18,000$  are depicted in figure 58. The experiments were conducted by towing a slender, axisymmetric body in a water channel. The outer-layer device used in figure 58a consists of two NACA-0009 airfoil-section rings placed in tandem 1.5 m downstream of the nose of the 3.7-m-long body. The second device used in figure 58b consists of two Clark Y low Reynolds number airfoil section rings, again placed in tandem. Both devices were optimized to yield lowest skin friction downstream. The figure depicts the downstream trends of the local skin friction, normalized with the skin friction at the same location but without the OLD.

Although both devices used by Anders (1990a) consistently lead to lower skin friction at all Reynolds numbers tested, net drag will, of course, be increased by the device drag penalty. This penalty depends on, among other factors, the thickness and angle of attack of the device, whether the boundary layer on the device itself is laminar, transitional, or turbulent, and the presence and extent of any separation bubble that might form on the outer-layer ribbon/airfoil. Anders (1990a) reports a very modest net drag reduction for his airfoil devices of around 2 percent at the lowest Reynolds number but a net drag increase of 1-5 percent at higher Reynolds numbers.

Bandyopadhyay (1986a) used a large-area drag balance to investigate, systematically, the Reynolds number effects on both single- and tandem-ribbon devices. His Reynolds number range of  $1300 \leq Re_\theta \leq 3600$  ( $5 \times 10^5 \leq Re_L \leq 1.8 \times 10^6$ ) is lower than that of Anders' (1990a), but the

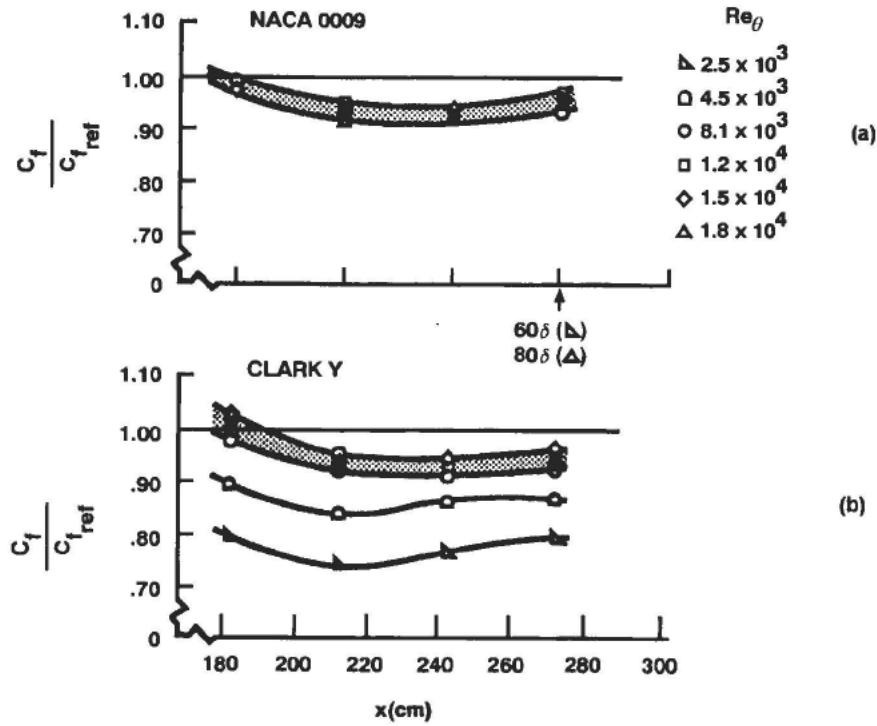


**Figure 58. Reynolds Number Effects on Viscous Drag Reduction Due to OLD for  $2500 \leq Re_\theta \leq 18,000$  (Anders, 1990a)**

loss-of-performance trends are the same as shown in figure 59. The net drag reduction as a percentage of the reference drag is plotted as a function of Reynolds number  $Re_L$  based on the freestream speed and the total length of the flat plate. Note that the drag penalty for the thin-ribbon devices used by Bandyopadhyay should be far smaller than that for the airfoil devices used by Anders. The conclusion was made that for both low  $Re_\theta (< 6 \times 10^3)$  and high  $Re_\theta (> 6 \times 10^3)$ , the effectiveness of OLD diminishes with the increase of Reynolds number.

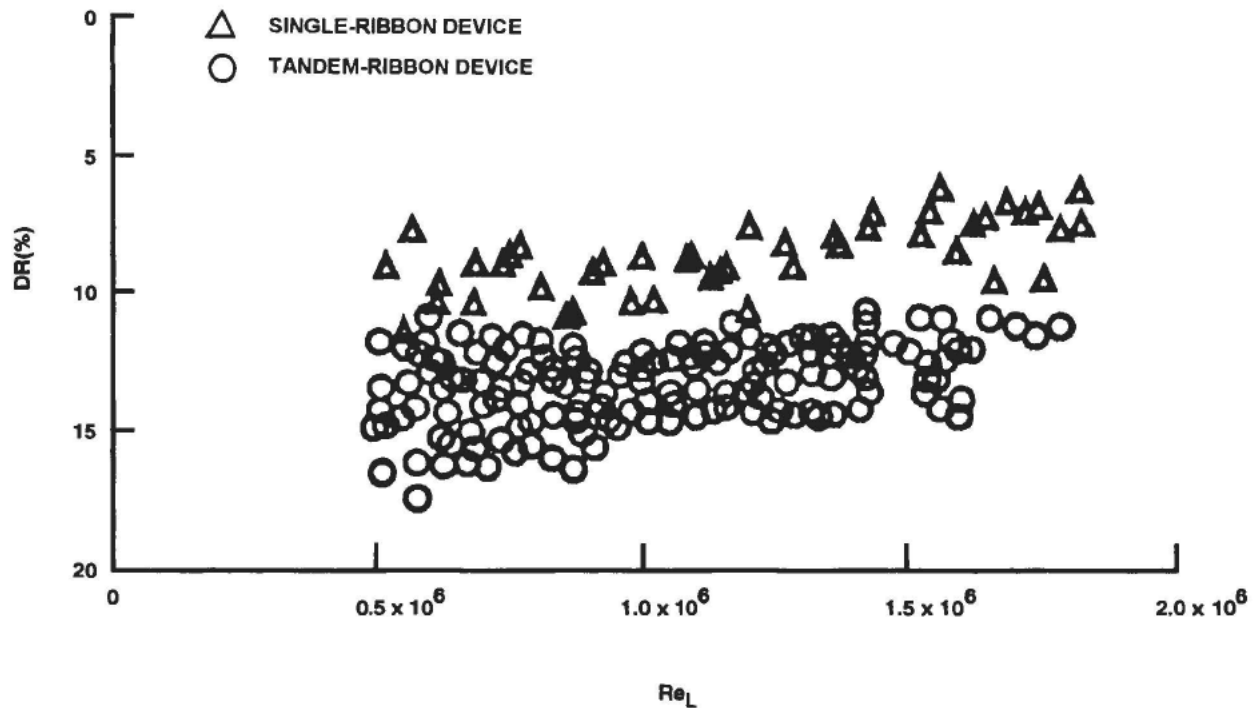


**Figure 59. Large Area Drag Balance Measurements Showing Reynolds Number Effects on Viscous Drag Reduction Due to Outer-Layer Devices for  $1300 \leq Re_\theta \leq 3600$  (Bandyopadhyay, 1986a)**

The continued drop in the skin-friction reduction with Reynolds number comes as a surprise because the mean flow analysis of Coles (1962) indicates an asymptotic state of the outer layer to have been reached above  $Re_\theta > 6 \times 10^3$ . The slow drop in  $\Delta U^+$  does not start until  $Re_\theta > 6 \times 10^3$  (see figures 11 and 12 of this report). Anders (1990a) attributed the irreproducibility of the low-Reynolds number behavior at higher values to a significant change in the turbulence structure at higher  $Re_\theta$  as discussed by Head and Bandyopadhyay (1981). The structural changes as the Reynolds number increases provide a simple explanation for the performance deterioration of outer-layer devices. These devices presumably work by selectively suppressing the normal velocity fluctuations, thus decorrelating the streamwise and normal velocities. As discussed in section 7, at high Reynolds numbers, fewer hairpin vortices reach the edge of the boundary layer because of increased interactions among these vortices. The overturning motion of the large eddies observed at low Reynolds numbers is less at higher Reynolds numbers, which reduces the  $v$  turbulence suppression role for the OLD.

### 8.3.2 Disturbances Close to Wall

From the preceding subsection, it is clear that knowledge of Reynolds number effects on the mean turbulent flow alone does not allow one to address all practical problems. This can be further demonstrated in the following post-transition unexpected result. Klebanoff and Diehl (1952) have made measurements on artificially thickened boundary layers at zero pressure gradient. The first 60 cm of their splitter plate was covered with No. 16 floor sanding paper. The measurements were carried out over a length of 320 cm at freestream velocities of 11, 17, and 33 m/s, giving three ranges of Reynolds numbers and producing a maximum  $Re_\theta$  of 14,850. The Reynolds number  $Re_\theta$  at the end of the sand roughness (at  $x = 60$  cm) was 2640, 4050, and 7990 at the three above mentioned speeds, respectively. Figure 60 shows the recovery response of the turbulent boundary layer to the same wall disturbance (meaning the same sand roughness) at the three different reference Reynolds numbers (that is, freestream speeds). One normally expects the recovery from wall disturbances to be the quickest (in  $x$ ) at the highest Reynolds numbers. Therefore, it comes as a surprise that, on the contrary, the return to the apparent "equilibrium" state (given by the broken line in figure 60) is clearly slowed down as the reference Reynolds number is *increased* and not *decreased*. Note that at  $U_\infty = 33$  m/s,  $\delta = 2.54$  cm at  $x = 60$  cm, which occurs immediately after the sand roughness. Figure 60 shows that even at the last station where  $x = 320$  cm and  $\Delta x / \delta = 100$ , the recovery is not yet complete. The recovery length in the figure for an incoming  $Re_\theta$  of about  $8 \times 10^3$  for the near-wall disturbance case is similar to the

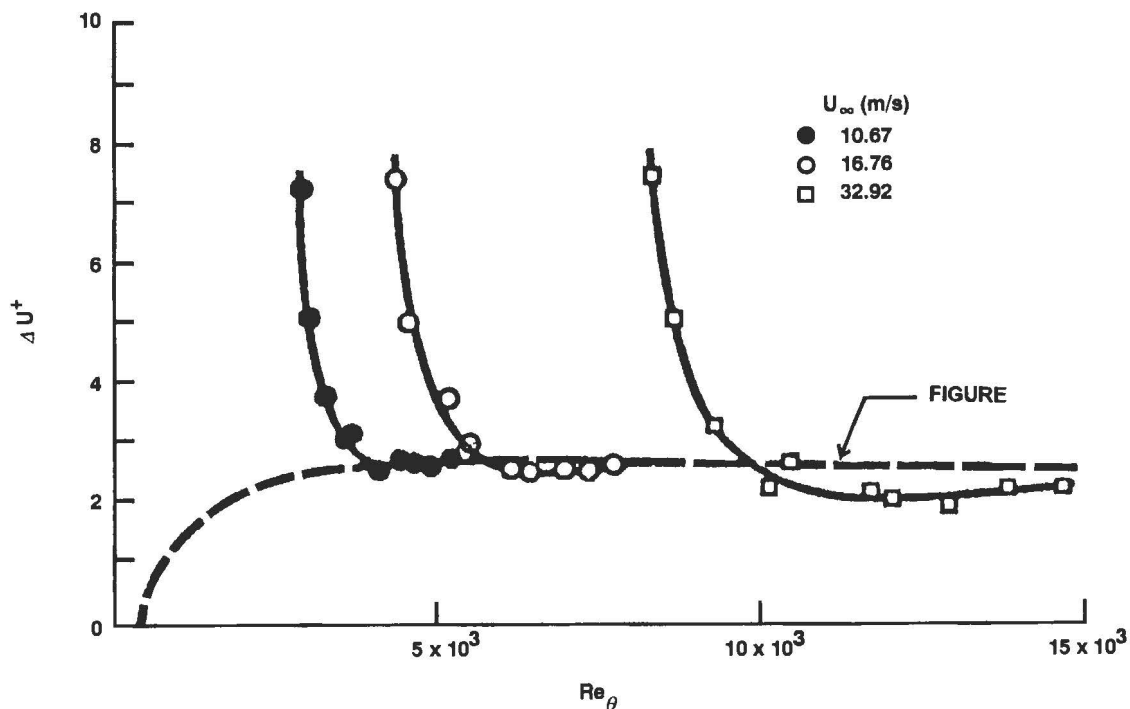


Figure 60. Approach to Equilibrium After Tripping Device at Moderately High Reynolds Numbers (Coles, 1962)

outer-layer disturbance case shown in figure 58 at a similar Reynolds number. This puzzling behavior leads to the question: why are the near-wall transition-trip disturbances surviving even beyond an  $x/\delta$  of 100 at such high Reynolds numbers as  $15 \times 10^3$  much like it is known for outer-layer devices at much lower Reynolds numbers? This question is clearly important to model testing in wind tunnels and code validation data, where roughness is used to trip and thicken the boundary layer to simulate high Reynolds numbers or flight conditions.

## 8.4 CONTROL OF HIGH REYNOLDS NUMBER FLOWS

The above discussion indicates that post-transition memory is longer at higher Reynolds numbers for certain trips. Wall-layer control may, therefore, have a long-lasting effect, say  $O(100\delta)$ , if applied during transition. On the other hand, as per Clauser (1956), if the wall control is applied in the fully developed turbulent region of the flow, the effect does not last long. The relevance of Reynolds number effects to flow control is particularly telling in case of full numerical simulation because it is currently limited to Reynolds numbers that are not far from transitional values.

It is instructive to recall here, typical Reynolds numbers encountered in the laboratory and in the field. Other than a handful of large-scale facilities (see section 5.4), boundary layers generated in wind tunnels and water tunnels typically have Reynolds numbers of  $Re_\theta = O(1000)$ . A commercial aircraft traveling at a speed of 300 m/s at an altitude of 10 km would have a unit Reynolds number of  $10^7/\text{m}$ . Because of the much smaller kinematic viscosity of water, a nuclear submarine moving at a modest speed of 10 m/s ( $\approx 20$  knots) would have the same unit Reynolds number of  $10^7/\text{m}$ . This unit Reynolds number translates to a momentum thickness Reynolds number near the end of either vehicle of roughly  $Re_\theta = 300,000$ . The Reynolds number on the space shuttle is as high as  $Re_\theta = 430,000$ ; on an aircraft carrier,  $Re_\theta$  can have a maximum of  $Re_\theta = 1.5 \times 10^6$ ; and in the atmospheric boundary layer,  $Re_\theta$  is typically  $10^6$ - $10^7$ . These ranges of Reynolds numbers together with the scopes of operation of typical wind and water tunnels, direct numerical simulations and three large-scale facilities, the National Transonic Tunnel, NASA-Langley towing tank, and the super-pipe are schematically shown in figure 61.

It is clear from the discussion thus far in this section and from the strong Reynolds number effects on the mean flow, higher-order statistics and coherent structures demonstrated in sections 5-7, that control devices developed and tested in the laboratory cannot, in general, be readily extrapolated to field conditions. Detailed knowledge of high Reynolds number consequences is required prior to attempting to control practical wall-bounded flows.

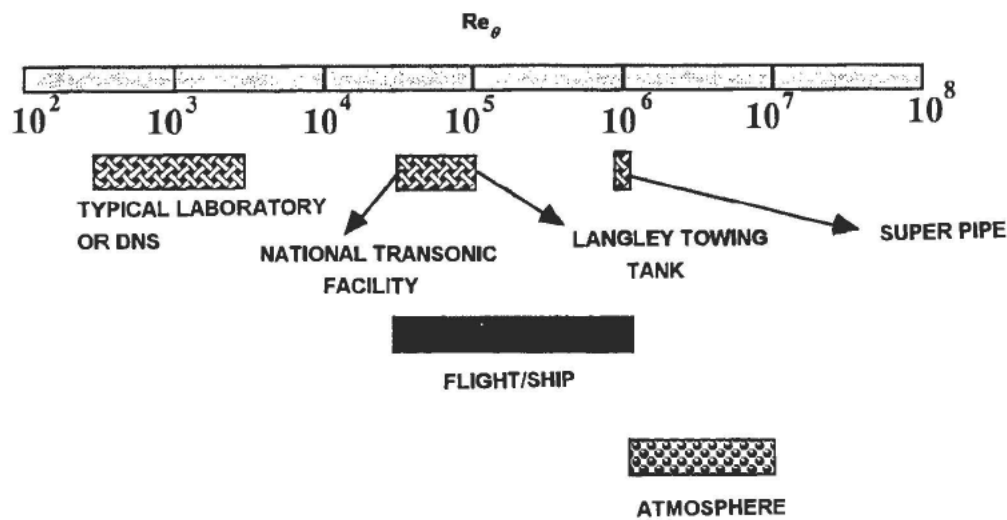


**Figure 61. Ranges of Momentum Thickness Reynolds Number for Different Facilities and Field Conditions**

## 9. NUMERICAL SIMULATIONS

### 9.1 GENERAL REMARKS

The principles of conservation of mass, momentum, and energy govern all fluid motions. In general, a set of partial, nonlinear differential equations expresses these principles and together with appropriate boundary and initial conditions constitute a well-posed problem. For a turbulent flow, the dependent variables are random functions of space and time, and no straightforward method exists for analytically obtaining stochastic solutions to nonlinear differential equations. Hence, the increased reliance on large-memory, high-speed digital computers to integrate the equations of motion. Large numbers of articles that specifically review turbulence computations are available (e.g., Launder and Spalding, 1974; Reynolds, 1976; Lumley, 1978, 1983; Rogallo and Moin, 1984; Speziale, 1991). Understanding and modeling of turbulence via numerical simulations can solve a variety of engineering problems and lead to important technological advances.

A distinguishable characteristic of high Reynolds number turbulent flows is their large range of excited space and time scales. In homogeneous turbulence, for example, the energy-containing eddies are  $O(Re_t^{3/4})$  times larger than the length scale of the smallest eddies (Kolmogorov length scale), where  $Re_t = u'L/\nu$  is the turbulence Reynolds number (see, for example, Landau and Lifshitz, 1987). To resolve the flow adequately, a computer storage (at each time step) of  $O(Re_t^{9/4})$  and a total number of arithmetic operations of at least  $Re_t^3$  are needed.

DNS attempted to integrate the instantaneous equations and resolve all scales with an appreciable kinetic energy but are limited to simple geometries and Reynolds numbers well below the values encountered in most practical situations. The reason is due to the enormous computer capacity required to resolve the necessarily time-dependent, three-dimensional velocity and pressure fields (as well as density and temperature fields if the flow is compressible). As indicated above, the number of active degrees of freedom in an incompressible turbulent flow is of the order of  $Re_t^{9/4}$  per unit volume. At Reynolds number of  $10^8$ , modest by geophysical standards, there are on the order of  $10^{18}$  active degrees of freedom per  $L^3$ , where  $L$  is the characteristic length of the flow (Frisch and Orszag, 1990). This colossal number challenges the capabilities of both the algorithms and fastest supercomputers available now or in the foreseeable future.

Even if it can be carried out, the brute-force numerical integration of the equations of motion using the supercomputer is prohibitively expensive even at modest Reynolds numbers. For example, a single direct numerical simulation of a canonical wall-bounded flow at  $Re_\theta = O(1000)$  requires about 1000 CPU hours and costs, at commercial supercomputer rates, close to \$1 million. This requirement increases roughly by an order of magnitude if the Reynolds number is doubled.

For now and the foreseeable future, a statistical approach, where a temporal, spatial, or ensemble mean is defined and the equations of motion are written for the various moments of the fluctuations about this mean, is the only route available to get meaningful engineering results. Unfortunately, the nonlinearity of the Navier-Stokes equations guarantees that the process of averaging to obtain moments results in an open system of equations, where the number of unknowns is always greater than the number of equations, and more or less heuristic modeling is used to close the equations. Such modeling can take a variety of forms and levels of sophistication, including the simple one-point first and second moments, the two-point closures or spectral models, the subgrid-scale models for large-eddy simulations, and models based on the joint probability density function.

In the simplest kind of turbulence modeling, the Reynolds stress is related to the mean-velocity gradient via a suitably assumed eddy viscosity, which may depend on position. Calculations of one-point first and second moments, such as mean velocity, mean pressure, and turbulence kinetic energy are then possible. Although gradient-transport models produce reasonable results in very few simple cases, they are in principle faulty (see, for example, Corrsin, 1974). Lumley (1992) summarizes the potential pitfalls in using first-order closure schemes. These are basically local models which, on introducing the Prandtl's (1925) concept of mixing length, make direct analogy between turbulent transport processes and molecular ones, an ill-fated assumption considering the lack of a clear-cut separation of scales in the former kind of transport.

A turbulent flow is, by necessity, nonlocal in nature. Conditions at a point depend on the history of all fluid particles that arrive at that point due to the hyperbolicity of the Navier-Stokes equations (Bradshaw et al., 1967). Ideally, therefore, a turbulence model should be nonlocal depending on the weighted integral, with fading memory and progressively broadening domain of integration, back over the mean path through the point in question. Second-order closure models essentially do that for second-order quantities, but the approximations used there for third-order quantities are again local, and so on. The structural models also satisfy this non-local requirement well.

Second-order models attempt to close the Reynolds-stress transport equations. Because these models are based on the two-point velocity correlation tensor, they provide more detailed information about the turbulence structure. The original idea for second-order closure schemes is due to Rotta (1951), but the massive computational requirement for solving six additional transport equations delayed its practical implementation for over two decades.

An alternative approach to conventional closure schemes uses the renormalization group (RNG) theory. The dynamic RNG method, first developed for use in the quantum field theory, together with a correspondence principle have been formalized for the turbulence problem by Yakhot and Orszag (1986). The method uses dynamic scaling and invariance together with iterated perturbation techniques to evaluate the transport coefficients and transport equations for the large-scale modes. RNG computations have been shown to produce better comparisons with experiments for complex situations where conventional closure methods often fail; for example, for separated flows, swirling flows, etc. A major advantage of the RNG analysis is its independence of any experimentally adjustable parameters.

Perhaps the next best computational strategy to direct numerical simulations is large-eddy simulations (LES), where the energy-containing eddies are directly computed but the more universal small scales are modeled. LES uses a fixed spatial resolution and the effects of eddies not resolved are modeled using gradient transport ideas (Galperin and Orszag, 1993) or the more sophisticated dynamic localization models. The two approaches are contrasted below.

Inertial transfer of energy over a wide range of spatial scales is a distinguishing characteristic of turbulent flows and one which strongly influences their evolution. This energy transfer originates from the nonlinear convective derivative term in the Navier-Stokes equation and gives rise to the familiar closure problem. The use of large-eddy simulation as a tool to explore the physics of complex turbulent flows is limited by current subgrid scale (SGS) models (Rogallo and Moin, 1984). Implicit in each SGS model currently in use are fairly simplistic assumptions regarding the nature of inertial energy transfer over the subgrid wavenumber range. For example, the simple Smagorinsky (1963) model lumps the effect of the subgrid eddies into an effective subgrid viscosity in the Heisenberg sense. The effect of shear at subgrid scales is neglected and the validity of the Smagorinsky model has been questioned by Kim et al. (1987). Such a model encounters particular difficulty when applied to complex nonequilibrium flows with extra strain rates. In the more recent dynamic SGS model (Germano et al. 1991), the eddy viscosity concept is retained, but a space time-dependent Smagorinsky constant is computed that allows the constant to adjust to the local flow dynamics. A disadvantage of dynamic localization SGS models with regard to their application in wall-bounded turbulent flows lies in the failure to

include effects associated with the anisotropy of small scales. The models can also predict energy backscatter that is too large and consequently gives rise to negative eddy viscosity values.

## 9.2 DIRECT NUMERICAL SIMULATIONS

Notwithstanding the colossal computer requirement, it is clear that integrating the instantaneous equations of motion is physically more sound than the heuristic closure required for any of the alternative approaches discussed above. DNS is not, however, without its detractors. A legitimate question is: What exactly is being simulated? It is not clear that DNS and a corresponding physical experiment at the same Reynolds number are simulating the same flow. When the numerical results are compared with experiments, at first glance, many points of agreement become evident. But some subtle disagreements remain, for example, in higher-order statistics. Admittedly, such quantities are not easy to measure in the laboratory either, and the observed differences may be fairly blamed on the experimentalists. However, notwithstanding that the full Navier-Stokes equations are being integrated, there are several potential pitfalls that are unique to DNS. These pitfalls include the imposed periodic boundary conditions, the unnatural way by which a boundary layer becomes turbulent<sup>†</sup> (it is neither properly tripped nor evolving through natural transition), and the sterilized environment in which the calculations progress (perfectly smooth wall and precisely irrotational, disturbance-free freestream). None of these conditions is possible in a physical experiment, and their detailed effects on the computed flow remain unknown. Two specific discrepancies between physical and numerical experiments will be elaborated later in this section.

More to the main topic of the present report is the ability to extrapolate low Reynolds number physical or numerical experiments to practical situations. Reynolds-averaged Navier-Stokes simulations model all the turbulent fluctuations and are not limited to low Reynolds numbers. The problem is to figure out the proper model to use for each range of Reynolds numbers. DNS, on the other hand, is by necessity a viable tool only at very modest Reynolds numbers. Without knowing Reynolds number effects on the mean and turbulence quantities, DNS results cannot be readily extended to engineering applications.

Now let us return to the subtle discrepancies between DNS and experiments. In the channel-flow direct numerical simulations of Moin and Kim (1982), the ratio of RMS spanwise vorticity fluctuations to RMS streamwise vorticity fluctuations computed at the wall is less than one-half of that computed from the near-wall velocity measurements of Kreplin and Eckelmann (1979) or the fluctuating shear stress right at the wall as measured by Fortuna and Hanratty (1971) and Sreenivasan and Antonia (1977). It seems that this discrepancy is a consequence of insufficient resolution in the viscous sublayer in the numerical simulations.

---

<sup>†</sup> Some researchers call DNS boundary layers *bastardized* turbulence (Robinson, 1991; Private Communication).

The second discrepancy concerns vortical structures, admittedly very difficult to detect experimentally. This report has shown that in a turbulent boundary layer, for  $Re_\theta < 10^3$ , Reynolds number affects the mean flow in the outer layer and the turbulence even down to  $y^+ = 4$ . In spite of that, the DNS studies of the flat-plate boundary layers (Robinson et al., 1989) give us information on the organized turbulence structures that would be valuable at higher Reynolds numbers. In the following, the simulation structure at  $Re_\theta = 670$  is compared with the experimentally observed structure at  $600 \leq Re_\theta \leq 17.5 \times 10^3$  (Head and Bandyopadhyay, 1981).

Figure 62 shows the numerically obtained vortical structures in a volume of several  $\delta^3$  (Robinson et al., 1989). The fact that vortex cores used here are always associated with regions of low pressure is used here to identify the vortical structures. This way, regions of significant vorticity are not confused with vortices, a potentially serious problem when dealing with unsteady viscous flows (Saffman and Baker, 1979; Robinson et al. 1989; Robinson, 1991). Compared with flow visualization experiments at  $Re_\theta = 600$  (Head and Bandyopadhyay, 1978), the immediate impression is that the number of structures per unit wall area is less and it is not difficult to track a structure all the way to the wall much like in the transitional layer. This gives credence to the criticism that what is being simulated numerically is not a fully developed turbulent flow but more like a transitional boundary layer.

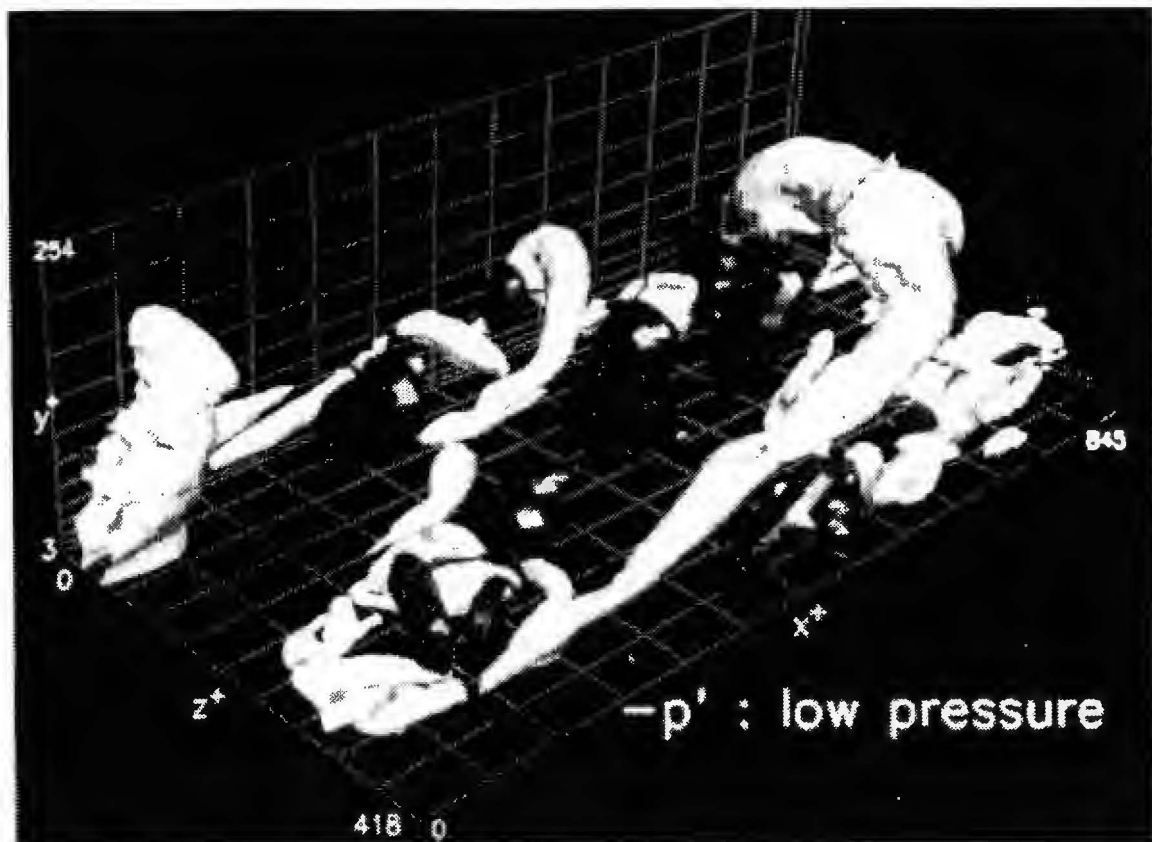


**Figure 62. Vortical Structures in Simulated Turbulent Boundary Layers**  
(Direct Numerical Simulation Results From Robinson et al., 1989)

A large structure can be defined as an agglomeration of successively forming hairpin vortices creating a linear upstream interface. However, Theodorsen (1952) and most others consider only one horseshoe vortex and not any agglomerations of them to describe a turbulent boundary layer. This causes a paucity of scales and restricts the models in their ability to better describe the turbulent boundary layer at high Reynolds numbers.

A longitudinal section of figure 62 contains one or two structures. In the constant-mixing-length region of the simulated boundary layer ( $\delta^+ = 280 > y^+ > 150$ ),  $d^+ = 60 \pm 20$ , where  $d$  is the vortex diameter (Robinson 1990; Bushnell et al., 1975). This gives a small range of  $\delta^+ / d_{\max}^+$ , viz., 3.5-7.0, which means there is a paucity of scales and that the overturning in the individual structures dominates the entire boundary layer. The overturning in the boundary layer diminishes with  $Re_\theta$  (Head and Bandyopadhyay, 1981). The value in the constant-mixing-length layer, viz.,  $d^+ / \delta^+ = 0.21_{14}^{29}$  compares with the mean value of Falco-Newman's (1974) typical-eddy<sup>†</sup> length scale  $C_y / \delta = 0.31$  at this  $Re_\theta$  (see figure 56).

It has been argued elsewhere (Bandyopadhyay, 1989) that increased vortex stretching and vortex-vortex interaction could lead the hairpin vortices to first spiral around themselves into a double helix and then onto further spiraling between neighboring double helices. Such process at  $Re_\theta = 600$  was depicted in figure 57 of this report. Vortex-vortex interactions are not present, however, in the direct numerical simulations at approximately the same Reynolds number ( $Re_\theta = 670$ ).

The high-resolution velocity and vorticity measurements by Klewicki et al. (1994) also indicate some disagreement with the numerical results of Spalart (1988). The experimental profile of turbulence kinetic energy production is consistently lower, predominantly resulting from differences in the Reynolds stress profiles. Both their turbulence diffusion and viscous diffusion terms peak closer to the wall than the computational profiles. In the experiment, the negative peak in the diffusion profile occurs closer to one wall than the positive peak in the production profile. In contrast, an opposite situation is observed in the numerical simulations, where the diffusion term exhibits its negative peak further from the wall and crosses zero near the positive peak in the production profile (figure 8 of Klewicki et al.'s paper).

---

<sup>†</sup> This is the cross-section of the hairpin vortices according to Head and Bandyopadhyay (1981) and Klewicki et al. (1994).

## 10. NON-CANONICAL BOUNDARY LAYERS

Thus far in this report, the focus has been on the canonical, turbulent wall-bounded flow. The incompressible, isothermal, zero-pressure-gradient boundary layer developing over a smooth, rigid, semi-infinite flat plate, or the closely related two-dimensional channel flow, is the *simplest* problem to study analytically, experimentally, or numerically. Practical wall-bounded flows, however, have one or more complicating influences such as freestream turbulence, pressure gradient, compressibility, roughness, surface curvature, three-dimensionality, wall compliance, heat transfer, stratification, change of phase, presence of side-walls and corners, etc. Such flows are naturally more difficult to deal with analytically, experimentally, or numerically but are nevertheless important to study for at least two reasons. Firstly, their behavior is often quite different from that of the canonical problem and therefore must be determined prior to rational design of practical devices. Secondly, as suggested by Clauser (1956), who in turn was inspired by Maxwell's concept of a *black box*, the physical understanding of a canonical turbulent flow (the black box) could be improved by observing the response of the flow to different external influences. In other words, studying a boundary layer over a rough wall, for example, might shed more light on the smooth-wall flow.

From the point of view of Reynolds number effects on the non-canonical wall-bounded flows, it is intuitively appealing to conclude that these effects are at least as strong as those reviewed in the bulk of the present paper for the canonical flow. Corroborating data, one way or the other, are unfortunately not available. The few existing experiments dealing with complex wall-bounded flows were not specifically designed to search for Reynolds number effects. In other words, such experiments were carried out at a particular Reynolds number or at a rather narrow range of Reynolds numbers. For example, if the RMS-velocity profiles, do not scale with inner variables in the canonical flow, there is little reason to believe that the corresponding profiles in the non-canonical case would do so. There is, however, one notable exception to this argument. Unlike the canonical problem, wall-bounded flows over rough walls may indeed achieve true Reynolds number-independence. This trait will be elaborated below.

In the present authors opinion, a complicating influence that is particularly useful to add to the arsenal of tools available to better understand the canonical wall-bounded flow is the non-smooth wall perturbation. Roughness is simple to implement, at least in physical experiments, and its effect on the flow is pronounced (see Raupach et al., 1990, for a recent review of rough-wall turbulent boundary layers). At sufficiently high Reynolds numbers, the skin friction becomes independent of viscosity and depends solely on the relative roughness scale. In this so-called fully-rough regime, the constant skin-friction coefficient contrasts the ever decreasing skin friction for a smooth wall. This has important consequences on the flow equilibrium as illustrated below.

According to Clauser (1954), an equilibrium turbulent boundary layer is characterized by similarity of its velocity-defect profile in the course of its downstream development. True equilibrium is achieved when the velocity-defect ratio becomes a function of  $(y/\delta)$  only and, therefore, independent of Reynolds number. Tani and Motohashi's (1985a, 1985b) results of analyzing available data seem to negate the existence of an equilibrium state for smooth, zero-pressure-gradient boundary layers. Tani (1986, 1987), on the other hand, shows that equilibrium is possible for boundary layers in favorable pressure gradients over smooth as well as k-type

rough surfaces. For a roughness height that increases linearly with the streamwise direction, equilibrium is achieved in zero pressure gradient. For d-type roughness, equilibrium exists for a certain range of pressure gradients, from favorable to adverse. These useful properties of rough walls may be exploited to better understand Reynolds number effects on smooth-wall boundary layers.

There is at least one more argument in favor of studying wall-bounded flows over rough walls. As discussed by Kailasnath (1993), changes in the wall-bounded flow physics are due to changing the scale ratio  $\delta^+$  or  $a^+$  and not the Reynolds number per se. While the mean flow is primarily influenced by  $Re_\theta$ ,  $\delta^+$  may be the more significant parameter for the turbulence and coherent structures. Such assertion is difficult to prove for the canonical flow case because a change in Reynolds number leads to a corresponding change in the scale ratio. However, this is not the case for fully-rough walls, making them particularly useful to study. In that case, the scale ratio at a given Reynolds number could be simply changed by systematically varying the roughness height.

A glimpse of the complexity of Reynolds number effects in non-canonical turbulent boundary layers can be had by examining such effects in the presence of freestream turbulence (Blair, 1983; Hancock and Bradshaw, 1983; Castro, 1984; Bandyopodhyay, 1992). This is a complicating factor that is particularly important for turbo-machinery blades where the Reynolds number is low ( $Re_\theta < 5000$ ) and the freestream turbulence is high. The effect of freestream turbulence is to increase the skin friction. However, as Bradshaw and Hancock (1983) have shown, freestream turbulence cannot be measured by turbulence intensity ( $u'/U_o$ ) alone, but also jointly with the ratio of the dissipation length scale in the freestream and the boundary layer thickness, ( $L_o/\delta$ ). The freestream turbulence parameter that combines these two effects is defined as

$$f = \left\{ \left[ \frac{u'}{U_o} \right] / \left[ \left( \frac{L_o}{\delta} \right) + 2 \right] \right\}. \quad (40)$$

The simultaneous involvement of the scale ratio greatly complicates the Reynolds number dependence of the freestream turbulence effects (Bandyopodhyay, 1992). For example, due to freestream turbulence in the range of  $f > 0.0115$ , the wake component  $\Delta U^+$  increases with  $Re_\theta$ , and in the range of  $0.0025 < f < 0.0095$ ,  $\Delta U^+$  drops with  $Re_\theta$ . On the other hand, in the two ranges of  $f \leq 0.0025$  and  $0.0095 \leq f \leq 0.0115$ , there is no apparent dependence on  $Re_\theta$ .

To account for low-Reynolds number effects, Blair (1983) empirically arrived at the following damping factor:

$$\beta = \left[ 1 + 3e^{-(Re_\theta/425)} \right]. \quad (41)$$

According to Bandyopodhyay (1992), the fractional increase in skin friction is then a function of only  $f_\beta = f \cdot \beta^n$ , where the exponent  $n$  takes the values -1, 1, or 0 depending, respectively, on whether  $\Delta U^+$  increases, decreases, or remains constant with increasing  $Re_\theta$ . Figure 63 is a summary of the increase in skin friction caused by freestream turbulence when the just mentioned dependence on  $Re_\theta$  is taken into account. The dashed lines indicate a  $\pm 5$  percent scatter band about the least-squares-fit solid line, and the arrows indicate uncertainties.

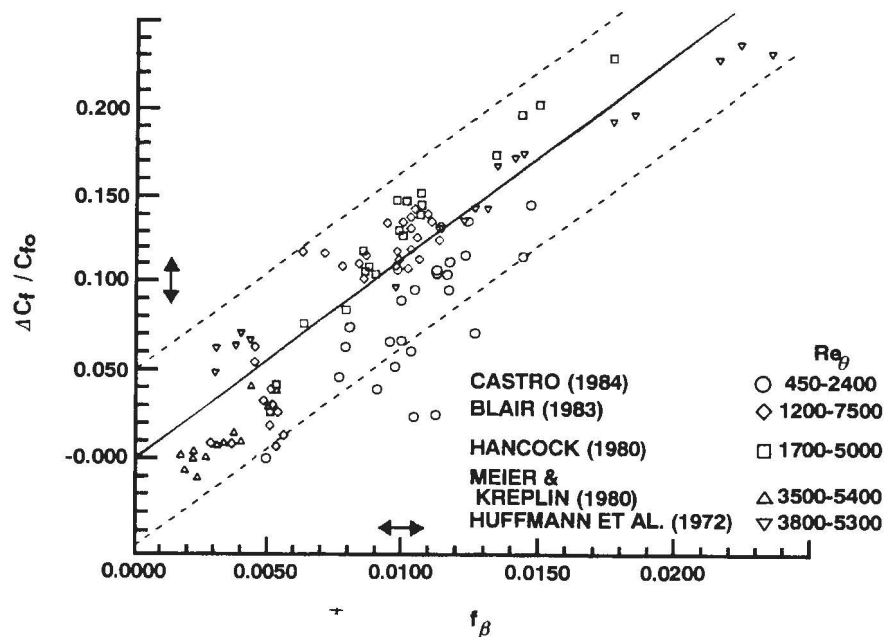


**Figure 63. Reynolds Number Dependence of Fractional Increase in Skin Friction Caused by Freestream Turbulence (Bandyopadhyay, 1992)**

## 11. CONCLUSIONS

In this report, an attempt was made to assimilate the considerable volume of experimental and numerical boundary-layer data that have been accumulated since the mean flow review of Coles (1962). Attention is drawn to some aspects of the emerging description of the structure of high-Reynolds number turbulent boundary layers. Both the inner- and outer-layer structures are affected by Reynolds number. The turbulence quantities do not accurately scale with wall-layer variables in the inner layer. The outer-layer turbulence structure ( $S_u$ , peak  $R_{uv}$ , intermittency,  $u$   $v$  quadrant distributions, streamwise scales) is greatly changed at extremely high Reynolds numbers (Smits et al., 1989, Smits 1990) and new structures probably evolve because of vortex-vortex interactions. As aptly illustrated by Kailasnath (1993), the classical similarity theory of wall-bounded flows that asserts a universal description for the near-wall flow is found to be increasingly deficient as the questions become more detailed.

The numerically simulated low Reynolds number, flat-plate turbulent boundary layers are characterized by a paucity of scale and a lack of vortex-vortex interaction. Studies of the very low Reynolds number turbulent boundary layer structure might not inherently involve several aspects of the high Reynolds number structure, which may be crucial to flow control through turbulence manipulation.

Why does the mean flow scale with wall-layer variables in the inner layer yet turbulence quantities do not? At a relatively low Reynolds number, for example,  $Re_\theta = 500$ , the inner-layer mean flow is already universal; so why should the low  $Re_\theta$  structure not be universal? These questions erroneously imply that there is a first-order direct connection between the mean flow and turbulence in a wall-bounded flow as in a free-shear flow. In a mixing layer, for example, the experimentally observed two-dimensional rollers are the direct result of an inviscid instability of the mean-velocity profile. Their characteristic dimension is equal to the layer thickness, and they contain almost all of the mean-flow vorticity. In a wall-bounded flow, on the other hand, the three-dimensional hairpin vortices are the result of a secondary or a tertiary instability, and their diameters are typically much smaller than the boundary layer thickness. The hairpins contain only a portion of the mean flow vorticity -- that is, they are further removed from the mean flow

Experience with turbulence modeling also suggests that the turbulence in a wall-bounded flow is not derived directly from the mean flow. In the earliest turbulence models, shear stress is derived from the mean-velocity profile. Such models have not been widely successful. Townsend (1976) and Bradshaw et al. (1967) have argued that instead there is a much closer connection between the shear stress and the turbulence structure. Townsend's work was limited to the near-wall region, while Bradshaw et al., have extended the argument to the entire shear layer. Direct measurements of typical eddies have supported their assertion (Falco, 1974; Newman, 1974).

It should be realized that ensemble averaging is a useful mathematical tool for computing typical characteristics as long as the variability in the quantities of interest is sufficiently low. The large variability in the measurements of streak spacing (standard deviation  $\sim 0.3$  to  $0.4$  of mean) and of vortex diameter even in full simulation at one low  $Re_\theta$  of 670 (maximum diameter about

twice minimum one) is disturbing and this issue has not yet been addressed. The following questions are raised:

1. Is the turbulence production mechanism independent of Reynolds number?
2. Even at one  $Re_\theta$  is there only one mechanism of turbulence production?
3. Can there be several mechanisms simultaneously in play each of which has a different Reynolds number dependence?

In the context of these questions the conclusion arrived at by Keith et al. (1992) for wall-pressure spectra, viz., that the scaling changes from mixed to outer layer as  $Re_\theta$  is increased, is intriguing. The answer to question 1 seems no longer an unequivocal affirmative.

A summary of conclusions of the Reynolds number effects follows:

1. The widely accepted "asymptotic" state of the wake component is present only in the range  $6 \times 10^3 < Re_\theta < 1.5 \times 10^4$ . At higher values, it drops although at a much slower rate than that in the range  $Re_\theta < 6 \times 10^3$ .
2. The Clauser's shape parameter is strongly Reynolds number dependent at  $Re_\theta < 10^3$ , and weakly above that.
3. Alternatives to the logarithmic mean velocity profile have been periodically proposed. Such *heretical* ideas deserve further scrutiny. Independent confirmation in well-controlled experiments that cover a wide range of Reynolds numbers is necessary.
4. The freestream turbulence effect is dependent on Reynolds number.
5. Turbulence measurements with probe lengths greater than the viscous sublayer thickness ( $\approx 5$  wall units) appear to be unreliable, particularly near the wall.
6. Unlike the mean flow, the statistical turbulence quantities do not scale accurately with the wall-layer variables over the entire inner layer. Such scaling applies over only a very small portion of the inner layer adjacent to the wall.
7. At low Reynolds numbers, the peak  $u$  turbulence intensity increases slightly with Reynolds number in both channels and flat plates.
8. The distance from the wall where the streamwise turbulence intensity peaks appears to scale with inner variables.
9. In contrast, the corresponding distances, expressed in wall units, for both the normal fluctuations and the Reynolds stress move away from the wall as the Reynolds number increases.

At high  $Re$ , the peak normal turbulence intensity and the peak Reynolds stress occur substantially outside the viscous region.

10. The wall pressure RMS increases slightly with Reynolds number.

11. Systematic changes in the mean and higher order statistics as the Reynolds number varies could be considered as proper first-order trends within the framework of an asymptotic theory. At finite Reynolds numbers, the additive composite expansion formed from the inner and outer expansions of any turbulence quantity provides the only uniformly valid approximation in the matched region.

12. In flat plates, trip memory can survive the statistical turbulence quantities at even  $Re_\theta > 6 \times 10^3$ , where the mean flow is said to have reached an asymptotic state.

13. The Reynolds number dependence of the post-transition relaxation length of both the mean and turbulence quantities is not well understood.

14. In pipe flows, the wave nature of the viscous sublayer that is observable at low Reynolds numbers gives way to a poorly understood random process at high Reynolds numbers.

15. While the variously defined (small) length scales differ greatly from each other at low Reynolds numbers, they all asymptote to the mixing length at much higher Reynolds numbers ( $Re_\theta > 1.0 \times 10^4$ ).

16. The outer-layer structure changes continuously with Reynolds number, and very little is known about the structure of very high Reynolds number turbulent boundary layers.

17. The aspect ratio of the hairpin vortices increases with Reynolds number as they also become skinnier. In a large structure, the number of constituent hairpin vortices per unit wall area (dimensional) increases with Reynolds number.

18. Changes in the wall-bounded flow physics can also be described as due to changing the scale ratio,  $\delta^+$  or  $a^+$ , which changes downstream in a given flow at a rate slightly lower than  $Re_\theta$ .

19. There is a dire need for high-resolution, reliable measurements of mean and statistical turbulence moments at high Reynolds numbers in smooth, flat-plate turbulent boundary layers.

20. Reynolds number effects in canonical flows cannot always be extrapolated to non-canonical cases in a simple straightforward manner.

It is obvious that our knowledge of Reynolds number effects in wall-bounded turbulent flows is basically phenomenological and a good theoretical foundation is largely lacking. Consequently, many of the controversies regarding the effects will remain with us for sometime to come. Direct, well-resolved and non-intrusive measurements will go a long way in resolving many of the controversies.

## BIBLIOGRAPHY

- Acarlar, M. S., and C. R. Smith (1987a), "A Study of Hairpin Vortices in a Laminar Boundary Layer, Part 1, Hairpin Vortices Generated by a Hemisphere Protuberance," *Journal of Fluid Mechanics*, vol. 175, pp. 1-41.
- Acarlar, M. S., and C. R. Smith (1987b), "A Study of Hairpin Vortices in a Laminar Boundary layer, Part 2, Hairpin Vortices Generated by Fluid Injection," *Journal of Fluid Mechanics*, vol. 175, pp. 43-83.
- Achia, B. U., and D. W. Thompson (1977), "Structure of the Turbulent Boundary Layer in Drag-Reducing Pipe Flow," *Journal of Fluid Mechanics*, vol. 81, pp. 439-464.
- Afzal, N. (1976), "Millikan's Argument at Moderately Large Reynolds Number," *Physics of Fluids*, vol. 1, pp 600-602.
- Afzal, N., and W. B. Bush (1985), "A Three-Layer Asymptotic Analysis of Turbulent Channel Flow," *Proceedings of the Indian Academy of Science (Mathematical Sciences)*, vol. 94, pp. 135-148.
- Alfredsson, P. H., and A. V. Johansson (1984), "On the Detection of Turbulence-Generating Events," *Journal of Fluid Mechanics*, vol. 139, pp. 325-345.
- Allan, J. F., and R. S. Cutland (1953), "Wake Studies of Plane Surfaces," *Transactions of the North East Coast Institute of Engineers and Shipbuilders*, vol. 69, pp. 245-266.
- Alving, A. E., A. J. Smits, and J. H. Watmuff (1990), "Turbulent Boundary Layer Relaxation from Convex Curvature," *Journal of Fluid Mechanics*, vol. 211, pp. 529-556.
- Anders, J. B. (1990a), "Boundary Layer Manipulators at High Reynolds Numbers," in *Structure of Turbulence and Drag Reduction*, A. Gyr, Ed., Springer-Verlag, Berlin, pp. 475-482.
- Anders, J. B. (1990b), "Outer-Layer Manipulators for Turbulent Drag Reduction," in *Viscous Drag Reduction in Boundary Layers, AIAA Progress in Astronautics and Aeronautics*, Volume 123, D. M. Bushnell and J. N. Hefner, Eds., Washington, DC, pp. 263-284.
- Andreopoulos, J., F. Durst, Z. Zaric, and J. Jovanovic (1984), "Influence of Reynolds Number on Characteristics of Turbulent Wall Boundary Layers," *Experiments in Fluids*, vol. 2, pp. 7-16.
- Antonia, R. A., D. K. Bisset, and L. W. B. Browne (1990), "Effect of Reynolds Number on the Topology of the Organized Motion in a Turbulent Boundary Layer," *Journal of Fluid Mechanics*, vol. 213, pp. 267-286.

- Antonia, R. A., S. Rajagopalan, C. S. Subramanian, and A. J. Chambers (1982), "Reynolds-Number Dependence of the Structure of a Turbulent Boundary Layer," *Journal of Fluid Mechanics*, vol. 121, pp. 123-140.
- Antonia, R. A., M. Teitel, J. Kim, and L. W. B. Browne (1992), "Low-Reynolds-Number Effects in a Fully Developed Turbulent Channel Flow," *Journal of Fluid Mechanics*, vol. 236, pp. 579-605.
- Ashkenas, H. I., and F. R. Riddell (1955), "Investigation of the Turbulent Boundary Layer on a Yawed Flat Plate," NACA Technical Note TN-3383, National Advisory Committee for Aeronautics, Hampton, VA.
- Aubrey, N., P. Holmes, J. L. Lumley, and E. Stone (1988), "The Dynamics of Coherent Structures in the Wall Region of a Turbulent Boundary Layer," *Journal of Fluid Mechanics*, vol. 192, pp. 115-173.
- Bakewell, H. P., and J. L. Lumley (1967), "Viscous Sublayer and Adjacent Wall Region in Turbulent Pipe Flow," *Physics of Fluids*, vol. 10, pp. 1880-1889.
- Bandyopadhyay, P. R. (1980), "Large Structure with a Characteristic Upstream Interface in Turbulent Boundary Layers," *Physics of Fluids*, vol. 23, pp. 2326-2327.
- Bandyopadhyay, P. R. (1982), "Period Between Bursting in Turbulent Boundary Layers," *Physics of Fluids*, vol. 25, pp. 1751-1754.
- Bandyopadhyay, P. R. (1983), "Turbulent Spot-Like Features of a Boundary Layer," *Annals of New York Academy of Sciences*, vol. 404, pp. 393-395.
- Bandyopadhyay, P. R. (1986a), "Drag Reducing Outer-Layer Devices in Rough Wall Turbulent Boundary Layers," *Experiments in Fluids*, vol. 4, pp. 247-256.
- Bandyopadhyay, P. R. (1986b), "Review -- Mean Flow in Turbulent Boundary Layers Disturbed to Alter Skin Friction," *Journal of Fluids Engineering*, vol. 108, pp. 127-140.
- Bandyopadhyay, P. R. (1987), "Rough-Wall Turbulent Boundary Layers in the Transition Regime," *Journal of Fluid Mechanics*, vol. 180, pp. 231-266.
- Bandyopadhyay, P. R. (1989), "Effect of Abrupt Pressure Gradients on the Structure of Turbulent Boundary Layers," in *Proceedings of the 10<sup>th</sup> Australasian Fluid Mechanics Conference*, Volume 1, A. E. Perry et al., Eds., University of Melbourne, Australia, pp. 1.1-1.4.
- Bandyopadhyay, P. R. (1990), "Convex Curvature Concept of Viscous Drag Reduction," in *Viscous Drag Reduction in Boundary Layers, AIAA Progress in Astronautics and Aeronautics*, Volume 123, D. M. Bushnell and J. N. Hefner, Eds., Washington, DC, pp. 285-324.

- Bandyopadhyay, P. R. (1991), "Comments on Reynolds Number Effects in Wall-Bounded Shear Layers," *AIAA Paper* 91-0231, New York.
- Bandyopadhyay, P. R. (1992), "Reynolds Number Dependence of the Freestream Turbulence Effects on Turbulent Boundary Layers," *AIAA Journal*, vol. 30, pp. 1910-1912.
- Bandyopadhyay, P. R., and A. Ahmed (1993), "Turbulent Boundary Layers Subjected to Multiple Curvatures and Pressure Gradients," *Journal of Fluid Mechanics* vol. 246, pp. 503-527.
- Bandyopadhyay, P. R., and A. K. M. F. Hussain (1984), "The Coupling Between Scales in Shear Flows," *Physics of Fluids*, vol. 27, pp. 2221-2228.
- Bandyopadhyay, P. R., and R. Balasubramanian (1993), "A Vortex Model for Calculating Wall Pressure Fluctuations," *ASME Symposium on Flow Noise Modeling, Measurement and Control*, T. M. Farabee, W. L. Keith, and R. Lueptow, Eds., New Orleans, LA, 28 November - 3 December 1993, NCA vol. 15, FED vol. 168, pp. 503-527.
- Bandyopadhyay, P. R., and R. Balasubramanian (1994), "On the Role of Vortex Reynolds Number in Turbulent Boundary Layers," *Theoretical and Computational Fluid Dynamics* (in press).
- Bandyopadhyay, P. R., and R. D. Watson (1988), "Structure of Rough-Wall Turbulent Boundary layers," *Physics of Fluids*, vol. 31, pp. 1877-1883.
- Barenblatt, G. I. (1979), *Similarity, Self-Similarity, and Intermediate Hypothesis*, Plenum Press, New York.
- Barenblatt, G. I. (1993), "Scaling Laws for Fully Developed Turbulent Shear Flows, Part 1, Basic Hypothesis and Analysis," *Journal of Fluid Mechanics*, vol. 248, pp. 513-520.
- Barenblatt, G. I., and V. M. Prostokishin (1993), "Scaling Laws for Fully Developed Turbulent Shear Flows, Part 2, Processing of Experimental Data," *Journal of Fluid Mechanics*, vol. 248, pp. 521-529.
- Berkooz, G., P. Holmes, and J. L. Lumley (1991), "Intermittent Dynamics in Simple Models of the Turbulent Boundary Layer," *Journal of Fluid Mechanics*, vol. 230, pp. 75-95.
- Bhatt, W. V. (1971), "Flight Test Measurement of Exterior Turbulent Boundary Layer Pressure Fluctuations on Boeing Model 737 Airplane," *Journal of Sound and Vibration*, vol. 14, pp. 439-457.
- Black, T. J. (1966), "Some Practical Applications of a New Theory of Wall Turbulence," in *Proceedings of the 1966 Heat Transfer and Fluid Mechanics Institute*, M. A. Saad and J. A. Miller, Eds., Stanford University Press, Stanford, CA, pp. 366-386.

- Black, T. J. (1968), "An Analytical Study of the Measured Wall Pressure Field Under Supersonic Turbulent Boundary Layers," NASA Contractor Report CR-888, National Aeronautics and Space Administration, Langley, VA.
- Blackwelder, R. F. (1978), "The Bursting Process in Turbulent Boundary Layers," in *Workshop on Coherent Structures of Turbulent Boundary Layers*, C. R. Smith and D. E. Abbott, Eds., Lehigh University, Bethlehem, PA, pp. 211-227.
- Blackwelder, R. F. (1988), "Coherent Structures Associated with Turbulent Transport," in *Transport Phenomena in Turbulent Flows*, M. Hirata and N. Kasagi, Eds., Hemisphere, New York, pp. 69-88.
- Blackwelder, R. F., and H. Eckelmann (1978), "The Spanwise Structure of the Bursting Phenomenon," in *Structure and Mechanisms of Turbulence I, Lecture Notes in Physics*, Volume 75, H. Fiedler, Ed., Springer-Verlag, Berlin, pp. 190-204.
- Blackwelder, R. F., and H. Eckelmann (1979), "Streamwise Vortices Associated with the Bursting Phenomenon," *Journal of Fluid Mechanics*, vol. 94, pp. 577-594.
- Blackwelder, R. F., and J. H. Haritonidis (1983), "Scaling of the Bursting Frequency in Turbulent Boundary Layers," *Journal of Fluid Mechanics*, vol. 132, pp. 87-103.
- Blackwelder, R. F., and R. E. Kaplan (1976), "On the Wall Structure of the Turbulent Boundary Layer," *Journal of Fluid Mechanics*, vol. 76, pp. 89-112.
- Blackwelder, R. F., and L. S. G. Kovasznay (1972), "Time-Scales and Correlations in a Turbulent Boundary Layer," *Physics of Fluids*, vol. 15, pp. 1545-1554.
- Blair, M. F. (1983), "Influence of Free-Stream Turbulence on Turbulent Boundary Layer Heat Transfer and Mean Profile Development, Part II--Analysis of Results," *Journal of Heat Transfer*, vol. 105, pp. 41-47.
- Blair, M. F., and M. J. Werle (1980), "The Influence of Free-Stream Turbulence on the Zero Pressure Gradient Fully Turbulent Boundary Layer," Report R80-914388-12, United Technologies Research Center, Hartford, CT.
- Bradshaw, P. (1967), "'Inactive' Motion and Pressure Fluctuations in Turbulent Boundary Layers," *Journal of Fluid Mechanics*, vol. 30, pp. 241-258.
- Bradshaw, P., D. H. Ferriss, and N. P. Atwell (1967), "Calculations of Boundary-Layer Development Using the Turbulent Energy Equation," *Journal of Fluid Mechanics*, vol. 28, pp. 593-616.
- Bremhorst, K., and T. B. Walker (1974), "Spectral Measurements of Turbulent Momentum Transfer in Fully Developed Pipe Flow," *Journal of Fluid Mechanics*, vol. 61, pp. 173-186.

- Brown, G. L., and A. S. W. Thomas (1977), "Large Structure in a Turbulent Boundary Layer," *Physics of Fluids*, vol. 20, pp. S243-S252.
- Bushnell, D. M. (1983), "Turbulent Drag Reduction for External Flows," *AIAA Paper*, 83-0227, New York.
- Bushnell, D. M., and G. C. Greene (1991), "High-Reynolds-Number Test Requirements in Low-Speed Aerodynamics," in *High Reynolds Number Flows Using Liquid and Gaseous Helium*, R. J. Donnelly, Ed., Springer-Verlag, New York, pp. 79-85.
- Bushnell, D. M., and J. N. Hefner, Eds. (1990), *Viscous Drag Reduction in Boundary Layers, AIAA Progress in Astronautics and Aeronautics*, Volume 123, Washington, DC.
- Bushnell, D. M., and C. B. McGinley (1989), "Turbulence Control in Wall Flows," *Annual Review of Fluid Mechanics*, vol. 21, pp. 1-20.
- Bushnell, D. M., A. M. Cary, and B. B. Holley (1975), "Mixing Length in Low Reynolds Number Compressible Turbulent Boundary Layers," *AIAA Journal*, vol. 13, pp. 1119-1121.
- Butler, K. M., and B. F. Farrell (1993), "Optimal Perturbations and Streak Spacing in Wall-Bounded Shear Flow," *Physics of Fluids A*, vol. 5, pp. 774-777.
- Cantwell, B. J. (1990), "Organized Motion in Turbulent Flow," *Annual Review of Fluid Mechanics*, vol. 13, pp. 457-515.
- Castro, I. P. (1984), "Effects of Free Stream Turbulence on Low Reynolds Number Boundary Layers," *Journal of Fluids Engineering*, vol. 106, pp. 298-306.
- Chiwanga, S. C., and B. R. Ramaprian (1993), "The Effect of Convex Wall Curvature on the Large-Scale Structure of the Turbulent Boundary Layer," *Experiments in Thermal Fluid Sciences*, vol. 6, pp. 168-176.
- Choi, K. S. (1989), "Near-Wall Structure of a Turbulent Boundary Layer with Riblets," *Journal of Fluid Mechanics*, vol. 208, pp. 417-458.
- Clauser, F. H. (1954), "Turbulent Boundary Layers in Adverse Pressure Gradient," *Journal of Aeronautical Sciences*, vol. 21, pp. 91-108.
- Clauser, F. H. (1956), "The Turbulent Boundary Layer," *Advances in Applied Mechanics*, vol. 4, pp. 1-51.
- Coles, D. (1956), "The Law of the Wake in the Turbulent Boundary Layer," *Journal of Fluid Mechanics*, vol. 1, pp. 191-226.
- Coles, D. E. (1962), "The Turbulent Boundary Layer in a Compressible Fluid," Report R-403-PR, Rand Corporation, Santa Monica, CA.

- Comte-Bellot, G. (1963), "Contribution à l'Étude de la Turbulence de Conduite," Doctoral Thesis, University of Grenoble, France.
- Comte-Bellot, G. (1965), "Ecoulement Turbulent entre Deux Parois Paralleles," *Publications Scientifiques et Techniques du Ministere de l' Air*, No. 419, Paris, France.
- Corino, E. R., and R. S. Brodkey (1969), "A Visual Investigation of the Wall Region in Turbulent Flow," *Journal of Fluid Mechanics*, vol. 37, pp. 1-30.
- Corrsin, S. (1957), "Some Current Problems in Turbulent Shear Flow," in *Symposium on Naval Hydrodynamics*, F.S. Sherman, Ed., National Academy of Sciences/National Research Council, No. 515, Washington, DC, pp. 373-400,
- Corrsin, S. (1974), "Limitations of Gradient Transport Models in Random Walks and Turbulence," in *Turbulent Diffusion in Environmental Pollution, Advances in Geophysics*, Volume 18A, F. N. Frenkiel and R. E. Munn, Eds., Academic Press, New York, pp. 25-60.
- Donnelly, R. J. (1991), *High Reynolds Number Flows Using Liquid and Gaseous Helium*, Springer-Verlag, New York.
- Donohue, G. L., W. G. Tiederman, and M. M. Reischman (1972), "Flow Visualization of the Near-Wall Region in a Drag-Reducing Channel Flow," *Journal of Fluid Mechanics*, vol. 56, pp. 559-575.
- Dutton, R. A. (1955), "Experimental Studies of the Turbulent Boundary Layer on a Flat Plate With and Without Distributed Suction," Ph.D. Dissertation, Cambridge University, England.
- Eckelmann, H. (1974), "The Structure of the Viscous Sublayer and the Adjacent Wall Region in a Turbulent Channel Flow," *Journal of Fluid Mechanics*, vol. 65, pp. 439-459.
- Elena, M., and R. Dumas (1978), "Turbulence Scales in a Pipe Flow With a Slightly Heated Wall," *American Society of Mechanical Engineers*, Paper No. 78-HT-4, Inst de Mec Stat de la Turbul, France.
- Erm, L. P., A. J. Smits, and P. N. Joubert (1987), "Low Reynolds Number Turbulent Boundary Layers on a Smooth Flat Surface in a Zero Pressure Gradient, in "Fifth Symposium on Turbulent Shear Flows, F. Durst et al., Eds., Springer-Verlag, Berlin, pp. 2.13-2.18.
- Falco, R. E. (1974), "Some Comments on Turbulent Boundary Layer Structure Inferred From the Movements of a Passive Contaminant," *AIAA Paper 74-99*, New York.
- Falco, R. E. (1977), "Coherent Motions in the Outer Region of Turbulent Boundary Layers," *Physics of Fluids*, vol. 20, pp. S124-S132.
- Falco, R. E. (1980), "The Production of Turbulence Near a Wall," *AIAA Paper 80-1356*, New York.

- Falco, R. E. (1983), "New Results, a Review and Synthesis of the Mechanism of Turbulence Production in Boundary Layers and its Modification," *AIAA Paper* 83-0377, New York.
- Falco, R. E. (1991), "A Coherent Structure Model of the Turbulent Boundary Layer and its Ability to Predict Reynolds Number Dependence," *Philosophical Transactions of the Royal Society of London, Series A*, vol. 336, pp. 103-129.
- Farabee, T. M., and M. J. Casarella (1991), "Spectral Features of Wall Pressure Fluctuations Beneath Turbulent Boundary Layers," *Physics of Fluids, A*, vol. 3, pp. 2410-2420.
- Fiedler, H. E. (1986), "Coherent Structures," in *Advances in Turbulence*, G. Comte-Bellot and J. Mathieu, Eds., Springer-Verlag, Berlin, pp. 320-336.
- Fiedler, H. E. (1988), "Coherent Structures in Turbulent Flows," *Progress in Aerospace Sciences*, vol. 25, pp. 231-269.
- Fiedler, H. E., and H.-H. Fernholz (1990), "On Management and Control of Turbulent Shear Flows," *Progress in Aerospace Sciences*, vol. 27, pp. 305-387.
- Fiedler, H. E., and M. R. Head (1966), "Intermittency Measurements in the Turbulent Boundary Layer," *Journal of Fluid Mechanics*, vol. 25, pp. 719-735.
- Fortuna, G., and T. J. Hanratty (1971), "The Influence of Drag-Reducing Polymers on Turbulence in the Viscous Sublayer," *Journal of Fluid Mechanics*, vol. 53, pp. 575-586.
- Frisch, U., and S. A. Orszag, (1990), "Turbulence: Challenges for Theory and Experiment," *Physics Today*, vol. 43, no. 1, pp. 24-32.
- Gad-el-Hak, M. (1989), "Flow Control," *ASME Applied Mechanics Reviews*, vol. 42, pp. 261-293.
- Gad-el-Hak, M. (1990), "Control of Low-Speed Airfoil Aerodynamics," *AIAA Journal*, vol. 28, pp. 1537-1552.
- Gad-el-Hak, M. (1993), "Innovative Control of Turbulent Flows," *AIAA Paper* 93-3268, Washington, DC.
- Gad-el-Hak, M., and D. M. Bushnell (1991), "Separation Control: Review," *Journal of Fluids Engineering*, vol. 113, pp. 5-30.
- Gad-el-Hak, M., R. F. Blakwelder, and J. J. Riley (1981), "On the Growth of Turbulent Regions in Laminar Boundary Layers," *Journal of Fluid Mechanics*, vol. 110, pp. 73-95.
- Gad-el-Hak, M., R. F. Blakwelder, and J. J. Riley (1984), "On the Interaction of Compliant Coatings With Boundary-Layer Flows," *Journal of Fluid Mechanics*, vol. 140, pp. 257-280.

- Gallagher, J. A., and A. S. W. Thomas (1984), "Turbulent Boundary Layer Characteristics Over Streamwise Grooves," *AIAA Paper* 84-2185, New York.
- Galperin, B., and S. A. Orszag, Eds. (1993), *Large Eddy Simulations of Complex Engineering and Geophysical Flows*, Cambridge University Press, London.
- George, W. K. and L. Castillo (1993), Boundary Layers With Pressure Gradient: Another Look at the Equilibrium Theory," in *Near-Wall Turbulent Flows*, R. M. C. SO et. al., Eds., Elsevier, Amsterdam.
- George, W. K., L. Castillo, and P. Knecht (1992) "The Zero-Pressure Gradient Turbulent Boundary Layer Revisited," in *Thirteenth Symposium on Turbulence*, X. B. Reed, Ed., University of Missouri, Rolla, MO, 21-23 April.
- George, W. K., L. Castillo, and P. Knecht (1993) "The Zero-Pressure Gradient Turbulent Boundary Layer," in *William C. Reynolds Anniversary Symposium*, Asilomar, CA.
- George, W. K., L. Castillo, and P. Knecht (1994) "The Zero-Pressure Gradient Turbulent Boundary Layer," submitted to *Physics of Fluids*.
- Germano, M., U. Piomelli, P. Moin, and W. H. Cabot ( 1991), "A Dynamic Subgrid-Scale Eddy Viscosity Model," *Physics of Fluids, A*, vol. 3, pp. 1760-1765.
- Gillis, J. C. (1980), "Turbulent Boundary Layer on a Convex, Curved Surface," Ph.D. Dissertation, Stanford University, Stanford, CA.
- Grant, H. L. (1958), "The Large Eddies of Turbulent Motion," *Journal of Fluid Mechanics*, vol. 4, pp. 149-190.
- Granville, P. S. (1977), "Drag and Turbulent Boundary Layer of Flat Plates at Low Reynolds Numbers," *Journal of Ship Research*, vol. 21, pp. 30-39.
- Grass, A. J. (1971), "Structural Features of Turbulent Flow over Smooth and Rough Boundaries," *Journal of Fluid Mechanics*, vol. 50, pp. 233-255.
- Gupta, A. K., and R. E. Kaplan (1972), "Statistical Characteristics of Reynolds Stress in a Turbulent Boundary Layer," *Physics of Fluids*, vol. 15, pp. 981-985.
- Hama, F. R. (1947), "The Turbulent Boundary Layer Along a Flat Plate, Parts I and II," in *Reports of the Institute of Science and Technology, University of Tokyo, Japan*, Volume 1, pp. 13-16 and 49-50.
- Hama, F. R. (1954), "Boundary-Layer Characteristics for Smooth and Rough Surfaces," *Transactions of the Society of Naval Architects and marine Engineers*, vol. 62, pp. 333-358.

- Hancock, P. E., and P. Bradshaw (1983), "The Effect of Free-stream Turbulence on Turbulent Boundary Layers," *Journal of Fluids Engineering*, vol. 105, pp. 284-289.
- Hanratty, T. J. (1989), "A Conceptual Model of the Viscous Wall Region," in *Near Wall Turbulence*, S. J. Kline and N. H. Afgan, Eds., Hemisphere, New York, pp. 81-103.
- Harder, K. J., and W. G. Tiederman (1991), "Drag Reduction and Turbulent Structure in Two-Dimensional Channel Flows," *Philosophical Transactions of the Royal Society of London, Series A*, vol. 336, pp. 19-34.
- Head, M. R., and P. R. Bandyopadhyay (1978), "Combined Flow Visualization and Hot-Wire Measurements," in *Coherent Structure of Turbulent Boundary Layers*, C. R. Smith and D. E. Abbott, Eds., Lehigh University, Bethlehem, PA, pp. 98-129.
- Head, M. R., and P. R. Bandyopadhyay (1981), "New Aspects of Turbulent Boundary-Layer Structure," *Journal of Fluid Mechanics*, vol. 107, pp. 297-338.
- Hinze, J. O. (1975), *Turbulence*, Second Edition, McGraw-Hill, New York.
- Hopkins, E. J., E. R. Keener, and T. E. Polek (1972), "Hypersonic Turbulent Skin Friction and Boundary Layer Profiles on Nonadiabatic Flat Plates," *AIAA Journal*, vol. 10, pp. 40-48.
- Hussain, A. K. M. F. (1983), "Coherent Structures -- Reality and Myth," *Physics of Fluids*, vol. 26, pp. 2816-2850.
- Hussain, A. K. M. F. (1986), "Coherent Structures and Turbulence," *Journal of Fluid Mechanics*, vol. 173, pp. 303-356.
- Hussain, A. K. M. F. and W. C. Reynolds (1975), "Measurements in Fully Developed Turbulent Channel Flow," *Journal of Fluids Engineering*, vol. 97, pp. 568-580.
- Izakson, A. (1937), "Formula for the Velocity Distribution Near a Wall," *Zhurnal Eksperimental' No. 11 Teoreticheskoy i Fiziki*, vol. 7, pp. 919-924.
- Johansson, A. V., and P. H. Alfredsson (1982), "On the Structure of Turbulent Channel Flow," *Journal of Fluid Mechanics*, vol. 122, pp. 295-314.
- Johansson, A. V., and P. H. Alfredsson (1983), "Effects of Imperfect Spatial Resolution on Measurements of Wall-Bounded Turbulent Shear Flows," *Journal of Fluid Mechanics*, vol. 137, pp. 409-421.
- Johansson, A. V., J.-Y. Her, and J. H. Haritonidis (1987), "On the Generation of High-Amplitude Wall-Pressure Peaks in Turbulent Boundary Layers and Spots," *Journal of Fluid Mechanics*, vol. 175, pp. 119-142.

- Kailasnath, P. (1993), "Reynolds Number Effects and the Momentum Flux in Turbulent Boundary Layers," Ph.D. Thesis, Yale University, New Haven, CT.
- Karlsson, R. I., and T. G. Johansson (1986), "LDV Measurements of Higher Order Moments of Velocity Fluctuations in a Turbulent Boundary Layer," in *Proceedings of the Third International Symposium on Applications of Laser Anemometry to Fluid Mechanics*, D. F. G. Durão et al., Eds., Paper No. 12.1, Lisbon, Portugal.
- Karniadakis, G. Em, and S. A. Orszag (1993), "Nodes, Modes, and Flow Codes," *Physics Today*, vol. 46, No. 3, pp. 34-42.
- Kastrinakis, E. G., and H. Eckelmann (1983), "Measurement of Streamwise Vorticity Fluctuations in a Turbulent Channel Flow," *Journal of Fluid Mechanics*, vol. 137, pp. 165-186.
- Keith, W. L., D. A. Hurdis, and B. M. Abraham (1992), "A Comparison of Turbulent Boundary Layer Wall-Pressure Spectra," *Journal of Fluids Engineering*, vol. 114, pp. 338-347.
- Kim, H. T., S. J. Kline, and W. C. Reynolds (1971), "The Production of Turbulence Near a Smooth Wall in a Turbulent Boundary Layer," *Journal of Fluid Mechanics*, vol. 50, pp. 133-160.
- Kim, J., and P. Moin (1986), "The Structure of the Vorticity Field in Turbulent Channel Flow, Part 2, Study of Ensemble-Averaged Fields," *Journal of Fluid Mechanics*, vol. 162, pp. 339-363.
- Kim, J., P. Moin, and R. D. Moser (1987), "Turbulence Statistics in Fully-Developed Channel Flow at Low Reynolds Number," *Journal of Fluid Mechanics*, vol. 177, pp. 133-166.
- Klebanoff, P. S. (1954), "Characteristics of Turbulence in a Boundary Layer with Zero Pressure Gradient," NACA Report R-1247, National Advisory Committee for Aeronautics, Hampton, VA.
- Klebanoff, P. S., and Z. W. Diehl (1952), "Some Features of Artificially Thickened Fully Developed Turbulent Boundary Layers with Zero Pressure Gradient," NACA Report 1110, National Advisory Committee for Aeronautics, Hampton, VA.
- Klebanoff, P. S., K. D. Tidstrom, and L. M. Sargent (1962), "The Three-Dimensional Nature of Boundary-Layer Instability," *Journal of Fluid Mechanics*, vol. 12, pp. 1-34.
- Klewicki, J. C., J. A. Murray, and R. E. Falco (1994), "Vortical Motion Contributions to Stress Transport in Turbulent Boundary Layers," *Physics of Fluids, A*, vol. 6, pp. 277-286.
- Kline, S. J. (1967), "Observed Structure Features in Turbulent and Transitional Boundary Layers," in *Fluid Mechanics of Internal Flow*, G. Sovran, Ed., Elsevier, Amsterdam, pp. 27-79.

- Kline, S. J., and P. W. Runstadler (1959), "Some Preliminary Results of Visual Studies of the Flow Model of the Wall Layers of the Turbulent Boundary Layer," *ASME Journal of Applied Mechanics*, vol. 26, pp. 166-170.
- Kline, S. J., W. C. Reynolds, F. A. Schraub, and P. W. Runstadler (1967), "The Structure of Turbulent Boundary Layers," *Journal of Fluid Mechanics*, vol. 30, pp. 741-773.
- Kolmogorov, A. N. (1941a), "The Local Structure of Turbulence in an Incompressible Viscous Fluid for Very Large Reynolds Numbers," *Comptes Rendus Academy of Science, U.S.S.R.*, vol. 30, pp. 301-305.
- Kolmogorov, A. N. (1941b), "On Degeneration of Isotropic Turbulence in an Incompressible Viscous Liquid," *Comptes Rendus Academy of Science, U.S.S.R.*, vol. 31, p. 538.
- Kolmogorov, A. N. (1941c), "Dissipation of Energy in Locally Isotropic Turbulence," *Comptes Rendus Academy of Science, U.S.S.R.*, vol. 32, pp. 16-18.
- Kolmogorov, A. N. (1962), "A Refinement of Previous Hypothesis Concerning the Local Structure of Turbulence in a Viscous Incompressible Fluid at High Reynolds Number," *Journal of Fluid Mechanics*, vol. 13, pp. 82-85.
- Koskie, J. E., and W. G. Tiederman (1991), "Turbulence Structure and Polymer Drag Reduction in Adverse Pressure Gradient Boundary Layers," Report PME-FM-91-3, Purdue University School of Mechanical Engineering, West Lafayette, IN.
- Kovaszny, L. S. G. (1970), "The Turbulent Boundary Layer," *Annual Review of Fluid Mechanics*, vol. 2, pp. 95-112.
- Kreplin, H.-P., and H. Eckelmann (1979), "Behaviour of the Three Fluctuating Velocity Components in the Wall Region of a Turbulent Channel Flow," *Physics of Fluids*, vol. 22, pp. 1233-1239.
- Kudva, A. K., and A. Sesonske (1972), "Structure of Turbulent Velocity and Temperature Fields in Ethylene Glycol Pipe Flow at Low Reynolds Number," *International Journal of Heat Mass Transfer*, vol. 15, pp. 127-145.
- Kutateladze, S. S., and E. M. Khabakhpasheva (1978), "Structure of Wall Boundary Layer (Forced Flow, Thermal Convection)," Institute of Thermodynamics, Siberian Branch of the USSR Academy of Science, Novosibirsk, USSR.
- Landahl, M. T. (1967), "A Wave-Guide Model for Turbulent Shear Flow," *Journal of Fluid Mechanics*, vol. 29, pp. 441-459.
- Landahl, M. T. (1972), "Wave Mechanics of Breakdown," *Journal of Fluid Mechanics*, vol. 56, pp. 775-802.

- Landahl, M. T. (1977) "Dynamics of Boundary Layer Turbulence and the Mechanism of Drag Reduction," *Physics of Fluids*, vol. 20, pp. S55-S63.
- Landahl, M. T. (1980), "A Note on an Algebraic Instability of Inviscid Parallel Shear Flows," *Journal of Fluid Mechanics*, vol. 98, pp. 243-251.
- Landahl, M. T. (1990), "On Sublayer Streaks," *Journal of Fluid Mechanics*, vol. 212, pp. 593-614.
- Landau, L. D., and E. M. Lifshitz (1987), *Fluid Mechanics*, Second Edition, Pergamon Press, Oxford, United Kingdom.
- Landweber, L. (1953), "The Frictional Resistance of Flat Plates at Zero Pressure Gradient," *Transactions of the Society of Naval Architects and Marine Engineers*, vol. 61, pp. 5-32.
- Landweber, L., and T. T. Siao (1958), "Comparison of Two Analyses of Boundary-Layer Data on a Flat Plate," *Journal of Ship Research*, vol. 1, pp. 21-33.
- Lauchle, G. C., and M. A. Daniels (1987), "Wall-Pressure Fluctuations in Turbulent Pipe Flow," *Physics of Fluids*, vol. 30, pp. 3019-3024.
- Laufer, J. (1951), "Investigation of Turbulent Flow in a Two-Dimensional Channel," NACA Report R-1053, National Advisory Committee for Aeronautics, Hampton, VA.
- Laufer, J. (1954), "The Structure of Turbulence in Fully Developed Pipe Flow," NACA Report R-1174, National Advisory Committee for Aeronautics, Hampton, VA.
- Laufer, J. (1975) "New Trends in Experimental Turbulence Research," *Annual Review of Fluid Mechanics*, vol. 7, pp. 307-326.
- Launder, B. E., and D. B. Spalding (1974), "The Numerical Computation of Turbulent Flows," *Computer Methods in Applied Mechanics and Engineering*, vol. 3, pp. 269-289.
- Lee, R. E., W. J. Yanta, and A. C. Leonas (1969), "Velocity Profile, Skin Friction Balance, and Heat Transfer Measurements of the Turbulent Boundary Layer at M 5 and Zero Pressure Gradient," NOL-TR69-106, Naval Ordnance Laboratory, White Oak, MD.
- Ligrani, P. M., and P. Bradshaw (1987), "Spatial Resolution and Measurements of Turbulence in the Viscous Sublayer Using Subminiature Hot-Wire Probes," *Experiments in Fluids*, vol. 5, pp. 407-417.
- Long, R. R., and T.-C. Chen (1981), "Experimental Evidence for the Existence of the "Mesolayer" in Turbulent Systems," *Journal of Fluid Mechanics*, vol 105, pp. 19-59.

- Löfdahl, L., G. Stemme, and B. Johansson (1989), "A Sensor Based on Silicon Technology for Turbulence Measurements," *Journal of Physics E: Scientific Instruments*, vol. 22, pp. 391-393.
- Löfdahl, L., G. Stemme, and B. Johansson (1991), "Reynolds Stress Measurements Using Direction Sensitive Double-Chip Silicon Sensors," *Measurements in Scientific Technology*, vol. 2, pp. 369-373.
- Löfdahl, L., G. Stemme, and B. Johansson (1992), "Silicon Based Flow Sensors Used for Mean Velocity and Turbulence Measurements," *Experiments in Fluids*, vol. 12, pp. 270-276.
- Long, R. R., and T.-C. Chen (1981), "Experimental Evidence for the Existence of the 'Mesolayer' in Turbulent Systems," *Journal of Fluid Mechanics*, vol. 105, pp. 19-59.
- Luchik, T. S., and W. G. Tiederman (1986), "Effect of Spanwise Probe Volume Length on Laser Velocimeter Measurements in Wall Bounded Turbulent Flows," *Experiments in Fluids*, vol. 3, pp. 339-341.
- Lumley, J. L. (1978), "Computational Modeling of Turbulent Flows," *Advances in Applied Mechanics*, vol. 18, pp. 123-176.
- Lumley, J. L. (1983), "Turbulence Modeling," *ASME Journal of Applied Mechanics*, vol. 50, pp. 1097-1103.
- Lumley, J. L. (1992), "Some Comments on Turbulence," *Physics of Fluids, A*, vol. 4, pp. 203-211.
- Mabey, D. G. (1979), "Influence of the Wake Component on Turbulent Skin Friction at Subsonic and Supersonic Speeds," *Aeronautical Quarterly*, vol. 30, pp. 590-606.
- Mabey, D. G., H. U. Meier, and W. G. Sawyer (1976), "Some Boundary Layer Measurements on a Flat Plate at Mach Numbers from 2.5 to 4.5," Technical Report RAE-74127, Royal Aeronautical Establishment, London.
- Malkus, W. V. R. (1956), "Outline of a Theory of Turbulent Shear Flow," *Journal of Fluid Mechanics*, vol. 1, pp. 521-539.
- Malkus, W. V. R. (1979), "Turbulent Velocity Profiles from Stability Criteria," *Journal of Fluid Mechanics*, vol. 90, pp. 401-414.
- Mickley, H. S., and R. S. Davis (1957), "Momentum Transfer for Flow over a Flat Plate with Blowing," NACA Technical Note 4017, *National Advisory Committee for Aeronautics*, Hampton, VA.

- Millikan, C. B. (1939), "A Critical Discussion of Turbulent Flows in Channels and Circular Tubes," in *Proceedings of the Fifth International Congress Applied Mechanics*, J. P. Den Hartog and H. Peters, Eds., Wiley, New York, pp. 386-392,.
- Moin, P., and J. Kim (1982), "Numerical Investigation of Turbulent Channel Flow," *Journal of Fluid Mechanics*, vol. 118, pp. 341-377.
- Moin, P., and J. Kim (1985), "The Structure of the Vorticity Field in Turbulent Channel Flow, Part 1, Analysis of Instantaneous Fields and Statistical Correlations," *Journal of Fluid Mechanics*, vol. 155, pp. 441-464.
- Monin, A. S., and A. M. Yaglom (1971), *Statistical Fluid Mechanics*, Volume I, Massachusetts Institute of Technology Press, Cambridge, MA.
- Morrison, W. R. B. (1969), "Two-Dimensional Frequency-Wavenumber Spectra and Narrow-Band Shear Stress Correlations in Turbulent Pipe Flow," Ph.D. Thesis, University of Queensland, Queensland, Australia.
- Morrison, W. R. B., K. J. Bullock, and R. E. Kronauer (1971), "Experimental Evidence of Waves in the Sublayer," *Journal of Fluid Mechanics*, vol. 47, pp. 639-656.
- Murlis, J., H. M. Tsai, and P. Bradshaw (1982), "The Structure of Turbulent Boundary Layers at Low Reynolds Numbers," *Journal of Fluid Mechanics*, vol. 122, pp. 13-56.
- Nagano, Y., and M. Tagawa (1990), "A Structural Turbulence Model for Triple Products of Velocity and Scalar," *Journal of Fluid Mechanics*, vol. 215, pp. 639-657.
- Naguib, A. M., and C. E. Wark (1992), "An Investigation of Wall-Layer Dynamics Using a Combined Temporal Filtering and Correlation Techniques," *Journal of Fluid Mechanics*, vol. 243, pp. 541-560.
- Narasimha, R., and S. V. Kailas (1986), "Energy Events in the Atmospheric Boundary Layer," Report 86-AS-8, Indian Institute of Science, Bangalore, India.
- Narasimha, R., and S. V. Kailas (1987), "Energy Events in the Atmospheric Boundary Layer," in *Perspectives in Turbulent Studies*, H. U. Meier and P. Bradshaw, Eds., Springer-Verlag, Berlin, pp. 188-222.
- Narasimha, R., and S. V. Kailas (1990), "Turbulent Bursts in the Atmosphere," *Atmospheric Environment*, vol. 24A, pp. 1635-1645.
- Narasimha, R., and H. W. Liepmann (1988), "Introduction," in *Turbulence Management and Relaminarisation*, H. W. Liepmann and R. Narasimha, Eds., Springer-Verlag, Berlin, pp. xii-xx.

- Narasimha, R., and K. R. Sreenivasan (1988), "Flat Plate Drag Reduction by Turbulence Manipulation," *Sādhānā*, vol. 12, pp. 15-30.
- Newman, G.R. (1974), "An Experimental Study of Coherent Structures in the Turbulent Boundary Layer," Certificate of Post-Graduate Study Dissertation, Cambridge University, Cambridge, United Kingdom.
- Nikuradse, J. (1932), "Gesetzmässigkeit der turbulenten Strömung in glatten Rohren," *Forschung Arbeiten Auf Dem Gebiete Des Ingenieurwesens*, No. 356, Germany.
- Nikuradse, J. (1933), "Strömungsgesetze in rauhen Rohren," *Forschung Arbeiten Auf Dem Gebiete Des Ingenieurwesens*, No. 361, Germany.
- Offen, G. R., and S. J. Kline (1974), "Combined Dye-Streak and Hydrogen-Bubble Visual Observations of a Turbulent Boundary Layer," *Journal of Fluid Mechanics*, vol. 62, pp. 223-239.
- Offen, G. R., and S. J. Kline (1975), "A Proposed Model of the Bursting Process in Turbulent Boundary Layers," *Journal of Fluid Mechanics*, vol. 70, pp. 209-228.
- Oldaker, D. K., and W. G. Tiederman (1977), "Spatial Structure of the Viscous Sublayer in Drag-Reducing Channel Flows," *Physics of Fluids*, vol. 20, pp. S133- 144.
- Owen, F. K., and C. C. Horstman (1972), "On the Structure of Hypersonic Turbulent Boundary Layers," *Journal of Fluid Mechanics*, vol. 53, pp. 611-636.
- Owen, F. K., C. C. Horstman, and M. I. Kussoy (1975), "Mean and Fluctuating Flow Measurements of a Fully-Developed, Non-Adiabatic, Hypersonic Boundary Layer," *Journal of Fluid Mechanics*, vol. 70, pp. 393-413.
- Panton, R. L. (1989), "Inner-Outer Structure of the Wall-Pressure Correlation Function," in *Near-Wall Turbulence*, S. J. Kline and N. H. Afgan, Eds., Hemisphere, New York, pp. 381-396.
- Panton, R. L. (1990a), "Scaling Turbulent Wall Layers," *Journal of Fluids Engineering*, vol. 112, pp. 425-432.
- Panton, R. L. (1990b), "The Role of Dimensional Analysis in Matched and Composite Asymptotic Expansions," in *Ocean Waves Mechanics, Computational Fluid Dynamics and Mathematical Modeling*, M. Rahman, Ed., Computational Mechanics, Boston, MA, pp. 363-379.
- Panton, R. L. (1991), "The Effects of Reynolds Number on Turbulent Wall Flows," *Proceedings of the Eighth Symposium on Turbulent Shear Flows*, Paper No. I-15, Technical University of Munich, 9-11 September.

- Panton, R. L., and J. H. Linebarger (1974), "Wall-Pressure Spectra Calculations for Equilibrium Boundary Layers," *Journal of Fluid Mechanics*, vol. 65, pp. 261-287.
- Panton, R. L., and G. Robert (1993), "The Wall-Pressure Spectrum Under a Turbulent Boundary Layer: Part 2, Theory and Results," *ASME Fluid Engineering Conference*, M. J. Morris and B. F. Carroll, Eds., ASME, New York, FED-vol. 155, pp. 43-48.
- Panton, R. L., and G. Robert (1994), "The Wavenumber-Phase Velocity Representation for the Turbulent Wall-Pressure Spectrum," *Journal of Fluids Engineering*, (in press).
- Panton, R. L., A. L. Goldman, R. L. Lowery, and M. M. Reischman (1980), "Low Frequency Pressure Fluctuations in Axisymmetric Turbulent Layers," *Journal of Fluid Mechanics*, vol. 97, pp. 299-319.
- Perry, A. E., and C. J. Abell (1975), "Scaling Laws for Pipe-Flow Turbulence," *Journal of Fluid Mechanics*, vol. 67, pp. 257-271.
- Perry, A. E., and C. J. Abell (1977), "Asymptotic Similarity of Turbulence Structures in Smooth- and Rough-Walled Pipes," *Journal of Fluid Mechanics*, vol. 79, pp. 785-799.
- Perry, A. E., and M. S. Chong (1982), "On the Mechanism of Wall Turbulence," *Journal of Fluid Mechanics*, vol. 119, pp. 173-217.
- Perry, A. E., S. M. Henbest, and M. S. Chong (1986), "A Theoretical and Experimental Study of Wall Turbulence," *Journal of Fluid Mechanics*, vol. 165, pp. 163-199.
- Perry, A. E., J. D. Li, S. Henbest, and I. Marusic (1989), "The Attached Eddy Hypothesis in Wall Turbulence," in *Near Wall Turbulence*, S. J. Kline and N. H. Afgan, Eds., Hemisphere, New York, pp. 715-735.
- Perry, A. E., T. T. Lim, and E. W. Teh (1981), "A Visual Study of Turbulent Spots," *Journal of Fluid Mechanics*, vol. 104, pp. 387-405.
- Peters, H. (1938), "A Study in Boundary Layers," in *Proceedings of the Fifth International Congress Applied Mechanics*, J. P. Den Hartog and H. Peters, Eds., Wiley, New York, pp. 393-395.
- Phillips, W. R. C. (1987), "The Wall Region of a Turbulent Boundary Layer," *Physics of Fluids*, vol. 30, pp. 2354-2361.
- Phillips, W. R. C., and J. T. Ratnanather (1990), "The Outer Region of a Turbulent Boundary Layer," *Physics of Fluids, A*, vol. 2, pp. 427-434.
- Prandtl, L. (1925), "Bericht über Untersuchungen zur ausgebildeten Turbulenz," *Zeitschrift für Angewandte Mathematik und Mechanik*, vol. 5, pp. 136-139.

- Praturi, A. K., and R. S. Brodkey (1978), "A Stereoscopic Visual Study of Coherent Structures in Turbulent Shear Flows," *Journal of Fluid Mechanics*, vol. 89, pp. 251-272.
- Preston, J. H. (1958), "The Minimum Reynolds Number for a Turbulent Boundary Layer and the Selection of a Transition Device," *Journal of Fluid Mechanics*, vol. 3, pp. 373-384.
- Preston, J. H., and N. E. Sweeting (1944), "The Velocity Distribution in the Boundary Layer of a Plane Wall at High Reynolds Numbers with Suggestions for Further Experiments," Report ARC-FM-671, Aeronautical Research Council, London.
- Purtell, L. P., P. S. Klebanoff, and F. T. Buckley (1981), "Turbulent Boundary Layer at Low Reynolds Number," *Physics of Fluids*, vol. 24, pp. 802-811.
- Rajagopalan, S., and R. A. Antonia (1984), "Conditional Averages Associated with the Fine Structure in a Turbulent Boundary Layer," *Physics of Fluids*, vol. 27, pp. 1966-1973.
- Rajagopalan, S., and R. A. Antonia (1993), "RMS Spanwise Vorticity Measurements in a Turbulent Boundary Layer," *Experiment in Fluids*, vol. 14, pp. 142-144.
- Rao, K. N., R. Narasimha, and M. A. Badri Narayanan (1971), "The 'Bursting' Phenomenon in a Turbulent Boundary Layer," *Journal of Fluid Mechanics*, vol. 48, pp. 339-352.
- Raupach, M. R., R. A. Antonia, and S. Rajagopalan (1991), "Rough-Wall Turbulent Boundary Layers," *Applied Mechanics Reviews*, vol. 44, pp. 1-25.
- Reischman, M. M., and W. G. Tiederman (1975), "Laser-Doppler Anemometer Measurements in Drag-Reducing Channel Flows," *Journal of Fluid Mechanics*, vol. 70, pp. 369-392.
- Reynolds, O. (1883), "An Experimental Investigation of the Circumstances Which Determine Whether the Motion of Water Shall be Direct or Sinuous, and of the Law of Resistance in Parallel Channels," *Philosophical Transactions of the Royal Society of London, Series A*, vol. 174, pp. 935-982.
- Reynolds, O. (1895), "On the Dynamical Theory of Incompressible Viscous Fluids and the Determination of the Criterion," *Philosophical Transactions of the Royal Society of London, Series A*, vol. 186, pp. 123-164.
- Reynolds, W. C. (1976), "Computation of Turbulent Flows," *Annual Review of Fluid Mechanics*, vol. 8, pp. 183-208.
- Richardson, L. F. (1922), *Weather Prediction by Numerical Process*, Cambridge University Press, London.
- Robert, G. (1993), "The Wall-Pressure Spectrum Under a Turbulent Boundary Layer: Part 1, Experiments," *ASME Fluid Engineering Conference*, M. J. Morris and B. F. Carroll, Eds., ASME, NY, FED-vol. 155, pp. 37-42.

- Robinson, S. K. (1990), "A Review of Vortex Structures and Associated Coherent Motions in Turbulent Boundary Layers," in *Structure of Turbulence and Drag Reduction*, A. Gyr, Ed., Springer-Verlag, Berlin, pp. 23-50..
- Robinson, S. K. (1991), "Coherent Motions in the Turbulent Boundary Layer," *Annual Review of Fluid Mechanics*, vol. 23, pp. 601-639.
- Robinson, S. K., S. J. Kline, and P. R. Spalart (1989), "A Review of Quasi-Coherent Structures in a Numerically Simulated Turbulent Boundary Layer," NASA Technical Memorandum 102191, National Aeronautics Space Administration, Langley, VA..
- Rogallo, R. S., and P. Moin (1984), "Numerical Simulation of Turbulent Flows," *Annual Review of Fluid Mechanics*, vol. 16, pp. 99-137.
- Roshko, A. (1992), "Bluff-Body and Other Shear Flows," in *Proceedings of the NUWC Division Newport Seminar Series on Turbulence and its Control*, P. R. Bandyopadhyay and J. C. S. Meng, Compilers, NUWC-NPT Technical Memorandum, 922089, Naval Undersea Warfare Center Division, Newport, RI, pp. 4.1-4.3.4.
- Rotta, J. C. (1951), "Statistische Theorie nichthomogener Turbulenz," *Zeitschrift fuer Physik*, vol. 129, pp. 547-572.
- Rotta, J. C. (1962), "Turbulent Boundary Layers in Incompressible Flow," in *Progress in Aeronautical Sciences*, Volume 2, pp. 1-219.
- Runstadler, P. G., S. J. Kline, and W. C. Reynolds (1963), "An Experimental Investigation of Flow Structure of the Turbulent Boundary Layer," Report MD-8, Stanford University, Department of Mechanical Engineering, Stanford, CA.
- Saffman, P. G. (1978), "Problems and Progress in the Theory of Turbulence," in *Structure and Mechanisms of Turbulence II, Lecture Notes in Physics*, Volume 76, H. Fiedler, Ed., Springer-Verlag, Berlin, pp. 273-306.
- Saffman, P. G., and G. R. Baker (1979), "Vortex Interactions," *Annual Review of Fluid Mechanics*, vol. 11, pp. 95-122.
- Sasaki, K., and M. Kiya (1991), "Three-Dimensional Vortex Structure in a Leading-Edge Separation Bubble at Moderate Reynolds Numbers," *Journal of Fluids Engineering*, vol. 113, pp. 405-410.
- Schewe, G. (1983), "On the Structure and Resolution of Wall-Pressure Fluctuations Associated with Turbulent Boundary-Layer Flow," *Journal of Fluid Mechanics*, vol. 134, pp. 311-328.
- Schildknecht, M., J. A. Miller, and G. E. A. Meir (1979), "The Influence of Suction on the Structure of Turbulence in Fully Developed Pipe Flow," *Journal of Fluid Mechanics*, vol. 90, pp. 67-107.

- Schlichting, H. (1979) *Boundary-Layer Theory*, Seventh Edition, McGraw-Hill, New York.
- Shah, D. A., and R. A. Antonia (1989), "Scaling of the 'Bursting' Period in Turbulent Boundary Layer and Duct Flows," *Physics of Fluids, A*, vol. 1, pp. 318-325.
- Simpson, R. L. (1970), "Characteristics of Turbulent Boundary Layers at Low Reynolds Numbers With and Without Transpiration," *Journal of Fluid Mechanics*, vol. 42, pp. 769-802.
- Simpson, R. L. (1976), "Comment on 'Prediction of Turbulent Boundary Layers at Low Reynolds Numbers'," *AIAA Journal*, vol. 14, pp. 1662-1663.
- Smagorinsky, J. (1963), "General Circulation Experiments with the Primitive Equations," *Monthly Weather Review*, vol. 91, pp. 99-164.
- Smith, C. R., and S. P. Metzler (1982), "A Visual Study of the Characteristics, Formation, and Regeneration of Turbulent Boundary Layer Streaks," in *Developments in Theoretical and Applied Mechanics*, Volume XI, T. J. Chung and G. R. Karr, Eds., University of Alabama, Huntsville, AL, pp. 533-543.
- Smith, C. R., and S. P. Metzler (1983), "The Characteristics of Low-Speed Streaks in the Near-Wall Region of a Turbulent Boundary Layer," *Journal of Fluid Mechanics*, vol. 129, pp. 27-54.
- Smith, C. R., and S. P. Schwartz (1983), "Observation of Streamwise Rotation in the Near-Wall Region of a Turbulent Boundary Layer," *Physics of Fluids*, vol. 26, pp. 641-652.
- Smith, D. W., and J. H. Walker (1959), "Skin-Friction Measurements in Incompressible Flow," NACA Report R-26, National Advisory Committee for Aeronautics, Hampton, VA.
- Smith, R. W. (1994), "Effect of Reynolds Number on the Structure of Turbulent Boundary Layers," Ph.D. Thesis, Princeton University, Princeton, NJ.
- Smits, A. J. (1990), "New Developments in Understanding Supersonic Turbulent Boundary Layers," in *Proceedings of the Twelfth Symposium on Turbulence*, X. B. Reed, Jr., et al., Eds., University of Missouri, Rolla, MO, pp. IL4.1-IL4.19.
- Smits, A. J., E. F. Spina, A. E. Alving, R. W. Smith, E. M. Fernando, and J. F. Donovan (1989), "A Comparison of the Turbulence Structure of Subsonic and Supersonic Boundary Layers," *Physics of Fluids*, vol. 1, pp. 1865-1875.
- Spalart, P. R. (1986), "Direct Simulation of a Turbulent Boundary Layer up to  $R_q = 1410$ ," NASA Technical Memorandum TM-89407, National Aeronautics and Space Administration, Langley, VA.
- Spalart, P. R. (1988), "Direct Simulation of a Turbulent Boundary Layer up to  $R_q = 1410$ ," *Journal of Fluid Mechanics*, vol. 187, pp. 61-98.

- Speziale, C. G. (1991), "Analytical Methods for the Development of Reynolds-Stress Closures in Turbulence," *Annual Review of Fluid Mechanics*, vol. 23, pp. 107-157.
- Spina, E. F., J. F. Donovan, and A. J. Smits (1991), "On the Structure of High-Reynolds-Number Supersonic Turbulent Boundary Layers," *Journal of Fluid Mechanics*, vol. 222, pp. 293-327.
- Sreenivasan, K. R. (1988), "A Unified View of the Origin and Morphology of the Turbulent Boundary Layer Structure," in *Turbulence Management and Relaminarisation*, H. W. Liepmann and R. Narasimha, Eds., Springer-Verlag, Berlin, pp. 37-61.
- Sreenivasan, K. R. (1989), "The Turbulent Boundary Layer," in *Frontiers in Experimental Fluid Mechanics, Lecture Notes in Engineering*, Volume 46, M. Gad-el-Hak, Ed., Springer-Verlag, Berlin pp. 159-209.
- Sreenivasan, K. R., and R. A. Antonia (1977), "Properties of Wall Shear Stress Fluctuations in a Turbulent Duct," *Journal of Applied Mechanics*, vol. 44, pp. 389-395.
- Tani, I. (1986), "Some Equilibrium Turbulent Boundary Layers," *Fluid Dynamics Research*, vol. 1, pp. 49-58.
- Tani, I. (1987), "Turbulent Boundary Layer Development over Rough Surfaces," in *Perspectives in Turbulent Studies*, H. U. Meier and P. Bradshaw, Eds., Springer-Verlag, Berlin, pp. 223-249.
- Tani, I. (1988), "Drag Reduction by Riblet Viewed as Roughness Problem," *Proceedings of the Japanese Academy B*, vol., 64, pp. 21-24.
- Tani, I., and T. Motohashi (1985a), "Non-Equilibrium Behavior of Turbulent Boundary Layer Flows, Part I, Method of Analysis," *Proceedings of the Japanese Academy B*, vol. 61, pp. 333-336.
- Tani, I., and T. Motohashi (1985b), "Non-Equilibrium Behavior of Turbulent Boundary Layer Flows, Part II, Results of Analysis," *Proceedings of the Japanese Academy B*, vol. 61, pp. 337-340.
- Theodorsen, Th. (1952), "Mechanism of Turbulence," in *Proceedings of the 2<sup>nd</sup> Midwestern Conference on Fluid Mechanics*, Ohio State University, Columbus, OH. pp. 1-18.
- Theodorson, Th. (1955), "The Structure of Turbulence," in *50 Jahre Grenzschichtsforschung (Ludwig Prandtl Anniversary Volume)*, H. Görtler and W. Tollmien, Eds., Friedrick Vieweg und Sohn, Braunschweig, Germany, pp. 55-62.
- Thomas, A. S. W., and M. K. Bull (1983), "On the Role of Wall-Pressure Fluctuations in Deterministic Motions in the Turbulent Boundary Layer," *Journal of Fluid Mechanics*, vol. 128, pp. 283-322.

- Tiederman, W. G., T. S. Luchik, and D. G. Bogard (1985), "Wall-Layer Structure and Drag Reduction," *Journal of Fluid Mechanics*, vol. 156, pp. 419-437.
- Townsend, A. A. (1961), "Equilibrium Layers and Wall Turbulence," *Journal of Fluid Mechanics*, vol. 11, pp. 97-120.
- Townsend, A. A. (1970), "Entrainment and the Structure of Turbulent Flow," *Journal of Fluid Mechanics*, vol. 41, pp. 13-46.
- Townsend, A. A. (1976), *The Structure of Turbulent Shear Flow*, Second Edition, Cambridge University Press, London.
- Tsai, H. M., and D. C. Leslie (1990), "Large Eddy Simulation of a Developing Turbulent Boundary Layer at Low Reynolds Number," *International Journal of Numerical Methods in Fluids*, vol. 10, pp. 519-555.
- Tu, B. J., and W. W. Willmarth (1966), "An Experimental Study of the Structure of Turbulence Near the Wall through Correlation Measurements in a Thick Turbulent Boundary Layer," Report 02920-3-T, University of Michigan Department of Aerospace Engineering, Ann Arbor, MI.
- Ueda, H., and J. O. Hinze (1975), "Fine Structure Turbulence in the Wall Region of a Turbulent Boundary Layer," *Journal of Fluid Mechanics*, vol. 67, pp. 125-143.
- Ueda, H., and T. Mizushima (1979), "Turbulence Structure in the Inner Part of the Wall Region in a Fully Developed Turbulent Flow," in *Proceedings of the 5<sup>th</sup> Biennial Symposium on Turbulence*, G. K. Patterson and J. L. Zakin, Eds., Science Press, Princeton, NJ, pp. 357-366.
- Van Dyke, M. (1964), *Perturbation Methods in Fluid Mechanics*, Academic Press, New York.
- Von Kármán, Th. (1930), "Mechanische Ähnlichkeit und Turbulenz," *Nachr. Ges. Wiss. Göttingen. Math.-Phys. Kl.*, pp. 58-76.
- Walker, J. D. A., and S. Herzog, (1988), "Eruption Mechanisms for Turbulent Flows Near Walls," in *Transport Phenomena in Turbulent Flows*, M. Hirata and N. Kasagi, Eds., pp. 145-156, Hemisphere, New York, pp. 145-156.
- Walsh, M. J. (1990), "Riblets," in *Viscous Drag Reduction in Boundary Layers*, *AIAA Progress in Astronautics and Aeronautics*, Volume 123, D. M. Bushnell and J. N. Hefner, Eds, Washington, DC, pp. 203-261.
- Walsh, M. J., W. L. Sellers III, and C. B. McGinley (1989), "Riblet Drag at Flight Conditions," *Journal of Aircraft*, vol. 26, pp. 570-575.
- Wark, C. E., and H. M. Nagib (1991), "Experimental Investigation of Coherent Structures in Turbulent Boundary Layers," *Journal of Fluid Mechanics*, vol. 230, pp. 183-208.

- Wei, T., and W. W. Willmarth (1989), "Reynolds-Number Effects on the Structure of a Turbulent Channel Flow," *Journal of Fluid Mechanics*, vol. 204, pp. 57-95.
- Wiegardt, K. (1943), "Über die Wandschubspannung in turbulenten Reibungsschichten bei veränderlichem Aussendruck," *Kaiser Wilhelm Institut für Strömungsforschung*, U&M-6603, Göttingen, Germany.
- Wilkinson, S. P., J. B. Anders, B. S. Lazos, and D. M. Bushnell (1988), "Turbulent Drag Reduction Research at NASA Langley: Progress and Plans," *International Journal of Heat and Fluid Flow*, vol. 9, pp. 266-277.
- Willmarth, W. W. (1959), "Space-Time Correlations and Spectra of Wall Pressure in a Turbulent Boundary Layer," NASA Memorandum 3-17-59W, National Aeronautics and Space Administration, Langley, VA.
- Willmarth, W. W. (1975a), "Structure of Turbulence in Boundary Layers," *Advances in Applied Mechanics*, vol. 15, pp. 159-254.
- Willmarth, W. W. (1975b), "Pressure Fluctuations Beneath Turbulent Boundary Layers," *Annual Review of Fluid Mechanics*, vol. 7, pp. 13-37.
- Willmarth, W. W., and T. J. Bogar (1977), "Survey and New Measurements of Turbulent Structure Near the Wall," *Physics of Fluids*, vol. 20, pp. S9-S21.
- Willmarth, W. W., and L. K. Sharma (1984), "Study of Turbulent Structure with Hot Wires Smaller Than the Viscous Length," *Journal of Fluid Mechanics*, vol. 142, pp. 121-149.
- Willmarth, W. W., and B. J. Tu (1967), "Structure of Turbulence in the Boundary Layer Near the Wall," *Physics of Fluids*, vol. 10, pp. S134-S137.
- Yajnik, K. S. (1970), "Asymptotic Theory of Turbulent Shear Flows," *Journal of Fluid Mechanics*, vol. 42, pp. 411-427.
- Yakhot, V., and S. A. Orszag (1986), "Renormalization Group Analysis of Turbulence. I. Basic Theory," *Journal of Scientific Computing*, vol. 1, pp. 3-51.
- Zakkay, V., V. Barra, and K. Hozumi (1980), "Turbulent Boundary Layer Structure at Low and High Subsonic Speeds," in *Turbulent Boundary Layers - Experiments, Theory, and Modelling*, AGARD Conference Proceedings, No. 271, pp. 4.1-4.20.
- Zaric, Z. (1972), "Wall Turbulence Studies," *Advances in Heat Transfer*, vol. 8, pp. 285-350.
- Zilberman, M., I. Wygnanski, and R. E. Kaplan (1977), "Transitional Boundary Layer Spot in a Fully Turbulent Environment," *Physics of Fluids*, vol. 20, pp. S258-S271.

## INITIAL DISTRIBUTION LIST

Addressee	No. of Copies
Naval Postgraduate School (T. Sarpkaya)	1
National Aeronautics and Space Administration, Langley Research Center (J. B. Anders, D. M. Bushnell, D. Dwoyer, G. Green, L. Weinstein, M. Y. Hussaini)	6
Defense Technical Information Center	2
Center for Naval Analyses	1
Catholic University of America (M. Casarella)	1
University of Illinois (C. Dutton)	1
Cambridge University (J. E. Ffowcs-Williams)	1
Yale University (K. R. Sreenivasan)	1
Melbourne University (A. E. Perry)	1
University of Notre Dame (M. Gad-el-hak)	1
Clarkson University (W. R. C. Phillips)	1
Brown University (L. Sirovich)	1
Old Dominion University (R. L. Ash)	1
State University of New York (W. George)	1
Virginia Polytechnic Institute and State University (D. Telionis)	1